Homogeneous Catalysis: Synthesis of Liquid Crystals to Diboration of Alkenes

by

Chaoyang Dai

A thesis
presented to the University of Waterloo
in fulfillment of the
thesis requirement for the degree of
Doctor of Philosophy
in
Chemistry

Waterloo, Ontario, Canada, 1998

© Chaoyang Dai 1998

National Library of Canada
Acquisitions and Bibliographic Services
395 Wellington Street
Ottawa ON K1A 0N4
Canada

Bibliothèque nationale du Canada
Acquisitions et services bibliographiques
395, rue Wellington
Ottawa ON K1A 0N4
Canada

Your file Votre référence

Our file Notre référence

The author has granted a non-exclusive licence allowing the National Library of Canada to reproduce, loan, distribute or sell copies of this thesis in microform, paper or electronic formats.

The author retains ownership of the copyright in this thesis. Neither the thesis nor substantial extracts from it may be printed or otherwise reproduced without the author's permission.

L'auteur a accordé une licence non exclusive permettant à la Bibliothèque nationale du Canada de reproduire, prêter, distribuer ou vendre des copies de cette thèse sous la forme de microfiche/film, de reproduction sur papier ou sur format électronique.

L'auteur conserve la propriété du droit d'auteur qui protège cette thèse. Ni la thèse ni des extraits substantiels de celle-ci ne doivent être imprimés ou autrement reproduits sans son autorisation.

0-612-30600-3

Canada

The University of Waterloo requires the signatures of all persons using or photocopying this thesis. Please sign below, and give address and date.

Abstract

Palladium/copper catalyzed cross-coupling methodology involving terminal alkynes and arylhalides provided a general route to a series of rigid-rod 1,4-bis(p-R-phenylethynyl)benzenes (R-C_6H_4-C≡C-C_6H_4-C≡C-C_6H_4-R, BPEB) and their partially and fully fluorinated analogs. Liquid crystal (LC) studies have demonstrated that a change in terminal substituents or fluorination of various parts of the molecule can affect not only the melting and clearing points but also the type of liquid crystalline phases that are formed. Extensive single crystal X-ray diffraction studies have been conducted in order to attempt to correlate the solid state crystalline structures with their liquid crystalline phase behaviors. An analysis of the molecular packing in crystals of the four parent BPEBs containing 0, 4, 10, or 14 fluorines, and three related tolan (C_6H_5-C≡C-C_6H_5) derivatives as well as several co-crystals is described, with particular emphasis being placed on the intermolecular interactions between phenyl and perfluorophenyl units.

In connection with the development of catalyst systems for the diboration of unsaturated organic substrates, a detailed study on the oxidative addition of the B-B bond in $(RO)_2B$-$B(OR)_2$ diboron compounds to low valent late transition metals Co(0), Ir(I) and Rh(I) has been carried out. Several interesting metal boryl [M-$B(OR)_2$] complexes were synthesized and characterized by X-ray crystallography. The paramagnetic Co(II) bis(boryl) [*cis*-$Co(PMe_3)_3(Bcat)_2$] (cat = 1,2-$O_2C_6H_4$) is the first well characterized Co bis(boryl) complex and the small B-Co-B bond angle indicates a possible remaining B···B interaction. Likewise, the novel Rh(I) mono(boryl) [$Rh(PMe_3)_4(Bcat)$] and Rh(III) tris(boryl) [*fac*-$Rh(PMe_3)_3(Bcat)_3$] complexes were obtained by reactions of [$Rh(PMe_3)_4Me$] with one or two equivalents of B_2cat_2, respectively. The Ir(III) bis(boryl) [*cis*-*fac*-$Ir(PMe_3)_3Cl(Bcat)_2$] is the first bis(boryl) complex with two distinctive boryl environments.

It has also been found that Rh(I) complexes such as [$Rh(PMe_3)_4Me$] and [$CpRh(PMe_3)_2$] can react with B_2cat_3, a reagent which has always been considered to be an undesired side product in the metal catalyzed hydroboration and diboration processes. The rational design of reactions between B_2cat_3 and [$(acac)RhL_2$] led exclusively to the formation of (acac)Bcat and a series of novel zwitterionic complexes [$(\eta^6\text{-}Bcat_2)RhL_2$] (L = C_2H_4, COE, PPh_2Me; L_2 = COD, dppm, dppe, dppp, dppb, dppf), some of which have been demonstrated to be extremely efficient hydroboration catalysts. This $(acac)RhL_2$ / B_2cat_3 system was readily applied to the catalytic addition of B_2cat_2 to 4-vinylanisole, and the reaction was complete within one hour with 89% of the desired 1,2-bis(boronate)ester product formed when 4 mol% $(acac)Rh(dppm)/B_2cat_3$ was employed. Moreover, diborations of unstrained internal alkenes such as *trans*-stilbene and *trans*-β-methylstyrene were realized for the first time and with excellent selectivities by applying the $(acac)Rh(dppm)/B_2cat_3$ catalyst system.

To my beloved wife,

Yanni

Acknowledgments

I would like to express my deepest gratitude to my supervisor, Dr. Todd Marder, for providing me with the opportunity to work on such interesting and challenging projects. I will never forget that chilly early January evening four years ago, when he received me at the Toronto Pearson Airport and led me to the Grand China Restaurant to have a warm noodle meal on my arrival to this strange snowy world. Thanks for all your patience and consideration over the years to me and to my family. Sometimes I tried to adapt to the new environment by myself without bothering you too much, but, whenever things did not turn out as expected, you were always there for me. Thanks for all your guidance, encouragement and continuing support throughout my research work. I enjoyed working on different research projects and making new things, although it is hard in the end to not be able to include everything into the thesis. (Can you make this compound? Someone in Chile asked me for it!)

Thanks to the past members of the Marder lab who, over the years, have made my experience in the group so enjoyable. Thanks to Paul Nguyen for giving me the lifts to get my first Social Insurance Number and my first several batches of groceries, and for showing me how to do the cross-coupling reactions and how to operate the GC/MS. Thanks to Gerry Lesley for your patience and help on the boron chemistry. Thanks to Fabio Souza for helping me tear down the Marder lab completely when Todd got his new Chair in England, and for constructing some of my favorite crystal structure drawings; also thanks for staying at Waterloo where I can still find someone to tell my stories to. Thanks are also due to Dr. Graham Stringer for your help with my preparation for the comprehensive examination and for showing me how to operate the dry box, and to Dr. Sylvain Nlate for sharing the lab packing moments and for blasting off the glove of the dry box but not allowing me to be sucked in through the glove port! Special thanks to Dr.

Francisco Somera and his wife Neusa for their friendship and driving lessons. The English visitors Fiona Lawlor, Ed Robins and Nigerian visitor Tolu Fasina, undergraduate students Alden Woodward, Monica Hirsch, and Rosana Souza are all greatly acknowledged for their delighted smiles and patience in the lab.

Special thanks to Dr. Scott Collins for his advice and continuing support throughout my research, for his hospitable accommodation, and for allowing me to use his computer to write this thesis when our lab turned out to be only benches and chairs. Also, thanks to Dr. Nick Taylor for his excellent crystallographic work, to Mrs. Jan Venne, Dr. Sandra Mooibroek, and Dr. Bill Power for their helpful discussions and assistance with the NMR spectroscopy, to Linda Steele and Cathy Van Esch for helping me sort through the piles of forms, and to Scott Nicoll for helping me rescue about five hundred rigid-rod phenylacetylene compounds and others from a big drum of trash which were carelessly disposed of while "cleaning-up the lab". What an experience!

I am in debt to our collaborators: Dr. Christopher Viney (Oxford University) for his colorful liquid crystal studies, Dr. Andrew Scott and Dr. Bill Clegg (University of Newcastle-upon-Tyne) for their powerful CCD detector and synchrotron X-ray radiation work; they are crystallographic geniuses (no decent NMR spectrum? no problem, show me the crystals!).

Financial support for this project was provided by the Natural Sciences and Engineering Research Council of Canada (NSERC), the Guelph-Waterloo Center for Graduate Work in Chemistry $(GWC)^2$, and was greatly appreciated. I would also like to thank the organizers of the 1996 NATO Summer School on "Crystal Engineering" for inviting me to participate and for covering my expenses; it helped me gain more knowledge in this amazing field. Special thanks to the J. T. Shaw Foundation for a scholarship which helped my family get through our financial hardship in our early years and let me concentrate on my research work.

Most importantly, I would like to thank my beloved wife Yanni for her understanding and sacrifices for me over the many years, for her willingness to give up her promising career as a young scientific editor and following me to this new country, for not complaining about staying home to raise our young baby in our difficult times. I thank our lovely son Yiyi for all the joys he has brought to us.

I would especially thank Anne Brunelle for her help to me and to our family, particularly for her encouragement and for making corrections to my thesis. Also thanks to little Ian for setting a role model for Yiyi. (What a nice big brother!)

To my parents back in China, who have fed me and educated me and pushed me up, to my brother and sister for the good times we enjoyed together, to my parents-in-law for their understanding and endless support, to my former supervisors at Wuhan University, Professors Daoyu Liu and Jingui Qin, who have taught me so much not only on the attitude towards scientific research but also on daily life by their own examples.

The past four years have sadly seen the loss of two of my deeply respected relatives: Mr. Shao-Chi Jem, my grand-uncle, former general manager of Grand Pacific Petrochemical Corp. in Taiwan, and my grandaunt, Mrs. Zhen-Yi Yin Li at Wuhan. Mr. Jem was one of those inspiring figures throughout my childhood, and without his generous support it would have been impossible for me to come to Canada to pursue Ph. D. studies. He will be remembered for generations in our family. I still remember vividly those happiest times Yanni and I spent at Mrs. Li's house at Wuhan University. We learned a lot from their true life stories. Finally, I would like to thank Mrs. Jem and Professor Li for their love and continuous encouragement. We love you all!

Table of Contents

Author's Declaration ii

Borrower's Page iii

Abstract iv

Dedication vi

Acknowledgments vii

Table of Contents x

List of Tables xv

List of Illustrations xvi

List of Abbreviations xxi

Chapter 1. Scope and Organization of the Thesis 1

Chapter 2. Pd/Cu Catalyzed Cross-Coupling Reactions of Arylhalides with Terminal Alkynes as a Route to A Variety of Functional Materials 4

2.1 Introduction 4

2.2 Pd/Cu Catalyzed Cross-Coupling of Arylhalides with Terminal Alkynes 5

2.3 Phenylacetylenic Compounds as Building Blocks for Functional Materials 11

2.3.1 Arylethynylene Polymers and Oligomers 11

2.3.2 Precisely Defined Oligomers and Polymers 12

2.4 References 19

Chapter 3. Synthesis, Crystal Structure, and Liquid Crystalline Phase Behaviors of Rigid-Rod 1,4-Bis(phenylethynyl) benzene (BPEB) Derivatives 26

3.1 Introduction 26

3.2 Results and Discussion 28

3.2.1 Synthesis 28

3.2.2 UV/Vis and Fluorescence Studies 33

3.2.3 Single Crystal Structure Study 35

3.2.4 Single Crystal Study on Parent BPEBs 38

3.2.4.1 Phenyl-perfluorophenyl Interactions 38

3.2.4.2 Molecular Structures of Parent BPEBs 43

3.2.4.3 Molecular Packings of Parent BPEBs 51

3.2.5 Liquid Crystal Study 64

3.2.5.1 Liquid Crystal Phases and Liquid Crystal Materials 65

3.2.5.2 Liquid Crystal Properties of BPEBs 69

3.2.5.2.1 Unsubstituted BPEBs 71

3.2.5.2.2 Substituted BPEBs 73

3.3 Conclusions 75

3.4 Experimental 77

3.4.1 General 77

3.4.2 Synthesis 78

3.4.3 Single Crystal Studies 85

3.4.3.1 Work at Waterloo 85

3.4.3.2 Work at Newcastle, England 85

3.4.3.3 Work at Daresbury, England 86

3.4.4 Liquid Crystal Studies 87

3.4.4.1 Differential Scanning Calorimetry 87

3.4.4.2 Transmitted Polarized Light Microscopy 88

3.5 References 90

Chapter 4. B-B Oxidative Addition to Low Valent Transition Metal Complexes 102

4.1 Introduction 102

4.1.1 Transition Metal Boryl Complexes 102

4.1.2 B-B Oxidative Addition to Transition Metal Complexes 103

4.1.3 Other Routes to Metal Bis(boryl) Complexes 105

4.1.4 Our Objectives 108

4.2 Results and Discussion 109

4.2.1 B-B Oxidative Addition to $[Co(PMe_3)_4]$ 109

4.2.2 B-B Oxidative Addition to $[Ir(PMe_3)_3Cl(COE)]$ 114

4.2.3 B-B Oxidative Addition to $[Rh(PMe_3)_4Me]$ 119

4.2.3.1 Synthesis of Rh(I) Boryl and Rh(III) Tris(boryl) Complexes 119

4.2.3.2 Reactions with Other Boron Compounds 128

4.2.3.2.1 With $B_2(4\text{-}Bu^t\text{-}cat)_2$ and $B_2(3,5\text{-}Bu^t{}_2\text{-}cat)_2$ 128

4.2.3.2.2 With B_2pin_2 and B_2neop_2 129

4.2.3.2.3 With MeBcat 134

4.2.3.3 Mechanistic Consideration 137

4.3 Experimental 143

4.4.1 General Procedures 143

4.4.2 Experimental Procedures 144

4.4.3 Molecular Structure Determinations 150

4.4.3.1 Work at Waterloo 150

4.4.3.2 Work at Newcastle, England 151

4.4 References 152

Chapter 5. Reactions Between B_2cat_3 and Rh(I) Complexes: New Homogeneous Catalysts for the Diboration of Alkenes 157

5.1 Introduction 157

5.1.1 Pt(0) Catalyzed Diboration of Alkynes 159

5.1.2 Pt(0) Catalyzed Diboration of Alkenes 164

5.1.3 Pd(0) Catalyzed Cross-Coupling Reactions between Arylhalides and Diboron Compounds 168

5.1.4 Rh(I) Catalyzed Diboration of Alkenes 169

5.1.5 Our Objectives 172

5.2 Results and Discussions 175

5.2.1 B_2cat_3 and Its Reactions with Low Valent Rh(I) Complexes 175

5.2.1.1 Reaction of B_2cat_3 with $[Rh(PMe_3)_4Me]$ 179

5.2.1.2 Reaction of B_2cat_3 with $[CpRh(PMe_3)_2]$ 182

5.2.2 Synthesis of Zwitterionic Complexes $[(\eta^6\text{-}Bcat_2)RhL_2]$ 185

5.2.2.1 Synthesis of $[(\eta^6\text{-}Bcat_2)RhL_2]$ Complexes 186

5.2.2.2 Spectroscopic Properties of $[(\eta^6\text{-}Bcat_2)RhL_2]$ Complexes 189

5.2.2.3 Crystal Structures of $[(\eta^6\text{-}Bcat_2)RhL_2]$ Complexes 197

5.2.3 Catalytic Diborations of Alkenes 215

5.2.3.1 Effectiveness of the $[(acac)RhL_2]/B_2cat_3$ Catalyst Systems 215

5.2.3.2 B_2cat_2 Addition to 4-Vinylanisole 216

5.2.3.3 Catalyzed Diboration of Other Alkenes Using $[(acac)RhL_2]/B_2cat_3$ 220

5.3 Conclusions 224

5.4 Experimental 226
5.4.1 General Procedures 226
5.4.2 Synthesis 226
5.4.3 Catalysis 233
5.4.4 Molecular Structure Determinations 236
5.5 References 238

Chapter 6. Conclusions and Future Work 244
6.1 Pd/Cu Catalyzed Cross-Coupling Reactions of Arylhalides with Terminal Alkynes as a Route to Multifunctional Materials 244
6.2 Pd Catalyzed Cross-Coupling Reactions as a Route to Arylborons 251
6.3 The Implications of Arene-Perfluoroarene Interactions in Homogeneous Catalysis 253
6.4 Topochemical Synthesis for Organoboranes? 258
6.5 References 260

List of Tables

Table 3.1 Absorption and Emission Data for Fluorinated BPEBs 34

Table 3.2 Crystallographic Data for BPEBs 36

Table 3.3 Crystal Data, Structure Solution and Refinement for Parent BPEBs and Tolans 44

Table 3.4 Interplanar Angle, C-C Triple Bond Length, C(ar)-C(sp) Bond Lengths for Parent BPEBs and Tolans 51

Table 3.5 Axial Ratio and Phase Transitions of BPEBs 70

Table 4.1 Reactions Between [$Rh(PMe_3)_4Me$] and Rhodium Boryl Complexes with Some Organoboranes 137

Table 5.1 $Pt(dba)_2$-Catalyzed Diboration of Alkenes 165

Table 5.2 $Pt(COD)_2$ or $Pt(NBE)_2$-Catalyzed Diboration of Alkenes 167

Table 5.3 Transition Metal Catalyzed Addition of B_2cat_2 to 4-Vinylanisole 171

Table 5.4 $^{31}P\{^1H\}$ and $^{11}B\{^1H\}$ NMR Data for [(acac)RhP_2] and [$(\eta^6\text{-}Bcat_2)RhP_2$] 190

Table 5.5 "Ring Contributions", Δ_R to ^{31}P Chemical Shifts in [$(\eta^6\text{-}Bcat_2)RhP_2$] 191

Table 5.6 Chemical Shifts of Catecholate Protons and Carbons in Some [$(\eta^6\text{-}Bcat_2)RhL_2$] Complexes 194

Table 5.7 Crystallographic Data for (acac)Bcat and [$(\eta^6\text{-}Bcat_2)RhL_2$] 198

Table 5.8 Selected Structural Features of Complexes [$(\eta^6\text{-}Bcat_2)RhL_2$] and [$Rh(PMe_3)_4$]($Bcat_2$) 203

Table 5.9 [$(\eta^6\text{-}Bcat_2)RhL_2$] Catalyzed Addition of B_2cat_2 to 4-Vinylanisole 218

Table 5.10 [(acac)Rh(dppm)]/B_2cat_3 Catalyzed Diboration of Alkenes 221

List of Illustrations

Scheme 2.1 Palladium-Catalyzed Cross-Coupling Reactions 5

Scheme 2.2 Proposed Mechanism for the Pd/Cu Catalyzed Cross-Coupling of Arylhalides with Terminal Alkynes 8

Figure 2.1 The Iterative Divergent/Convergent Synthetic Approach to the Linear Phenylacetylene Oligomers 13

Figure 2.2 A Representative Random Coil Conformation and the Helical Conformation of a *meta*-Phenylacetylene Octadecamer 15

Figure 2.3 A Well Defined Cyclic Phenylacetylene Oligomer 17

Figure 2.4 A Phenylacetylene 127-mer with a 124 Å Diameter..... 18

Scheme 3.1 Synthesis of Terminal Alkynes **4a-h** 30

Scheme 3.2 Synthesis of Tetrafluorinated 1,4-Bis(*p*-R-phenylethynyl)-benzenes **8a-f** 32

Scheme 3.3 Synthesis of Deca- and Octafluorinated 1,4-Bis(*p*-R-phenyl-ethynyl)benzenes **10a, 8c** 32

Scheme 3.4 Synthesis of Perfluorinated 1,4-Bis(*p*-R-phenylethynyl)-benzenes **12a, 12c** 33

Figure 3.1 Molecular Structure of **8e**, with 50% Probability Ellipsoids 37

Figure 3.2 Packing Diagram for **8e** 37

Figure 3.3 Overlap Diagram for **8e** 37

Figure 3.4a Williams' Packing Plot of the $C_6H_6 \bullet C_6F_6$ Complex 41

Figure 3.4b Another View of $C_6H_6 \bullet C_6F_6$ and Overlap Diagram 41

Figure 3.5 Molecular Structure of **1a**, with 50% Probability Ellipsoids 47

Figure 3.6 Molecular Structure of **12a**, with 50% Probability Ellipsoids..... 47

Figure 3.7 Molecular Structure of **8a**, with 50% Probability Ellipsoids 48

Figure 3.8 Molecular Structure of **10a**, with 50% Probability Ellipsoids 49

Figure 3.9 Molecular Structure of **8a•10a**, with 50% Probability Ellipsoids 49
Figure 3.10 Overlap Diagram of **1a** 52
Figure 3.11 Packing Plot for **1a** 52
Figure 3.12 Space Filling Overlap Diagram of **12a** 53
Figure 3.13 Short Intermolecular Contact Distances of **12a** 53
Figure 3.14 Packing Diagram of **14** 53
Figure 3.15 Overlap Diagram of **8a** 54
Figure 3.16 Overlap Diagram of **10a** 54
Figure 3.17 Short Interstack Distances of **8a** 54
Figure 3.18 Short Interstack Distances of **10a** 55
Figure 3.19 Packing Diagram of **8c** 56
Figure 3.20 Packing Diagram of **8a** 56
Figure 3.21 Packing Diagram of **10a** 57
Figure 3.22 Packing Diagram of **8a•10a** 57
Figure 3.23 Stacking Geometry of **8a•10a** 58
Figure 3.24 Short Interstack Contact Distances of **8a•10a** 59
Figure 3.25 Overlap Diagram of **13•14** 60
Figure 3.26 Stacking Geometry of **13•14** 60
Figure 3.27 Short Interstack Contact Distances of **13•14** 61
Figure 3.28 Overlap Diagram of **15** 61
Figure 3.29 Stacking Geometry of **15** 62
Figure 3.30 Short Interstack Contact Distances in **15** 62
Figure 3.31 Arrangement of Molecules in BPEB•3C_6F_6 (Preliminary Result) 64
Figure 3.32 Physical Description of Solid, Liquid Crystal and Isotropic Phases 65
Figure 3.33 Schematic Illustration of the Various Phases of Calamitic Molecules 66

Figure 3.34 Schematic Representation of Molecular Arrangement in Some Smectic Phases 68

Figure 3.35 Three Representative Liquid Crystal Mesogens 69

Figure 4.1 Projection of the Molecular Structure of **21** Showing the Atom Numbering Scheme and Illustrating the Distorted Square-Pyramidal Description of the Coordination Environment 110

Figure 4.2 Projection of the Molecular Structures of **21** and **22** Illustrating the Distorted Square-Pyramidal Description of the Coordination Environment 113

Figure 4.3 $^{31}P\{^{1}H\}$ NMR Spectrum of **26** in $CDCl_3$ 115

Figure 4.4 $^{11}B\{^{1}H\}$ NMR Spectrum of **26** in $CDCl_3$ 115

Figure 4.5 Molecular Structure of **26**, with 50% Probability Ellipsoids 117

Figure 4.6 $^{11}B\{^{1}H\}$ and $^{31}P\{^{1}H\}$ NMR Spectra of $[Rh(PMe_3)_4Me] + B_2cat_2$ in C_6D_6 121

Figure 4.7 $^{31}P\{^{1}H\}$ NMR Spectrum of $[Rh(PMe_3)_4Bcat]$ at 193K..... 122

Figure 4.8 Molecular Structure of $[Rh(PMe_3)_4Bcat]$, with 50% Probability Ellipsoids 123

Figure 4.9a $^{31}P\{^{1}H\}$ NMR Spectrum of $[Rh(PMe_3)_4Me]$+ 2 B_2cat_2 in C_6D_6... 125

Figure 4.9b $^{11}B\{^{1}H\}$ NMR Spectrum of $[Rh(PMe_3)_3(Bcat)_3]$ in C_6D_6..... 125

Figure 4.10 Molecular Structure of $[Rh(PMe_3)_3(Bcat)_3]$, with 50% Probability Ellipsoids 127

Figure 4.11 $^{31}P\{^{1}H\}$ NMR Spectrum of $[Rh(PMe_3)_4Me]$ + 3 B_2pin_2 in C_6D_6 130

Figure 4.12 $^{31}P\{^{1}H\}$ NMR Spectrum of $[Rh(PMe_3)_4Me]$ + 2.5 B_2neop_2 in C_6D_6 130

Figure 4.13 $^{31}P\{^{1}H\}$ NMR Spectrum of $[Rh(PMe_3)_4Me]$ + B_2neop_2 + B_2cat_2 (1:1:1) in C_6D_6 133

Figure 4.14 $^{31}P\{^{1}H\}$ NMR Spectrum of $[Rh(PMe_3)_4Me]$ + B_2cat_2 + B_2neop_2 (1:1:1) in C_6D_6 133

Figure 4.15 Molecular Structure of $[Rh(PMe_3)_4](Bcat_2)$, with 50% Probability Ellipsoids 136

Scheme 4.1 Possible Reaction Pathways for $[Rh(PMe_3)_4Me]$ and B_2R_4 138

Scheme 4.2 Possible Reaction Pathways for $[Rh(PMe_3)_3(Bcat)_3]$ and $[Rh(PMe_3)_4Me]$ 141

Figure 5.1 Mechanism for Uncatalyzed Diboration of Alkenes 157

Figure 5.2 Three-Center π-Complex Intermediate 158

Figure 5.3 Synthesis of *Z*-(±)-5,6-dimethylcyclododec-5-en-1-ol (**11**)..... 160

Figure 5.4 Synthesis of Tetrasubstituted Ethylenes on Solid Support..... 161

Scheme 5.1 Proposed Catalytic Cycle for Diboration of Alkynes 163

Figure 5.5 $[Pt(PPh_3)_4]$-Catalyzed Diboration of 1,3-Dienes..... 164

Figure 5.6 Synthesis of Diboron Compounds **1a-d**..... 168

Figure 5.7 Pd(0)-Catalyzed Cross-Coupling of **1d** with Arylhalides 169

Scheme 5.2 Proposed Catalytic Cycle for Rh(I) Catalyzed Diboration of Alkenes 170

Scheme 5.3 Possible Products Resulting from the β-H Elimination Pathway 172

Figure 5.8 Molecular Structure of B_2cat_3 (**38**) 178

Figure 5.9 Molecular Structure of $[Rh(PMe_3)_4(H)_2](Bcat_2)$, with 50% Probability Ellipsoids 180

Figure 5.10 $^{31}P\{^{1}H\}$ and $^{11}B\{^{1}H\}$ NMR Spectra of $[CpRh(PMe_3)_2]$ + B_2cat_3 in CD_3CN..... 184

Figure 5.11 Reaction between $[CpRh(PMe_3)_2]$ and B_2cat_3 185

Figure 5.12 $^{31}P\{^{1}H\}$ and $^{11}B\{^{1}H\}$ NMR Spectra of [(acac)Rh(dppb)] + B_2cat_3 in C_6D_6 188

Figure 5.13 $^{1}H\{^{13}C\}$ 2D HMQC NMR Spectrum of $[(\eta^6\text{-}Bcat_2)Rh(dppb)]$

in C_6D_6 196

Figure 5.14 Molecular Structure of (acac)Bcat, with 50% Probability Ellipsoids 202

Figure 5.15 Molecular Structure of [(η^6-$Bcat_2$)Rh($COE)_2$], with 50% Probability Ellipsoids 206

Figure 5.16 Molecular Structure of [(η^6-$Bcat_2$)Rh(COD)], with 50% Probability Ellipsoids 208

Figure 5.17 Molecular Structure of [(η^6-$Bcat_2$)Rh(dppm)], with 50% Probability Ellipsoids 210

Figure 5.18 Molecular Structure of [(η^6-$Bcat_2$)Rh(dppe)], with 50% Probability Ellipsoids 212

Figure 5.19 Molecular Structure of [(η^6-$Bcat_2$)Rh(dppb)], with 50% Probability Ellipsoids 213

Figure 5.20 Molecular Structure of [(η^6-$Bcat_2$)Rh(dppf)], with 50% Probability Ellipsoids 214

Figure 5.21 Products Obtained from the Addition of B_2cat_2 to 4-Vinylanisole 217

Figure 5.22 Molecular Structure of the Product of Diboration of *trans*-Stilbene, with 50% Probability Ellipsoids 223

Scheme 6.1 A General Route to NLO Chromophores with Heteroaromatic Rings 250

Scheme 6.2 Pd(0) Catalyzed Cross-Coupling Reactions Involving Diboron Compounds 253

List of Abbreviations

Å	Ångstrom
Ac	Acetyl
acac	Acetylacetonate
AMS	the Accessible Molecular Surface
β	First Order Molecular Hyperpolarizability
B_2cat_2	Bis(catecholate) Diboron
B_2cat_3	Tris(catecholate) Diboron
B_2neop_2	Bis(neopentylglycolate) Diboron
B_2neop_3	Tris(neopentylglycolate) Diboron
B_2pin_2	Bis(pinacolate) Diboron
B_2pin_3	Tris(pinacolate) Diboron
BBE	Bis(boronate) Ester
BDEs	Bond Dissociation Energies
BINOL	1,1'-Binapthol
BPEB	Bis(phenylethynyl)benzene
br	Broad
Bu	Butyl
5CB	*p*-n-Pentyl-*p'*-cyanobiphenyl
CCD	Charge-Coupled Device
COD	*cis*,*cis*-1,5-Cyclooctadiene
COE	*cis*-Cyclooctene
δ	Chemical Shift in ppm
dba	Dibenzylideneacetone
dcpe	1,2-Bis(dicyclohexylphosphino)ethane

diop	O-Isopropylidene-2,3-dihydroxy-1,4-bis(diphenylphosphino)butane
diphos	Bis(phosphine)
Dippe	1,2-Bis(diisopropylphosphino)ethane
DMF	Dimethylformamide
dmpe	1,2-Bis(dimethylphosphino)ethane
dppb	1,4-Bis(diphenylphosphino)butane
dppe	1,2-Bis(diphenylphosphino)ethane
dppf	1,1'-Bis(diphenylphosphino)ferrocene
dppm	1,1-Bis(diphenylphosphino)methane
dppp	1,3-Bis(diphenylphosphino)propane
DR1	Disperse Red 1
DSC	Differential Scanning Calorimetry
esu	Electrostatic Unit
Et	Ethyl
EtOAc	Ethylacetate
GC	Gas Chromatography
η	Hapticity
h	Hour
HBcat	Catecholborane ($HBO_2C_6H_4$)
hfac	Hexafluoroacetylacetonate
HFB	Hexafluorobenzene
I	Isotropic Phase
^{i}Pr	Isopropyl
IR	Infrared
K	Crystalline Phase
KTP	$KTiOPO_4$

LC	Liquid Crystal
LCD	Liquid Crystal Display
λ_{max}	Maximum Absorption (Emission) Wavelength
μ	Bridging
μ	Dipole Moment
Me	Methyl
mg	Miligram
mL	Mililiter
mp	Melting Point
MS	Mass Spectroscopy
N	Nematic Phase
NBE	Norbornadiene
neop	Neopentyl Glycolate
NLO	Nonlinear Optics
NMR	Nuclear Magnetic Resonance
OMe	Methoxy
OTf	$[O_3SCF_3]^-$
ov	Overlapped
%	Percentage
Ph	Phenyl
pin	Pinacolate
PMe_3	Trimethylphosphine
PPE	Poly(phenylene ethynylene)
PPh_3	Triphenylphosphine
ppm	Parts per Million
Py	Pyridine

q	Quartet
S	Smectic Phase
s	Singlet
S_A	Smectic A Phase
S_B	Smectic B Phase
S_C	Smectic C Phase
SHG	Second Harmonic Generation
t	Triplet
TBE	Tris(boronate) Ester
T_d	Decomposition Temperature
THF	Tetrahydrofuran
TMS	Tetramethylsilane
TMS	Trimethylsilyl
tol-BINAP	2,2'-Bis(di-*p*-tolylphosphino)-1,1'-binapthyl
tolan	Diphenylacetylene
Ts	$4\text{-}CH_3C_6H_4SO_2$
UV	Ultraviolet
VBE	Vinylboronate Ester
Vis	Visible
vt	Virtual Triplet
°	Degree
Δ_R	Ring Contribution Factor (^{31}P NMR)

Chapter 1

Scope and Organization of the Thesis

This thesis presents our work on two main projects: (i) Pd/Cu catalyzed cross-coupling reactions between arylhalides and terminal acetylenes, and (ii) transition metal boryl chemistry and Rh(I) catalyzed diboration of alkenes. Chapters 2 and 3 illustrate the Pd/Cu catalyzed cross-coupling methodology and its applications to the synthesis of a wide range of rigid-rod symmetric 1,4-bis(*p*-R-phenylethynyl)benzenes (BPEB) and their partially and fully fluorinated analogs. Chapters 4 and 5 describe the B-B bond activation in $B_2(OR)_4$ diboron compounds by low valent group 9 transition metals and Rh(I) catalyzed diboration of alkenes. Chapter 6 concludes our work and attempts to apply the knowledge gained from both projects to propose a few ideas for future work.

In addition to the above symmetric BPEBs, several unsymmetrically substituted BPEB compounds have also been synthesized for nonlinear optics (NLO), as have a series of symmetrically and unsymmetrically substituted bis(*p*-R-phenyl)acetylenes (tolans) and *trans*-1,2-bis(*p*-R-phenylethynyl)ethenes. However, these are not included in the thesis because some of the physical property measurements are not complete at this time. The study of rigid-rod phenylacetylene derivatives as multifunctional materials is a continuing research theme in our laboratory, for which many physical measurements are being carried out in collaboration with several research groups in England and France. Therefore, other researcher's contributions, where necessary, will be discussed and acknowledged in the appropriate sections of the thesis.

Chapter 2 reviews the discovery and development of the Pd/Cu catalyzed cross-coupling methodology for the synthesis of arylacetylene derivatives. It provides a powerful tool for the construction of phenylacetylene based organic and polymeric

functional materials. A wide variety of cyclic or acyclic, straight or branched phenylacetylene oligomers, polymers and dendrimers have been synthesized in recent years.

In **Chapter 3**, we present our work in the Pd/Cu catalyzed synthesis of a series of symmetric 1,4-bis(*p*-R-phenylethynyl)benzenes (BPEB) and their partially and fully fluorinated analogs. Due to their conjugated structures, these molecules have considerable potential as fluorescent and electroluminescent materials. Moreover, their rod-like geometry makes them ideal model compounds for the study of thermotropic liquid crystalline behavior. The widely used long chain aliphatic end groups are not required for many of them to achieve stable meso phases, thus enabling us to grow reasonably large high quality single crystals of our materials. Extensive single crystal X-ray diffraction studies have been conducted, particularly, a detailed molecular packing analysis is presented on the parent BPEB (C_6H_5-C≡C-C_6H_4-C≡C-C_6H_5, **1a**) and tolan (C_6H_5-C≡C-C_6H_5, **13**), and their partially and fully fluorinated analogs, which reflects the characteristic features of molecular interactions between phenyl and perfluorophenyl units. One interesting example is that two partially fluorinated BPEBs, C_6H_5-C≡C-C_6F_4-C≡C-C_6H_5 (**8a**) and C_6F_5-C≡C-C_6H_4-C≡C-C_6F_5 (**8a**) readily form co-crystals with alternative parallel intermolecular phenyl-perfluorophenyl interactions. Furthermore, the co-crystals exhibit a characteristic liquid crystal phase with a range of about 10°C. The two components, on their own, show no or only transient tendency to liquid crystallinity when heated.

Transition metal boryl complexes are currently of great interest because they play an important role in the catalytic addition of B-E (E = H, B, Si, Sn) bonds to alkenes and alkynes. In **Chapter 4**, oxidative addition of B-B bonds of several diboron compounds of the form $B_2(OR)_4$ to low valent metal complexes has been examined. Thus, B_2cat_2 (cat = 1,2-$O_2C_6H_4$) adds readily to [$Co(PMe_3)_4$] and [$Ir(PMe_3)_3Cl(COE)$] (COE = *cis*-

cyclooctene) resulting in a paramagnetic Co(II) bis(boryl) *cis*-[$Co(PMe_3)_3(Bcat)_2$] and a diamagnetic Ir(III) bis(boryl) *mer-trans*-[$Ir(PMe_3)_3Cl(Bcat)_2$] complex, respectively. Likewise, B_2cat_2 reacts with [$Rh(PMe_3)_4Me$] to generate both mono(boryl) [$Rh(PMe_3)_4Bcat$] and tris(boryl) *fac*-[$Rh(PMe_3)_3(Bcat)_3$] complexes respectively when 1 or 2 equivalents of B_2cat_2 are employed. However, the alkoxy analogs such as B_2pin_2 (pin = pinacolate) only form the mono(boryl) complex [$Rh(PMe_3)_4Bpin$] even when 3 equivalents of B_2pin_2 are added, which indicates the relative reactivities of different diboron reagents. These electron rich Rh(I) mono(boryl) compounds [$Rh(PMe_3)_4B(OR)_2$] are important for further reactivity and catalytic studies.

Chapter 5 reports the reactions between B_2cat_3 (triscatecholato diboron) and some Rh(I) complexes. The finding of a simple and direct route to [$(\eta^6\text{-}Bcat_2)RhL_2$] zwitterionic complexes *via* reaction of [$(acac)RhL_2$] with B_2cat_3 is a major synthetic breakthrough. The combination of [$(acac)RhL_2$] and B_2cat_3 thus provides easy access to a variety of complexes of ligands such as COE, COD, and monodentate or bidentate phosphines, and they were spectroscopically or crystallographically characterized. This series of zwitterionic complexes has been applied to the catalytic addition of B_2cat_2 to 4-vinylanisole, and excellent efficiency as well as selectivity has been achieved when [$(\eta^6\text{-}Bcat_2)Rh(dppm)$] is employed as the catalyst. The scope of applications of the binary catalyst system [(acac)Rh(dppm)]/ B_2cat_3 has been expanded to other alkenes. It has been demonstrated that it is also an effective catalyst for the diboration of unstrained internal alkenes.

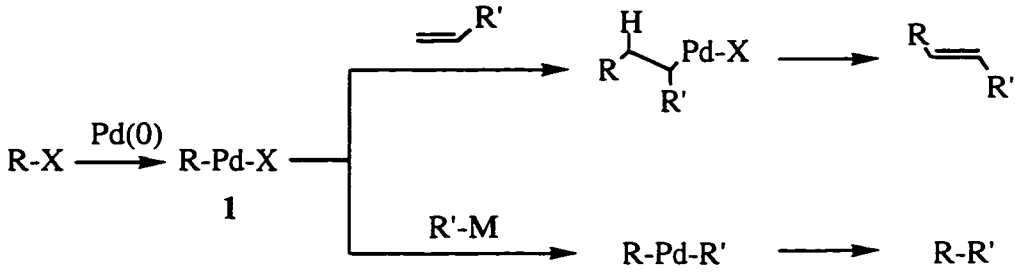
Finally, **Chapter 6** provides brief overall conclusion on the results of the present work, and presents some suggestions to extend the functionality of the BPEBs, to further the application of Pd catalysis in organoborane synthesis, and to apply our knowledge on the arene-perfluoroarene interactions in organic synthesis and crystal engineering.

Chapter 2

Pd/Cu Catalyzed Cross-Coupling Reactions of Arylhalides with Terminal Alkynes as a Route to a Variety of Functional Materials

2.1 Introduction

In recent years, the palladium-catalyzed cross-coupling reaction has evolved as a powerful tool for carbon-carbon bond formation in organic synthesis. The common feature of this palladium chemistry is that organic halides or triflates undergo facile oxidative addition to Pd(0) to form complexes $[PdL_n(R)(X)]$ (**1**) which have a Pd-C bond.[1] Then, in general, two transformations of these intermediate complexes follow: insertion or transmetallation. Unsaturated compounds such as alkenes and conjugated dienes can insert into the Pd-C bond, followed by β–hydride elimination. This forms the basis for the notable Heck reaction,[2] which is the cross-coupling of aryl or alkenyl halides with alkenes. Alternatively, transmetallation can take place with main group organometallic compounds of Li, Mg, Zn, B, Al, Sn, Si, Hg, etc., and the reaction terminates by reductive elimination. Among those nucleophilic reagents, organotin[3] and organoboron[4] compounds are particularly attractive and have found widespread applications; these processes are generally referred to as the Stille reaction[3] and the Suzuki-Miyaura[4] coupling reaction, respectively.



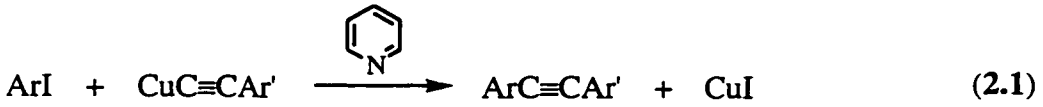
R, R' = aryl, alkenyl, alkynyl, alkyl, acyl
X = halides, triflates
M = main group metals (Li, Mg, Zn, B, Al, Sn, Si, Hg)

Scheme 2.1 Palladium-catalyzed cross-coupling reactions.

Over the past several years, we have been particularly interested in the cross-coupling reaction involving arylhalides with terminal alkynes for the preparation of a variety of rigid-rod phenylacetylene derivatives. We have synthesized a series of π-conjugated organic and organometallic complexes and investigated their linear and nonlinear optical (NLO) properties as well as their liquid crystalline (LC) phase behaviors.[5] In this chapter, a brief discussion will be presented on the methodology of Pd/Cu catalyzed cross-coupling reaction of arylhalides with terminal alkynes, and its application in the synthesis of various phenylacetylene-based functional materials.

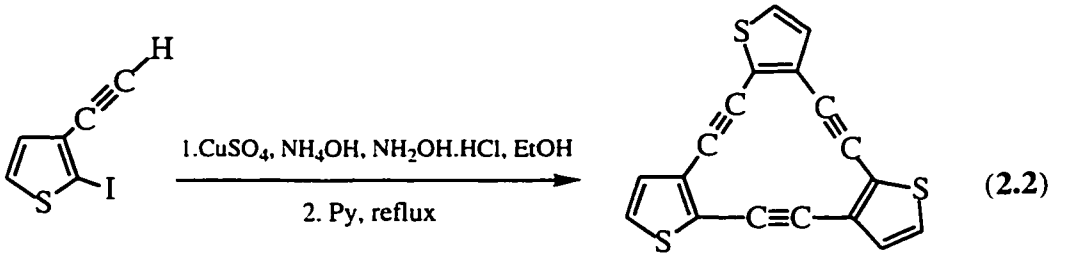
2.2 Pd/Cu Catalyzed Cross-Coupling of Arylhalides with Terminal Alkynes.

In the early 1960s, Castro and co-workers[6] reported that a variety of diphenylacetylenes (tolans) could be obtained in good yield by reacting aryl iodides with cuprous acetylides in refluxing pyridine (Reaction **2.1**).



(2.1)

This method, known as the Castro coupling reaction, generally gives very clean products, and it is still in wide use today. One interesting example is the synthesis of a cyclic thiophene acetylene compound (**2**) [7] (Reaction **2.2**). It has also been applied by Gladysz et al.[8] to synthesize metal-capped oligomers of sp carbon atoms or "molecular wires". However, it is not a very convenient method for organic chemists because cuprous acetylide complexes must be prepared prior to use. Therefore, modifications of this type of reaction were developed.



2 (2.2)

Suzuki et al.[9] in 1989 demonstrated that copper (I) species can promote the reaction of vinyl halides with terminal alkynes directly, but, as with the Castro reaction, a stoichiometric amount of copper salt is needed. In 1992, Miura et al.[10a,b] found that aryl and vinyl iodides react smoothly with terminal alkynes in the presence of a catalytic amount of CuI (5 mol%) using K_2CO_3 as base in DMF or DMSO at 120°C when an appropriate amount of PPh_3 is added. They observed that the addition of PPh_3 is essential for the reaction to proceed catalytically. Recently, Kang et al.[10c] also reported that CuI can catalyze the Stille coupling reaction in the presence of sodium chloride without using palladium.

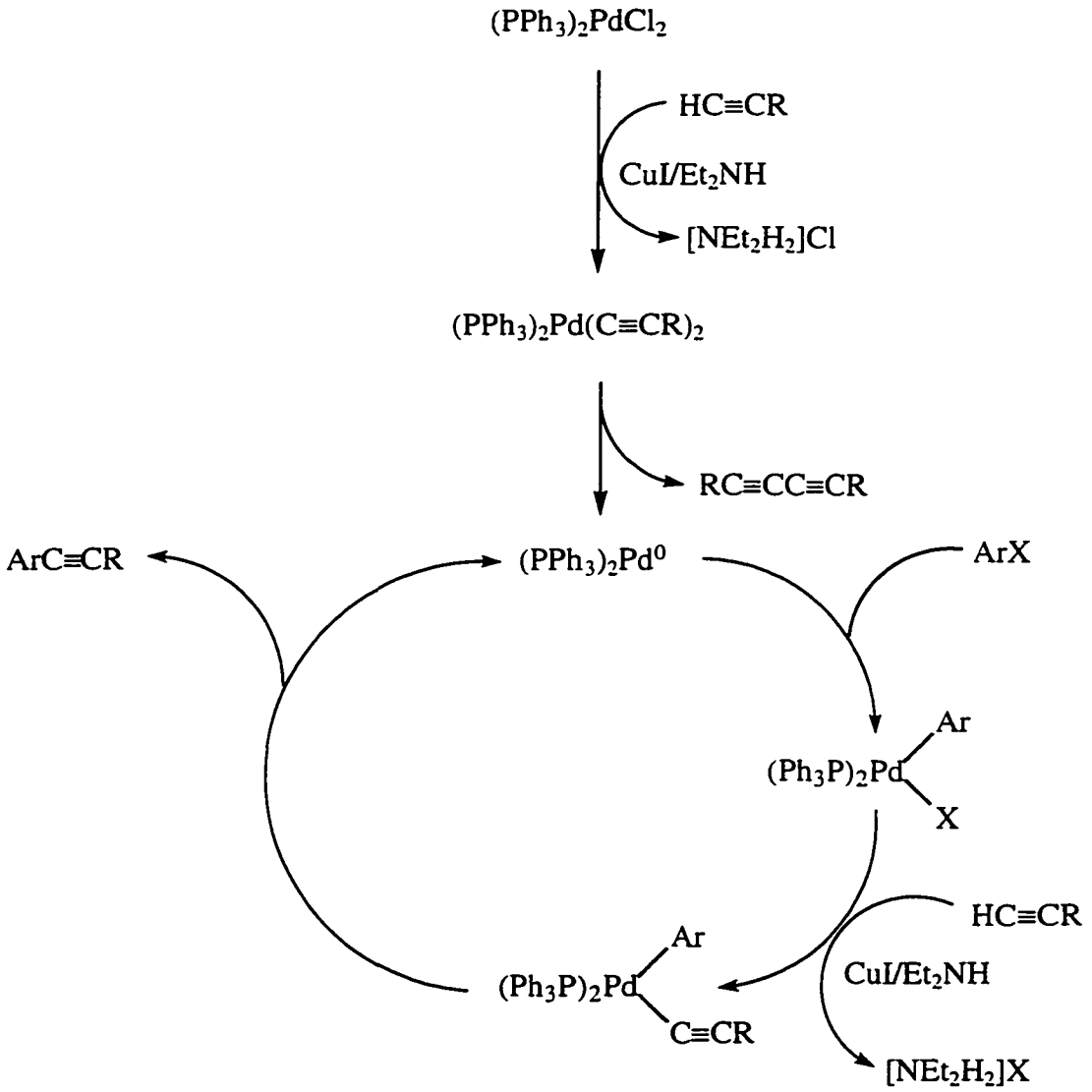
In 1975, Cassar[11] and Heck[12] simultaneously discovered that palladium phosphine complexes can catalyze the coupling of aryl halides with terminal alkynes in the presence of a base ($NaOCH_3$, or amine) under mild conditions. The reaction was proposed to undergo an initial oxidative addition of arylhalide to Pd(0) to form the Pd-C complex intermediate **1**, followed by an attack of an incipient acetylide anion to **1** and

terminated by reductive elimination of the product. Later that year, Sonogashira et al.[13] demonstrated that addition of CuI as a co-catalyst gives better results. It has been proposed that CuI activates alkynes by forming a copper acetylide[14], which undergoes transmetallation with arylpalladium halide to form the alkynylarylpalladium species. Now, this Pd/Cu catalyzed coupling reaction of aryl or vinyl halides with terminal alkynes is generally called the Sonagashira coupling reaction (Reaction **2.3**).[15] Although some recent reports indicated that the coupling also proceeds smoothly without the addition of CuI on some occasions,[16] or, as indicated above, CuI alone can catalyze the coupling reaction,[10] the palladium-copper catalytic system is always superior to the single catalyst systems in terms of higher reactivity and milder conditions, and thus it has found the widest application in the synthesis of aryl acetylene derivatives.

$$\text{Ar-I} + \text{H-C}\equiv\text{C-R} \xrightarrow[\text{Et}_2\text{NH, r.t.}]{\text{Pd(PPh}_3\text{)}_2\text{Cl}_2\text{-CuI}} \text{Ar-C}\equiv\text{C-R} \qquad (2.3)$$

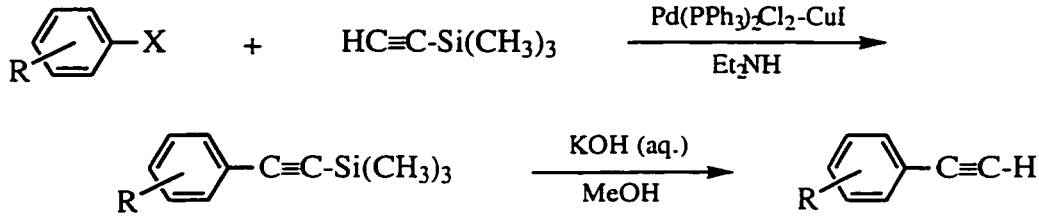
Pd(0) complexes such as $Pd(PPh_3)_4$ can be used as a catalyst for the above coupling reaction, or, the other commercially available and yet air-stable Pd(0) complex $Pd(dba)_2$ (dba = dibenzylideneacetone) is more conveniently used in combination with phosphine ligands. However, the Pd(II) complex $Pd(PPh_3)_2Cl_2$ is, above all, the most widely used catalyst precursor. It is air-stable and can be employed directly to the reaction system. Other forms of Pd(II) complexes have also been employed such as $PdCl_2/PPh_3$, $Pd(OAc)_2/PPh_3$, $Pd(PhCN)_2Cl_2/PPh_3$, $Pd(PPh_3)_2(OAc)_2$, $PdI(Ph)(PPh_3)_2$, etc.[17] Pd on carbon and PPh_3[18a] or on glass[18b] is also an active catalyst. A plausible mechanism for the Pd(II)/Cu(I) catalyzed cross-coupling of terminal alkynes and aryl halides was proposed by Sonogashira in 1975 (Scheme **2.2**).[13] The initial step involves reduction of Pd(II) to the active catalytic Pd(0) species, "$Pd(PPh_3)_2$", *via* oxidative homocoupling of the alkyne to give one equivalent of the 1,3-butadiyne. The actual chemical nature of the highly reactive, and coordinatively unsaturated Pd moiety is

unknown. It has been proposed recently to exist as an aggregate mixture of anionic species, $[Pd(PPh_3)_2Cl]_2^{2-}$, $[Pd(PPh_3)_2Cl]^-$ and $[Pd(PPh_3)_2Cl_2]^{2-}$.[19] The catalytic cycle begins with the oxidative addition of an aryl halide to the Pd(0) center to form $(PPh_3)_2Pd(Ar)(X)$, followed by a trans-metallation reaction which gives $(PPh_3)_2Pd(Ar)(C{\equiv}CR)$, and finally C-C bond reductive elimination to afford ethynylarene and regenerate $Pd(PPh_3)_2$.



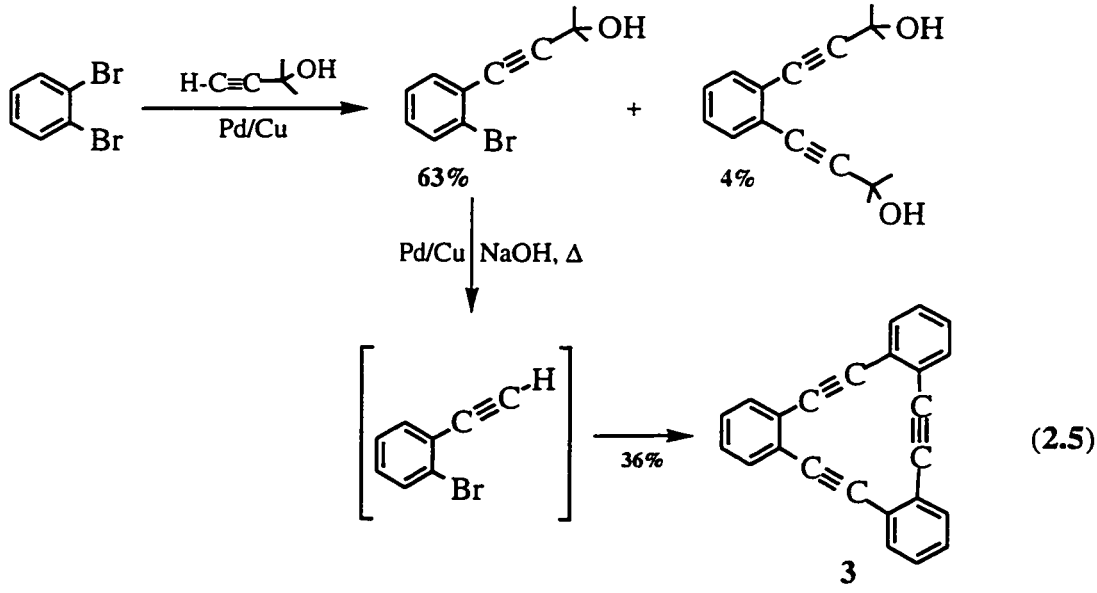
Scheme 2.2 Proposed mechanism for the Pd/Cu catalyzed cross-coupling of arylhalides with terminal alkynes.

Monosubstitution of acetylene itself is not easy. Therefore, protected acetylenes are used to make various terminal arylacetylenes, among which trimethylsilylacetylene ($HC{\equiv}C\text{-}SiMe_3$)[20] is the most widely used. After the coupling, the silyl group can be very easily removed by treating with dilute alkaline solution (KOH or K_2CO_3) in methanol or with fluoride anion at room temperature (Reaction **2.4**). Another much less



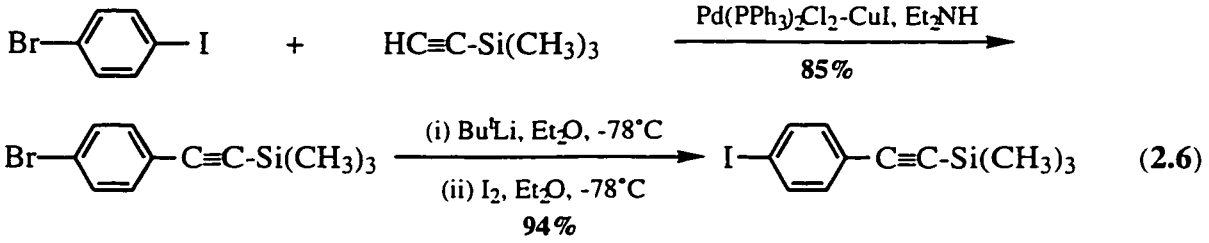
(2.4)

expensive masked acetylene is 2-methyl-3-butyn-2-ol ($HC{\equiv}C\text{-}C(OH)Me_2$), but the deprotection step requires much harsher conditions, such as refluxing with KOH or NaOH in toluene or butanol.[21] Also, the liberation of acetone will not proceed smoothly if the aromatic ring is substituted by strong electronic donor groups such as H_2N, Me_2N, etc.; so its application is relatively limited. An interesting example is the one-pot synthesis of dehydro[12]annulene (**3**) from 1,2-dibromobenzene [21d] (Reaction **2.5**).



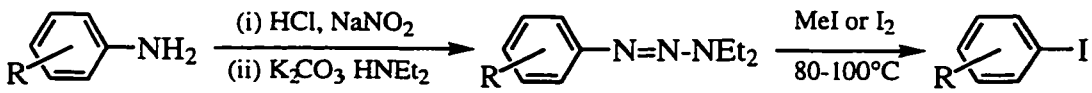
(2.5)

Due to the different reactivity of C-X bonds towards oxidative addition to the Pd(0) center, the reactivity of the aromatic halides towards coupling with terminal alkynes decreases in the order of I > Br >> Cl. Likewise, the reactivity of substituted aryl halides decreases in going from electron-withdrawing substituents to unsubstituted aryl halides to electron-donating substituents. So, aryl iodides, when possible, are preferred, particularly in the synthesis of elongated conjugated phenylacetylene oligomers. Otherwise, aryl iodide can be obtained by halogen exchange reactions.[5j] For example, the useful synthon 4-(trimethylsilylethynyl)phenyliodide was synthesized from commercially available 1-bromo-4-iodobenzene in 80% overall yield[22] (Reaction **2.6**).



(**2.6**)

However, the best method of obtaining aryl iodides was identified by Moore.[23] Thus, N,N-dialkylaryltriazenes can be transformed to aryl iodides in high yield by treatment with iodomethane or I_2 at ca. 100°C (Reaction **2.7**). The triazene group is stable to conditions used in Pd/Cu catalyzed cross-coupling reactions as well as those used to unmask the terminal alkynes protected by a $SiMe_3$ group, so it can serve as an excellent protecting group for iodide. Moreover, the $SiMe_3$ group is also stable to the conditions used in the triazene to iodide transformation. Therefore, these two protecting groups are complementary to each other for the cross-coupling reaction under discussion, and numerous conjugated arylacetylene oligomers have been synthesized.



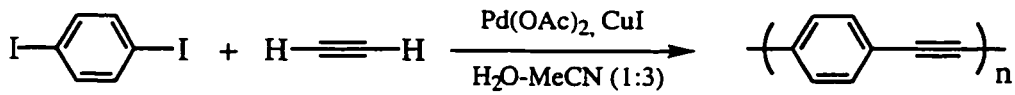
(**2.7**)

2.3 Phenylacetylenic Compounds as Building Blocks for Functional Materials

In the past decade, acetylene chemistry has experienced a major renaissance in modern organic chemistry.[24] Phenylacetylenic compounds, in particular, provide a conjugated and rigid scaffolding that can be further incorporated with a wide variety of functionalities. They have been extensively studied in the last several years as suitable building blocks for a wide variety of functional materials. This topic has been reviewed twice by Moore recently.[25] Thus, this section is not intended to be comprehensive, but rather, only a few selected examples are given.

2.3.1 Arylethynylene Polymers and Oligomers

Poly(phenylene ethynylene)s (PPE) are an important class of conjugated polymers exhibiting properties such as photoluminescence, electronic conductivity and nonlinear optics.[26] They were conveniently obtained by the cross-coupling of aryl dihalides with aryldiacetylenes, and the *ortho*-, *meta*- and *para*- PPEs were all synthesized.[27] Polymers with other functional units such as thiophene, pyridine, [28] 2,2'-bipyridine,[29] optically active binaphthol[30] etc. were also very easily prepared by the same cross-coupling methodology. The polymerization of aryl diiodide with acetylene gas was reported to take place in an aqueous medium[31] (Reaction **2.8**). This Pd/Cu catalytic system works smoothly in the presence of water. However, in order to obtain characterizable PPEs of high molecular weight, it is necessary to maintain solubility by using long chain alkyl- or alkoxy-substituted arenes.[27e,k]



(2.8)

2.3.2 Precisely Defined Oligomers and Polymers

Due to the statistical nature of the polymerization process, the above cross-coupling reactions generate polydisperse materials, that is, polymer chains with varying molecular weights. However, there is a growing interest in the past several years in the study of precisely defined systems.[32] Such oligomers and polymers with precise length and constitution can serve as excellent models for their corresponding polydispersive macromolecular analogs. They are far easier to characterize, furthermore, they may exhibit distinctive unique properties in applications such as molecular device or nanotechnology.[33] Toward this end, phenylacetylene has been widely chosen as a versatile building block, and the efficient Pd/Cu catalyzed cross-coupling methodology has been extensively applied to the construction of both straight chain and branched, monodisperse, sequence-specific phenylacetylene oligomers and polymers.[25, 32a]

Using trimethylsilyl and triazene as protecting groups and starting from compound **4**, Tour[34] has successfully applied an iterative divergent/convergent approach to synthesize a series of oligo(*p*-phenylene ethynylene)s (Figure **2.1**). In each step, the monomeric unit is doubled. The only limitation of this growing method is the solubility of the resulting products. Thus, with R = 3-ethylheptyl, a 16-mer compound (**5**) was isolated and well characterized. It has an estimated length of 128 Å, and has been expected to act as a "molecular wire"[33a]. The modern state-of-the-art nanopatterning techniques allow lithographic probe assemblies to be engineered down to the 100 Å gap regime, and **5** exhibits two reactive termini which could be used to "clip" the molecular wire to the metal electrodes. The analogous oligo(thiophene ethynylene)s were also obtained in a similar fashion.[35] Later, Moore and co-workers[36] developed a solid-phase method to simplify the purification process and to increase the reaction rates. They demonstrated that the synthesis of a *meta*-poly (phenylene ethynylene) chain attached to a

polystyrene support can be performed in a similar iterative manner to give a 64-unit chain.

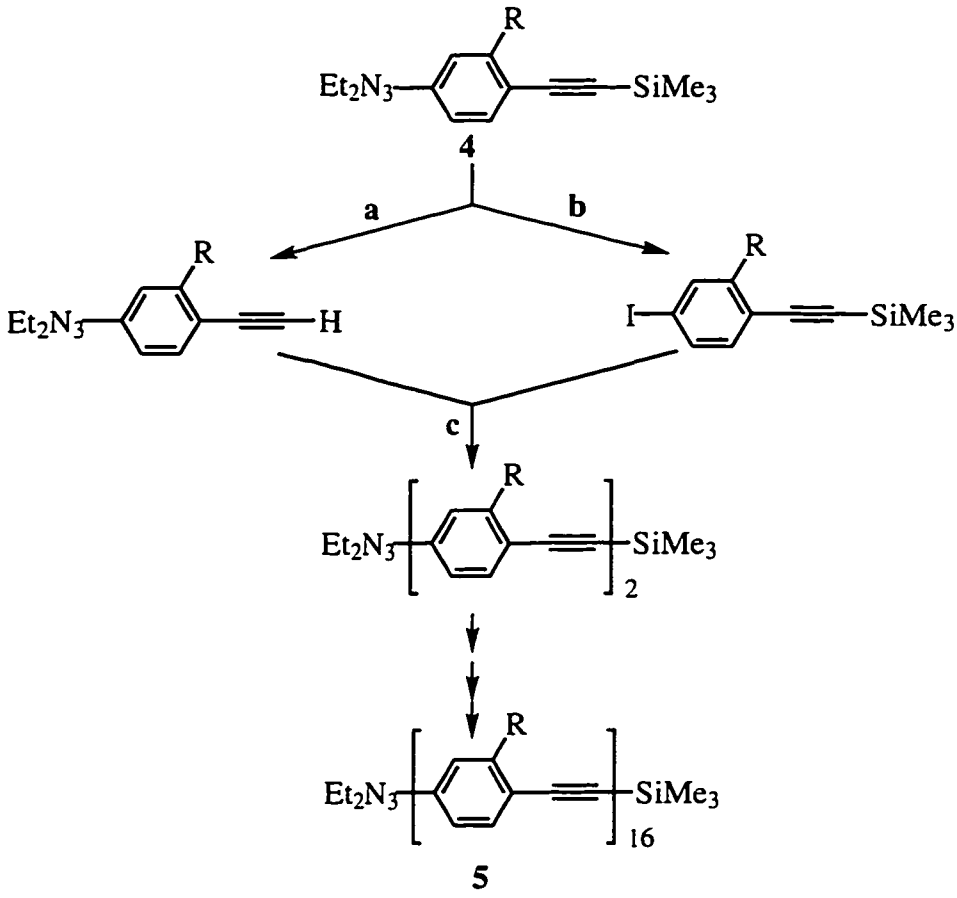


Figure **2.1** The iterative divergent/convergent synthetic approach to the linear phenylacetylene oligomers. (a) K_2CO_3, MeOH, 23°C; (b) MeI as solvent, 120°C, in a screw-cap tube; (c) [Pd(dba)$_2$] (5 mol%), CuI (10 mol%), PPh_3 (20 mol%), Pr^i_2NH/THF (1:5), 23°C.

It is a very interesting topic to analyze the possible conformations that these highly conjugated phenylacetylene oligomers may obtain. The *para*-poly(phenylene ethynylene)s (**5**) may adapt a pseudolinear straight chain structure so that they can be

applied as a molecular wire. While the credibility of this statement may still be in question, the *meta*- analogs, however, have been demonstrated recently by Moore and co-workers[37] (for chains with n > 8) to readily coil into a helix in solution, which is one of the basic folding motifs of proteins, and thus form a cavity which has potential application in molecular recognition etc. In Figure **2.2**, an octadecamer **6** is depicted in a representative random coil conformation, but both computational and spectroscopic studies have shown that it adapts a compact helical conformation in polar solvents. This new "foldamer", like proteins, can be made to fold, unfold, and then fold again. It was reasoned that intramolecular aromatic stacking maximizes solvent interactions with the polar side chains, maximizes aromatic-aromatic contacts, and minimizes interactions of hydrocarbon backbone with solvent. This is the first example of the solvophobically driven folding of nonbiological polymers, and more studies on this aspect are expected to come in the near future.

The above acyclic oligo(phenylene ethynylene)s have also been cyclized into various sized phenylacetylene macrocycles by utilizing the same Pd/Cu catalyzed cross-coupling methodology. These well-defined macrocycles of precise size and functionality have potential use in the construction of supramolecular assemblies. Here, only one example[38] is shown below (Fig. **2.3**). Compound **7** with a cavity size of 22 Å was synthesized in 70% yield. By applying different topologies such as altering substitution positions and different degrees of linking, many other related macrocycle systems were obtained by Moore's group and others.[39]

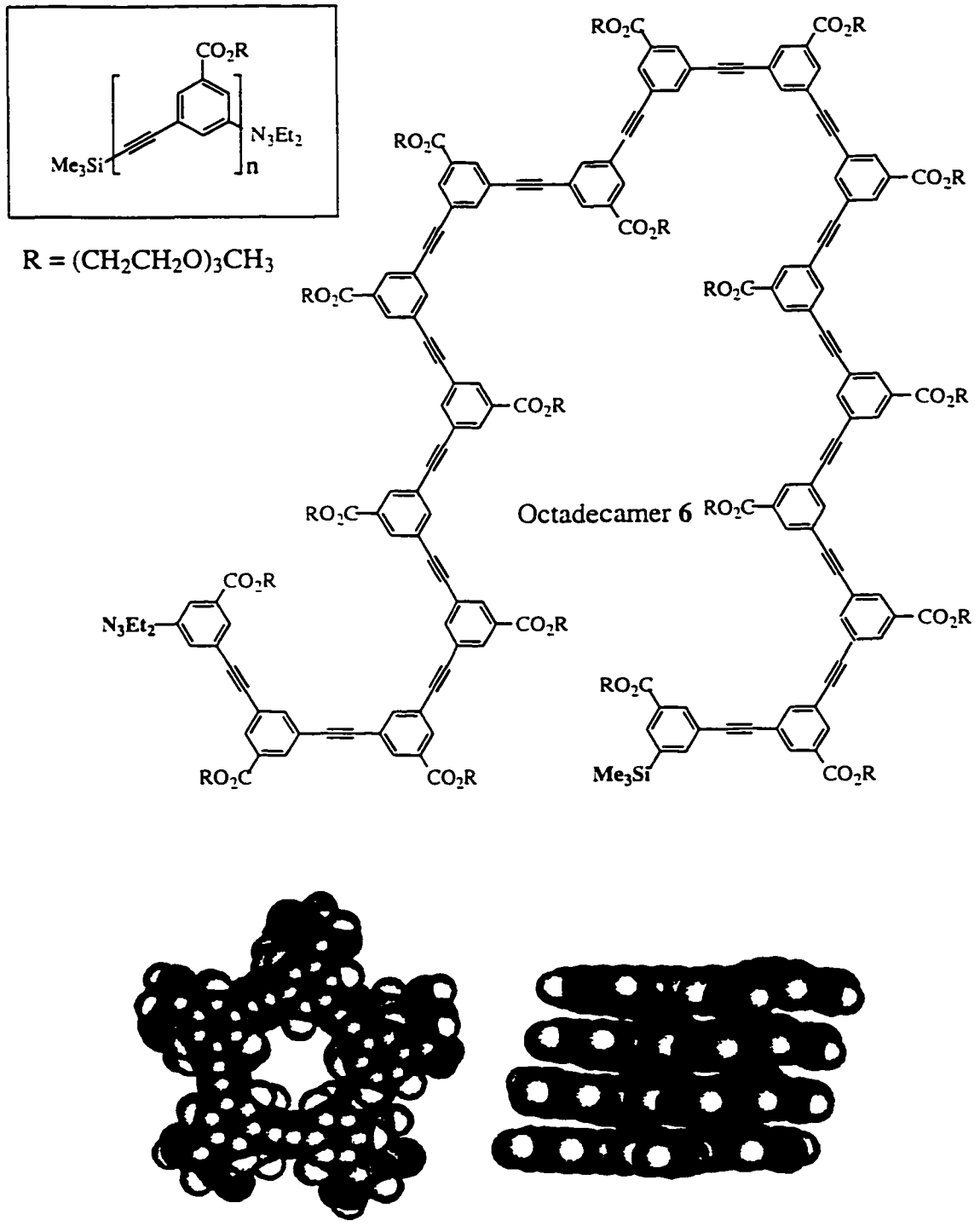


Figure 2.2 A representative random coil conformation (**top**) and the helical conformation (**bottom**) of a *meta*-phenylacetylene octadecamer (n = 18)

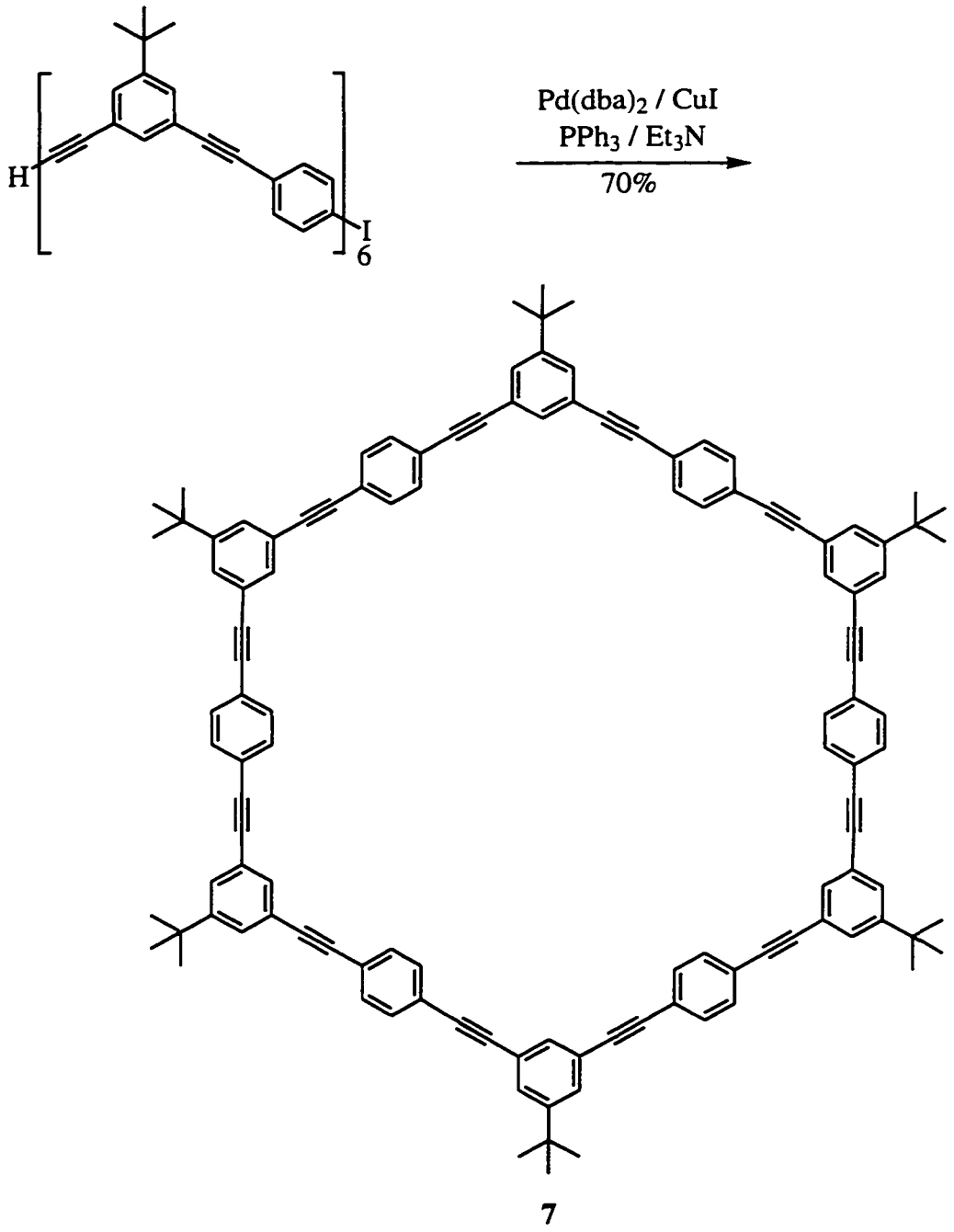


Figure **2.3** A well-defined cyclic phenylacetylene oligomer

Our understanding of polymers has changed to some extent since 1985 when Tomalia and Newkome[40] discovered a new type of polymer - dendritic macromolecules. Dendrimers are structures that possess cores with successively increasing branches of precise length and constitution. It is not surprising to see that the phenylacetylene architecture has been extensively applied to the construction of the only type of fully conjugated dendrimers to date.[41] The obstacle of solubility problems were readily overcome when 3,5-di-tert-butylphenyl groups were utilized as termini. As a matter of fact, Moore and co-workers stated that the solubility increases with increasing generation beyond the 15-mer. Sophisticated rapid growing methods such as the "double exponential growth" [41e] were developed to obtain very large dendrimers, such as the 127-mer[41b] (Figure **2.4**), which has a chemical formula of $C_{1398}H_{1278}$ (18.1 KDa). Even larger systems such as a 255-mer ($C_{3066}H_{3079}N_3$, 39.957 kDa) were able to be synthesized in pure form.[41e] These giant molecules are believed to have the potential to function as an energy funnel for electronic excitations, etc. The solid-phase synthetic approach was also readily applied to the synthesis of dendritic or hyperbranched macromolecules, and it was found that the confined spaces that exist when a dendrimer attaches to the solid-support provide a means to control the molecular weight in hyperbranched polymerizations.[42]

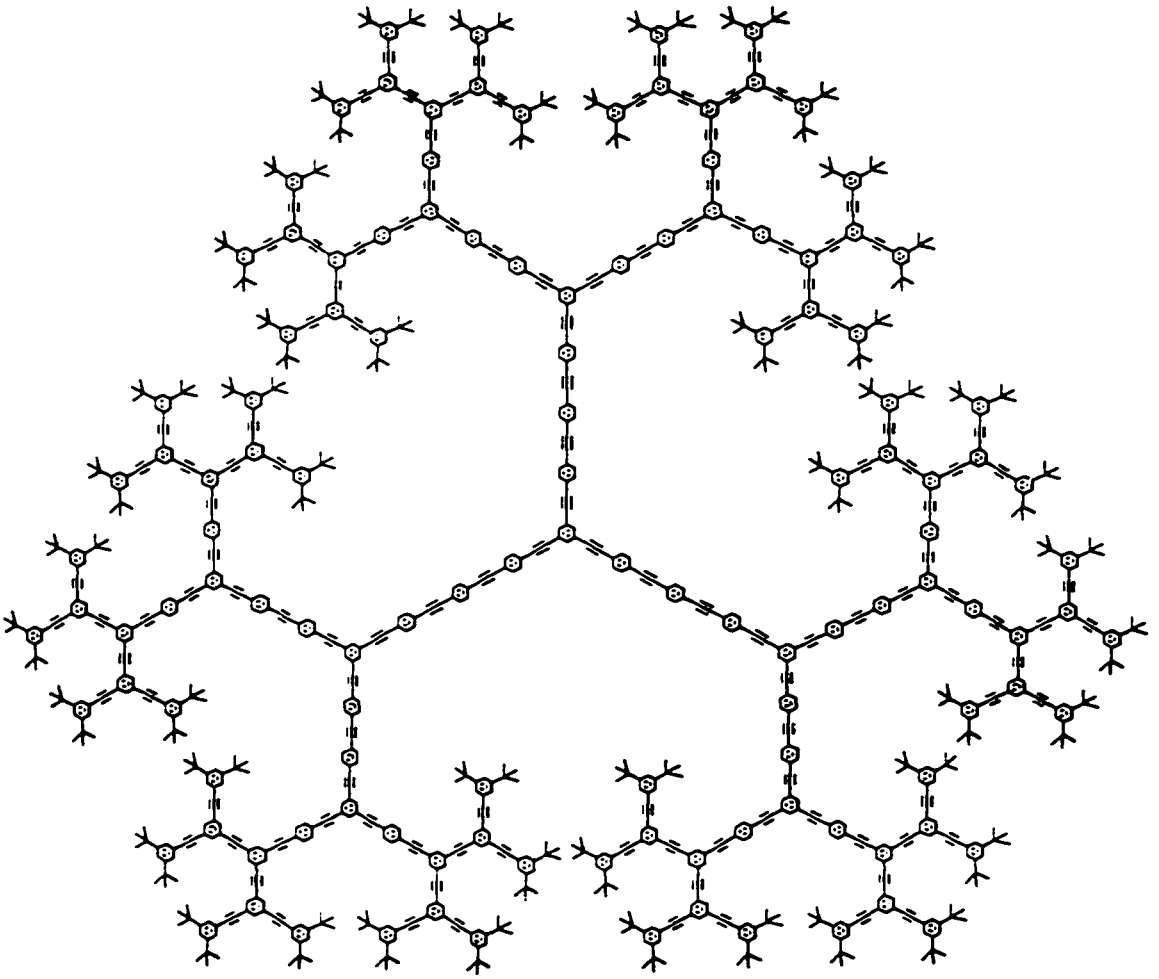


Figure 2.4. A phenylacetylene 127-mer with a 125 Å diameter. It can act as an energy funnel for electronic excitation.

2.4 References

1. (a) Heck, R. F., *Palladium Reagents in Organic Synthesis*, Academic Press: London, **1985**. (b) Tsuji, J., *Organic Synthesis with Palladium Compounds*, Springer: Berlin, **1980**. (c) Tsuji, J., *Palladium Reagents and Catalysts*, John Wiley & Sons: Chichester, **1995**.

2. Reviews: (a) Heck, R. F. *Org. React.* **1980**, *27*, 345; (b) Heck, R. F. *Adv. Catal.*, **1977**, *26*, 323; (c) Heck, R. F. *Acc. Chem. Res.* **1979**, *12*, 146; (d) Heck, R. F. in *Comprehensive Organic Synthesis*, Vol. 4, Trost, B. M.; Fleming, L. (Eds.), Pergamon Press: Oxford, **1991**, p. 833. (e) de Meijere, A.; Meyer, F. E. *Angew. Chem. Int. Ed. Engl.* **1994**, *33*, 2379.

3. Reviews: (a) Stille, J. K. *Angew. Chem. Int. Ed. Engl.*, **1986**, *25*, 508. (b) Mitchell, T. N. *Synthesis* **1992**, 803.

4. Reviews: (a) Suzuki, A. *Acc. Chem. Res.* **1982**, *15*, 178. (b) Miyaura, N.; Suzuki, A. *Chem. Rev.* **1995**, *95*, 2457.

5. (a) Marder, T. B.; Lesley, G.; Yuan, Z.; Fyfe, H. B.; Chow, P.; Stringer, G.; Jobe, I. R.; Taylor, N. J.; Williams, I. D.; Kurtz, S. K. in *Materials for Nonlinear Optics: Chemical Perspectives*, Marder, S. R.; Sohn, J. E.; Stucky, G. D. (Eds.), ACS Symp. Ser. 455, American Chemical Society: Washington, DC, **1991**, p. 605. (b) Fyfe, H. B.; Mlekuz, M.; Zargarian, D.; Taylor, N. J.; Marder, T. B. *J. Chem. Soc., Chem. Commun.* **1991**, 188. (c) Yuan, Z.; Taylor, N. J.; Marder, T. B.; Williams, I. D.; Kurtz, S. K.; Cheng, L.-T. in *Organic Materials for Nonlinear Optics II*, Hahn, R. A.; Bloor, D. (Eds.), Spec. Publ. No. 91, R. Soc. Chem.: Cambridge, **1991**, p. 190. (d) Lesley, G.; Yuan, Z.; Stringer, G.; Jobe, I. R.; Taylor, N. J.; Koch, L.; Marder, T. B.; Williams, I. D.; Kurtz, S. K. *Ibid.* p. 197.

(e) Fyfe, H. B.; Mlekuz, M.; Stringer, G.; Taylor, N. J.; Marder, T. B. in *Inorganic and Organometallic Polymers with Special Properties*, Laine, R. M. (Ed.), NATO ASI Ser. 206, Kluwer Acad. Publ.: Dordrecht, **1992**, p. 331. (f) Yuan, Z.; Taylor, N. J.; Marder, T. B.; Williams, I. D.; Kurtz, S. K.; Cheng, L.-T. *J. Chem. Soc., Chem. Commun.* **1990**, 1489. (g) Lewis, J.; Khan, M. S.; Kakkar, A. K.; Johnson, B. F. G.; Marder, T. B.; Fyfe, H. B.; Wittmann, F.; Friend, R. H.; Dray, A. E. *J. Organomet. Chem.* **1992**, *425*, 165. (h) Nguyen, P.; Todd, S.; Van den Biggelaar, D.; Taylor, N. J.; Marder, T. B.; Wittmann, F.; Friend, R. H. *Synlett*, **1994**, 299. (i) Nguyen, P.; Lesley, G.; Dai, C.; Taylor, N. J.; Marder, T. B.; Chu, V.; Viney, C.; Ledoux, I.; Zyss, J. in *Applications of Organometallic Chemistry in the Preparation and Processing of Advanced Materials*, Harrod, J. F.; Laine, R. M. (eds.) Kluwer Academic Publishers: Dordrecht, **1995**, p. 333; (j) Nguyen, P.; Yuan, Z.; Agocs, L.; Lesley, G.; Marder, T. B.; *Inorg. Chim. Acta* **1994**, *220*, 289. (k) Nguyen, P.; Lesley, G.; Marder, T. B.; Ledoux, I.; Zyss, J. *Chem. Mater.* **1997**, *9*, 406.

6. (a) Stephens, R. D.; Castro, C. E. *J. Org. Chem.* **1963**, *28*, 2163. (b) Stephens, R. D.; Castro, C. E. *J. Org. Chem.* **1963**, *28*, 3313. (c) Castro, C. E.; Gaughan, E. J.; Owsley, D. C. *J. Org. Chem.* **1966**, *31*, 4071.

7. Solooki, D.; Bradshow, J. D.; Tessier, C. A.; Youngs, W. J. *Organometallics*, **1994**, *13*, 451.

8. Bartik, T.; Bartik, B.; Brady, M.; Dembinski, R.; Gladysz, J. A. *Angew. Chem. Int. Ed. Engl.*, **1996**, *35*, 414.

9. Ogawa, T.; Kusume, K.; Tanaka, M.; Hayami, K.; Suzuki, H. *Synth. Commun.* **1989**, *19*, 2199.

10. (a) Okuru, K.; Furune, M.; Miura, M.; Norumu, M. *Tetrahedron Lett.* **1992**, *422*, 301. (b) (a) Okuru, K.; Furune, M.; Enna, M.; Miura, M.; Norumu, M. *J. Org. Chem.* **1993**, *58*, 4716. (c) Kang, S. -K.; Kim, J. -S.; Choi, S. -C. *J. Org. Chem.*, **1997**, *62*, 4208.

11. Cassar, L. *J. Organomet. Chem.* **1975**, *93*, 253.

12. Dieck, H. A.; Heck, R. F. *J. Organomet. Chem.* **1975**, *93*, 259.

13. Sonogashira, K; Toda, Y.; Hagihara, N. *Tetrahedron Lett.* **1975**, 4467.

14. (a) Sonogashira, K.; Yatake, T.; Tohda, Y.; Takahashi, S.; Hagihara, N. *J. Chem. Soc. Chem. Commun.* **1977**, 291. (b) Takahashi, S.; Kuroyama, Y.; Sonogashira, K.; Hagihara, N. *Synthesis* **1980**, 627.

15. Sonogashira, K. in *Comprehensive Organic Synthesis*, Pergamon Press: Oxford, **1990**, Vol. 3, p. 521.

16. (a) Genet, J. P.; Blart, E.; Savignac, M. *Syn. Lett.* **1992**, 715. (b) Alami, M.; Ferri, F.; Linstrumelle, G. *Tetrahedron Lett.* **1993**, *34*, 6403.

17. (a) Kasahara, A.; Izumi, T.; Shimizu, I.; Satou, M.; Katou, T. *Bull. Chem. Soc. Jpn.* **1982**, *55*, 2434. (b) d'Alarcao, M.; Leonard, N. J. *J. Am. Chem. Soc.* **1983**, *105*, 5958. (c) Mikami, K.; Azuma, K.- I.; Nakai, T. *Tetrahedron* **1984**, *40*, 2308. (d) Arcadi, A.; Cacchi, S.; Marinelli, F. *Ibid.* **1985**, *41*, 5121. (e) Gibson, K. J.; d'Alarcao, M.; Leonard, N. J. *J. Org. Chem.* **1985**, *50*, 2462. (f) Duchene, K.-H.; Vogtle, F. *Synthesis* **1986**, 659. (g) Diercks, R.; Armstrong, J. C.; Boese, R.; Vollhardt, K. P. C. *Angew. Chem. Int. Ed. Engl.* **1986**, *25*, 268. (h) Diercks, R.; Vollhardt, K. P. C. *Ibid.* **1986**, *25*, 266. (g) Tischler, A. N.; Lanza, T. J. *Tetrahedron Lett.* **1986**, *27*, 1653. (h) Blade, R. J.; Robinson, J. E.; Peek, R. J.; Weston, J. B. *Ibid.* **1987**, *28*, 3857. (i) Trost, B. M.; Chan, C.; Ruhter, G. *J. Am.*

Chem. Soc. **1987**, *109*, 3486. (j) Nye, S. A.; Potts, K. T. *Synthesis* **1988**, 375. (k) Zhang, Y.; Wen, J. *Ibid.* **1990**,727.

18. (a) Dela Rosa, M. A.; Velarde, E.; Guzman, A. *Synth. Commun.* **1990**, *20*, 2059. (b) Li, J.; Mau, A. M. -H.; Strauss, C. R. *Chem. Commun.* **1997**, 1275.

19. (a) Negishi, Ei-I.; Takahashi, T.; Akiyoshi, K. *J. Chem. Soc., Chem. Commun.* **1986**, 1338. (b) Amatore, C.; Azzbi, M.; Jutand, A. *J. Am. Chem. Soc.* **1991**, *113*, 8375.

20. (a) Takahashi, S.; Kuroyama, Y.; Sonogashira, K.; Hagihara, N. *Synthesis*, **1980**, 627. (b) Austin, W. B.; Bilow, N.; Kelleghan, W. J.; Lau, K. S. Y. *J. Org. Chem.* **1981**, *46*, 2280. (c) Brandsma, L.; van den Heuvel, H. G. M.; Verkruijsse, H. D. *Synth. Commun.* **1990**, *20*, 1889.

21. (a) Ames, D. E.; Bull, D.; Takundwa, C. *Synthesis* **1981**, 364. (b) Sabourin, E. T.; Onopchenko, A. *J. Org. Chem.* **1983**, *48*, 5135. (c) Havens, S. J.; Hergenrother, P. M. *J. Org. Chem.*, **1985**, *50*, 1763. (d) Huynh, C.; Linstrumelle, G. *Tetrahedron* **1988**, *44*, 6337. (e) Melissaries, A. P.; Litt, M. *J. Org. Chem.* **1992**, *57*, 6998.

22. Hsung R. P.; Chidsey, C. E. D.; Sita, L. R. *Organometallics* **1995**, *14*, 4808.

23. Moore, J. S.; Weinstein, E. J.; Wu, Z. *Tetrahedron Lett.* **1991**, *32*, 2465. (b) Wu, Z.; Moore, J. S. *Tetrahedron Lett.* **1994**, *35*, 5539.

24. Stang, P. J.; Diederich, F. *Modern Acetylene Chemistry;* VCH: Weinheim, 1995.

25. (a) Young, J. K.; Moore, J. S. In *Modern Acetylene Chemistry;* Stang, P. J.; Diederich, F. (Eds.); VCH: Weinheim, 1995; Chapter 12. (b) Moore, J. S. *Acc. Chem. Res.* **1997**, *30*, 402.

26. (a)Yamamoto, T.; Takagi, M.; Kizu, K.; Maruyama, K.; Kubota, H.; Kanbara, T.; Kurihara, T.; Kaino, T. J. *Chem. Soc., Chem. Commun.* **1993**, 797. (b) Baughman, R. H.; Bredas, J. L.; Chance, R. R.; Elsenbaumer, R. L.; Shacklette, L. W. *Chem. Rev.* **1982**, *82*, 209. (c) Skotheim, T. A.; Dekker, M. *Handbook of Conductive Polymers*, New York, **1986**. (d) Salaneck, W. R.; Clark, D. T.; Samuelsen, E. J., *Science and Applications of Conducting Polymers*, Adam Hilger: Bristol, **1990**. (e) Bredas, J. L.; Chance, R. R., *Conjugated Polymeric Materials: Opportunities in Electronics, Optoelectronics, and Molecular Electronics*, NATO ASI Series Vol. 182, Kluwer Academic Publishers: Dordrecht, **1990**.

27. (a) Sanechika, K.; Yamamoto, T.; Yamamoto, A. *Bull. Chem. Soc. Jpn.* **1984**, *57*, 752. (b) Trumbo, D. L.; Marvel, C. S. *J. Polym. Sci., Part A: Polym. Chem.* **1986**, *24*, 2231. (c) Trumbo, D. L.; Marvel, C. S. *J. Polym. Sci., Part A: Polym. Chem.* **1986**, *24*, 2311. (d) Trumbo, D. L.; Marvel, C. S. *J. Polym. Sci., Part A: Polym. Chem.* **1987**, *25*, 839. (e) Giesa, R.; Schulz, R. C. *Makromol. Chem.* **1990**, *191*, 857. (f) Kondo, K.; Okuda, M.; Fujitani, T. *Macromolecules* **1993**, *26*, 7382. (g) Grubbs, R. H.; Kratz, D. *Chem. Ber.* **1993**, *126*, 149. (h) Solomin, V. A.; Heitz,W. *Macromol. Chem. Phys.* **1994**, *195*, 303. (i) Moroni, M.; Moigne, J. L. *Macromolecules* **1994**, *27*, 562. (j) Heitz, W. *Pure & Appl. Chem.* **1995**, *67*, 1951. (k) Mangel, T.; Eberhardt, A.; Schef, U.; Bunz, U. H. F.; Müllen, K. *Macromol. Rapid Commun.*, **1995**, *16*, 571.

28. Yamamoto, T.; Takagi, M.; Kizu, K.; Maruyama, T.; Kubota, K.; Kanbara, H.; Kurihara, T.; Kaino, T. *J. Chem. Soc., Chem. Commun.* **1993**, 797.

29. Ley, K. D.; Whittle, C. E.; Bartberger, M. D.; Schanze, K. S. *J. Am. Chem. Soc.* **1997**, *119*, 3423.

30. Ng, M.; Chow, H.; Chan, T.; Mak, T. C. W. *Tetrahedron Lett.* **1996**, *37*, 2979. (b) Cheng, H. ; Ma, L.; Hu, Q., Zheng, X.; Anderson, J.; Pu, L. *Tetrahedron: Asymmetry* **1996**, *7*, 3083. (c) Ma, L.; Hu, Pu, L. *Tetrahedron: Asymmetry* **1996**, *7*, 3103.

31. Li, C.; Slaven IV, W. T.; John, V. T.; Banerjee, S. *Chem. Commun.* **1997**, 1569.

32. (a) Tour, J. M. *Chem. Rev.* **1996**, *96*, 537. (b) Rothe, M. In *Chemistry and Physics of Macromolecules;* Fisher, E. W., Schulz, R. C., Sillescu, H., VCH: Weinheim, 1991; p 39. (c) Tour, J. M. *Trends Polym. Sci.* **1994**, *2*, 332.

33. (a) Ward, M. D. *Chem. & Ind.* **1996**, 568. (b) Diederich, F. *Nature* **1994**, *369*, 199. (c) Aviram, A. *J. Am. Chem. Soc.* **1988**, *110*, 5687.

34. Schumm, J. S.; Pearson, D. L.; Tour, J. M. *Angew. Chem., Int. Ed. Engl.* **1994**, *33*, 1360.

35. Pearson, D. L.; Schumm, J. S.; Tour, J. M. *Macromolecules* **1994**, *27*, 2348.

36. Young, J. K.; Nelson, J. C.; Moore, J. S. *J. Am. Chem. Soc.* **1994**, *116*, 10841.

37. Nelson, J. C.; Saven, J. G.; Moore, J. S.; Wolynes, P. G. *Science* **1997**, *277*, 1793.

38. Zhang, J.; Pesak, D. J.; Ludwick, J. L.; Moore, J. S. *J. Am. Chem. Soc.* **1994**, *116*, 4227.

39. (a) Wu, Z.; Lee, S.; Moore, J. S. *J. Am. Chem. Soc.* **1992**, *114*, 8730. (b) Venkataraman, D.; Lee, S.; Zhang, J.; Moore, J. S. *Nature* **1994**, *371*, 591. (c) Wu, Z.; Moore, J. S. *Angew. Chem. Int. Ed. Engl.* **1996**, *35*, 297. (d) Bedard, T. C.; Moore, J. S. *J. Am. Chem. Soc.* **1995**, *117*, 10662. (e) Shetty, A. S.; Zhang, J.; Moore, J. S. *J. Am. Chem. Soc.* **1996**, *118*, 1019. (f) Anderson, S.; Neidlein, U.; Gramlich, V.; Diederich, F. *Angew. Chem. Int. Ed. Engl.* **1995**, *34*, 1596. (g)

Morrison, D. L.; Höger, S. *Chem. Commun.* **1996**, 2313. (h) Höger, S.; Meckenstock, A. -D.; Pellen, H. *J. Org. Chem.* **1997**, *62*, 4556. (i) Kawase, T.; Ueda, N.; Darabi, H. R.; Oda, M. *Angew. Chem. Int. Ed. Engl.* **1996**, *35*, 1556. (j) Kawase,T;. Darabi, H. R.; Oda, M. *Angew. Chem. Int. Ed. Engl.* **1996**, *35*, 2664. (k) Boese, R.; Matzger, A. J.; Vollhardt, K. P. C. *J. Am. Chem. Soc.* **1997**, *119*, 2052. (l) Haley, M. M.; Brand, S. C.; Pak, J. J. *Angew. Chem. Int. Ed. Engl.* **1997**, *36*, 836.

40. (a) Tomalia, D. A.; Baker, H.; Dewald, J. R.; Hall, M.; Kallos, G.; Martin, S.; Ryder, J.; Smith, P. *Polymer J.* **1985**, *17*, 117. (b) Newkome, G. R.; Yao, Z. -Q.; Baker, G. R.; Gupta, V. K. *J. Org. Chem.* **1985**, *50*, 2003.

41. (a) Xu, Z.; Moore, J. S. *Angew. Chem. Int. Ed. Engl.* **1993**, *32*, 246. (b) Xu, Z.; Moore, J. S. *Angew. Chem. Int. Ed. Engl.* **1993**, *32*, 1354. (c) Xu, Z., Kahr, M.; Walker, K. L.; Wilkins, C. L.; Moore, J. S. *J. Am. Chem. Soc.* **1994**, *116*, 4537. (d) Bharathi, P.; Patel, U.; Kawaguchi, T.; Pesak, D. J.; Moore, J. S. *Macromolecules* **1995**, *28*, 5955. (e) Kawaguchi, T.; Walker, K. L.; Wilkins, C. L.; Moore, J. S. *J. Am. Chem. Soc.* **1995**, *117*, 2159. (f) Xu, Z.; Moore, J. S. *Acta Poly.* **1994**, *45*, 83. (g) Devadoss, C.; Bharathi, P.; Moore, J. S. *J. Am. Chem. Soc.* **1996**, *118*, 9635. (h) Kopelman, R.; Shotreed, M.; Shi, Z. Y.; Tan, W.; Xu, Z.; Moore, J.S.; Bar-Haim, A.; Klafter, J. *J. Phys. Rev. Lett.* **1997**, *78*, 1239.

42. Bharathi, P.; Moore, J. S. *J. Am. Chem. Soc.* **1997**, *119*, 3391.

Chapter 3

Synthesis, Crystal Structure, and Liquid Crystalline Phase Behaviors of Rigid-Rod 1,4-Bis(phenylethynyl) benzene (BPEB) Derivatives

3.1. Introduction

The synthesis of rigid conjugated organic molecules with novel structural, electronic and optical properties is currently an area of intensive activity.[1] Among all the construction strategies, phenylacetylene is certainly one of the most widely used building blocks for these materials.[2] The simple diphenylacetylene (tolan) derivatives, have long been demonstrated to exhibit reasonably large second order nonlinear optical (NLO) properties,[3a-e] good fluorescent properties,[3f,g] as well as liquid crystalline behaviors.[3h-l] Recently, much more effort has been put forward to the more extended oligomeric structures[4-6] (see previous chapter). The linear oligo(phenylene ethynylene) molecule with a precise length of 128 Å (16-mer) was reported,[4b] and the structurally related 64-mer was also prepared by the solid-phase synthetic method.[4c] Tritopic 1,3,5-tris(cyanophenylethynyl)benzenes have been used as ligands to construct infinite coordination networks with metals,[5a-c] and other branched poly phenylethynyl-substituted benzene systems exhibit interesting third-order optical nonlinearity [5d] or discotic liquid-crystalline phase behaviors.[5e,f] In the meantime, macrocycles based on phenylacetylene were synthesized by several different research groups.[6] The syntheses of fully conjugated rigid oligo(phenylene ethynylene) dendrimers and hyperbranched macromolecules were also achieved.[7] While the linear phenylacetylene polymers were

first prepared in the mid 1980's,[8a,b] more recent efforts have been applied to improve the solubility of these polymers and to utilize different polymerization strategies.[8c-f]

Along this line, however, considerably less emphasis has been placed on the study of the relatively smaller bis(phenylethynyl) benzene (BPEB) derivatives,[9] probably because of the general feeling of "the longer the better", which, of course, is not always true. For instance, several theoretical studies on the conjugation length and nonlinear optical hypersusceptibilities indicate a saturation response at a certain length.[10] The optimum effective conjugation length with respect to the third order optical nonlinearity (γ) for poly(thiophene) has been reported to be just 9-10 repeat units.[11] In the past several years, we have been engaged in a systematic investigation of the synthesis of symmetrically and unsymmetrically substituted 1,4-bis (*p*-R-phenylethynyl)benzene derivatives (**1**) and their linear and nonlinear optical properties as well as liquid crystalline phase behaviors.[12]



1

In the latter case, the rod-like geometry and their suitable axial ratio (i.e. length-to-diameter ratio) made them ideal model compounds for the study of thermotropic liquid crystalline properties.[13] One of our collaborators, C. Viney,[13a] has previously shown that an axial ratio of approximately 4.3 for this type of molecules is large enough to sustain nematic order at ambient pressure, whereas, the axial ratio of the parent unsubstituted BPEB (C_6H_5-C≡C-C_6H_4-C≡C-C_6H_5, **1a**) is estimated to be 4.45.[13c] Thus, the widely used long chain end substituents (for example, in the corresponding tolan derivatives) are not necessarily required for these compounds to achieve stable mesogenic phases. This, in turn, allowed us to explore the effect of soft interaction (i.e. charge distribution) on the liquid crystalline behavior easily by maintaining the core

structure of the molecules and changing the simple end substituents without too much axial ratio change. It also enabled us to grow reasonably large single crystals of these liquid crystal molecules and hence to try to correlate their solid state crystalline structures with their liquid crystalline phase behaviors.

In continuation of our studies on this BPEB system, we began to introduce perfluorophenyl units into the molecules. The fluorine atom combines large electronegativity with small size, so, it is expected to affect significantly the electronic polarizability of the molecules but without elimination of the possibility of mesophase formation. The introduction of fluorine atoms into mesogens is a very common strategy in liquid crystal studies.[14] In this work, we employed the Pd/Cu catalyzed cross-coupling methodology to synthesize a variety of partially and fully fluorinated BPEB molecules. The X-ray single crystal structure studies enable us to investigate the molecular packing patterns and hence to gain some insight into the nature of the intermolecular phenyl-perfluorophenyl interactions and furthermore, to rationalize the thermotropic properties of these molecules.

3.2. Results and Discussion

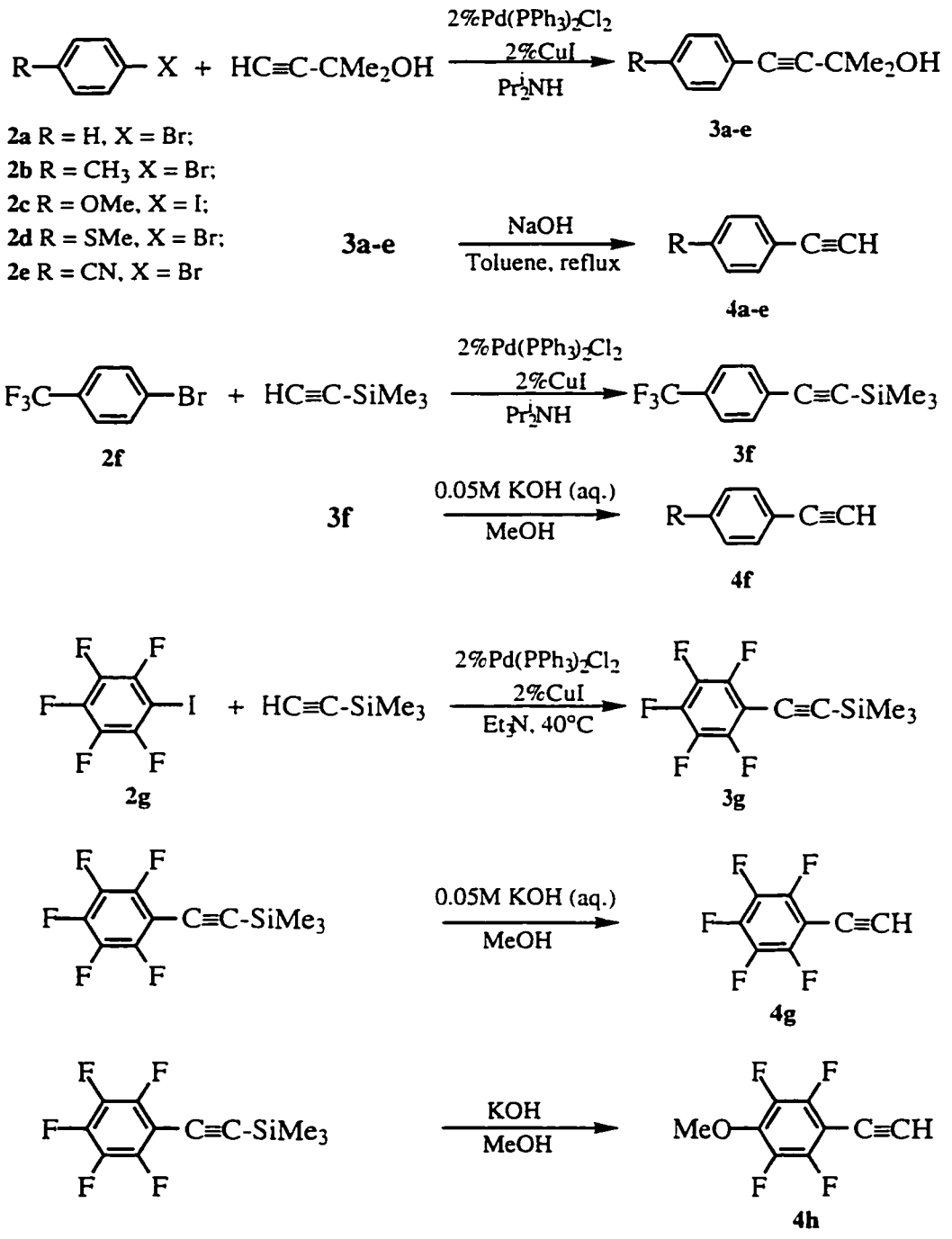
3.2.1. Synthesis

Both electron-donating and accepting *para*-substituted phenylacetylenes **4a-e** can be obtained readily from the cross-coupling reactions between the corresponding *para*-substituted phenylbromides (or iodide, **2c**) and 3-methylbut-1-yn-3-ol (**5**) catalyzed by 2 mol% $Pd(PPh_3)_2Cl_2$ and 2 mol% CuI in diisopropylamine, followed by deprotection with NaOH in refluxing toluene. The arylbromides were utilized wherever applicable for obvious economic reasons, however, 4-iodoanisole (**2c**) had to be used in order to secure an effective coupling reaction. When R = CF_3, the deprotection step from F_3C-C_6H_4-

$C{\equiv}C\text{-}C(Me_2)OH$ was unsuccessful due to the decomposition of the corresponding terminal alkyne, $F_3C\text{-}C_6H_4\text{-}C{\equiv}CH$ under refluxing conditions. So, trimethylsilylacetylene (**6**) was used instead of **5** (Scheme **3.1**). The Pd/Cu catalyzed cross-coupling reaction has been demonstrated to be an effective route for all the terminal alkynes **4a-f**; the overall yields from **2a-f** to the final products **4a-f** were over 70%.

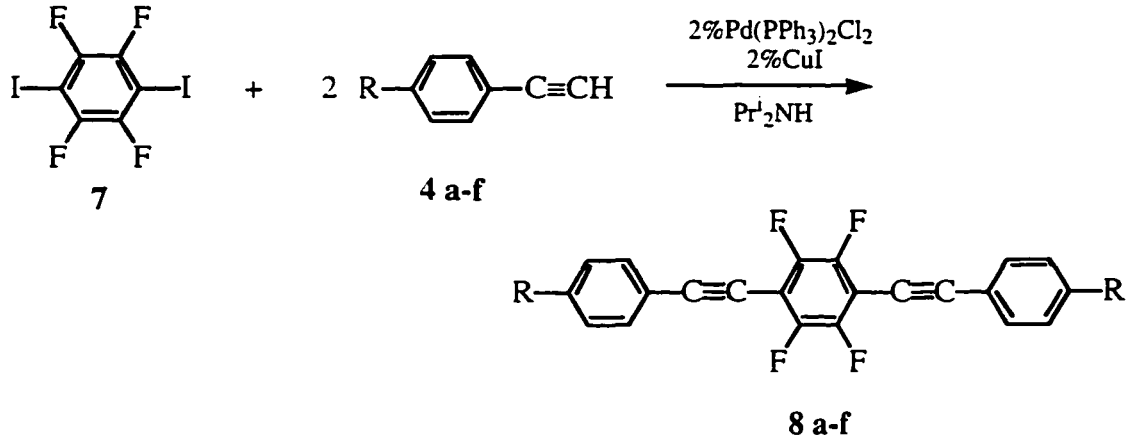
Pentafluorophenylacetylene (**4g**) was also synthesized in a similar fashion[15] by the cross-coupling reaction between iodopentafluorobenzene (**2g**) and **6**. The masking reagent **5** is obviously unsuitable for this purpose because **4g** can not tolerate the harsh deprotection reaction conditions. Triethylamine, instead of diisopropylamine, was used as the reaction medium, because perfluoroaryl compounds are known to undergo nucleophilic substitution reactions with primary or secondary amines in the presence of a base such as K_2CO_3.[16] (Trimethylsilyl)pentafluorophenylacetylene (**3g**) was obtained with the best isolated yield being 73% among several experiments when coupling between **2g** and 1.2 equiv of **6** was catalyzed by 2 mol% of $Pd(PPh_3)_2Cl_2$ / CuI in Et_3N for 24 h at 40°C. However, significant amounts of 1,4-bis(trimethylsilyl)butadiyne (*ca.* 20%) and pentafluorobenzene were also observed by *in situ* GC-MS analysis of the reaction mixture. We reasoned that they had arisen predominantly from the hydrodehalogenation side reaction where **2g** serves as an oxidizing reagent to promote the Pd/Cu catalyzed oxidative homo-coupling reaction of **6** to give $Me_3Si\text{-}C{\equiv}C\text{-}C{\equiv}C\text{-}SiMe_3$ and $C_6F_5\text{-}H$. This side reaction is more severe if bromopentafluorobenzene is applied for the cross-coupling reaction, an isolated yield of only 20% from $C_6F_5\text{-}Br$ was reported previously.[17] The compound $C_6F_5\text{-}C{\equiv}CH$ could be very easily deprotected by treating $C_6F_5\text{-}C{\equiv}C\text{-}SiMe_3$ (**3g**) with dilute KOH (aq) solution in MeOH; however, prolonged reaction time results in the formation of $4\text{-}MeO\text{-}C_6F_5\text{-}C{\equiv}CH$ (**4h**). Therefore, **4h** was obtained in 81% yield as a white solid when **3g** was treated with KOH in MeOH for 10 h (Scheme **3.1**).

Scheme 3.1 Synthesis of Terminal Alkynes **4a-h**



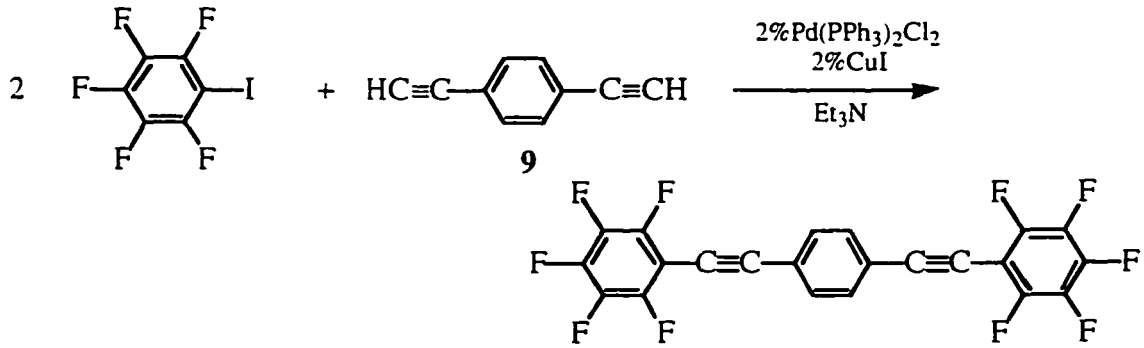
The 1,4-bis(*p*-R-phenylethynyl)tetrafluorobenzenes (**8a-f**) were prepared in good yields via the Pd/Cu catalyzed cross-coupling reactions between 1,4-diiodotetrafluorobenzene (**7**) and 2 equiv. of the corresponding *para*-substituted phenylacetylenes **4a-f** in diisopropylamine at reflux (Scheme **3.2**). The reactions were monitored by GC-MS for completion. The ammonium salt was removed by filtration, and the desired products were isolated either by direct recrystallization or after purification by column chromatography. These catalytic cross-coupling reactions all proceed smoothly; only minor side products due to competing processes such as terminal alkyne homo-coupling, dimerization, and hydrodehalogenation were detected by *in situ* GC-MS analysis. The decafluorinated 1,4-bis(pentafluorophenylethynyl)benzene (**10a**) was synthesized through the coupling of 1,4-diethynylbenzene (**9**) with two equiv. of iodopentafluorobenzene in triethylamine (Scheme **3.3**). Triethylamine was utilized throughout this synthetic work whenever iodopentafluorobenzene was used for the cross-coupling reactions, in order to avoid the possible nucleophilic substitution reactions by amines (*vide supra*). When the reactions were conducted in diisopropylamine, the related amine substitution products could be observed by GC-MS analysis, but it was only to a minor extent. Compound **10c** was prepared by the reaction of fluorinated terminal alkyne **4h** with 1,4-diiodobenzene. Likewise, by applying the same Pd/Cu catalyzed cross-coupling methodology, two perfluorinated BPEB analogs **12a**, **12c** have also been prepared with good yields (> 75%) (Scheme **3.4**). All these BPEBs have been fully characterized by NMR spectroscopy, IR, elemental analysis, MS, as well as single crystal X-ray diffraction analysis.

Scheme 3.2 Synthesis of Tetrafluorinated 1,4-Bis(*p*-R-phenylethynyl)benzenes **8a-f**

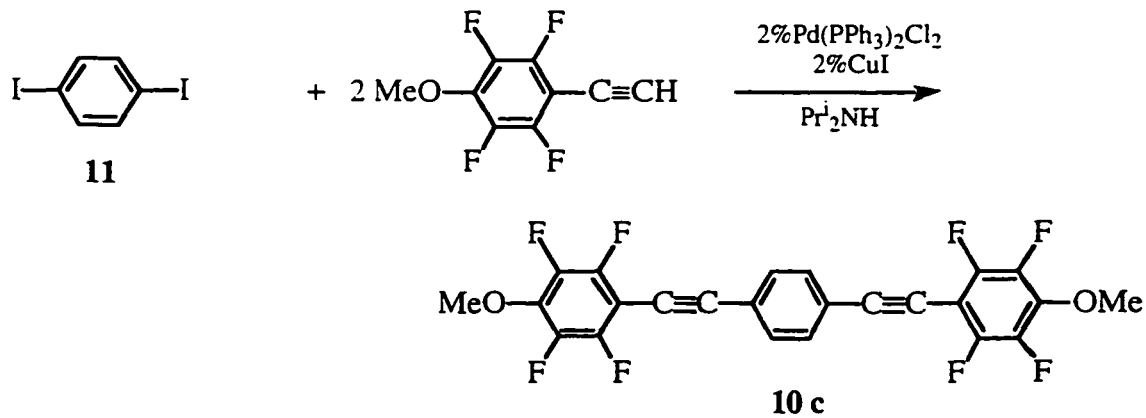


7 **4 a-f** **8 a-f**

Scheme 3.3 Synthesis of Deca- and Octafluorinated 1,4-Bis (*p*-R-phenylethynyl)benzenes **10a**, **8c**.

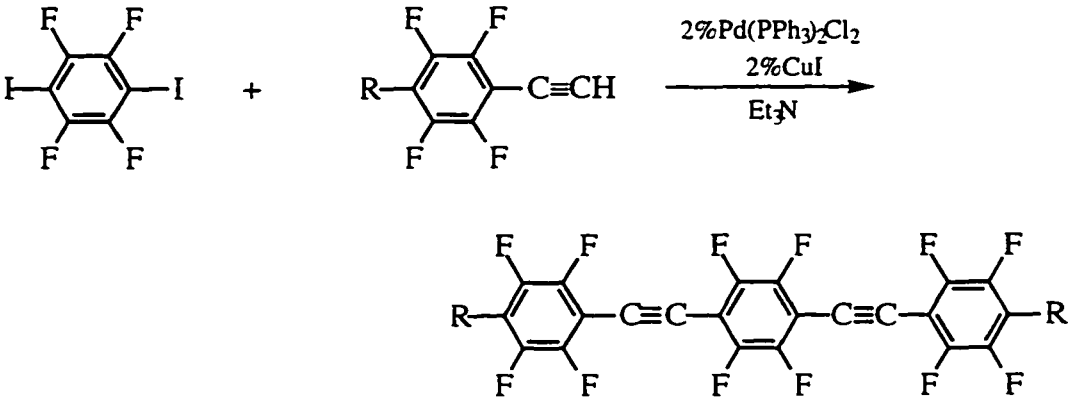


9 **10 a**



11 **10 c**

Scheme 3.4 Synthesis of perfluorinated 1,4-Bis(*p*-R-phenylethynyl)benzenes **12a**, **12c**.



12a R = F; **12c** R = OMe

3.2.2 UV/Vis and Fluorescence Studies

The above fluorinated BPEBs have strong absorptions in the near UV (316-354 nm) region, and are also highly fluorescent in the near UV-visible (342-487 nm) region. Their absorption and emission spectroscopic data are summarized in Table **3.1**. In the **8a-f** series compounds, both electron-donating (**8b-d**) and electron-accepting (**8e**) substituents affect the absorption as well as emission bathochromically, while terminal CF_3 groups, as in **8f**, have little effect on the absorption. Methoxy substitution on the phenyl rings leads to a similar effect on the absorption in the fluoroarene systems, whereas ring fluorination itself seems to result in a small blue shift of the absorption bands (compare the three series of compounds **8**, **10**, and **12**).

Table 3.1 Absorption and emission data for fluorinated BPEBs.[a]

R	Absorption	Emission
	λ/nm (log ε)	λ/nm (λex[b]/nm)
	R-C_6H_4-C≡C-C_6F_4-C≡C-C_6H_4-R	
H (**8a**)	322 (4.79), 340 (4.62)	350, 370 (322)
Me (**8b**)	328 (4.78), 346 (4.66)	369, 386 (328)
MeO (**8c**)	340 (4.70), 358 (4.63)	410, 423 (340)
MeS (**8d**)	284 (4.28), 354 (4.87)	487 (284)
CN (**8e**)	330 (4.88), 352 (4.70)	366, 395 (330)
CF_3 (**8f**)	320 (4.82), 340 (4.64)	350, 368 (320)
	R-C_6F_4-C≡C-C_6H_4-C≡C-C_6F_4-R	
F (**10a**)	316 (4.76), 336 (4.61)	342, 370 (316)
MeO (**10c**)	322 (4.79), 342 (4.59)	361, 384 (322)
	R-C_6F_4-C≡C-C_6F_4-C≡C-C_6F_4-R	
F (**12a**)	318 (4.81), 338 (4.66)	344, 370 (318)
MeO (**12c**)	328 (4.74), 346 (4.62)	415, 435 (328)

[a] Absorption and emission spectra were recorded in acetonitrile;

[b] λex, excitation wavelength.

3.2.3 Single Crystal Structure Study

The molecular structures of all the above compounds have been determined by single crystal X-ray diffraction, as have those of the non-fluorinated BPEB compounds **1a-f** which were prepared previously in our laboratory by P. Nguyen.[18] These linear molecules are prone to crystallize as flat plates or long needles. Some structures were determined at Waterloo by Dr. N. J. Taylor, but most of them were solved in Prof. W. Clegg's research group at the University of Newcastle-Upon-Tyne, England. With the newly developed CCD area detector, particularly with the use of ultra-high intensity synchrotron X-ray radiation, they were able to determine structures from very small single crystals, e.g. 0.24 x 0.15 x 0.05 mm (**1f**) or less with high precision. It is not our intention in this thesis to present a detailed analysis of all of the structures in this series of compounds, instead, some crystallographic data are listed in Table **3.2** and only one example is given in detail.

Compound **8e** ($NC\text{-}C_6H_4\text{-}C{\equiv}C\text{-}C_6F_4\text{-}C{\equiv}C\text{-}C_6H_4\text{-}CN$) (Figure **3.1**) crystallizes in the monoclinic space group, $P2_1/c$ with a = 14.638, b = 5.0625, c = 11.679 Å, and β = 95.158°. The molecule is essentially planar, the angles between the mean planes of the outer and inner phenyl rings averaging 8.9°. The C≡C triple bonds are 1.068(7) Å, which are shorter than those of the non-fluorinated analog **1e** (1.1742(19) Å), whilst both C(ar)-C(sp) lengths are slightly longer than the corresponding lengths in **1e** (1.477(8), 1.512(8) Å compared with 1.4386(18), 1.4368(18) Å). The molecular packing in **8e** occurs along the short b-axis (Figure **3.2**). The molecules are found to pack in a flattened, herringbone fashion, the main C····C interactions being between parallel translated molecules. The overlap diagram is shown in Figure **3.3**. The molecules adopt an offset parallel packing configuration. Very similar packing arrangements can be seen in other structures of this series of compounds (**8**, $R\text{-}C_6H_4\text{-}C{\equiv}C\text{-}C_6F_4\text{-}C{\equiv}C\text{-}C_6H_4\text{-}R$).

Table 3.2 Crystallographic data for BPEBs

R	Space Group	Axial Ratio	Packing Coefficient
	R-C_6H_4-C≡C-C_6H_4-C≡C-C_6H_4-R		
H (**1a**)	P-1	4.52	0.680
Me (**1b**)	$P2_1/c$		
MeO(**1c**)[a,b]	Pbca		
MeS (**1d**)	P-1	5.63	0.696
CN (**1e**)	$P2_1/c$		
CF_3 (**1f**)	$P2_1/c$		
	R-C_6H_4-C≡C-C_6F_4-C≡C-C_6H_4-R		
H (**8a**)	$P2_1/c$	3.91	0.705
Me (**8b**)[b]	$P2_1/c$		
MeO (**8c**)[b]	$P2_1/n$	4.36	
MeS (**8d**)	P-1	4.84	0.710
CN (**8e**)	$P2_1/c$	4.62	0.737
CF_3 (**8f**)	$P2_1/c$		0.728
	R-C_6F_4-C≡C-C_6H_4-C≡C-C_6F_4-R		
F (**10a**)	$P2_1/c$	4.07	0.737
MeO(**10c**)	P-1	4.82	0.716
	R-C_6F_4-C≡C-C_6F_4-C≡C-C_6F_4-R		
F (**12a**)	C2/m	4.07	0.745
MeO (**12c**)	C2/c	4.87	0.743

[a] Work done by P. Nguyen; [b] Structure determined by Dr. N. J. Taylor at Waterloo.

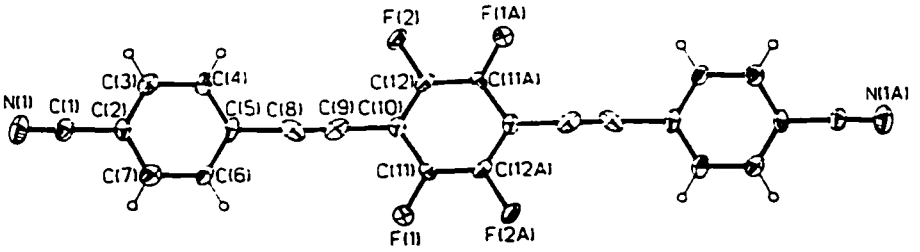


Figure 3.1 Molecular structure of **8e**, with 50% probability ellipsoids

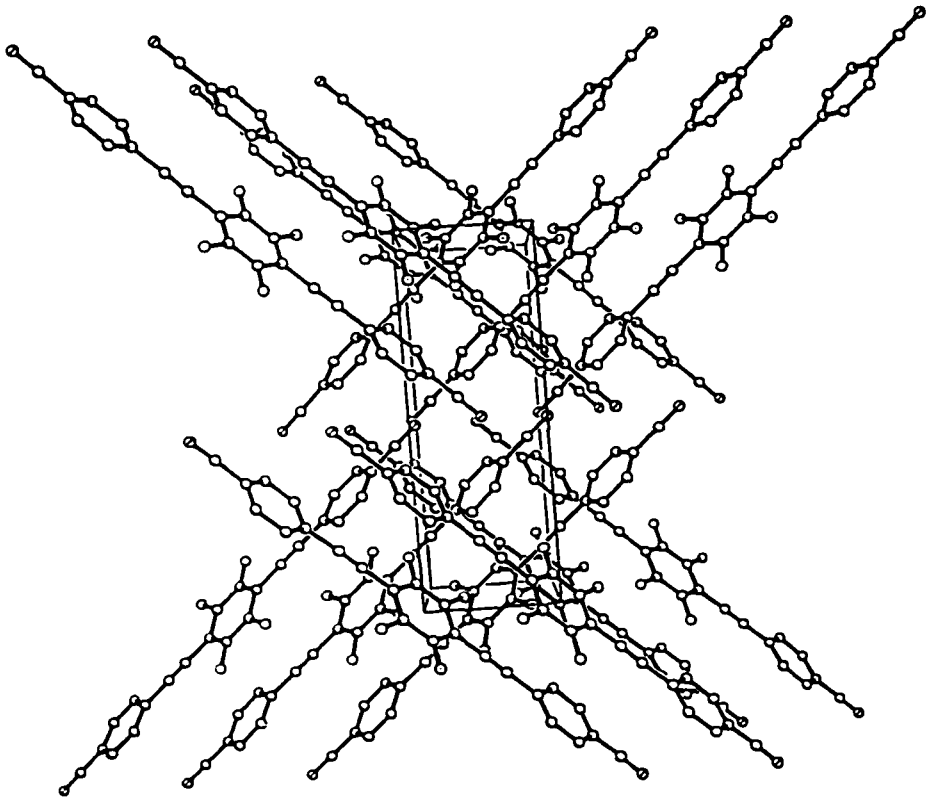


Figure 3.2 Packing diagram for **8e**

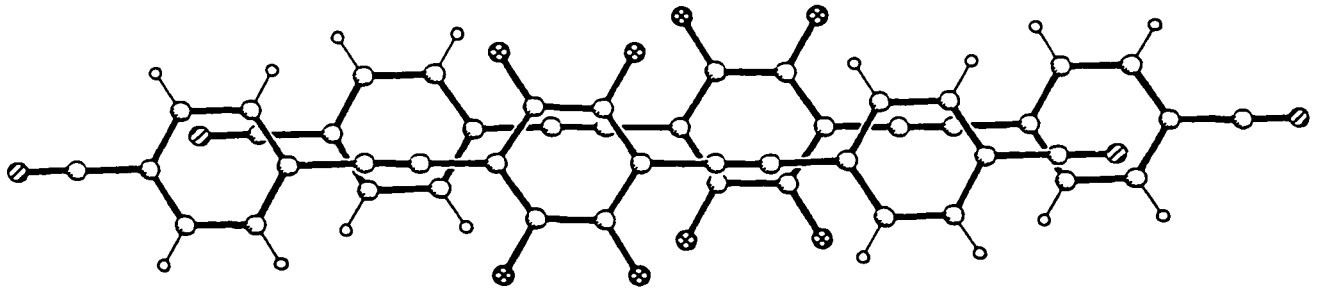


Figure 3.3 Overlap diagram for **8e**

3.2.4 Single Crystal Study on Parent BPEBs

In this section, we will take a closer look at the crystal structures of the four parent unsubstituted compounds (**1a**, **8a**, **10a** and **12a**) of the above series of BPEBs. During our investigations, we also found that when equimolar amounts of **8a** and **10a** were dissolved in $CHCl_3$, a 1:1 co-crystal of **8a•10a** was formed which was also characterized by X-ray diffraction. However, 1:1 co-crystals of **1a•12a** were apparently not obtained when the same procedure was applied to **1a** and **12a**. GC-MS analysis indicated that the first recrystallization of an equimolar mixture of **1a** and **12a** from $CHCl_3$ gave rise to a mixture of the two in a ratio of *ca.* 1:3. Subsequent recrystallization of this solid from $CHCl_3$ resulted in only pure **12a**. While preliminary X-ray powder diffraction studies on the 1:1 mixture of **1a** and **12a** did show some new patterns in addition to those of the pure components, further investigation of this binary system is obviously necessary. Herein, we report a molecular packing analysis on the parent BPEB (**1a**) and its partially (**8a**, **10a**) and fully (**12a**) fluorinated analogs. In addition, the structures of the 1:1 co-crystal of tolan/decafluorotolan (**13•14**) and of the partially fluorinated tolan (**15**, C_6H_5-C≡C-C_6F_5) will also be included for the purpose of completion. We believed that the alternation of perfluorophenyl and phenyl units in the molecules should change the way in which they pack in the crystalline phase. Thus, by carrying out a detailed molecular packing analysis, we can examine the influence of fluorination on the arene-arene interactions, with particular interest in the interactions between phenyl and perfluorophenyl units.

3.2.4.1 Phenyl-perfluorophenyl Interactions

Non-covalent interactions between aromatic units are currently of great interest because they play a significant role in determining the structures and properties of molecular assemblies in biology, chemistry and material science.[19] They are important

for the tertiary structures of proteins, [20] for the vertical base pair stacking which stabilizes the double helical structure of DNA,[21] and for a variety of biological activities such as the intercalation of small molecules between nucleotides, and enzyme recognition of substrates and inhibitors etc.[22] Recently, π–stacking interaction between base pairs has been proposed for the still controversial electronic conductivity of the DNA double helix.[23] In a variety of chemical phenomena, the arene-arene interaction has long been realized to play a key role in the aggregation of porphyrins and other macrocycles in solution.[24] In the past ten years or so, arene-arene interactions have been widely employed in supramolecular chemistry,[25] and to some extent to facilitate chiral recognition in organic synthesis and catalysis.[26] The π–stacking was rationalized to be a control element for the steric selectivity of certain Ziegler-Nata metallocene polymerization catalysts.[27] Furthermore, numerous examples can be found in the solid state where arene-arene interaction is of great importance to the packing of organic molecules in crystals and to crystal engineering for the design of functional materials.[28] The stability and phase behavior of many liquid crystals have also been reported to originate from these arene-arene interactions.[29]

The nature of this arene-arene interaction is now realized to be based essentially on dispersion forces and electrostatic interactions; other concepts such as "charge transfer" or "electron donor acceptor interaction" are of much less importance.[19] One unique example of the arene-arene interactions involves those between arene and perfluoroarene units. In 1960, Patrick and Prosser discovered that when benzene was mixed with hexafluorobenzene (HFB) in equimolar quantities, a solid 1:1 molecular complex of the two components was formed.[30] The melting points of the two pure components are similar, being 5.5°C for benzene and 4°C for HFB, while the 1:1 mixture has a melting point of 24°C. This binary system has been the subject of extensive research both experimentally[31] and theoretically[32] for the past 38 years. The crystal structure of the molecular complex revealed that in the crystalline phase, benzene and

hexafluorobenzene are packed in a face-to-face manner alternately forming infinite columns.[33] This differs remarkably from the packing of its two pure constituents wherein the aromatic rings are oriented perpendicular to one another.[34] Despite the absence of any charge-transfer bands in the spectra, and the low electron affinity of hexafluorobenzene, the striking features of this binary complex still led early researchers to interpret it as one kind of "charge transfer" complex,[30] which was indeed a widespread theory on stacked, planar organic molecules in the 1960's.[35] As the discussion of arene-arene interactions progressed, the basis of this benzene-hexafluorobenzene type of interaction has gradually been rationalized to be predominantly electrostatic in nature. One simple model that has been utilized widely in the past 24 years,[32a-d] and has been invoked by Williams recently,[32e] is based on the interaction between electric quadrupole moments. Thus, benzene has a large and negative quadrupole moment of -29.0 x 10^{-40} Cm^2, while that of hexafluorobenzene is also large but with a positive sign, 31.7 x 10^{-40} Cm^2, owing to the strong electronegativity of the fluorine atoms. It is easy to comprehend that benzene and hexafluorobenzene are prone to stack in a face-to-face manner which represents the lowest energy assembly of two dissimilar quadrupolar molecules.[32e] However, this description may not be entirely correct. As already pointed out by Williams[32e,f] and others[19e,36] there is a fundamental obstacle to describing the electric potential as a multipole expansion when the molecular separation is comparable to or smaller than the dimensions of the molecules in discussion, as in the case of $C_6H_6 \cdot C_6F_6$. Dougherty[37] recently pointed out the same argument in the description of cation-arene interactions.

It is apparent that the most commonly used packing diagrams in the crystallographic literature always display a projection along one of the crystallographic axes rather than one normal to the plane of the molecules. This may well distort one's view of the true nature of the intermolecular packing and thus be misleading (see Figure **3.4a** and **3.4b**) as the crystallographic axis is often inclined with respect to the plane of

the arene. It seems to us that it would be more appropriate to use the latter view or both views side-by-side.

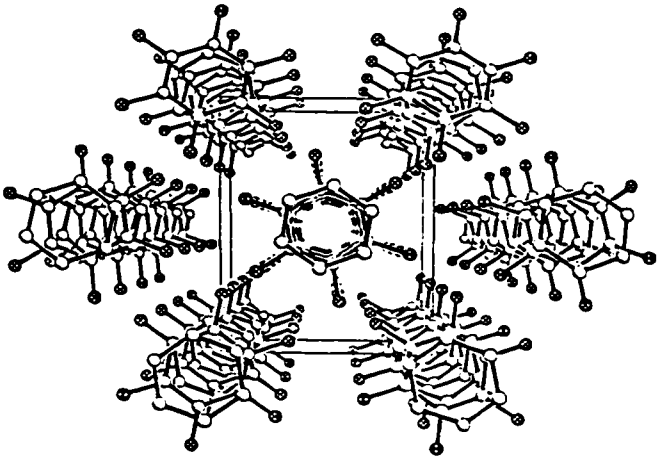
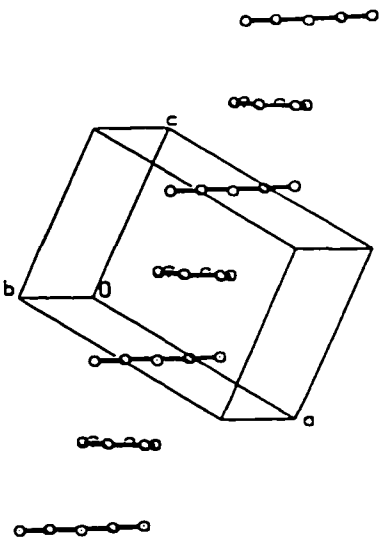


Figure 3.4a Williams' packing plot of the $C_6H_6 \cdot C_6F_6$ complex viewed down the c-axis.



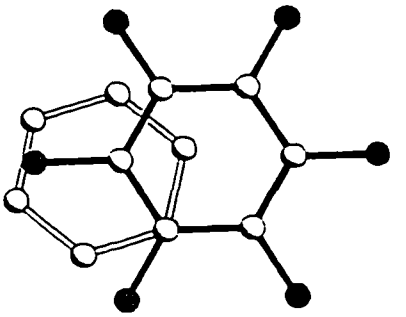


Figure 3.4b Another view of $C_6H_6 \cdot C_6F_6$ (left) and overlap diagram (right).

Perhaps the most profound method of interpreting arene-perfluoroarene interaction relies on atom-atom potential calculations, and entropic contributions may also be taken into account. The corresponding structure would be the balance of various attractive and repulsive forces, neither of which should be overestimated or ignored. With electrostatic interactions alone, the arene-perfluoroarene system can be visualized as comprising C, H and F atoms with appropriate charges. Hunter and coworkers[38] have conducted an energy calculation on a $[M(OC_6H_5)(OC_6F_5)]$ system by using a variety of empirical charge models, and their results are quite promising.

Although a more sophisticated description of the nature of the arene-perfluoroarene interaction still requires further investigation, the remarkable ability of hexafluorobenzene to form molecular complexes with almost all simple aromatic hydrocarbon compounds[31a] implies that systems containing perfluoroaromatic units have potential utility in supramolecular chemistry. It is therefore surprising to note that examples of this application were very limited until the last few years[39]. One example was reported by Fujita[39b,c] in that specific recognition of the electron-rich aromatic guest molecules is observed by host macrocycles containing the $-C_6F_4-$ unit. No such specificity is found by the non-fluorinated cavity. Very recently, Grubbs and coworkers[40] reported an elegant example in which diphenylbutadiyne and decafluorodiphenylbutadiyne adopt a face-to-face stacking configuration in the crystalline phase, enabling the topochemical polymerization of the 1,3-diyne in this co-crystal to occur in a unique *cis* fashion. Again, the stacking is not in an idealized ring centroid over ring centroid fashion (and the separation is somewhat wider due to this offset) so that the polymerization conversion reached only 50% after 24 hours of UV radiation, resulting in various *cis*-specific oligomers. Nonetheless, the experiment demonstrated the utility of the perfluoroarene/arene interaction in controlling crystal architecture.

As the molecular packing in crystals depends on various intermolecular interactions, X-ray crystallography has always been an important method for the study of those forces. In the recent years, there is a growing demand for systematic analysis of the packing patterns of groups of related molecules, in order to draw general conclusions on some intermolecular interactions which may not be easy to reach from individual analyses.[36] In the context of arene-perfluoroarene interactions, systematic crystallographic studies on 1:1 molecular complexes containing hexafluorobenzene have been conducted by Dahl[41] and others[33] in the past 27 years. Besides the above mentioned diphenylbutadiyne/decafluorodiphenylbutadiyne co-crystal,[40] other structures such as 1:1 molecular complexes of decafluorobiphenyl / biphenyls,[42] octafluoronaphthalene / naphthalene,[43] and decafluorobiphenyl / naphthalene[44] have also been determined, so has that of *trans*-decafluoroazobenzene/*trans*-stilbene.[45] In all cases, both component molecules are stacked alternatively face-to-face to varying extents to form infinite columns. A similar pattern can be seen in the structures of partially fluorinated molecules such as 2,3,4,5,6-pentafluorodiphenylbutadiyne,[40] 2,3,4,5,6-pentafluorobiphenyl[46] and N-pentafluorophenyl-4-methylphenyl aldimine[47] where the molecules packed in a head-to-tail parallel fashion exhibiting the unique arene-perfluoroarene interaction.

3.2.4.2 Molecular Structures of Parent BPEBs

The crystallographic data on the unsubstituted BPEB and its fluorinated analogs and tolans along with the co-crystals are summarized in Table **3.3**. The parent BPEB compound (**1a**, C_6H_5-C≡C-C_6H_4-C≡C-C_6H_5), crystallizes in the triclinic space group $P\bar{1}$, with Z = 2. The structure consists of two non-equivalent BPEB molecules (Figure 3.5), each with a crystallographically imposed center of symmetry. The molecules are essentially planar, the angles between the mean planes of the outer and center phenyl

Table 3.3. Crystal data, structure solution and refinement for parent BPEBs and tolans.

	1a	8a	10a	12a	8a•10a	13•14	15
Formula	$C_{22}H_{14}$	$C_{22}H_{10}F_4$	$C_{22}H_4F_{10}$	$C_{22}F_{14}$	$C_{44}H_{14}F_{14}$	$C_{28}H_{10}F_{10}$	$C_{14}H_5F_5$
MW	278.33	350.30	458.25	530.22	808.55	536.36	268.18
Crystal system	Triclinic	Monoclinic	Monoclinic	Monoclinic	Triclinic	Triclinic	Triclinic
Space group	$P\bar{1}$	$P2_1/n$	$P2_1/c$	C2/m	$P\bar{1}$	$P\bar{1}$	$P\bar{1}$
a(Å)	6.0202(10)	8.595(2)	15.1000(14)	8.956(4)	6.0931(7)	6.0939(13)	6.1305(10)
b (Å)	9.662(2)	4.9721(14)	4.9040(5)	7.671(4)	7.5393(9)	7.5286(15)	7.2444(12)
c (Å)	13.692(2)	18.837(5)	11.7091(11)	13.260(6)	19.114(2)	12.491(3)	12.764(2)
α (deg)	90.719(4)	90	90	90	96.044(3)	85.554(6)	85.229(4)
β (deg)	94.732(4)	95.329(7)	99.580(2)	98.959(12)	99.102(3)	86.478(6)	84.793(4)
γ (deg)	103.859(4)	90	90	90	96.538(3)	84.095(6)	85.766(4)
V ($Å^3$)	770.2(2)	801.5(4)	854.97(14)	899.8(7)	854.54(17)	567.5(2)	560.88(16)
Z	2	2	2	2	1	1	2
d_{calc} (g cm^{-3})	1.200	1.451	1.780	1.957	1.571	1.569	1.588

Crystal size (mm)	0.78 x 0.28 x 0.18	0.46 x 0.20 x 0.06	0.62 x 0.24 x 0.04	0.70 x 0.52 x 0.04	0.62 x 0.18 x 0.02	0.40 x 0.40 x 0.06	0.40 x 0.16 x 0.02
Crystal color	Colorless	Colorless	Pale Yellow	Colorless	Colorless	Colorless	Colorless
Temperature (K)	160(2)	160(2)	160(2)	286(2)	160(2)	160(2)	160(2)
μ (mm^{-1})	0.068	0.116	0.180	0.216	0.145	0.149	0.150
F (000)	292	356	452	516	404	268	268
Reflections for cell refinement	1921 (θ range 2.59 to 25.80°)	2182 (θ range 2.17 to 26.30°)	3637 (θ range 2.40 to 28.29°)	1031 (θ range 1.56 to 26.28°)	2327 (θ range 2.17 to 27.88°)	2140 (θ range 2.72 to 28.01°)	1891 (θ range 2.83 to 28.19°)
θ range	1.49 to 25.82°	2.17 to 26.38°	0.37 to 28.33°	1.55 to 25.00°	1.09 to 25.00°	2.73 to 28.01°	2.83 to 28.25°
Index ranges	$-7 \le h \le 7$,	$-6 \le h \le 10$,	$-16 \le h \le 19$,	$-10 \le h \le 11$,	$-7 \le h \le 4$,	$-7 \le h \le 6$,	$-7 \le h \le 7$,
	$-11 \le k \le 11$,	$-6 \le k \le 6$,	$-6 \le k \le 6$,	$-8 \le k \le 9$,	$-9 \le k \le 9$,	$-9 \le k \le 5$,	$-9 \le k \le 7$,
	$-16 \le l \le 8$	$-23 \le l \le 18$	$-15 \le l \le 12$	$-16 \le l \le 16$	$-24 \le l \le 25$	$-15 \le l \le 15$	$-16 \le l \le 15$
Refl measd	3417	4023	5033	2035	4426	3470	3479
Independent refl	2498(R_{int}= 0.0381)	1582(R_{int}= 0.0987)	1984(R_{int}= 0.0506)	851(R_{int}= 0.0753)	2918(R_{int}= 0.0449)	2403(R_{int}= 0.0323)	2409(R_{int}= 0.0273)
Refl with $I>2\sigma(I)$	1975	1274	1726	655	2217	1486	1527
Weighting parameters a, b	0.0566, 0.1524	0.0384, 0.9074	0.0338, 0.9306	0.1104, 1.2132	0.0340, 1.5407	0.1017, 0.000	0.0890, 0.000
No. of parameters	200	119	146	92	263	172	173

GOF on F^2	1.132	1.222	1.203	1.113	1.239	0.947	1.059
Final R indices [I>2σ(I)]	R1 = 0.0415	R1 = 0.0712	R1 = 0.0489	R1 = 0.0690	R1 = 0.0685	R1 = 0.0675	R1 = 0.0623
	wR2 = 0.1173	wR2 = 0.1533	wR2 = 0.1206	wR2 = 0.1836	wR2 = 0.1442	wR2 = 0.1640	wR2 = 0.1584
R indices (all data)[a]	R1 = 0.0540	R1 = 0.0920	R1 = 0.0578	R1 = 0.0844	R1 = 0.0931	R1 = 0.0961	R1 = 0.0971
	wR2 = 0.1344	wR2 = 0.1683	wR2 = 0.1278	wR2 = 0.2040	wR2 = 0.1661	wR2 = 0.1782	wR2 = 0.1767
Extinction coeff.	0.032(5)	0.018(6)	0.008(3)	0.002(2)	0.0034(11)		0.005(10)
Largest shift/esd	0.000	0.000	0.000	0.000	0.000	0.000	0.000
Largest diff. peak and hole (e Å^{-3})	0.169, -0.137	0.265, -0.212	0.333, -0.224	0.440, -0.482	0.295, -0.302	0.442, -0.479	0.344, -0.433

[a] $R = \Sigma(|F_o|-|F_c|)/\Sigma(|F_o|)$, $wR = \{\Sigma[w(F_o^2-F_c^2)^2]/\Sigma[w(F_o^2)^2]\}^{1/2}$, $GOF = S = \{\Sigma[w(F_o^2-F_c^2)^2]/(n-p)\}^{1/2}$ for n reflections and p parameters in the refinement.

rings averaging 3.1°. The C-C triple bond lengths average 1.203 (2)Å. The C(ar)-C(sp) lengths are almost identical, ranging from 1.428 (2) to 1.432(2) Å.

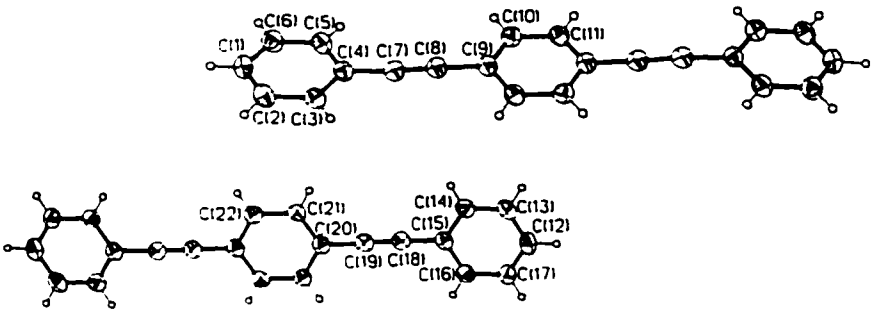


Figure 3.5 Molecular structure of **1a**, with 50% probability ellipsoids

The fully fluorinated BPEB (**12a**, C_6F_5-C≡C-C_6F_4-C≡C-C_6F_5, Figure **3.6**) crystallizes in the monoclinic space group, C2/m. Like **1a**, the molecules are even closer to planarity (interplanar angle, 1.1°), but smaller endocyclic angles (mean 117.2(4)°) are observed at C(4) and C(7) due to the fluorine substituents on the phenyl rings. The C-C triple bond length is similar to those in **1a** (1.194(7) vs 1.203(2) Å). The two C(ar)-C(sp) bond lengths are identical and also similar to those in **1a** (1.426(2) Å compared with 1.431(2) Å). The phenyl rings are sufficiently separated from each other by the C-C triple bond linkage and the fluorine atoms are small enough, so that there are no steric interactions between the fully fluorinated phenyl rings.

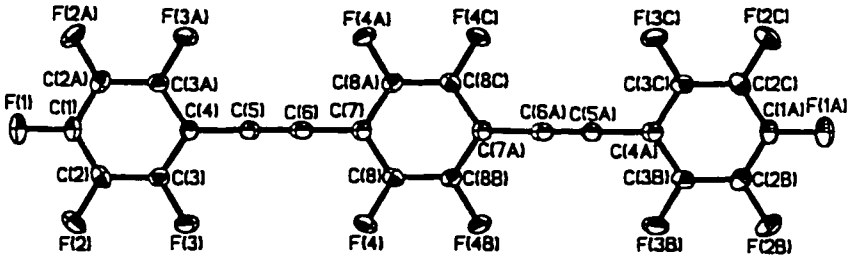


Figure 3.6 Molecular structure of **12a**, with 50% probability ellipsoids

The two partially fluorinated BPEB's (**8a**, C_6H_5-C≡C-C_6F_4-C≡C-C_6H_5; **10a**, C_6F_5-C≡C-C_6H_4-C≡C-C_6F_5) both crystallize in monoclinic space groups, $P2_1/n$ and $P2_1/c$ respectively (Figure **3.7** and **3.8**). In comparison to the previous non-fluorinated (**1a**) or fully fluorinated (**12a**) structures, these two molecules deviate significantly from planarity in the solid state, the angles between the mean planes of the outer and inner rings being 16.7 and 9.7° for **8a** and **10a** respectively. The C-C triple bond lengths in these two molecules are essentially identical (1.199(4) for **8a** and 1.198(3) for **10a**) and are not significantly different from those of **1a** and **12a**. It is significant that the two C(ar)-C(sp) lengths, C(4)-C(7) and C(8)-C(9) for both **8a** and **10a** are quite different: the C(ar)-C(sp) bond adjacent to the fluorinated phenyl ring (**8a**: 1.424(4); **10a**: 1.424(3) Å) is notably shorter than the equivalent bond adjacent to the non-fluorinated ring (**8a**: 1.440(4); **10a**: 1.438(3) Å). The 1:1 co-crystal between **8a** and **10a** crystallizes in the triclinic space group $P\bar{1}$, with Z = 1 (Figure **3.9**). The component molecules in **8a•10a** are both much closer to planarity in the co-crystal than is observed for individual **8a** and **10a**. The angles between the mean planes of the outer and inner phenyl rings are 3.9 and 3.0° for the centrally fluorinated and terminally fluorinated molecules respectively. No other significant differences in the bond lengths and angles are observed. The interplanar angles, C-C triple bond length, and C(ar)-C(sp) bond lengths for the parent BPEBs and tolans are summarized in Table **3.4**.

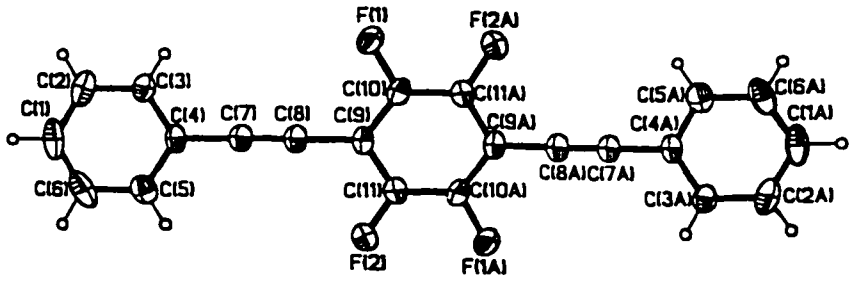


Figure 3.7 Molecular structure of **8a**, with 50% probability ellipsoids

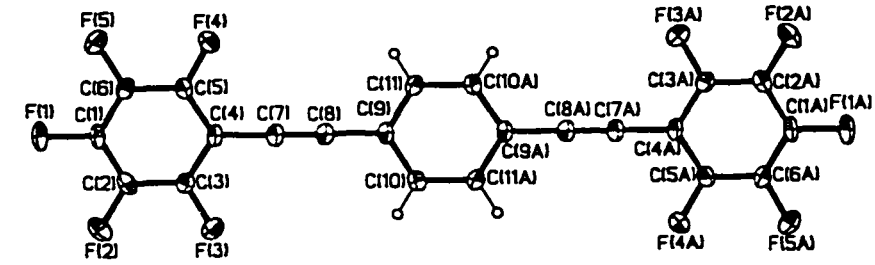


Figure 3.8 Molecular structure of **10a**, with 50% probability ellipsoids

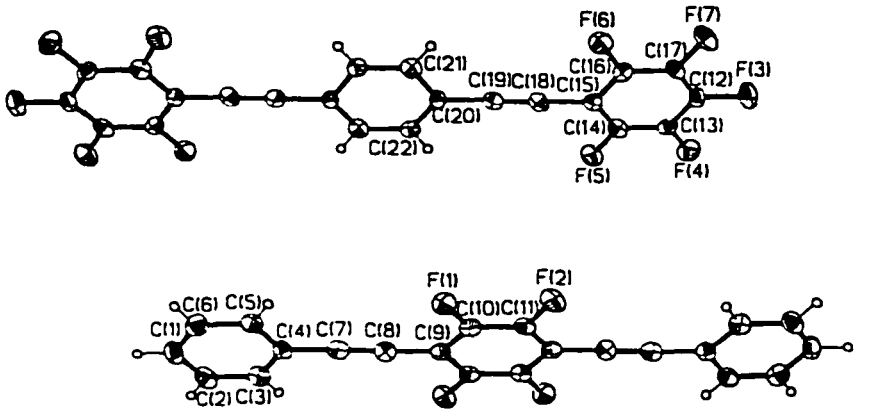


Figure 3.9 Molecular structure of **8a•10a**, with 50% probability ellipsoids

The planarity of tolan (**13**) and related molecules is a subject of considerable interest. Steric interactions between phenyl rings are negligible, so the conformation for an isolated molecule is expected to be dominated by electronic factors. The torsion angle between the two mean planes would be mainly determined by the rotation of the C(ar)-C(sp) single bonds, which may depend on the conjugation of the phenyl rings with C-C triple bond. A planar geometry (D_{2h} symmetry) may result from overlapping pπ-orbitals of both phenyl rings with the same pπ-orbital of the C(sp)-C(sp) triple bond fragment. On the other hand, the overlapping of the phenyl π-system with different pπ-orbitals of the C(sp)-C(sp) triple bond would lead to a perpendicular molecular configuration (D_{2d} symmetry). While theoretical calculations[48, 49] predicted a slightly favorable perpendicular form, experimental studies[49, 50] on tolan revealed a planar

geometry. Nevertheless, both sides indicated that these two forms are quite similar in energy and that the extent of π-π overlapping and thus the barrier to rotate is small. The Pauling bond number of the C(ar)-C(sp) single bond in tolan was estimated to be 1.18, that is, 18% double bond character in the ground state.[48] Experimentally, the activation energy for torsion rotation is found to be less than 0.60 kcal/mol.[50] However, several crystallographic studies[48, 51, 52] on tolan demonstrated that the molecules are planar in the crystalline state. Its perfluorinated analog **14** also adopts a nearly planar configuration (interplanar angle, 2.2°).[53] The planarity seems to be maintained in the elongated parent BPEB (**1a**) and its fully fluorinated analog (**12a**) as shown here. While the two partially fluorinated BPEB compounds **8a** and **10a** each deviate significantly from planarity in their own crystals (16.7 and 9.7°), both molecules exhibit remarkably more planar configurations in the co-crystal of **8a•10a** (3.9 and 3.0°). From the above analysis, we can conclude that the interplanar angle in tolan or BPEB compounds in the crystalline state is mainly the result of crystal packing forces. Different intermolecular packing patterns may result in very different molecular configurations. A Cambridge Structural Database search done in 1988 by Desiraju and Krishna[54] indicated that unsymmetrically substituted tolans are likely to adopt non-planar configurations in the solid state. However, we found an interplanar angle of only 4.8° in the partially fluorinated tolan **15**. We have also recently determined the crystal structures of four unsymmetrically substituted tolan compounds (D-C_6H_4-C≡C-C_6H_4-A, D = MeO, MeS; A = NO_2, CN). These molecules are also found to be essentially planar in the solid-state (interplanar angles ranging from 3.6 to 8.5°), and, moreover, polymorphs were found for MeO-C_6H_4-C≡C-C_6H_4-NO_2. The ease of C(ar)-C(sp) single bond rotation may be partially responsible for the phenomenon of polymorphism in tolan derivatives.

Table 3.4 Interplanar angle, C-C triple bond length, C(ar)-C(sp) bond lengths for parent BPEBs and tolans.

	Interplanar Angle (°)	C≡C (Å)	C(ar)-C(sp) (Å)
C_6H_5-C≡C-C_6H_4-C≡C-C_6H_5 (**1a**)	3.1	1.203(2)	1.428(2), 1.432(2)
C_6F_5-C≡C-C_6F_4-C≡C-C_6F_5 (**12a**)	1.1	1.194(7)	1.426(2)
C_6H_5-C≡C-C_6F_4-C≡C-C_6H_5 (**8a**)	16.7	1.199(4)	1.424(4), 1.440(4)
C_6F_5-C≡C-C_6H_4-C≡C-C_6F_5 (**10a**)	9.7	1.198(3)	1.424(3), 1.438(3)
C_6H_5-C≡C-C_6F_4-C≡C-C_6H_5 C_6F_5-C≡C-C_6H_4-C≡C-C_6F_5	3.9 3.0	1.208(5) 1.196(5)	1.413(5), 1.428(5) 1.421(5), 1.434(5)
C_6H_5-C≡C-C_6H_5 (**13**)[a]		1.198(4)	1.438(4)
C_6F_5-C≡C-C_6F_5 (**14**)[b]	2.2	1.198(5)	1.422(6), 1.415(6)
C_6H_5-C≡C-C_6H_5 C_6F_5-C≡C-C_6F_5		1.189(5) 1.190(5)	1.439(4) 1.431(3)
C_6H_5-C≡C-C_6F_5 (**15**)	4.8	1.191(4)	1.433(4), 1.425(4)

[a] Mavridis, A.; Moustakali-Mavridis I. *Acta Cryst.*, **1977**, *B33*, 3612.

[b] Goodhand, N.; Hamor, T. A. *Acta Cryst.* **1979**, *B35*, 704.

3.2.4.3 Molecular Packings of Parent BPEBs

In the non-fluorinated BPEB compound, C_6H_5-C≡C-C_6H_4-C≡C-C_6H_5 (**1a**), the molecules pack in an approximate T-shaped arrangement (Figure **3.10**, **3.11**), which resembles the packing pattern in tolan (**13**).[48,51]

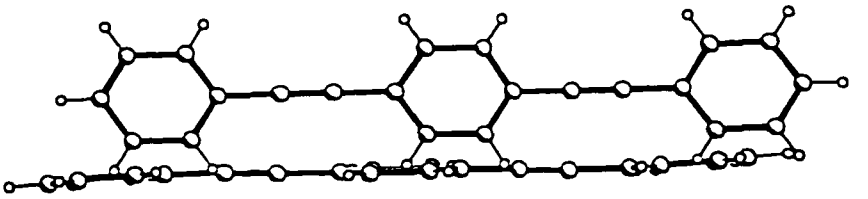


Figure 3.10 Overlap diagram of **1a**.

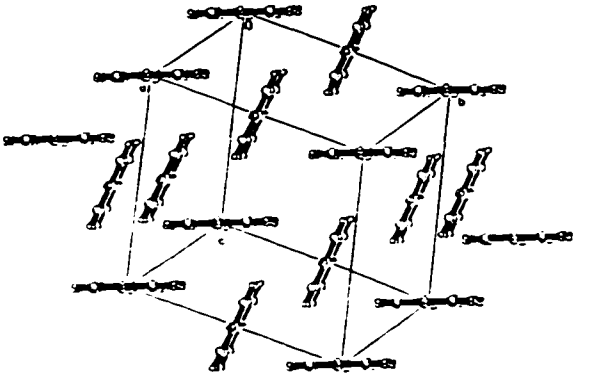


Figure 3.11 Packing plot for **1a**.

The packing coefficient, K, which was introduced by Kitaigorodskii,[55] is now often used as a parameter to describe the efficiency of molecular packing in the crystalline state. A value of 0.740 for K is estimated to be that of a close-packed arrangement of hard spheres. In crystals of **1a**, K has been calculated to be 0.680.

The fully fluorinated BPEB, C_6F_5-C≡C-C_6F_4-C≡C-C_6F_5 (**12a**), on the other hand, is extremely close packed in the crystalline state, K = 0.745. The molecules align parallel to each other, but avoid direct ring over ring or ring over triple bond configurations (Figure **3.12**). Intermolecular F····F contact distances of 2.912 to 2.969 Å are observed (Figure **3.13**). In comparison, the sum of the van der Waal's radii for this possible interaction is about 2.94 Å. Some intermolecular F····F distances fall well within their van der Waal's contact. Perfluorotolan, C_6F_5-C≡C-C_6F_5 (**14**), exhibits both face-face and face-edge intermolecular packing patterns (Figure **3.14**).

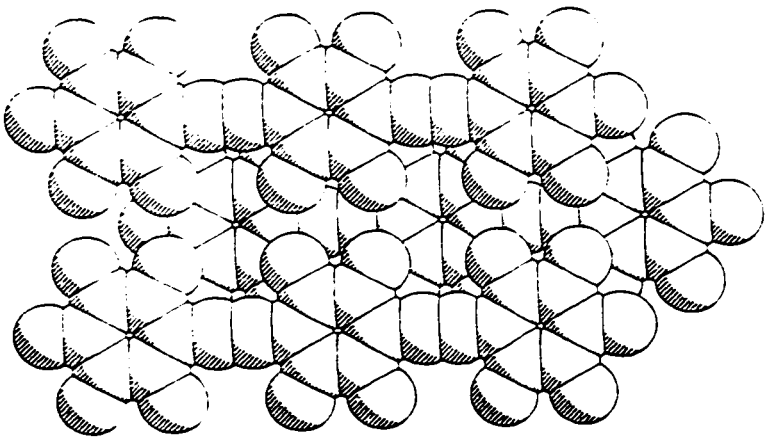


Figure 3.12 Space filling overlap diagram of **12a**.

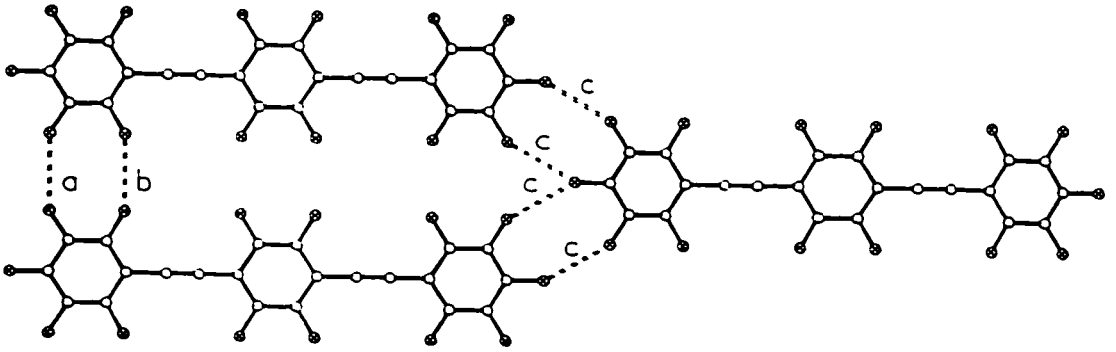


Figure 3.13 Short intermolecular contact distances of **12a**, a = 2.969, b = 2.959, c = 2.912

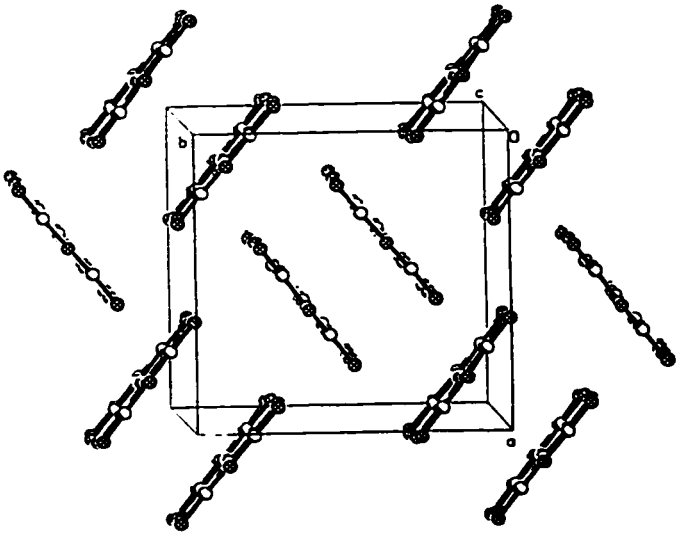


Figure 3.14 Packing diagram of **14**.

The two partially fluorinated BPEB compounds, C_6H_5-C≡C-C_6F_4-C≡C-C_6H_5 (**8a**) and C_6F_5-C≡C-C_6H_4-C≡C-C_6F_5 (**10a**) exhibit a similar packing pattern with each other in the crystalline state (Figure **3.15**, **3.16**). The molecules are found to sit ring on triple bond with short interstack distances between the inner ring center to the triple bond center being 3.737 and 3.498 Å, respectively (Figure **3.17**, **3.18**). Simply from these interstack distance values, we may conclude that the more heavily fluorinated molecule **10a** is obviously more closely packed than the tetrafluorinated BPEB **8a**. Indeed, their crystalline packing coefficients are 0.737 and 0.705, respectively.

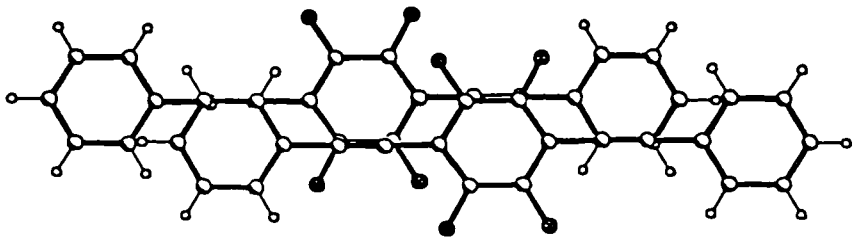


Figure 3.15 Overlap diagram of **8a**.

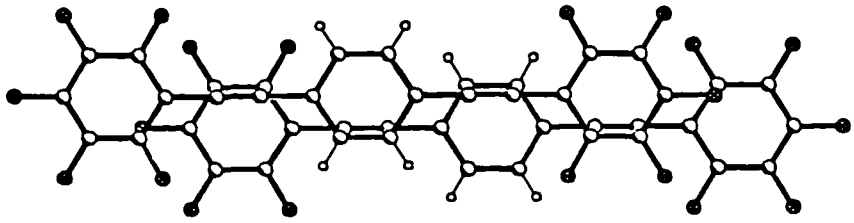


Figure 3.16 Overlap diagram of **10a**.

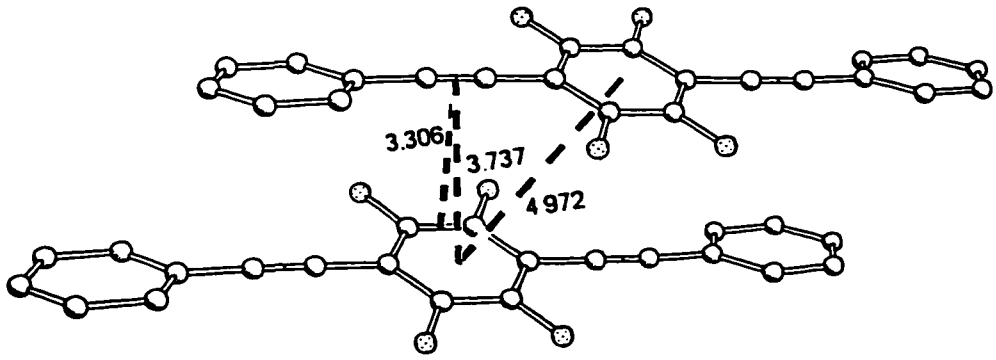


Figure 3.17 Short interstack distances of **8a**.

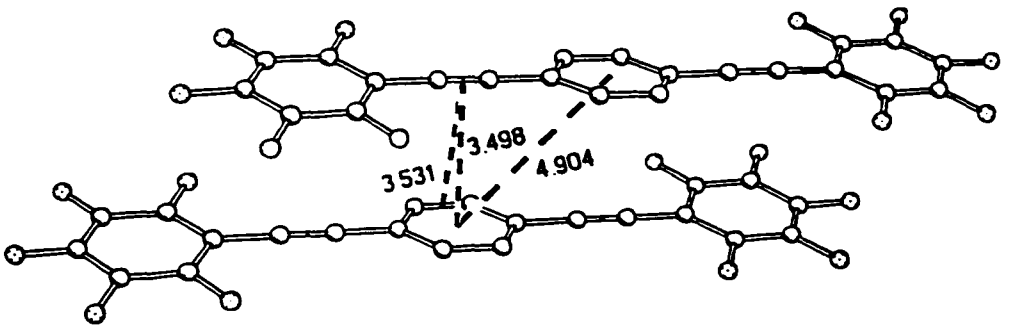


Figure 3.18 Short interstack distances of **10a**.

According to a Cambridge Structural Database search, Moore et al.[19s] recently concluded that the intermolecular interactions of neither arene-acetylene nor acetylene-acetylene is of significance to the crystal packing of conjugated phenylacetylene containing organic compounds. However, in the crystal structures of **8a** and **10a**, the acetylene units seem to sit offset right over phenyl or perfluorophenyl rings. It may need cautious consideration on whether this arrangement is the result of the seemingly favorable arene-acetylene interactions or it is the offset phenyl-perfluorophenyl packing mode between parallel molecules that drives the acetylene linkage to be occasionally over the rings. However, these two molecules with alternate phenyl and perfluorophenyl units obviously pack in a very different way to those of non-fluorinated (**1a**) or perfluorinated (**12a**) BPEBs. The interaction between phenyl and perfluorophenyl units must have played an important role in the determination of their crystal packings. Perhaps, the significance of phenyl-perfluorophenyl interaction can be viewed more directly from the structure of one of the substituted tetrafluorinated BPEBs, MeO-C_6H_4-C≡C-C_6F_4-C≡C-C_6H_4-OMe (**8c**), where alternative phenyls sit right over the perfluorophenyl group of next parallel molecule (Figure **3.19**).

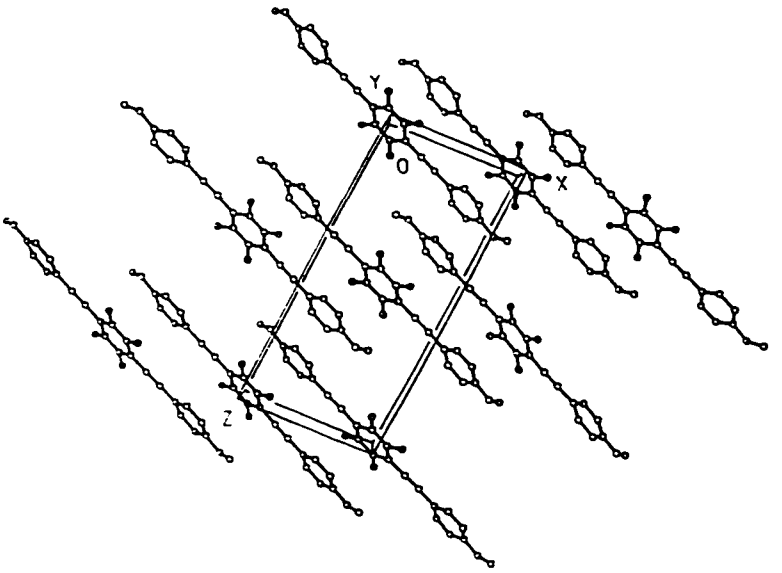


Figure 3.19 Packing diagram of **8c**.

Both **8a** and **10a** are packed in a flattened-out, herringbone fashion (Figure **3.20**, **3.21**), the main C····C interactions are between parallel translated molecules. According to Gavezzotti and Desiraju's classification,[28a,b] these structures would probably be described as having a γ-type packing mode.

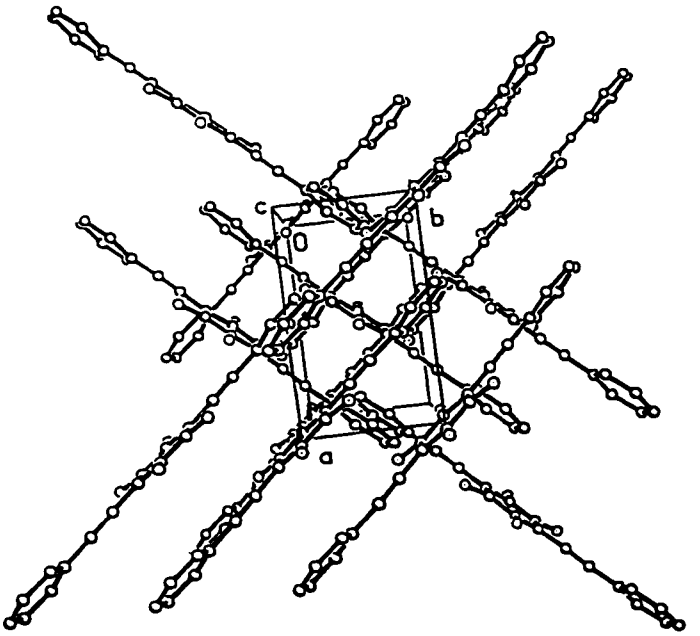


Figure 3.20 Packing diagram of **8a**.

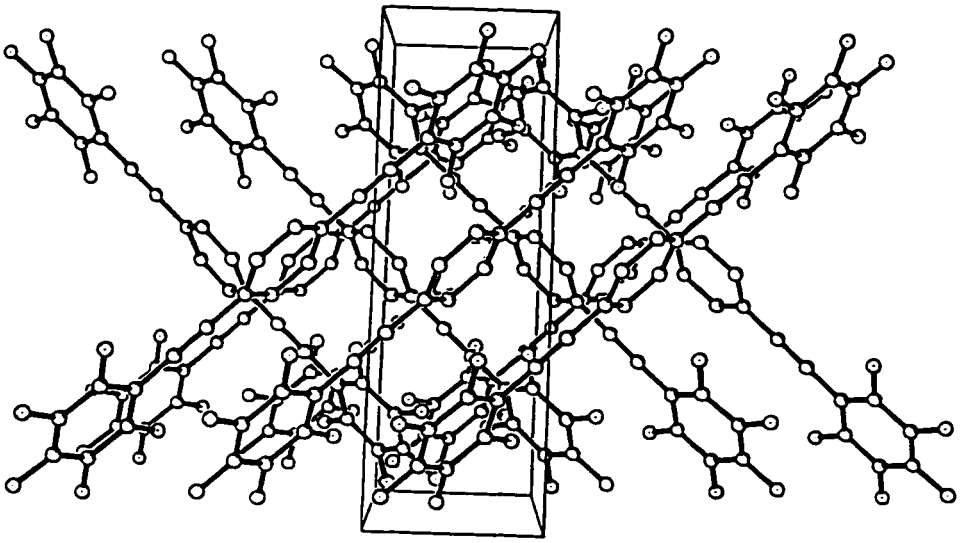


Figure 3.21 Packing diagram of **10a**.

The structure of the co-crystal of **8a** and **10a** is comprised of alternating layers of molecules in a columnar arrangement. The molecules are oriented such that the phenyl and perfluorophenyl rings sit approximately above each other (Figure **3.22**).

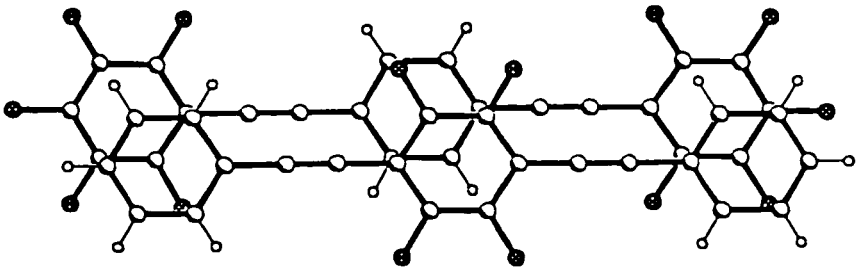


Figure 3.22 Overlap diagram of **8a•10a**.

The mean distance between the centers of the phenyl and perfluorophenyl rings within the stack is 3.770 Å. The interplanar distance averages 3.398 Å. The rings are not completely eclipsed, a slight lateral offset being observed (Figure **3.23**), which is very similar to that of the co-crystal of C_6H_6•C_6F_6.

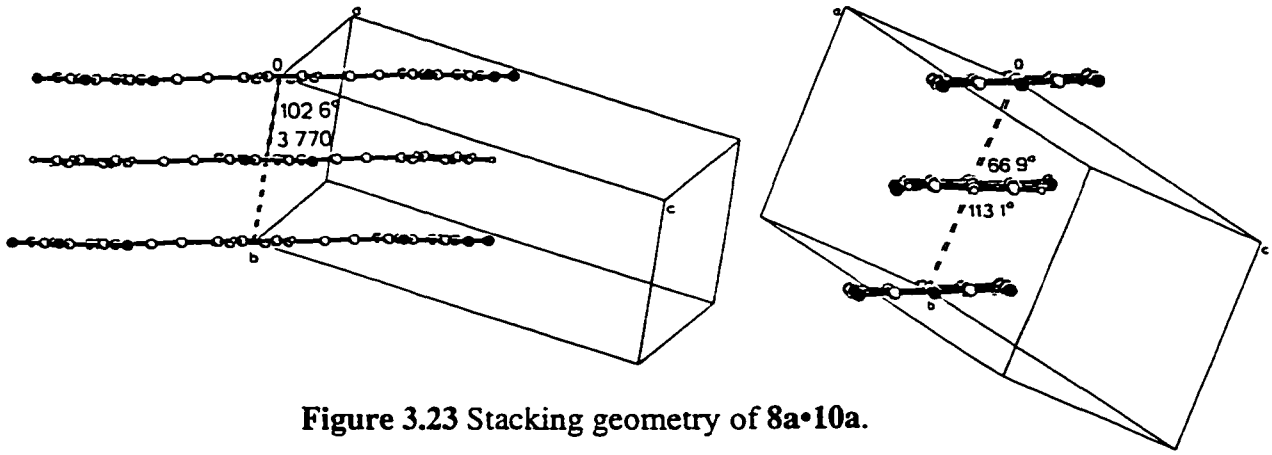


Figure 3.23 Stacking geometry of **8a•10a**.

The packing coefficient for **8a•10a** is only 0.700, which is less than either on the values for its two components in their homo structures (0.705 for **8a** and 0.737 for **10a**, respectively). Accordingly, the estimated crystal density for **8a•10a** (1.571) is well below the mean value of the crystals of **8a** and **10a** themselves (1.451 for **8a**, 1.780 for **10a**, averaging 1.615). The crystal structures of **8a** and **10a** may be viewed as comprising of two sets of parallel molecular stacks which interpenetrate each other in different angles to form a herringbone-type structure. In their co-crystals, on the other hand, molecule **8a**, C_6H_5-C≡C-C_6F_4-C≡C-C_6H_5 and molecule **10a**, C_6F_5-C≡C-C_6H_4-C≡C-C_6F_5 match up with each other perfectly in terms of direct parallel phenyl-perfluorophenyl interaction, so that all the comprising molecules are packed parallel to form stacks along only one direction, that is, the crystallographic b-axis. As in the structure of C_6H_6•C_6F_6, only slight interpenetration of the C-H and C-F bonds of molecules in neighboring columns can be found in the crystals of **8a•10a**. The molecular stacks in this arrangement are obviously less closely packed than in the previous interpenetrating herringbone fashions as seen in the structures of **8a** and **10a**. The significant impact of this packing to the thermal stability of this molecular complex will be discussed later in the context of liquid crystalline phase behaviors.

Intermolecular CH···F close contacts in **8a•10a** crystals are found to be within 2.598 to 2.715 Å (Figure **3.24**). The sum of the van der Waal's radii for H and F is 2.67

Å. It is thus possible to envision that these interactions may involve weak hydrogen bonding as the means to stabilize the columnar packing in the crystal structure. The same argument has been invoked before by Williams[32e] in the analysis of the structure of C_6H_6•C_6F_6. Recently, both Howard[56] and Dunitz[57] concluded independently from CSD searches and MO calculations that organic fluorine hardly ever accepts hydrogen bonds. However, more examples[58] are appearing to support the statement[56] which says "encouraging for the bio-organic chemists is that the substrate/protein interactions may offer an environment for optimal F···H bonding". Likewise, we may borrow the same argument here that the unique packing fashion in the crystals of **8a•10a** as well as C_6H_6•C_6F_6 makes the CH···F hydrogen bonding a reality which acts as a stabilizing factor to the crystal lattice.

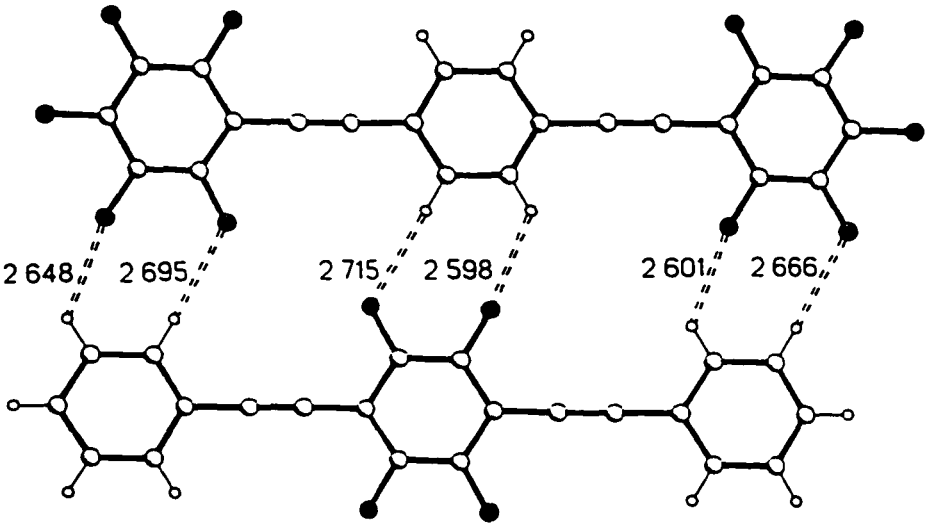


Figure 3.24 Short interstack contact distances of **8a•10a**.

The crystal structure of the molecular complex of tolan and perfluorotolan **13•14** is comprised of alternate layers of tolan and perfluorotolan molecules. No significant differences are observed in the geometries of the molecules in **13•14** compared with those in the crystal structures of the pure **13** or **14** compounds. Much like that of **8a•10a**, a slight offset arrangement is found in the structure of this complex (Figure **3.25**).

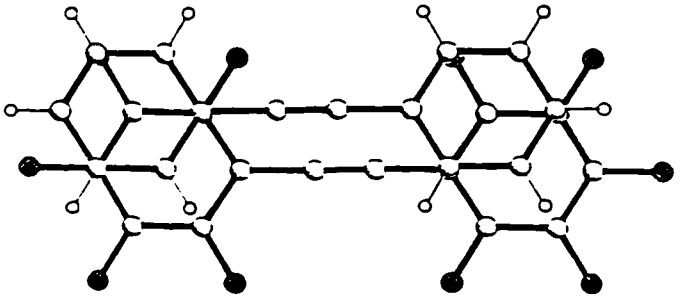


Figure 3.25 Overlap diagram of **13•14**.

The molecular columns are also stacked along the b-axis (Figure **3.26**). The mean distance between the centers of the phenyl and perfluorophenyl rings within the stack is 3.765 Å, the interplanar distance averaging 3.402 Å. The packing coefficient for **13•14** is estimated to be 0.695.

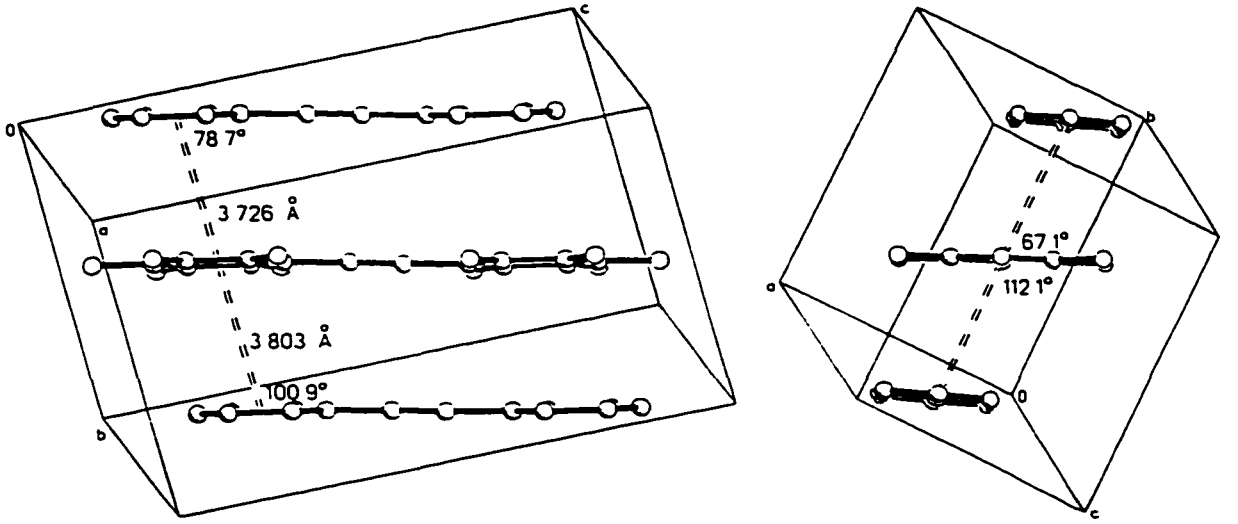


Figure 3.26 Stacking geometry of **13•14**.

Similar short intercolumn interactions as in **8a•10a** show H····F contacts ranging from 2.593 to 2.741 Å (Figure **3.27**).

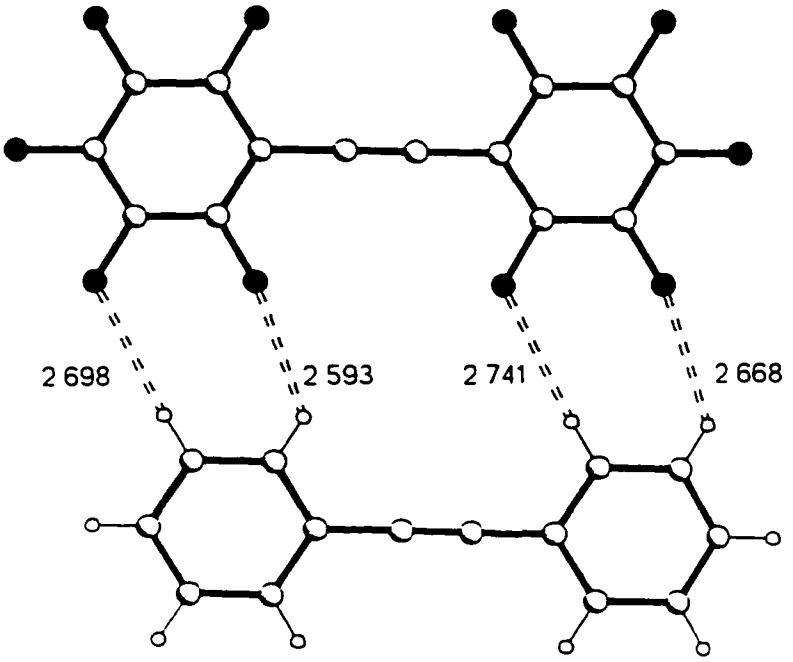


Figure 3.27 Short interstack contact distances of **13•14**.

The crystal structure of partially fluorinated tolan **15**, C_6H_5-C≡C-C_6F_5, is essentially identical with that of **13•14**. The similarities can be seen from their crystal data in Table **3.3** as well as their packing coefficients (0.701 for **15**). Crystals of **15** are composed of columns of molecules in a head to tail arrangement, with the phenyl unit sitting offset over the perfluorophenyl unit of the next parallel molecule (Figure **3.28**). The same arrangement has been previously found in the crystal structures of partially fluorinated diphenylbutadiyne[40] and pentafluorobiphenyl[46].

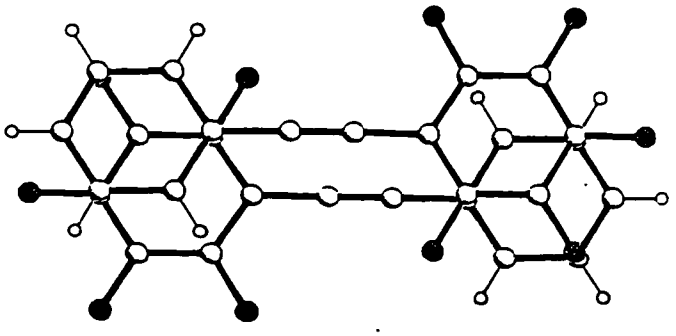


Figure 3.28 Overlap diagram of **15**.

Again, the molecular columns are stacked along the b-axis (Figure **3.29**). The mean distance between the centers of the phenyl and perfluorophenyl rings within the stack is 3.693 Å. The interlayer spacing is 3.462. Possible weak hydrogen bonding is observed with interstack CH···F distances of 2.545 Å (Figure **3.30**).

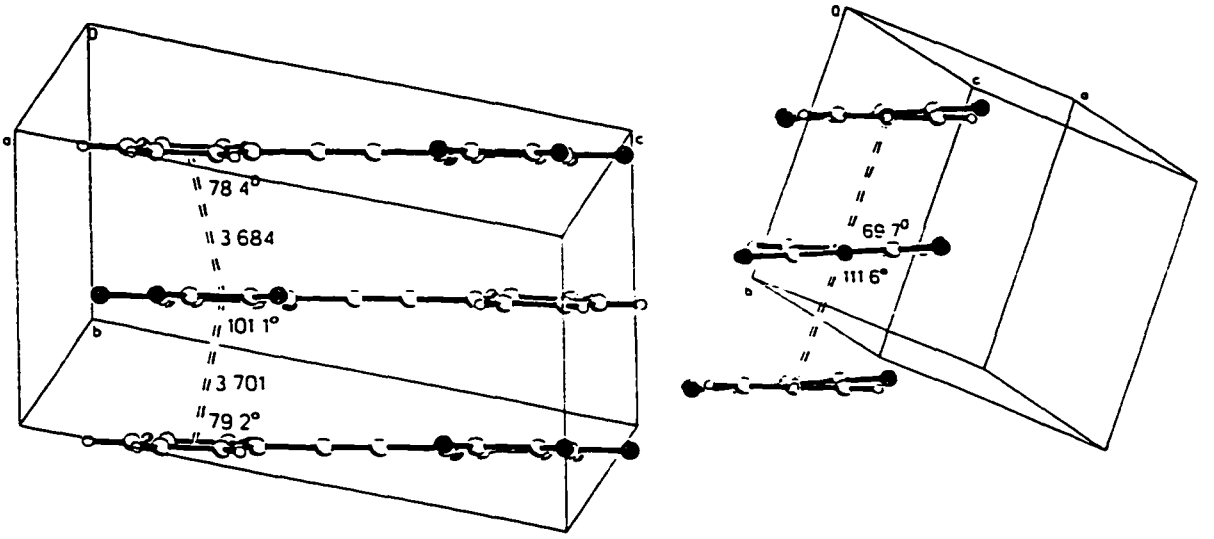


Figure 3.29 Stacking geometry of **15**.

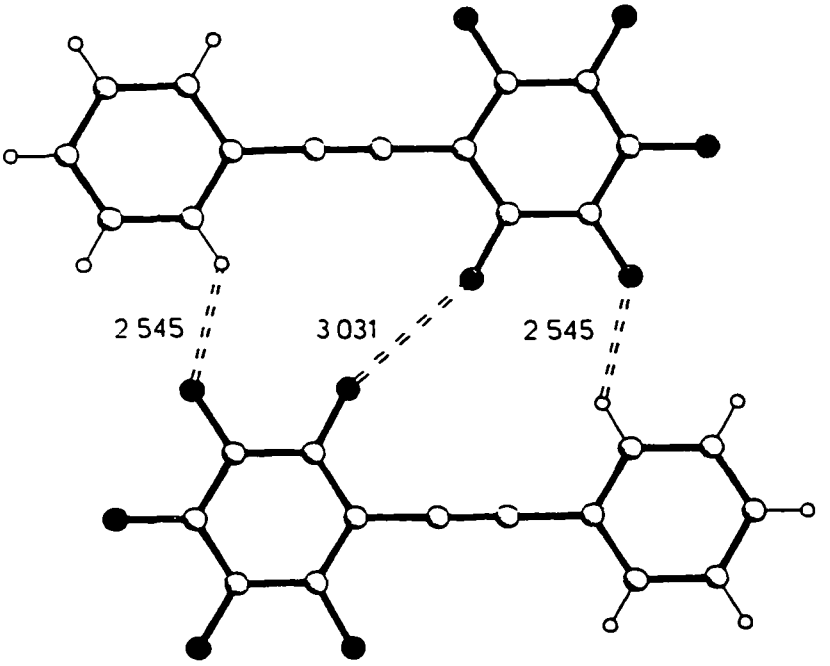


Figure 3.30 Short interstack contact distances in **15**.

To summarize, in the above seven crystal structures, we can at least conclude at present that the interactions between phenyl and perfluorophenyl units are an important driving force influencing the packing of these molecules in the crystalline phase. In the crystals containing an equal number of phenyl and perfluorophenyl groups (in the case of **8a•10a**, **13•14** and **15**), columnar packing arrangements have exclusively been observed with alternating phenyl and perfluorophenyl units one over the other. The interaction of the parent BPEB **1a** with the perfluorinated BPEB **12a** is still open to question at this stage as we have not yet obtained suitable single crystals for X-ray diffraction. However, our preliminary studies have indicated that a crystal of BPEB grown from C_6F_6 is comprised of one BPEB molecule associated with three C_6F_6 molecules. As expected, the C_6F_6 molecules are associated with the phenyl rings of the BPEB; with an offset geometry, the inter-ring distances are approximately 3.6 Å (Figure **3.31**). Due to the steric repulsions between C_6F_6 molecules, the BPEB molecule in this structure does not have the planar geometry found in **1a**; the angle between the outer and inner rings is approximately 60°. Further analysis is restricted by the very poor quality of this structure. However, this gives another good example of how the crystal packing can affect the interplanar angle in the tolan derivatives. The two partially fluorinated BPEB molecules **8a** and **10a** each bear unequal numbers of phenyl and perfluorophenyl groups, with phenyl or perfluorophenyl ring over acetylene being the pattern displayed in their crystal structures resulting in a flattened herringbone arrangement. With the cooperation of another polarizable substituent such as MeO in **8c** (Figure **3.19**), the alternate phenyl over perfluorophenyl packing mode is obtained in the crystal structure. The phenyl-perfluorophenyl interaction is certainly more favorable than the interactions between the homogeneous components. We cannot, however, from the current work, make a judgment on whether the parallel perfluorophenyl-perfluorophenyl interaction is stronger or weaker than that between phenyl and phenyl units, although notable differences are observed between the packing coefficients of BPEB and perfluorinated BPEB (0.680 *vs.*

0.745) as well as between tetrafluorinated and decafluorinated BPEBs (0.705 *vs.* 0.737). As we can see, the packing coefficient cannot be used alone to compare one particular type of intermolecular force in different crystals as there are many kinds of forces involved in the stabilization of a crystal lattice, particularly when different packing modes are observed in the crystals under comparison.

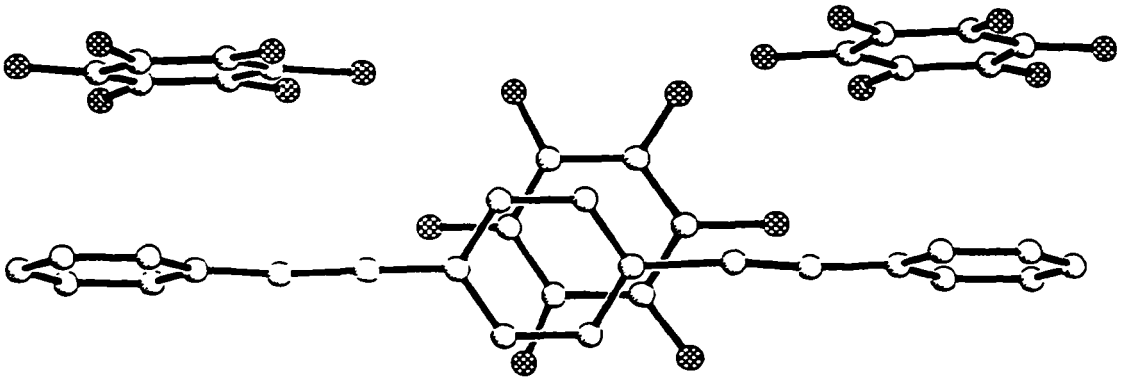


Figure 3.31 Arrangement of molecules in BPEB•3C_6F_6 complex (preliminary results).

3.2.5 Liquid Crystal Study

Liquid crystals are very important materials in modern society, yet they were virtually unknown before the 1960's. Today, they are all around us. They are used in the displays of calculators, lap-top computers, and pocket television sets; they are an important component of high-strength fibers; and they occur naturally in cell membranes of biological systems. Their greatest impact has been in display technology, where liquid crystal displays (LCD) are second only to the cathode ray tube in a multi-billion-dollar market. Their greatest potential is expected in emerging flat-panel television displays, optical computers, and integrated devices for communications. Multidisciplinary research is currently aiming to improve view angle, response time, and brightness of LCDs.[59]

3.2.5.1 Liquid Crystal Phases and Liquid Crystal Materials

The liquid crystal state is a distinct phase of matter observed between the crystalline (solid) and isotropic (liquid) states. In the solid state, the molecules occupy certain positions in the crystal lattice and are constrained in certain orientations with respect to each other. Thus, solid phases possess positional as well as orientational order. When a solid melts to a liquid, both types of order are lost completely. However, if it melts into a liquid crystal phase, the positional order may be lost, but some of the orientational order still remains. Figure **3.32** illustrates the order present in the three phases. This represents the first type of liquid crystals, namely *thermotropic liquid crystals,*[60] which are formed from compounds whose molecules are mainly rod-shaped (calamitic) or disc-shaped (discotic), either by heating the crystalline solid or by cooling the isotropic liquid, i.e. by thermal effects. The other type of liquid crystals is called *lyotropic liquid crystals*. They are formed from compounds with amphiphilic properties and solvents (commonly water). Common examples of such lyotropic liquid crystals are those produced from soaps and other detergent systems and water.

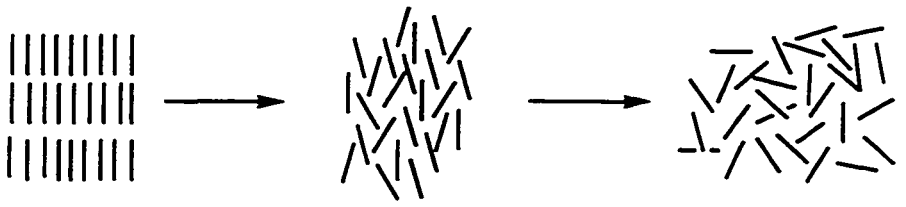


Figure 3.32 Physical description of solid, liquid crystal and isotropic phases.

The majority of thermotropic liquid crystals are composed of rod-like molecules which is the theme of discussion in the current work. The calamitic liquid crystals are generally classified into three groups: nematic, cholesteric (chiral nematic), and smectic phases (Figure **3.33**).

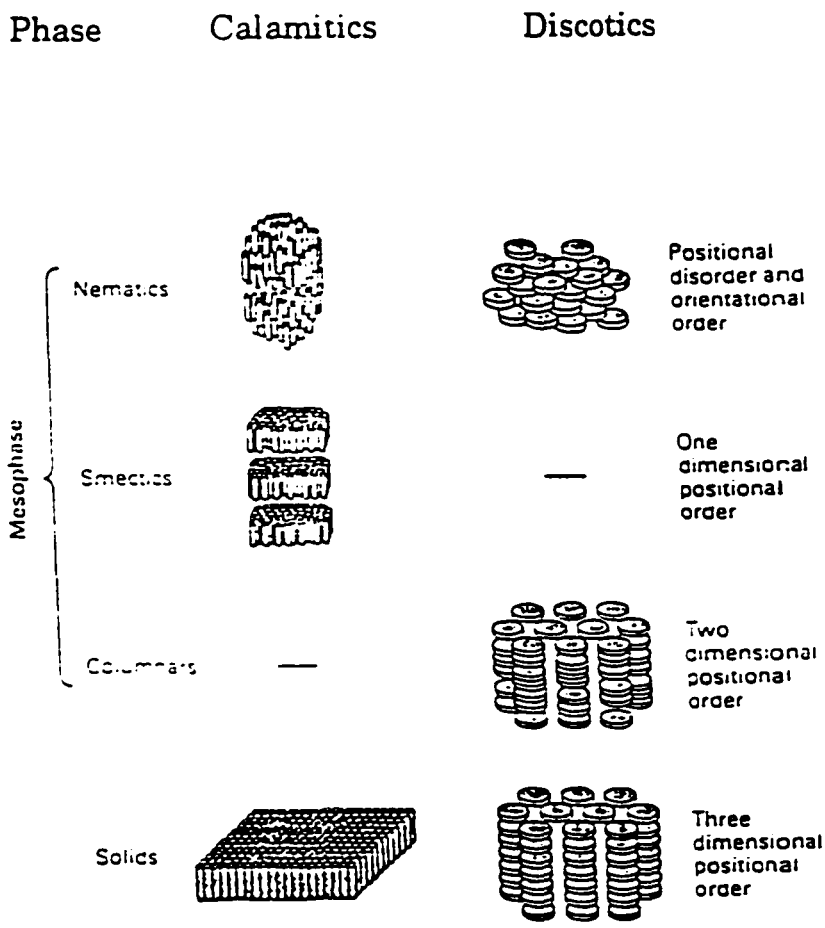


Figure 3.33 Schematic illustration of the various phases of calamitic molecules.

In *nematic* mesophases, there is a quasi-long-range orientational order of the molecules, but there is no long-range positional order. The long axes of the rod-like molecules tend to align along a common axis called the *director*. The *cholesteric* mesophase is also a nematic type liquid crystal which is composed of optically active molecules. This name stems from cholesterol derivatives in which the cholesteric liquid crystal phase was firstly observed. A more proper name for this phase is *chiral nematic* liquid crystal. The difference between nematic and chiral nematic phases lies in the direction of the preferred molecular orientation. The director is fixed in space for a nematic phase, but rotates throughout the sample in a chiral nematic phase. The rotation (or twist) may generate right-handed or left-handed helices depending on the molecular conformation.

In the *smectic* phase, not only is the small amount of orientational order of liquid crystals present, but there is also a small amount of positional order. The molecules tend to point along the director and arrange themselves in layers. There are a variety of possible molecular arrangements which make up the different smectic phases (12 right now) labeled through S_A to S_K (Figure **3.34**). The designation of smectic phases by letters is more historical than physical, in that additional letters have been used each time a new smectic phase is discovered.[60b] However, only the most distinct and representative phases are discussed here. In both smectic A and smectic C phases, the molecules randomly diffuse within each plane. No positional order exists within the plane, so, in a sense, the positional order is in one dimension only. In the smectic A phase, the director is perpendicular to the planes, while in smectic C phase the director makes an angle other than 90° to the planes. The smectic B phase differs from the S_A and S_C phases in that it has an ordered arrangement of the molecules in the layers. The positional order is three dimensional now. Such orderly arrangement tends to make the layers in the S_B phase much more rigid than that of the S_A and S_C phases.

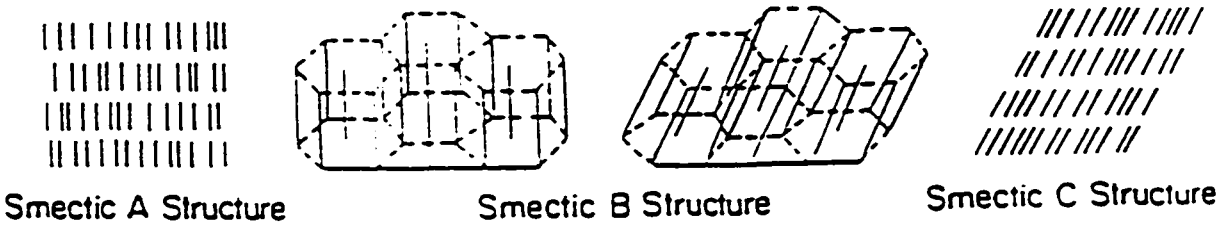
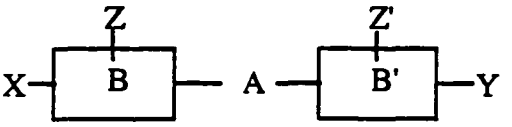


Figure 3.34 Schematic representation of molecular arrangement in some smectic phases.

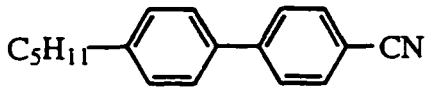
A large number of compounds are known to exhibit one or several types of liquid crystal phases. Since the subject of this chapter is solely on rod-like molecules, only calamitic liquid crystal materials will be discussed in this context. As a matter of fact, currently, only calamitic liquid crystals have found important technological applications. The anisotropic shape and resulting anisotropic forces of a rod-shaped molecule lead to the tendency to form liquid crystal phases. A typical calamitic liquid crystal molecule can be depicted as having the following molecular structure.



X, Y = terminal groups;
A = a linking group between two (or more) ring systems (B, B');
Z, Z' = lateral substituents.

The B, B' ring systems are often represented by phenyls. However, one or both B, B' can also be an alicyclic system, for example cyclohexyl, or a heteracyclic system such as pyridine or dioxane. Alternatively, B, B' can consist of more than one ring, for example phenylcyclohexane or phenyldioxane, etc. Biphenyl derivatives are a very typical type of

mesogens. The compound *p*-n-pentyl-*p'*-cyanobiphenyl (5CB) is the first room temperature liquid crystal compound discovered by Gray in 1970.



Other common linking groups (A) are -CH=CH-, -C≡C-, -CH=N-, N=N-, -CO-O-, and so on. The skeleton of only B-A-B' is often referred as the "core" structure of the liquid crystal molecules. However, by altering the magnitude of the molecules' terminal and lateral substituents, it is possible to vary the liquid crystal properties. Several other representative liquid crystal molecules are listed in Figure **3.35**.

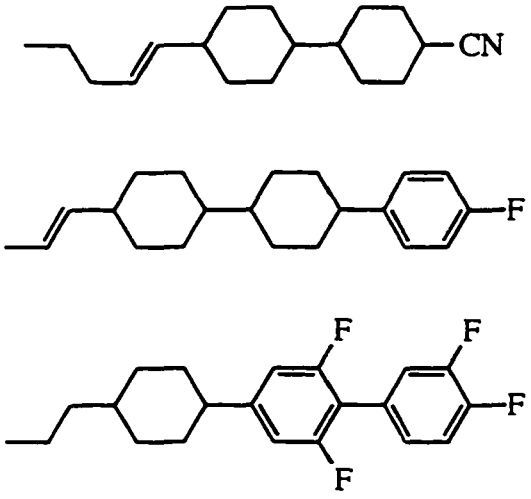


Figure **3.35** Three representative liquid crystal mesogens.

3.2.5.2 Liquid Crystal Properties of BPEBs

In the studies of calamitic liquid crystals, several theoretical analyses[61] have been put forth to predict the critical axial ratio (i.e. length-to-diameter ratio) needed for nematic phase formation. To test the predictions of these analyses, one of our

Table 3.5 Axial ratio and phase transitions of BPEBs

R	Axial Ratio	Phase Transitions (°C)
	R-C_6H_4-C≡C-C_6H_4-C≡C-C_6H_4-R	
H (**1a**)[a]	4.52	K 181.7 I
Me (**1b**)[a]		K 218.8 N (243.6)[b] I
MeO(**1c**)[a]		K 217.6 N ?[c] I
MeS (**1d**)[a]	5.63	K 249.9 N (285.5)[b] I
CN (**1e**)[a]		K 274 N ?[c] I
CF_3 (**1f**)[a]		K 200.0 S_B 222.3 I
	R-C_6H_4-C≡C-C_6F_4-C≡C-C_6H_4-R	
H (**8a**)	3.91	K 182.5 I
Me (**8b**)[b]		K 238.3 N ?[c] I
MeO (**8c**)[b]	4.36	K 184.4 N (~300)[b] I
MeS (**8d**)	4.84	K 173.7 S 197.0 S_B 203.7 N 260.3 I
CN (**8e**)	4.62	K 313.4 N ?[c] I
CF_3 (**8f**)		K 182.6 Rot 189.7 I
	R-C_6F_4-C≡C-C_6H_4-C≡C-C_6F_4-R	
F (**10a**)	4.07	K 196.5 N/I[d]
MeO(**10c**)	4.82	K 198.2 N ?[c] I
	R-C_6F_4-C≡C-C_6F_4-C≡C-C_6F_4-R	
F (**12a**)	4.07	K 226.1 I
MeO (**12b**)	4.87	K 188.2 N 200.7 I

[a] Compound was synthesized by P. Nguyen.

[b] Question mark denotes that no transition can be unambiquiously observed.

[c] Parentheses signify that microscopy reveals slow degradation above $T_{K \rightarrow N}$.
[d] N/I denotes that the nematic phase exists over a very narrow temperature, and is observed only transiently by microscopy.

collaborators, Dr. Viney[13a] started in 1990 to investigate a series of rigid-rod BPEB compounds, and he showed that the critical axial ratio for nematic phase formation in polytolans is close to 4.3 (about that of the parent BPEB, **1a**). It is widely accepted that hard interactions (excluded volume effects) are the principal cause of molecular ordering into a nematic phase. In such cases, rod axial ratio is a critical parameter. However, it is also expected that regardless of the shape anisotropy the charge distribution anisotropy in the molecule can also largely affect the liquid crystal properties. This aspect is often termed as soft interactions. Since 1994, we have been collaborating with Viney and others to synthesize and examine a series of substituted BPEB compounds. We are studying not only their liquid crystalline properties but also their molecular packings in the crystalline state as discussed in the previous section. The axial ratio and the phase transition data on some of the BPEB compounds are listed in Table **3.5**. The axial ratios are obtained from the crystal structure results. To identify possible transitions involving a liquid crystalline phase, the mesogenic phases were characterized by differential scanning calorimetry (DSC) and transmitted polarized light microscopy.

3.2.5.2.1 Unsubstituted BPEBs

The non-fluorinated BPEB, **1a**, was taken initially as the model compound with a core structure which has an approximately uniform charge distribution along the length of the molecule. It has an estimated axial ratio of 4.52 from its crystal structure. No mesophase is observed on heating the sample through crystalline phase to isotropic liquid (m.p. 181.7°C), however, when cooling the liquid slowly, a monotropic nematic mesophase is found at 164.3°C and a small nematic range of 5°C, I 164.3 N 159.5 K is observed. The undercooling helps the nucleation process to crystallinity, and hence the

mesophase is observed. This observation is consistent with the theoretical calculation[13a] that an axial ratio of 4.3 is barely sufficient to stabilize liquid crystallinity at ambient pressure.

The fully fluorinated BPEB, **12a**, with an axial ratio of 4.07, showed no liquid crystallinity either on heating or cooling processes. This can be understood in that it has too small an axial ratio. Perhaps consistent with its close packing in the crystals, it has a much higher melting point of 226.1°C.

The tetrafluorinated BPEB, **8a**, has an even lower molecular axial ratio (3.91). No mesophase is observed, and it melts to an isotropic liquid at essentially the same temperature as the model compound **1a** (182.5 *vs.* 181.7°C). However, surprisingly, the decafluorinated BPEB, **10a**, which has the same small axial ratio of 4.07 as that of **12a**, does show a transient nematic phase at 196.5°C. This observation reflects well our previous statement that even though this molecule lacks the necessary shape anisotropy (not elongated enough), the strong and anisotropic intermolecular "soft" interactions ensure the formation of a liquid crystalline phase.

As expected, the co-crystal **8a•10a** shows distinctively different thermal properties from its two component compounds **8a** and **10a** in their pure forms. Unlike the co-crystal of C_6H_6•C_6F_6 which exhibits a much higher melting point than either of its components,[30] this 1:1 molecular complex transits from its crystalline state at a higher temperature (189.3°C) than that of **8a** (182.5°C) but lower than that of **10a** (196.5°C). Most interesting of all, however, it does preserve a characteristic nematic liquid crystal phase in a range of about 10°C, K 189.3 N 199.0 I. This observation is interesting for at least two reasons. First, it has been reported that intermolecular arene-arene interactions help to form or stabilize the mesophases in liquid crystals,[29] and there are numerous examples of hydrogen-bonded liquid crystals which derive from two or more non-mesogenic components.[62] The current result is, however, to our knowledge, the first

example in which liquid crystallinity is promoted by co-crystallizing two compounds with dominant intermolecular arene-arene interactions, specifically, phenyl-perfluorophenyl interactions. The two components, on their own, show no or only transient tendency to form a liquid crystalline phase when heated. Second, it is well known[63] that mixing two mesogenic species can lead to a reduction in melting point and so expand the temperature range of liquid crystallinity exhibited by either constituent; often a simple eutectic phase diagram is obtained. However, in **8a•10a**, it is not only just the melting point that is lowered - *the clearing point of this binary mixture is also raised* above the temperature needed to render the respective constituents isotropic. This suggests that the phenyl-perfluorophenyl interaction between the molecules is not only important to the structure in the crystalline phase but also possibly significant in the liquid crystalline phase as well.

3.2.5.2.2 Substituted BPEBs

As expected, the bis-substituted non-fluorinated BPEBs **1b-1f** all exhibit liquid crystalline phase(s) when heated because of their elongated molecular shapes (Table **3.5**). Moreover, different thermal properties are observed for each compound as different substituents will change the charge distribution along the length of the molecule while the molecular geometry may not have been significantly altered. For instance, compounds **1b**, CH_3-C_6H_4-C≡C-C_6H_4-C≡C-C_6H_4-CH_3, and **1f**, CF_3-C_6H_4-C≡C-C_6H_4-C≡C-C_6H_4-CF_3 are expected to have very similar molecular shape (axial ratios are estimated to be 4.85 and 4.90, respectively). They also crystallizes in the same space group, $P2_1/c$ (Table **3.2**). However, **1b** (R = CH_3) exhibits a nematic mesophase at 218.8°C and a nematic range of 26°C, but in **1f** (R = CF_3), both lower melting points and clearing points are observed, and a more ordered smectic B phase in a range of 22°C is generated. This

clearly demonstrates that a small change in the charge distribution in the molecule can have a significant effect on the thermotropic behavior.

In the substituted tetrafluorinated BPEBs (**8a-8f**), R-C_6H_4-C≡C-C_6F_4-C≡C-C_6H_4-R, although axial ratios lower than 4.52 are observed in some of them, they all exhibit liquid crystal behaviors when heated (Table **3.5**). While similar melting points are observed for the two parent compounds **1a** and **8a** (181.7 and 182.5°C), compounds **8c** (MeO), **8d** (MeS) and **8f** (CF_3) experience lower melting points than the corresponding non-fluorinated compounds, but **8b** (CH_3) and **8e** (CN) have relatively higher melting points. No conclusions from these results can be drawn without the understanding of their molecular packings in the crystalline phase, because liquid crystallinity is a property that is dominated by the intermolecular interaction. Compounds **8a** to **8f** all crystallize in the orthorhombic or monoclinic system except **8d** which is composed of two independent molecules in the lattice. The molecules are all packed in a flattened herringbone fashion in that molecules sit parallel with phenyl or perfluorophenyl rings over triple bonds except in **8c** where phenyls are offset over perfluorophenyl units. Again, different liquid crystalline phase behaviors are seen with those two very similar compounds **8b** (CH_3) and **8f** (CF_3). In compound **8d** (MeS), both nematic and smectic mesophases are observed in the wide temperature range of 173.7 to 260°C, K 173.7 S 197.0 S_B 203.7 N 260.3 I. The presence of the -C_6F_4- units in these molecules must have a profound impact on the intermolecular interactions.

The octafluorinated BPEB compound **10c** (R = MeO) exhibits a nematic phase at 198.2°C, but the clearing point cannot be observed. Meanwhile, the related perfluorinated BPEB mesogen **12c** (R = MeO) shows both lowered melting and clearing points, K 188.2 N 200.7 I. It has been reported previously that the introduction of tetrafluoro substitution in the phenyl rings often decreases the thermal stability of the mesophase.[64] In the case of the octofluorinated 1,2-(4,4'-dialkoxyphenyl)acetylene, H(CH_2)$_m$O-C_6F_4-C≡C-C_6F_4-

$O(CH_2)_mH$, (m = 7-9), complete annihilation of liquid crystallinity was observed, compared with their non-fluorinated analogs. However, our results demonstrate that this is not necessarily true, particularly when intermolecular phenyl-perfluorophenyl interactions are involved.

3.3 Conclusions

We have demonstrated the utility of the Pd/Cu catalyzed cross-coupling methodology to the synthesis of a series of rigid-rod partially and fully fluorinated 1,4-bis(phenylethynyl)benzene derivatives.

Extensive single crystal structural analyses have been employed to determine the molecular packings in the crystalline phase. The intermolecular interactions between phenyl and perfluorophenyl units in the molecules has a profound impact on the crystal structures of the partially fluorinated compounds, particularly with regard to the formation of co-crystals.

The liquid crystalline behavior studies reveal that the parent non-fluorinated compound BPEB is a good model compound for the study of calamitic liquid crystals. It is clear that a small variation in the end substitution groups can affect not only the melting and clearing points but also the type of mesogenic phases that are formed. The introduction of perflurophenyl unit(s) to the molecules changes the charge distribution along the molecules, but perhaps more importantly, it changes the packing patterns of the molecules themselves in the crystals. Liquid crystallinity in the molecular complex **8a•10a** clearly originates from strong intermolecular phenyl-perfluorophenyl interaction between its two non-mesogenic components.

While we have determined all the crystal structures of the BPEB compounds discussed in this chapter, we are in a good place to start to correlate their crystalline structures with their liquid crystal properties. However, this task is never easy, as different packing modes are presented for different compounds. We expect that compound **10a**, C_6F_5-C≡C-C_6H_4-C≡C-C_6F_5 may be able to form co-crystal not only with **8a**, C_6H_5-C≡C-C_6F_4-C≡C-C_6H_5 but also with all the other substituted compounds **8b-8f**, in a very similar packing fashion, and their crystal structures will be related. Then their liquid crystal properties can be compared in terms of substituent effects. We also discovered that the substituted partially fluorinated tolan, NC-C_6H_4-C≡C-C_6F_5 has a very similar crystal structure as that of **15**, C_6H_5-C≡C-C_6F_5. A series of derivatives of the form of NC-C_6H_4-C≡C-C_6F_4-O$(CH_2)_m$H can be very easily synthesized, and their liquid crystal properties as well as crystal structures will be explored in future work. In summary, with the unique phenyl-perfluorophenyl interaction, numerous combinations can be formed from these compounds to investigate not only the liquid crystal properties but also crystal packings.

3.4 Experimental

3.4.1 General

All reactions were performed under a dry nitrogen atmosphere using standard Schlenk techniques. Triethylamine and diisopropylamine were distilled from CaH_2 under N_2.

Nuclear magnetic resonance experiments were performed on a Bruker AC200 spectrometer at the following frequencies: ^1H - 200 MHz; $^{13}C\{^1H\}$ -50 MHz; $^{19}F\{^1H\}$ - 188 MHz. ^1H chemical shifts were referenced to the internal standard tetramethylsilane (TMS), ^{13}C chemical shifts were referenced to the solvent resonances and are relative to the external standard TMS. ^{19}F chemical shifts were referenced to the external standard fluorotrichloromethane ($CFCl_3$). All spectra were recorded in $CDCl_3$. FT-IR spectra were recorded as Nujol mulls on a Bomem Michelson MB Series FT-IR spectrophotometer. Absorption spectra were recorded on a Hewlett-Packard 8452A Diode Array UV-VIS spectrophotometer. Emission spectra were recorded on a PTI MD-5020 spectrophotometer. Elemental analyses were obtained from M-H-W Laboratories, Phoenix, Arizona, and at the University of Newcastle Upon Tyne, the University of Bristol, England.

GC/MS analyses were performed on a Hewlett-Packard 5890 Series II/5971A MSD instrument equipped with an HP 7673A autosampler and a fused silica column (30 m x .25 mm x .25 mm, cross-linked 5% phenylmethyl silicone). The following operating conditions were used: injector, 260°C; detector, 280°C; oven temperature was ramped from 70°C to 260°C at the rate of 20°C/min. UHP grade helium was used as the carrier gas.

3.4.2 Synthesis

(Trimethylsilyl)pentafluorophenylacetylene (3g). To a solution of iodopentafluorobenzene (30 g, 0.102 mol) and trimethylsilylacetylene (12 g, 0.122 mol) in degassed triethylamine (200 mL) were added $PdCl_2(PPh_3)_2$ (0.72 g, 1.1 mmol) and CuI (0.200 g, 1.1 mmol) under nitrogen. The reaction mixture was allowed to stir at 40°C for 24 h. GC-MS test showed that iodopentafluorobenzene was completely reacted. Then, Et_2O (100 mL) was added into the suspension, the salt was filtered off and washed well with Et_2O. The filtrate was then washed with H_2O (150 mL x 3), 0.2 M HCl solution (150 mL x 3) and H_2O (150 mL x 2) again. The Et_2O solution was dried over Na_2SO_4, and distilled *in vacuo* to give (trimethyl)pentafluorophenylacetylene (19.7 g, 73%).

Pentafluorophenylacetylene (4g). Aqueous 0.05 M KOH solution (10 mL) was added to a solution of (trimethylsilyl)pentafluorophenylacetylene (7.0 g, 0.0265 mmol) in methanol (100 mL). The reaction mixture was allowed to stir at room temperature for 2 h, then was extracted with Et_2O (100 mL). The Et_2O solution was washed with 0.2 M HCl solution (100 mL x 3) and H_2O (100 mL x 3), and dried with Na_2SO_4. The product was obtained after removing the solvent by distillation, yielding 4.2 g (82%) as a colorless liquid.

4-Methoxytetrafluorophenylacetylene (4h). Solid KOH (30 mg) was added to a solution of (trimethylsilyl)pentafluorophenylacetylene (4.0 g, 0.015 mmol) in methanol (50 mL). The reaction mixture was allowed to stir at room temperature for 10 h, then was extracted with Et_2O (100 mL). The Et_2O solution was washed with 0.2 M HCl solution (100 mL x 3) and H_2O (100 mL x 3), and dried over Na_2SO_4. The solvent was removed, and the solid was recrystallized from hexane; 2.5 g (81%) of white solid was obtained. m.p. 56-57°C. ^1H NMR (200 MHz): δ 3.52 (s, 1H, C≡CH), 4.09 (m, 3H, CH_3O). $^{13}C\{^1H\}$ NMR (50.4 MHz): δ 62.2 (m, CH_3O), 68.6 (C≡C), 88.5 (C≡C), 96.6 (C), 138.1

(CF), 139.7 (C), 143.3 (CF), 145.6 (CF), 150.7 (CF). $^{19}F\{^{1}H\}$ (188 MHz): -158.01 (m, 2F), -137.89 (m, 2F). IR (Nujol, cm^{-1}): 2228 (C≡C). MS (EI), m/z (rel) 204 (M+,100), 189(52), 173(3), 161(89), 155(2), 141(10), 123(18), 117(3), 92(10).

1,4-Bis(phenylethynyl)tetrafluorobenzene (8a). A solution of phenylacetylene (1.0 g, 9.8 mmol) in diisopropylamine (20 mL) was added to a suspension containing 1,4-diiodotetrafluorobenzene (1.6g, 4 mmol), $PdCl_2(PPh_3)_2$ (0.070 g, 0.1 mmol) and CuI (0.019 g, 0.1 mmol) in diisopropylamine (10 mL) under nitrogen. The reaction mixture was allowed to stir at reflux for 4 h. The solvent was removed *in vacuo*, and the crude product was extracted into hot toluene and filtered through a 2 cm pad of silica gel (70-230 mesh). Compound **2** was obtained as colorless needle-shaped crystals by cooling the hot toluene solution. The yield was 0.55 g (71%). mp 182.5°C. ^{1}H NMR (200 MHz): δ 7.36-7.43 (m, 6H, phenyl H's), 7.58-7.62 (m, 4H, phenyl H's). $^{13}C\{^{1}H\}$ NMR (50.4 MHz): δ 74.6 (m, C≡C), 103.1 (C≡C), 121.6 (C, C_6H_5), 128.5 (CH), 129.7 (CH), 132.0 (CH), 143.8 (CF, m), 148.9 (CF, m). $^{19}F\{^{1}H\}$ NMR (188 MHz): -147.7 (s). IR (Nujol, cm^{-1}): 2226, 2209 (C≡C). MS (EI), m/z (rel) 350 (M^+,100), 330(4), 298(3), 274(2), 246(1), 175(1), 149(2), 123(1). UV-Vis (CH_3CN): λ (nm, (log ε)) 192(4.12), 226(3.36), 304(3.65), 322(3.79), 340 (3.62). Anal. Calcd. for $C_{22}H_{10}F_4$: C, 75.43; H, 2.86; F, 21.71. Found: C, 75.52; H, 2.68; F, 21.86

1,4-Bis(*p*-methylphenylethynyl)tetrafluorobenzene (8b). White crystals (yield 79%). ^{1}H NMR (200 MHz): δ 2.39 (s, 6H, CH_3), 7.24 (m, 4H, phenyl H's), 7.49 (m, 4H, phenyl H's). $^{19}F\{^{1}H\}$ NMR (188 MHz): -137.42 (s). IR (Nujol, cm^{-1}): 2224, 2206 (C≡C). MS (EI), m/z (rel) 378 (M^+,100), 356(3), 343(4), 312(3), 291(3), 243(3), 219(2), 189(14), 178(3). UV-Vis (CH_3CN): λ (nm, (log ε)) 328 (4.78), 346 (4.66). Anal. Calcd. for $C_{24}H_{14}F_4$: C, 76.12; H, 3.70. Found: C, 75.99; H, 3.68.

1,4-Bis(*p*-methoxyphenylethynyl)tetrafluorobenzene (8c). White plates (yield 70%). ^{1}H NMR (200 MHz): δ 3.64 (s, 6H, CH_3O), 6.90 (m, 4H, phenyl H's), 7.53 (m, 4H,

phenyl H's). $^{19}F\{^1H\}$ NMR (188 MHz): -137.74 (s). IR (Nujol, cm^{-1}): 2228, 2207 (C≡C). MS (EI), m/z (rel) 410 (M^+,100), 395(33), 367(13), 352(12), 325(5), 324(24), 298(6) 205(25), 162(27), 149(13), 136(5). UV-Vis (CH_3CN): λ (nm, (log ε)) 340 (4.70), 358 (4.63). Anal. Calcd. for $C_{24}H_{14}F_4O_2$: C, 70.25; H, 3.44. Found: C, 69.92; H, 3.78.

1,4-Bis(*p*-methylthiophenylethynyl)tetrafluorobenzene (8d). Pale yellow crystals (yield 91%). ^1H NMR (200 MHz): δ 2.51 (s, 6H, CH_3S), 7.23 (m, 4H, phenyl H's), 7.49 (m, 4H, phenyl H's). $^{19}F\{^1H\}$ NMR (188 MHz): -147.92 (s). IR (Nujol, cm^{-1}): 2221, 2205 (C≡C). MS (EI), m/z (rel) 442(M^+, 100), 443(23), 444(10), 445(2), 427(23), 412(11), 393(1), 368(2), 221(10). UV-Vis (CH_3CN): λ (nm, (log ε) 284 (4.29), 354 (4.87). Anal. Calcd. for $C_{24}H_{14}F_4S_2$: C, 65.15; H, 3.19. Found: C, 65.78; H, 3.36.

1,4-Bis(*p*-cyanophenylethynyl)tetrafluorobenzene (8e). Pale yellow flakes (yield 71%). ^1H NMR (200 MHz): δ 7.70 (s, phenyl H's). $^{19}F\{^1H\}$ NMR (188 MHz): -113.38 (s). IR (Nujol, cm^{-1}): 2235 (CN), 2207 (C≡C). MS (EI), m/z (rel) 400(M^+, 49), 401(12), 402(4), 223(4), 200(5), 191(2), 169(5), 149(100), 125(7), 111(15), 109(12). UV-Vis (CH_3CN): λ (nm, (log ε)) 330 (4.88), 352 (4.70). Anal. Calcd. for $C_{24}H_8F_4N_2$: C, 72.01; H, 2.01; N, 7.00. Found: C, 71.28; H, 2.00; N, 6.99.

1,4-Bis(*p*-trifluoromethylphenylethynyl)tetrafluorobenzene (8f). White plates (yield 80%). ^1H NMR (200 MHz): δ 7.69 (m, phenyl H's). $^{19}F\{^1H\}$ NMR (188 MHz): -136.12 (s, 4F, C_6F_4), -62.83 (s, 6F, CF_3). IR (Nujol, cm^{-1}): 2227, 2207 (C≡C). MS (EI), m/z (rel) 487 (M^+,100), 468(13), 467(55), 436(31), 497(12), 377(12), 366(18), 348(18), 346(16), 328(15), 327(10), 316(13), 297(12), 296(12), 278(9), 270(10), 217(34), 208(46), 198(12), 185(10), 183(11), 174(12), 173(10), 170(42), 144(8). UV-Vis (CH_3CN): λ (nm, (log ε)) 320 (4.82), 340 (4.64). Anal. Calcd. for $C_{24}H_8F_{10}$: C, 59.28; H, 1.66. Found: C, 59.16; H, 1.89.

1,4-Bis(pentafluorophenylethynyl)benzene (10a). A solution of iodopentafluorobenzene (7.0 g, 24 mmol) in triethylamine (50 mL) was degassed and added to a suspension containing 1,4-diethynylbenzene (1.5g, 12 mmol), $PdCl_2(PPh_3)_2$ (0.084 g, 0.12 mmol) and CuI (0.023 g, 0.12 mmol) in triethylamine (100 mL) under nitrogen. The reaction mixture was allowed to stir at 60°C for 6 h. After being cooled to room temperature, the reaction mixture was filtered and the brown solid was collected. This crude product was washed thoroughly with H_2O and dried in air. Recrystallization from hot toluene yielded pale yellow product 4.0 g (78%). mp 196.5°C. ^1H NMR (200 MHz): δ 7.60 (phenyl H, s). $^{19}F\{^1H\}$ NMR (188 MHz): -172.0 (4F, m), -162.3 (2F, m), -146.10 (4F, m),. IR (Nujol, cm^{-1}): 2223 (C≡C). MS (EI), m/z (rel) 458 (M^+,100), 420(7), 389(5), 320(1), 290(1), 242(1), 229(21), 194(3), 179(3), 147(2). UV-Vis (CH_3CN): λ (nm, (log ε)) 192(3.75), 214(3.45), 298(3.62), 316(3.76), 336 (3.61). Anal. Calcd for $C_{22}H_4F_{10}$: C, 57.64; H, 0.88; F, 41.88. Found: C, 57.63; H, 0.82; F, 41.63.

1,4-Bis(*p*-methoxytetrafluorophenylethynyl)benzene (10c). *p*-Methoxytetrafluoroacetylene (0.98 g, 4.4 mmol) and 1,4-diiodobenzene (0.66 g, 2 mmol) along with $PdCl_2(PPh_3)_2$ (0.028 g, 0.04 mmol) and CuI (0.008 g, 0.04 mmol) were charged into a 100 mL Schlenk flask under the protection of nitrogen. Diisopropylamine (50 mL) was then added to the flask, and the reaction solution was allowed to stir and reflux for 4 h. After being cooled to room temperature, the precipitate was collected by filtration. The solid was washed thoroughly with H_2O and dried in air. Recrystallization from hot toluene yielded white cotton-like product 0.87 g (90%). ^1H NMR (200 MHz): δ 4.13 (m, 6H, CH_3O), 7.59 (s, 4H, phenyl H's). $^{19}F\{^1H\}$ (188 MHz): -157.81 (4F, m), -137.43 (4F, m). IR (Nujol, cm^{-1}): 2220 (C≡C). MS (EI), m/z (rel) 482 (M^+,100), 467(59), 452(41), 346(37), 327(51), 283(39), 269(77), 255(39), 198(19), 148(17). UV-Vis (CH_3CN): λ (nm, (log ε)) 322(4.79), 342(4.59). Anal. Calcd for $C_{24}H_{10}F_8O_2$: C, 59.71; H, 2.07. Found: C, 59.53; H, 1.90.

1,4-Bis(pentafluorophenylethynyl)tetrafluorobenzene (12a). A solution of pentafluoroacetylene (1.37 g, 7.1 mmol) in triethylamine (10 mL) was degassed and added to a suspension containing 1,4-diiodotetrafluorobenzene (1.20 g, 3 mmol), $PdCl_2(PPh_3)_2$ (0.042 g, 0.06 mmol) and CuI (0.012 g, 0.06 mmol) in triethylamine (40 mL) under nitrogen. The reaction mixture was allowed to stir at reflux for 3 h. After being cooled to room temperature, the reaction mixture was filtered and the gray solid was collected. This crude product was washed thoroughly with H_2O and dried in air. Recrystallization from hot toluene yielded pale yellow product 0.99 g (75%). mp 226.1°C. $^{19}F\{^1H\}$ (188 MHz): -160.4 (4F, m), -148.7 (2F, m), -134.6 (central C_6F_4, 4F, m), -133.8 (4F, m). MS (EI), m/z (rel) 530 (M^+,100), 492(8), 461(14), 423(10), 392(8), 361(13), 337 (9), 306(6), 265(21), 230(12), 196(11), 165(11). UV-Vis (CH_3CN): λ (nm, (log ε)) 192(4.00), 210(354.), 302(3.69), 318(3.81), 338(3.66). Anal. Calcd for $C_{22}F_{14}$: C, 49.84; F, 50.16. Found: C, 50.02; F, 46.66.

1,4-Bis(*p*-methoxytetrafluorophenylethynyl)tetrafluorobenzene (12c). White plates (yield 79%) ^1H NMR (200 MHz): δ 4.17 (m, 6H, CH_3O). $^{19}F\{^1H\}$ (188 MHz): -157.25 (4F, m), -136.00 (4F, m), -135.31 (s, 4F). MS (EI), m/z (rel) 554 (M^+,100), 539(62), 524(38), 496(18), 468(16), 430(9), 399(24), 368(8), 361(10), 337(6), 331(8), 329(9), 281(6), 277(17), 256(5), 234(21), 215(9), 165(8). UV-Vis (CH_3CN): λ (nm, (log ε)) 328(4.74), 346(4.62). Anal. Calcd for $C_{24}F_{12}O_2$: C, 51.96; H 1.08 Found: C, 51.89; H, 0.96.

2,3,4,5,6-Pentafluorodiphenylacetylene (15). A solution of phenylacetylene (0.61 g, 6 mmol) in triethylamine (30 mL) was added to a suspension containing iodopentafluorobenzene (1.47g, 5 mmol), $PdCl_2(PPh_3)_2$ (0.035 g, 0.05 mmol) and CuI (0.010 g, 0.05 mmol) in triethylamine (30 mL) under nitrogen. The reaction mixture was allowed to stir at reflux for 4 h. The solvent was removed *in vacuo*, and the crude product was extracted into hexane and filtered through a 2 cm pad of silica gel (70-230

mesh). Compound **2** was obtained as colorless needle-shaped crystals by cooling the hexane solution to -20°C. The yield was 1.20 g (90%). ^{1}H (200 MHz): δ 7.32-7.40 (phenyl H's, 3H, m), 7.52-7.57 (phenyl H's, 2H, m). ^{19}F{^{1}H} (188 MHz): -172.6 (2F, m), -163.5 (1F, m), -146.7 (2F, m). IR (Nujol, cm^{-1}): 2228 (C≡C). MS (EI), m/z (rel) 268 (M^+,100), 249(7), 237(8), 216(8), 199(38), 179(2), 147(4), 134(9). UV-Vis (CH_3CN): λ (nm, (log ε)) 194(4.86), 266(3.38), 280(3.52), 296(3.45). Anal. Calcd for $C_{14}H_5F_5$: C, 62.70; H, 1.88; F, 35.42. Found: C, 62.91; H, 2.04; F, 35.56.

(*p*-Cyanophenylethynyl)pentafluorobenzene. Yellow crystals (yield 70%). m.p. 164-165°C. ^{1}H NMR (200 MHz): δ 7.59 (m, C_6H_4). ^{13}C{^{1}H} (50.4 MHz): 99.10 (br, C≡C), 113.01 (*C*N), 118.02 (s), 126.16 (s), 128.15 (s), 132.97 (s), 135.13 (m), 139.47 (m), 140.24 (m), 144.50 (m), 149.65 (m). MS (EI), m/z (rel) 293 (M^+, 100), 294(19), 295(2), 273(5), 262(6), 242(5), 216(9), 209(1), 192(4), 166(1), 146(9), 123(3).

4-(*p*-Iodophenylethynyl)benzaldehyde. A solution of *p*-ethynylbenzaldehyde (2.0 g, 15.4 mmol) in triethylamine (75 mL) was added dropwise to a suspension containing 1,4-diiodobenzene (15.23 g, 46.2 mmol), $PdCl_2(PPh_3)_2$ (0.108 g, 0.154 mmol) and CuI (0.029 g, 0.154 mmol) in 175 mL of triethylamine over a period of 24 h. At the end of the reaction, the mixture was filtered to remove the triethylammonium iodide salt, and the solvent was then removed *in vacuo*. The crude product was washed by hexane (50 mL x 2), the residue was then dissolved in hot toluene and purified via column chromatography on silica gel (70-230 mesh) with toluene as eluent. Pure product was obtained as pale yellow flakes (3.8 g, 74%). ^{1}H NMR (200 MHz): δ 7.25 (m, 2H), 7.68 (m, 4H), 7.85 (m, 2H), 10.01 (s, 1H, CHO). Anal. Calcd for $C_{15}H_9IO$: C, 54.24; H 2.73 Found: C, 54.50; H, 2.80.

Co-crystals of diphenylacetylene (13) and decafluorophenylacetylene (14) Co-crystals of diphenylacetylene and decafluorophenylacetylene were obtained from hexane.

Anal. Calcd for $C_{14}H_{10} \cdot C_{14}F_{10}$: C, 62.70; H, 1.88; F, 35.42. Found: C, 62.80; H, 1.75; F, 35.19.

Co-crystallization of 1,4-Bis(phenylethynyl)tetrafluorobenzene (8a) and 1,4-Bis(pentafluorophenylethynyl)benzene (10a) Solid samples of 1,4-bis(phenylethynyl)-tetrafluorobenzene (**8a**) (70 mg, 2 mmol) and 1,4-bis(pentafluorophenylethynyl)benzene (**10a**) (92 mg, 2 mmol) were dissolved in 5 mL of hot $CHCl_3$. Some colorless needle-like crystals were collected after cooling the solution to room temperature. GC/MS analysis showed that this solid contained (**8a**) and (**10a**) in a 1:1 ratio. Anal. Calcd for $C_{22}H_{10}F_4 \cdot C_{22}H_4F_{10}$: C, 65.53; H, 1.41; F, 32.56. Found: C, 65.36; H, 1.75; F, 32.89.

Co-crystallization attempts between 1,4-Bis(phenylethynyl)benzene (1a) and 1,4-Bis(pentafluorophenylethynyl)tetrafluorobenzene (12a). Solid samples of 1,4-bis(phenylethynyl)benzene (**1a**) (28 mg, 1 mmol) and 1,4-bis(pentafluorophenylethynyl)-tetrafluorobenzene (**12a**) (53 mg, 1 mmol) were dissolved in 10 mL of hot $CHCl_3$. Some pale yellow crystals (40 mg) were collected after cooling the solution to room temperature. However, GC/MS analysis showed that this solid contained (**1a**) and (**12a**) in an approximate 1:3 ratio. This solid was recrystallized from $CHCl_3$ again, but only pure **12c** was obtained which was indicated by GC-MS analysis.

In another experiment, solid samples of 1,4-bis(phenylethynyl)benzene (**1a**) (28 mg, 1 mmol) and 1,4-bis(pentafluorophenylethynyl)-tetrafluorobenzene (**12a**) (53 mg, 1 mmol) were dissolved in 10 mL of hot $CHCl_3$. Then the solution was evaporated to dryness, yielding a pale yellow solid. Powder X-ray diffraction analysis indicated that there was new species within this solid, and LC study showed the following phase transitions: $K_{178.5}$ $S_{B\ 196.2}$ bi $N/I_{231.5}$ I.

3.4.3 Single Crystal Studies

3.4.3.1 Work at Waterloo

Suitable crystals of **1c**, **8b** and **8c** were obtained by slow evaporation from a toluene solution. The data sets were collected at 295 K on a Siemens R3m/V diffractometer using graphite monochromated Mo Kα radiation (0.71073 Å) and ω scan methods with variable scan rates. Background measurements were made at the beginning and end of each scan for a total time equal to a quarter the scan time. Data were corrected for Lorentz and polarization effects and absorption (face-indexed numerical). The structures were solved by direct methods and refined by full-matrix least-squares methods using Siemens SHELXTL PLUS (VMS) software, with anisotropic thermal parameters for all non-hydrogen atoms and isotropic thermal parameters for hydrogen atoms. The function minimized was $\sum w (|F_o|-|F_c|)^2$. The atomic scattering factors were taken from the International Tables Vol. 4.

3.4.3.2 Work at Newcastle, England

Other structures in this chapter were determined at the University of Newcastle, and at CCLRC, Daresbury Laboratory, England.

Suitable single crystals were grown from toluene or $CHCl_3$. Measurements were made on a Siemens SMART CCD area-detector diffractometer; in all cases, graphite-monochromated MoKα radiation was used (λ = 0.71073Å). The crystals were mounted on a glass fiber with a coating of perfluoropolyether oil, cell parameters were refined from the observed setting angles and detector spot positions for selected reflections, and intensities were measured from a series of frames each covering a 0.3° oscillation in ω.

The structures were solved using direct methods, and refined by full-matrix least-

squares techniques. The refinement was on F^2 of all independent reflections, to minimize $\Sigma w(F_o^2 - F_c^2)^2$, with weighting $w^{-1} = \sigma^2(F_o^2) + (aP)^2/ bP$, where $P = (F_o^2 + 2F_c^2)/3$; the refined isotropic extinction parameter χ is defined such that F_c is multiplied by $(1 + 0.001\chi F_c^2 \lambda^3/ \sin 2\theta)^{-1/4}$. In each case, anisotropic displacement parameters were refined for all non-hydrogen atoms, and isotropic hydrogen atoms were constrained to ride on their parent carbon atoms with fixed bond lengths and idealized bond angles.

Programs were standard Siemens control and integration software, versions 4 and 5 of SHELXTL, and local programs.

3.4.3.3 Work at Daresbury, England

Data of **1b, 1f** were collected employing a wavelength of 0.6889 Å, on a Siemens SMART CCD area detector diffractometer, equipped with a silicon (111) crystal monochromator and a palladium coated focusing mirror on the single crystal diffraction station at the Daresbury Laboratory Synchrotron Radiation Sourse.

3.4.4 Liquid Crystal Studies

Liquid crystal studies were carried out by V. Chu and C. Viney, University of Washington, Seattle (**1a-f**), but mostly by C. Viney later at the Department of Materials at Oxford University.

3.4.4.1 Differential Scanning Calorimetry

Phase transitions were determined by differential scanning calorimetry on a Perkin Elmer DSC 7 system with aluminum sample and reference pans. Pans were closed with aluminum covers, using a Perkin Elmer crimper press to obtain a standard (non-hermetic) seal. An environment of dry argon was provided at a flow rate of 20 cm^3/min. In cases where a compound exhibited traces of retained solvent or volatile solid (as evidenced by a deposit forming outside the sample during an exploratory heating run), a programmable microscope hot stage was used to pre-heat each subsequent sample of that compound to 100°C for a few minutes in an open DSC pan. The 100°C temperature used to pre-heat samples is safely below the degradation temperature of any of the compounds discussed here.

The thermal history of each sample (after the pan was sealed) was as follows: heat to 300°C at 10°C/min, cool to ambient at 10°C/min, and re-heat to 300°C at 10°C/min. While each of these three steps can be used to provide phase transition temperatures, their information content is not necessarily identical:

- Results obtained during the first heating may depend on whether the as-synthesized material was precipitated from solution or crystallized from a melt. The conditions under which the initial solid forms a higher-temperature (less-ordered) phase can be sensitive to the molecular order that is present in the initial solid.

• A transition detected on cooling may occur at a lower temperature than the equivalent transition on heating, if the transition is limited by nucleation of the lower temperature phase. Also, the specimen may degrade during the first heating, so that the cooling step may in fact be characterizing a material that is different from the original sample.

• The second heating is performed on a material that may have degraded during the first heating.

Therefore, the results reported here present the transition temperatures from the first heating step and from the cooling step.

3.4.4.2 Transmitted Polarized Light Microscopy

Microscopy at the University of Washington: Specimens were observed with a Leitz Laborlux 12 POL microscope equipped with a Linkam THM 600 heating / freezing stage and PR 600 controller. A long working distance objective (32x; NA=0.4) was used to view micro structures at a resolution of approximately 1.5μm; the design of the stage (which optimizes temperature control at the specimen) effectively restricts the incident illumination to a parallel (orthoscopic) beam, so that resolution is not as good as it would be under Köhler illumination. Specimens were maintained between glass cover slides that had previously been rinsed in ethanol and allowed to air dry. The specific purpose of the microscopical observations was to confirm the existence (and if possible the nature) of liquid crystalline phases.

Microscopy at the University of Oxford: An Ultraphot II light microscope (Carl Zeiss, Oberkochen / Württemberg, Germany), equipped with a Xenon arc lamp and crossed polars, was used in transmission. The xenon arc lamp ensured good contrast from liquid crystalline samples. A Linkam THMS 600 heating / freezing stage and TP 92 temperature programmer / controller (Linkam Scientific Instruments Ltd., Tadworth,

Surrey, UK) were used to enable observation of sample microstructures *in situ* at elevated temperatures. Heating and cooling rates of $10°C/min^{-1}$ were typical. Occasionally, slower heating rates ($1°C/min^{-1}$ to $5°C/min^{-1}$) were used to facilitate distinction between phases that are stable over a narrow temperature range. Specimens were cleaned before use: a rinse in distilled and de-ionized water was followed by two rinses with acetone; they were then allowed to air dry under a dust cover.

In principle, microscopy could be used instead of DSC to determine the phase transition temperatures. However, aside from the fact that DSC offers a substantially quicker route to obtaining the transition temperatures, it also provides numbers that are more reliable. The limitations of microscopy in this respect arise because (a) an optically resolvable amount of the new phase has to have formed before the transition is detectable with the microscope, and (b) the scale and nature of the microstructure is sensitive to specimen-substrate interactions which may not be exactly reproducible from one preparation to the next.

3.5 References

1. (a) Tour, J. M. *Chem. Rev.*, **1996**, *96*, 537. (b) Ward, M. D. *Chem. & Ind.*, **1996**, 568. (c) Ward, M. D. *Chem. & Ind.*, **1997**, 640. (d) Dalton, L. R. *Chem. & Ind.*, **1997**, 510. (e) Bredas, J. L.; Silbey, R. *Conjugated Polymers*, Kluwer Academic Publishers: Dordrecht, **1991**. (f) Hide, F.; Díaz-García, M. A.; Schwartz, B. J.; Heeger, A. J. *Acc. Chem. Res.*, **1997**, *30*, 430.

2. (a) Stang, P. J. Diedrich, F. *Modern Acetylene Chemistry*, VCH: Weinheim, **1995**. (b) Gleiter, R.; Kratz, D. *Angew. Chem. Int. Ed. Engl.*, **1993**, *32*, 842. (c) Bunz, U. H. F. *Angew. Chem. Int. Ed. Engl.*, **1994**, *33*, 1073. (d) Diederich, F. *Nature* (London) **1994**, *369*, 199. (e) Tykwinski, R. R.; Diederich, F. *Liebigs Ann. Recueil* **1997**, 649. (f) Moore, J. S. *Acc. Chem. Res.* **1997**, *30*, 402.

3. (a) Stiegman, A. E.; Miskowski, V. M.; Perry, J. W.; Coulter, D. R. *J. Am. Chem. Soc.*, **1987**, *109*, 5884. (b) Stiegman, A. E.; Graham, E.; Perry, K. J.; Khundkar, L. R.; Cheng, L. -T.; Perry, J. W. *J. Am. Chem. Soc.*, **1991**, *113*, 7658. (c) Barzoukas, M.; Fort, A.; Klein, G.; Boeglin, A.; Serbutoviez, C.; Oswald L.; Nicoud, J. F. *Chem. Phys.* **1991**, *153*, 457. (d) Jungbauer, D.; Teraoka, I.; Yoon, D. Y.; Reck, B.; Swalen, J. D.; Twieg, R.; Willson, C. G. *J. Appl. Phys.* **1991**, *69*, 8011. (e) Dehu, C.; Meyers, F.; Brédas, J. L. *J. Am. Chem. Soc.*, **1993**, *115*, 6198. (f) Khundkar, L. R.; Stiegman, A. E.; Perry, J. W. *J. Phys. Chem.*, **1990**, *94*, 1224. (g) Khundkar, L. R.; Bartlett, J. T.; Biswas, M. *J. Phys. Chem.*, **1995**, *102*, 6456. (h) Malthete, J.; Leclercq, M.; Dvolaitzky, M.; Gabard, J.; Billard, J.; Pontikis, V.; Jacques, J. *Mol. Cryst. Liq. Cryst.* **1973**, *23*, 233. (i) Fouquey, C.; Lehn, J. -M.; Malthête, J. *J. Chem. Soc., Chem. Commun.*, **1987**, 1424. (j) Pugh, C.; Percec, V. *Mol. Cryst. Liq. Cryst.* **1990**, *178*, 193. (k) Pugh, C.;

Percec, V. *Chem. Mater.* **1991**, *3*, 107. (l) Takatsu, H.; Takeuchi, K.; Tanaka, Y.; Sasaki, M. *Mol. Cryst. Liq. Cryst.* **1986**, *141*, 279.

4. (a) Grubbs, R. H.; Kratz, D. *Chem. Ber.*, **1993**, *126*, 149. (b) Schumm, J. S.; Pearson, D. L.; Tour, J. M. *Angew. Chem. Int. Ed. Engl.*, **1994**, *33*, 1360. (c) Young, J. K.; Nelson, J. C.; Moore, J. S. *J. Am. Chem. Soc.*, **1994**, *116*, 10841. (d) Hsung, R. P.; Chidsey, C. E. D.; Sita, L. R. *Organometallics*, **1995**, *14*, 4808. (e) Anderson, S.; Anderson, H. L. *Angew. Chem. Int. Ed. Engl.*, **1996**, *35*, 1956.

5. (a) Gardner, G. B.; Venkataraman, D.; Moore, J. S.; Lee, S. *Nature*, **1995**, *374*, 792. (b) Venkataraman, D.; Gardner, G. B.; Lee, S.; Moore, J. S. *J. Am. Chem. Soc.*, **1995**, *117*, 11600. (c) Gardner, G. B.; Kiang, Y. -H.; Lee, S.; Asgaonkar, A.; Venkataraman, D. *J. Am. Chem. Soc.*, **1996**, *118*, 6946. (d) Kondo, K.; Yasuda, S.; Sakaguchi, T.; Miya, M. *J. Chem. Soc., Chem. Commun.*, **1995**, 55. (e) Langner, M.; Praefcke, K.; Krüerke, D.; Heppke, G. *J. Mater. Chem.*, **1995**, *5*, 693. (f) Booth, C. J.; Krüerke, D.; Heppke, G. *J. Mater. Chem.*, **1996**, *6*, 927.

6. (a) Wu, Z.; Lee, S.; Moore, J. S. *J. Am. Chem. Soc.*, **1992**, *114*, 8730. (b) Venkataraman, D.; Lee, S.; Zhang, J.; Moore, J. S. *Nature*, **1994**, *371*, 591. (c) Wu, Z.; Moore, J. S. *Angew. Chem. Int. Ed. Engl.*, **1996**, *35*, 297. (d) Bedard, T. C.; Moore, J. S. *J. Am. Chem. Soc.*, **1995**, *117*, 10662. (e) Shetty, A. S.; Zhang, J.; Moore, J. S. *J. Am. Chem. Soc.*, **1996**, *118*, 1019. (f) Anderson, S.; Neidlein, U.; Gramlich, V.; Diederich, F. *Angew. Chem. Int. Ed. Engl.*, **1995**, *34*, 1596. (g) Morrison, D. L.; Höger, S. *Chem. Commun.*, **1996**, 2313. (h) Höger, S.; Meckenstock, A. -D.; Pellen, H. *J. Org. Chem.* **1997**, *62*, 4556. (i) Kawase, T.; Ueda, N.; Darabi, H. R.; Oda, M. *Angew. Chem. Int. Ed. Engl.*, **1996**, *35*, 1556. (j) Kawase,T.; Darabi, H. R.; Oda, M. *Angew. Chem. Int. Ed. Engl.*, **1996**, *35*, 2664.

(k) Boese, R.; Matzger, A. J.; Vollhardt, K. P. C. *J. Am. Chem. Soc.*, **1997**, *119*, 2052. (l) Haley, M. M.; Brand, S. C.; Pak, J. J. *Angew. Chem. Int. Ed. Engl.*, **1997**, *36*, 836.

7. (a) Xu, Z.; Moore, J. S. *Angew. Chem. Int. Ed. Engl.*, **1993**, *32*, 246. (b) Xu, Z.; Moore, J. S. *Angew. Chem. Int. Ed. Engl.*, **1993**, *32*, 1354. (c) Bharathi, P.; Moore, J. S. *J. Am. Chem. Soc.*, **1997**, *119*, 3391.

8. (a) Sanechika, K.; Yamamoto, T.; Yamamoto, A. *Bull. Chem. Soc. Jpn.*, **1984**, *57*, 752. (b) Trumbo, D. L.; Marvel, C. S. *J. Polym. Sci., Part A: Polym. Chem*, **1986**, *24*, 2311. (c) Kondo, K.; Okuda, M.; Fujitani, T. *Macromolecules*, **1993**, *26*, 7382. (d) Solomin, V. A.; Heitz, W. *Macromol. Chem. Phys.*, **1994**, *195*, 303. (e) Mangel, T.; Eberhardt, A.; Schef, U.; Bunz, U. H. F.; Müllen, K. *Macromol. Rapid Commun.*, **1995**, *16*, 571. (f) Weiss, K.; Michel, A.; Auth, E. -M.; Bunz, U. H. F.; Mangel, T.; Müllen, K. *Angew. Chem. Int. Ed. Engl.*, **1997**, *36*, 506.

9. (a) Pugh, C.; Percec, V. *Polym. Bull.*, **1990**, *23*, 177. (b) Pugh, C.; Anderson, S. K.; Percec, V. *Liq. Cryst.*, **1991**, *10*, 229. (c) Nakatsuji, S.; Matsuda, K.; Uesugi, Y.; Nakashima, K.; Akiyama, A.; Fabian. W. *J. Chem. Soc., Perkin Trans. 1*, **1992**, 755. (c) Wautelet, P.; Le Moigne, J.; Turek, P. In "*Electrical, Optical, and Magnetic Properties of Organic Solid State Materials*", Garito, A. F.; Jen, A. K.-Y.; Lee, C. Y-C.; Dalton, L. R. Eds., MRS Symp. Proc. Vol. 328, **1994**. (d) Xu, Y.; Hu, Y.; Chen, Q.; Wen, J. *J. Mater. Chem.*, **1995**, *5*, 219. (e) Crisp, G. T.; Bubner, T. P. *Tetrahedron*, **1997**, *53*, 11899. (f) Bumm, L. A.; Arnold, J. J.; Cygan, M. T. ; Dunbar, T. D.; Burgin, T. P.; Jones II, L.; Allara, D. L.; Tour, J. M.; Weiss, P. S. *Science*, **1996**, *271*, 1705. (g) Andres, R. P.; Bielefeld, J. D.; Henderson, J. I.; Janes, D. B.; Kolagunta, V. R.; Kubiak, C. P.; Mahoney, W. J.; Osifchin, R. G. *Science*, **1996**, *273*, 1690. (h) Strukelj, M.; Jordan, R. H.; Dodabalapur, A. *J. Am. Chem. Soc.*, **1996**, *118*, 1213.

10. Bredas, J. L.; Adent, C.; Tackx, P.; Persoons, A. *Chem. Rev.* **1994**, *94*, 243.

11. Ming-Tang, Z.; Singh, B. P.; Prasad, P. N. *J. Chem. Phys.* **1988**, *89*, 5535.

12. (a) Nguyen, P.; Lesley, G.; Dai, C.; Taylor, N. J.; Marder, T. B.; Chu, V.; Viney, C.; Ledoux, I.; Zyss, J. In *Applications of Organometallic Chemistry in the Preparation and Processing of Advanced Materials* Harrod J. F.; Laine R. M. Eds., Kluwer Academic Publishers: Dordrecht, 1995, p. 333-347. (b) Nguyen, P.; Yuan, Z.; Agocs, L.; Lesley, G.; Marder, T. B. *Inorg. Chim. Acta*, **1994**, *220*, 289-296. (c) Nguyen, P.; Lesley, G.; Marder, T. B.; Ledoux, I.; Zyss, J. *Chem. Mater.* **1997**, *9*, 406-408.

13. (a) Viney, C.; Twieg, R. J.; Dannels, C. M.; Chang, M. Y. *Mol. Cryst. Liq. Cryst. Lett.*, **1990**, *7*, 147. (b) Viney, C.; Brown, D. J.; Dannels, C. M.; Twieg, R. J. *Liq. Cryst.*, **1993**, *13*, 95. (c) Twieg, R. J.; Chu, V.; Nguyen, C.; Dannels, C. M.; Viney, C. *Liq. Cryst.*, **1996**, *20*, 287.

14. (a) Gray, G. W.; Hird, M.; Lacey, D.; Toyne, K. J. *J. Chem. Soc., Perkin Trans. 2*, **1989**, 2041. (b) Gray, G. W.; Hird, M.; Lacey, D.; Toyne, K. J. *Mol. Cryst. Liq. Cryst.* **1989**, *172*, 165. (c) Gray, G. W.; Hird, M.; Lacey, D.; Toyne, K. J. *Mol. Cryst. Liq. Cryst.* **1991**, *195*, 221. (d) Gray, G. W.; Hird, M.; Lacey, D.; Toyne, K. J. *Mol. Cryst. Liq. Cryst.* **1991**, *204*, 43.

15. Zhang, Y.; Wen, J. *Synthesis*, **1990**, 727.

16. Tarrant, P. in *Fluorine Chemistry Reviews*, Tarrant, P. Ed.; Marcel Dekker: New York, **1974**, vol. 7.

17. Neenan, T. X.; Whitesides, G. M. *J. Org. Chem.*, **1989**, *53*, 2489.

18. Nguyen, P. Ph. D. Dissertation, University of Waterloo, **1995.**

19. (a) Hunter, C. A. *Angew. Chem. Int. Ed. Engl.*, **1993**, *32*, 1584. (b) Price, S. L.; Stone, A. J. *J. Chem. Phys.*, **1987**, *86*, 2859. (c) Jorgensen, W. L.; Severance, D. L. *J. Am. Chem. Soc.*, **1990**, *112*, 4768. (d) Hunter, C. A.; Sanders, J. K. M. *J. Am. Chem. Soc.*, **1990**, *112*, 5525. (e) Fowler, P. W.; Buckingham, A. D. *Chem. Phys. Lett.*, **1991**, *176*, 11. (f) Linse, P. *J. Am. Chem. Soc.*, **1992**, *114*, 4366. (g) Hunter, C. A. *Chem. Soc. Rev.*, **1994**, *23*, 101. (h) Williams, D. E.; Xiao, Y. *Acta Cryst.*, **1993**, *A49*, 1. (i) Hobza, P.; Selzle, H. L.; Schlag, E. W. *J. Am. Chem. Soc.*, **1994**, *116*, 3500. (j) Hobza, P.; Selzle, H. L.; Schlag, E. W. *Chem. Rev.*, **1994**, *94*, 1767. (k) Nishio, M.; Umezawa, Y.; Hirota, M.; Takeuchi, Y. *Tetrahedron*, **1995**, *51*, 8865. (l) Laatikainen, R.; Ratilainen, J.; Sebastian, R.; Santa, H. *J. Am. Chem. Soc.*, **1995**, *117*, 11006. (m) Cozzi, F.; Cinquini, M.; Annuziata, R.; Dwyer, T.; Siegel, J. S. *J. Am. Chem. Soc.*, **1992**, *114*, 5729. (n) Cozzi, F.; Cinquini, M.; Annuziata, R.; Siegel, J. S. *J. Am. Chem. Soc.*, **1993**, *115*, 5330. (o) Cozzi, F.; Ponzini, F.; Annuziata, R.; Cinquini, M.; Siegel, J. S. *Angew. Chem. Int. Ed. Engl.*, **1995**, *34*, 1019. (p) Cozzi, F.; Siegel, J. S. *Pure Appl. Chem.* **1995**, *67*, 683. (q) Newcomb, L. F.; Gellman, S. H. *J. Am. Chem. Soc.*, **1994**, *116*, 4993. (r) Zhang, J.; Moore, J. S. *J. Am. Chem. Soc.*, **1992**, *114*, 9701. (s) Shetty, A. S.; Zhang, J.; Moore, J. S. *J. Am. Chem. Soc.*, **1996**, *118*, 1019.

20. (a) Burley, S. K.; Presko, G. A. *Science*, **1985**, *229*, 23. (b) Burley, S. K;. Presko, G. A. *Adv. Protein Chem.*, **1988**, *39*, 125. (c) Hunter, C. A.; Sighn, J.; Thornton, J. M. *J. Mol. Biol.*, **1991**, *218*, 837.

21. (a) Saenger W. , *Principles of Nucleic Acid Structure*, Springer: New York, **1984**, p. 132-140. (b) Hunter, C. A. *J. Mol. Biol.*, **1993**, *230*, 1025.

22. (a) Wakelin, L. P. G. *Med. Res. Rev.*, **1986**, *6*, 275. (b) Ortiz, A. R.; Pisabarro, M. T.; Gallego, J.; Gago, F. *Biochemistry*, **1992**, *31*, 2887. (c) Breinlinger, E. C.;

Rotello, V. M. *J. Am. Chem. Soc.*, **1997**, *119*, 1165. (d) Deans, R.; Niemz, A.; Breinlinger, E. C.; Rotello, V. M. *J. Am. Chem. Soc.*, **1997**, *119*, 10863.

23. (a) Murphy, C. J.; Arkin, M. R.; Jenkins, Y.; Ghatlia, N. D.; Bossmann, S. H.; Turro, N. J. *Science*, **1993**, *262*, 1025. (b) Arkin, M. R.; Stemp, E. D. A.; Holmlin, R. E.; Barton, J. K.; Hormann, A.; Olson, E. J. C. *Science*, **1996**, *273*, 475. (c) Hall, D. B.; Holmlin, R. E.; Barton, J. K. *Nature*, **1996**, *382*, 731. (d) Taubes, G. *Science*, **1997**, *275*, 1420. (e) Dandliker, P. J.; Holmlin, R. E.; Barton, J. K. *Science*, **1997**, *275*, 1465. (f) Diederichsen, U. *Angew. Chem. Int. Ed. Engl.*, **1997**, *36*, 2317. (g) Holmlin, R. E.; Dandliker, P. J.; Barton, J. K. *Angew. Chem. Int. Ed. Engl.*, **1997**, *36*, 2715. (h) Fukui, K.; Tanaka, K. *Angew. Chem. Int. Ed. Engl.*, **1998**, *37*, 158. (i) Meggers, D.; Kusch, D.; Spichty, M.; Wille, U.; Giese, B. *Angew. Chem. Int. Ed. Engl.*, **1998**, *37*, 460.

24. (a) Hughes A., *Proc. R. Soc. London, Ser. A.* **1936**, *155*, 710. (b) Alexander, A. E. *J. Chem. Soc.*, **1937**, 1813. (c) Abraham, R. J.; Eivazi, F.; Pearson, H.; Smith, K. M. *J. Chem. Soc., Chem. Commun.*, **1976**, 698. (d) White, W. in *The Porphyrins*, Dolphin, D. Ed.; Academic Press: New York, **1978**, Vol. V, Chapter 7. (e) Leighton, P.; Cowan, J. A.; Abraham, R. J.; Sanders, J. K. M. *J. Org. Chem.*, **1988**, *53*, 733. (f) Hunter, C. A.; Meah, M. N.; Sanders, J. K. M. *J. Am. Chem. Soc*, **1990**, *112*, 5773. (g) Schneider, H. J.; Wang, M. *J. Org. Chem.*, **1994**, *59*, 7464. (h) Will, S.; Lex, J.; Vogel, E.; Schmickler, H.; Gisselbrecht, J. -P.; Haubtmann, C.; Bernard, M.; Gross, M. *Angew. Chem. Int. Ed. Engl.*, **1997**, *36*, 357. (i) Feiters, M. C.; Fyfe, M. C. T.; Martínez-Díaz, M. -V.; Menzer, S.; Nolte, R. J. M.; Stoddart, J. F.; van Kan, P. J. M.; Williams, D. J. *J. Am. Chem. Soc.*, **1997**, *119*, 8119.

25. (a) Benzing, T.; Tjivikua, T.; Wolfe, J.; Rebek Jr., J. *Science*, **1988**, *242*, 266. (b) Cram, D. J. *Angew. Chem. Int. Ed. Engl.*, **1988**, *27*, 1009. c) Lehn, J. -M. *Angew.*

Chem. Int. Ed. Engl., **1988**, *27*, 91. (d) Muehldorf, A.V.; Van Engen, D.; Warner, J. C.; Hamilton, A. D. *J. Am. Chem. Chem.*, **1988**, *110*, 6561. (e) Diederich, F. *Angew. Chem. Int. Ed. Engl.*, **1988**, *27*, 362. (f) Zimmerman, S. C.; Wu, W. *J. Am. Chem. Soc*, **1989**, *111*, 8054. (g) Pirkle, W. H.; Burke, J. A.; Wilson, S. R. *J. Am. Chem. Soc*, **1989**, *111*, 9222. (h) Rebek, Jr., J. *Angew. Chem. Int. Ed. Engl.*, **1990**, *29*, 245. (i) Cochran, J. E.; Parrott, T. J.; Whitlock, B. J.; Whitlock, H. W. *J. Am. Chem. Soc.*, **1992**, *114*, 2269. (j) Zimmerman, S. C. *Top. Cur. Chem.*, **1993**, 165, 71. (k) Bisson, A. P.; Carver, F. J.; Hunter, C. A.; Waltho, J. P. *J. Am. Chem. Soc.*, **1994**, *116*, 10292. (l) Pirkle, W. H.; Selness, S. R. *J. Org. Chem.*, **1995**, *60*, 3252. (m) Ashton, P. R.; Huff, J.; Menzer, S.; Parsons, I. W.; Preece, J. A.; Stoddart, J. F.; Tolly, M. S.; White, A. J. P.; Williams, D. J. *Chem. Eur. J.*, **1996**, 2, 31. (n) Ochiai, K.; Mazaki, Y.; Nashikiori, S.; Kobayashi, K.; Hayashi, S. *J. Chem. Soc., Perkin Trans. 2*, **1996**, 1139. (o) Hamilton, D. G.; Sanders, J. K. M.; Davies, J. E.; Clegg, W.; Treat, S. J. *Chem. Commun.* **1997**, 897. (p) Kickham, J. E.; Loeb, S. J.; Murphy, S. L. *Chem. Eur. J.*, **1997**, *3*, 1203.

26. (a) Maddaluno, J. F.; Gresh, N.; Giessner-Prettre, C. *J. Org. Chem.*, **1994**, *59*, 793. (b) Pirkle, W. H.; Welch, C. J. *Tetrahedron: Asymmetry*, **1994**, *5*, 777. (c) Norrby, P.-O.; Kolb, H. C.; Sharpless, K. B. *J. Am. Chem. Soc.*, **1994**, *116*, 8470. (d) Jones, G. B.; Chapman, B. J. *Synthesis*, **1995**, 475. (e) Corey, E. J.; Noe, M. C. *J. Am. Chem. Soc.*, **1996**, *118*, 319. (f) Quan, R. W.; Li, Z.; Jacobsen, E. N. *J. Am. Chem. Soc.*, **1996**, *118*, 8156. (g) Kawabata, T.; Nagata, M.; Takasu, K.; Fuji, K. *J. Am. Chem. Soc.*, **1990**, *119*, 3169.

27. Pietsch, M. A.; Rappé, A. K. *J. Am. Chem. Soc.*, **1996**, *118*, 10908.

28. (a) Desiraju, G. R.; Gavezzotti, A. *J. Chem. Soc., Chem. Commun.*, **1989**, 621. (b) Desiraju, G. R.; Gavezzotti, A. *Acta Cryst.*, **1989**, *B45*, 473. (c) Desiraju, G. R. *Crystal Engineering: the Design of Organic Solids*, Elsevier: New York, **1989**. (d)

Holligan, B. M.; Jeffery, J. C.; Ward, M. D. *J. Chem. Soc., Dalton Trans.*, **1992**, *23*, 3337. (e) Desiraju, G. R. *Angew. Chem. Int. Ed. Engl.*, **1995**, *34*, 2311. (f) Aoyama, Y.; Endo, K.; Anzai, T.; Yamahuchi, Y.; Sawaki, T.; Kobayashi, K.; Kanehisa, N.; Hashimoto, H.; Kai, Y.; Masuda, H. *J. Am. Chem. Soc.*, **1996**, *118*, 5562. (g) Lewis, F. D.; Yang, J. -S.; Stern, C. L. *J. Am. Chem. Soc.*, **1996**, *118*, 12029. (h) Desiraju, G. R. *Chem. Commun.*, **1997**, 1475. (i) König, O.; Bürgi, H.-B.; Armbruster, T.; Hulliger, J.; Weber, T. *J. Am. Chem. Soc* ., **1997**, *119*, 10632.

29. (a) Adam, D.; Schuhmacher, P.; Simmerer, J.; Häusslling, L.; Slemensmeyer, K.; Etzbach, K. H.; Ringsdorf, H.; Haarer, D. *Nature*, **1994**, *371*, 141. (b) Miyamura, K.; Mihara, A.; Fujii, T.; Gohshi, Y.; Ishii, Y. *J. Am. Chem. Soc.*, **1995**, *117*, 2377. (c) Zhang, J.; Moore, J. S. *J. Am. Chem. Soc.*, **1994**, *116*, 2655. (d) Lee, K. M.; Lee, C. K.; Lin, I. J. B. *Angew. Chem. Int. Ed. Engl.*, **1997**, *36*, 1850.

30. Patrick, C. R.; Prosser G. S. , *Nature (London)*, **1960**, *187*, 1021.

31. (a) Swinton, F. L.; in *Molecular Complexes*, Foster, R. Ed.; **1973**, Elek: London, p. 63-106. (b) Duncan, W. A.; Swinton, F. L. *Trans. Faraday Soc.*, **1966**, *62*, 1082. (c) Duncan, W. A.; Sheridan, J. P.; Swinton, F. L. *Trans. Faraday Soc.*, **1966**, *62*, 1090. (d) Gilson, D. F. R.; McDowell, C. A. *Can. J. Chem.*, **1966**, *44*, 945. (e) Beaumont, T. G.; David, K. M. C. *J. Chem. Soc. B*, **1967**, 1131. (f) Bauer, M. E.; Knobler, C. M.; Horsma, D. A.; Perez, P. *J. Phys. Chem.*, **1970**, *74*, 4594. (g) Brennan, J. S.; Brown, N. M. D.; Swinton, F. L. *J. Chem. Soc., Faraday Trans. 1*, **1974**, *70*, 1965. (h) Ripmeester, J. A.; Wright, D. A.; Fyfe, C. A.; Boyd, R. K. *J. Chem. Soc., Faraday Trans. 2*, **1978**, *74*, 1164. (i) Mackenzie, G. A.; Overell, J. S. W.; Pawley, G. S. *Solid State Commun.*, **1979**, *31*, 431. (j) Bailey, R. T.; Ferri, R. U.; *Spectrochim. Acta*, **1980**, *36A*, 69. (k) Bartsch, E.; Bertagnolli, H, *Ber. Bunsenges. Phys. Chem.*, **1986**, *90*, 34. (l) Goates, S. R.; Boerio-Goates, J.; Goates, J. R.; Ott, J. B. *J. Chem. Soc., Faraday Trans. 1*, **1987**, *83*, 1553. (m)

Suhm, M. A.; Weingartner, H. *Chem. Phys. Lett.*, **1989**, *159*, 193. (n) Williams, J. H. *Mol. Phys.*, **1991**, *73*, 99. (o) Williams, J. H.; White, R. P. *J. Chem. Phys.*, **1992**, *89*, 1755. (p) Williams, J. H. *Chem. Phys.*, **1992**, *167*, 215. (q) Duer, M. J. *J. Chem. Soc., Faraday Trans.*, **1993**, *89*, 823. (r) Laatikainen, R.; Santa, H.; Hilunen, Y.; Lounila, J. *J. Magn. Reson., Ser. A*, **1993**, *104*, 238. (s) Ott, J. B.; Goates, J. R. *J. Chem. Eng. Data*, **1996**, *41*, 669. (t) Neelakandan, M.; Pant, D.; Quitevis, E. L. *Chem. Phys. Lett.*, **1997**, *265*, 283.

32. (a) Brown, M. D.; Swinton, F. L. *J. Chem. Soc., Chem. Commun.* **1974**, 770. (b) Laidig, K. E. *Chem. Phys. Lett.*, **1991**, *185*, 483. (c) Hernández-Trujillo, J.; Costas, M.; Vela, A. *J. Chem. Soc., Faraday Trans.*, **1993**, *89*, 2441. (d) Luhmer, M.; Bartik, K.; Dejaegere, A.; Bovy, P.; Reisse, J. *Bull. Soc. Chim. Fr.*, **1994**, *131*, 603. (e) Williams, J. H. *Acc. Chem. Res.*, **1993**, *26*, 593. (f) Williams, J. H. *J. Chem. Phys.*, **1993**, *172*, 171. (g) Hernández-Trujillo, J.; Colmenares, F.; Cuevas, G.; Costas, M. *Chem. Phys. Lett.*, **1997**, *265*, 503.

33. (a) Overell, J. S. W.; Pawley, G. S.; *Acta Cryst.*, **1982**, *B38*, 1966. (b) Williams, J. H.; Cockcroft, J. K.; Fitch, A. N. *Angew. Chem. Int. Ed. Engl.*, **1992**, *31*, 1655.

34. (a) Bacon, G. E.; Curry, N. A.; Wilson, S. A. *Proc. R. Soc. London, Ser. A*, **1964**, *279*, 98. (b) Jeffrey, G. J.; Ruble, J. R.; McMullan, R. K.; Pople, J. A. *Proc. R. Soc. London, Ser. A*, **1987**, *414*, 47. (c) Boden, N.; Davis, P. P.; Stam, C. H.; Wesselink, G. A. *Mol. Phys.*, **1973**, *25*, 81.

35. (a) Mulliken, R. S. *J. Am. Chem. Soc.*, **1952**, *74*, 811. (b) Mulliken, R. S;. Person, W. B.*J. Am. Chem. Soc.*, **1969**, *91*, 3409. (c) Foster, R. *Organic Charge-Transfer Complexes*, **1969**, Academic Press: London.

36. Dunitz, J. D. in *The Crystal as a Supramolecular Entity,* Desiraju, G. R. Ed.; **1996**, John Wiley & Sons: Chichester; p. 1-30.

37. (a) Dougherty, D. A. *Science*, **1996**, *271*, 163. (b) Ma, J. C.; Dougherty, D. A. *Chem. Rev.*, **1997**, *97*, 1303.

38. Hunter, C. A.; Lu, X.; Kaptejn, G. M.; van Koten, G. *J. Chem. Soc., Faraday Trans.*, **1995**, *91*, 2009.

39. (a) Raasch, M. S. *J. Org. Chem.*, **1979**, *44*, 2629. (b) Fujita, M.; Nagao, S.; Iida, M.; Ogata, K.; Ogura, K. *J. Am. Chem. Soc.*, **1993**, *115*, 1574. (c) Fujita, M.; Ibukuro, F.; Hagihara, H.; Ogura, K. *Nature*, **1994**, *367*, 720. (d) Gillard, R. E.; Stoddart, J. F.; White, A. J. P.; Williams, B. J.; Williams, D. J. *J. Org. Chem.*, **1996**, *61*, 4504. (e) Ashton, P. R.; Boyd, S. E.; Claessens, C. G.; Gillard, R. E.; Menzer, S.; Stoddart, J. F.; Tolley, M. S.; White, A. J. P.; Williams, D. J. *Chem. Eur. J.*, **1997**, *3*, 788. (f) Ballardini, R.; Balzani, V.; Credi, A.; Brown, C. L.; Gillard, R. E.; Montalti, M.; Philp, D.; Stoddart, J. F.; Venturi, M.; White, A. J. P.; Williams, B. J., Williams, D. J. *J. Am. Chem. Soc.*, **1997**, *119*, 12503.

40. Coates, G. W.; Dunn, A. R.; Henling, L. M.; Dougherty, D. A.; Grubbs, R. H. *Angew. Chem. Int. Ed. Engl.*, **1997**, *36*, 248.

41. For review articles, see: (a) Dahl, T. *Acta Chem. Scand.*, **1988**, *A42*, 1. (b) Dahl, T. *Acta Cryst.*, **1990**, *B46*, 283. (c) Dahl, T. *Acta Chem. Scand.*, **1994**, *48*, 95.

42. (a) Naae, D. G. *Acta Cryst.*, **1979**, *B35*, 2765. (b) Pirtle, S. L.; Naae, D. G. *Am. Cryst. Assoc., Ser. 2*, **1980**, *7*, 10.

43. Potenza, J.; Mastropaolo, D. *Acta Cryst.*, **1975**, *B31*, 2527.

44. Foss, L. I.; Syed, A.; Stevens, E. D.; Klein, C. L. *Acta Cryst.*, **1984**, *C40*, 272.

45. Bruce, M. I.; Snow, M. R.; Tiekink, E. R. T. *Acta Cryst.*, **1987**, *C43*, 1640.

46. (a) Lin, T.; Naae, D. G. *Tetrahedron Lett.*, **1978**, *19*, 1653-1656. (b) Brock, C. P.; Naae, D. G. *Acta Cryst.* **1978**, *B34*, 3691-3696.

47. Li, A.; Bin, X.; Zhu, S.; Huang, Q.; Liu, J. *J. Fluorine Chem.*, **1994**, *68*, 145.

48. Marridis, A.; Moustakali-Mavridis, I. *Acta Cryst.* **1977**, *B33*, 3612.

49. Liberles, A.; Matlosz, B. *J. Org. Chem.* **1971**, *36*, 2710.

50. Okuyama, K.; Hasegawa, T.; Ito, M.; Mikami, N. *J. Phys. Chem.* **1984**, *88*, 1711.

51. Espiritu, A. A.; White, J. G. *Z. Krist.* **1978**, *147*, 177.

52. Abramenkov, A. V.; Almenningen, A.; Cyvin, B. N.; Jonvik, T.; Khaikin, L. S.; Rømming, C.; Vilkov, L. V. *Acta Chem. Scand.* **1988**, *A42*, 674.

53. Goodhand, N.; Hamor, T. A. *Acta Cryst.* **1979**, *B35*, 704.

54. Desiraju, G. R.; Krishna, T. S. R. *J. Chem. Soc., Chem. Commun.* **1988**, 192.

55. Kataigorodski, A. I. *Molecular Crystals and Molecules*, Academic Press: New York, **1973**, p. 33.

56. Howard, J. A. K.; Hoy, V. J.; O'Hagan, D.; Smith, G. T. *Tetrahedron*, **1996**, *53*, 12613.

57. Dunitz, J. D.; Taylor, R. *Chem. Eur. J.* **1997**, *3*, 89.

58. Evans, T. A.; Seddon, K. R. *Chem. Commun.* **1997**, 2023.

59. C & E News, December 16, **1996**, p. 33.

60. (a) Gray, G. W., Ed.; *Thermotropic Liquid Crystals*, **1987**, John Wiley & Sons: Chichester.

(b) Collings, P. J. *Liquid Crystals, Nature's Delicate Phase of Matter*, **1990**, Princeton University Press: Princeton,.

61. (a) Flory, P. J. *Adv. Polym. Sci.* **1984**, *59*, 1. (b) Singh, U. P.; Singh, Y. *Phys. Rev.* **1986**, *A33*, 2725. (c) Chick, L. A.; Viney, C. *Mol. Cryst. Liq. Cryst.* **1993**, *226*, 25.

62. (a) For a recent review, see: Paleos, M.; Tsiourvas, D. *Angew. Chem. Int. Ed. Engl.* **1995**, *34*, 1696. (b) For a recent example, see: Palmans, A. R. A.; Vekemans, J. A. J. M.; Fisher, F.; Hikmet, R. A.; Meijer, E. W. *Chem. Eur. J.* **1997**, *3*, 300.

63. Bahadur, B., Ed.; *Liquid Crystals - Applications and Uses*; **1990**, World Scientific: Singapore, Vol.1.

64. Xu, Y.; Hu, Y.; Chen, Q.; Wen, J. *J. Mater. Chem.*, **1995**, *5*, 219.

Chapter 4

B-B Oxidative Addition to Low Valent Transition Metal Complexes

4.1 Introduction

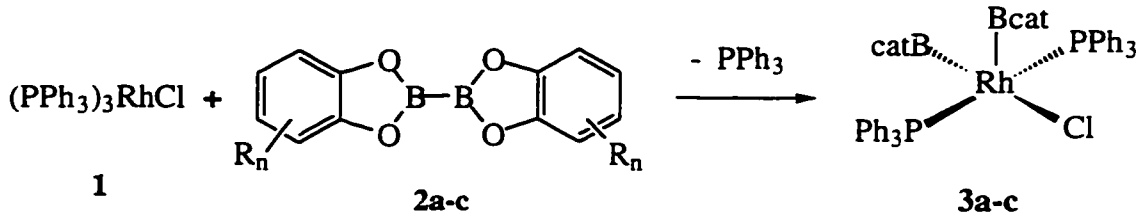
4.1.1 Transition Metal Boryl Complexes

The chemistry of transition metal boryl complexes is currently an active area of research owing to their significant applications in transition metal catalyzed B-H [1,2] and B-E (E= B[3], Si[4], Sn[5], S[6]) additions to unsaturated organic substrates and related organoborane generating processes.[7,8] These compounds are characterized by the presence of a BX_2 group bound to a mononuclear transition metal center (X = H, halogen, organo, amino, alkoxy, sulfido groups). It is remarkable that no metal compounds of boron (either transition metal or not) were known up to about 1960. In the 1960's, German chemists H. Nöth and G. Schmid started to synthesize different kinds of metal boryl compounds, all with transition metals except Sn. A review on this early period of studies appeared in 1970 by Schmid[9], and most of the compounds were poorly characterized and thus their authenticity was in question. It is interesting to note that there were few contributions from 1970 until 1985 when Männig and Nöth[10] discovered the transition-metal-catalyzed alkene hydroboration reaction using Wilkinson's catalyst [$Rh(PPh_3)_3Cl$] (1) with HBCat (Cat = 1,2-$O_2C_6H_4$). This discovery resulted from a clever combination of two earlier reported processes, namely the oxidative addition of HBcat to Wilkinson's catalyst[11] and the Rh(I) catalyzed addition of polyhedral boranes to alkenes.[12] Since then, intense studies in this area have been conducted, both in the applications to organic synthesis and in defining the transition metal's role in the catalyzed reactions. In the past three to four years, we have been particularly interested in the metal catalyzed diborations of alkenes and alkynes.[3a-d] A key step in this process

is believed to be the B-B oxidative addition to low valent transition metal complexes. Thus, in this chapter, we will focus on our results on the B-B oxidative addition to some group 9 metal (Co, Rh, Ir) complexes, and the structural studies of the resulting metal boryl complexes.

4.1.2 B-B Oxidative Addition to Transition Metal Complexes

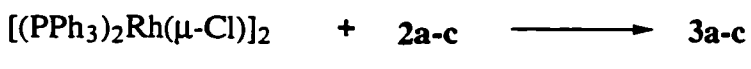
We have recently reported that B_2cat_2 and related diboron compounds (**2a-c**) underwent clean and facile reactions with Wilkinson's catalyst **1** or its dimer $[Rh(PPh_3)_2Cl]_2$ (**4**) at room temperature to generate the corresponding Rh(III) bis(boryl) complexes $[Rh(PPh_3)_2Cl(Bcat^*)_2]$ (**3a-c**) in quantitative yield (Reactions **4.1**, **4.2**).[13]



1 **2a-c** **3a-c**

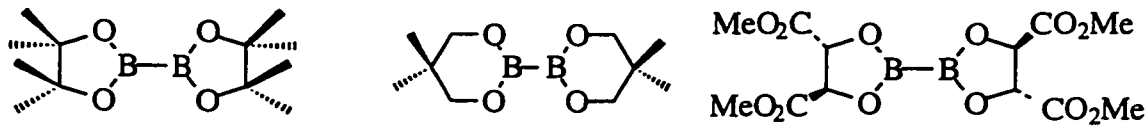
2a: $R_n=H_4$
2b: R_n=4-Bu^t-3,5,6-H_3
2c: R_n=3,5-Bu$^t_2$-4,6-H_2

(4.1)



4

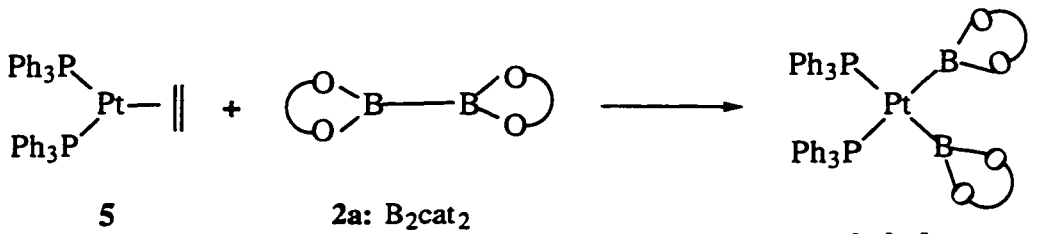
(4.2)



2d **2e** **2f**

Reaction of **2a** with **4** in CH_2Cl_2 was complete in *ca.* 10 min, whereas the analogous reaction involving **2b** took ca. 1.25 h. Interestingly, no reaction was observed when pure B_2pin_2 (pin = $OC(CH_3)_2C(CH_3)_2O$, **2d**) or B_2neop_2 (neop = $OCH_2C(CH_3)_2CH_2O$, **2e**) was treated with **4** at room temperature, even though B_2cat_2 demonstrated a *shorter* B-B bond distance than B_2pin_2 in the solid state. [13,14] On the other hand, compound **2f** with the electron withdrawing group CO_2Me does show reactivity toward complex **4**, but the reaction is notably slower, and it does not go to completion in 3 h. Clearly the reactivity of the tetrakis(alkoxy) diboron compounds is considerably lower than that of the catecholate analogs.

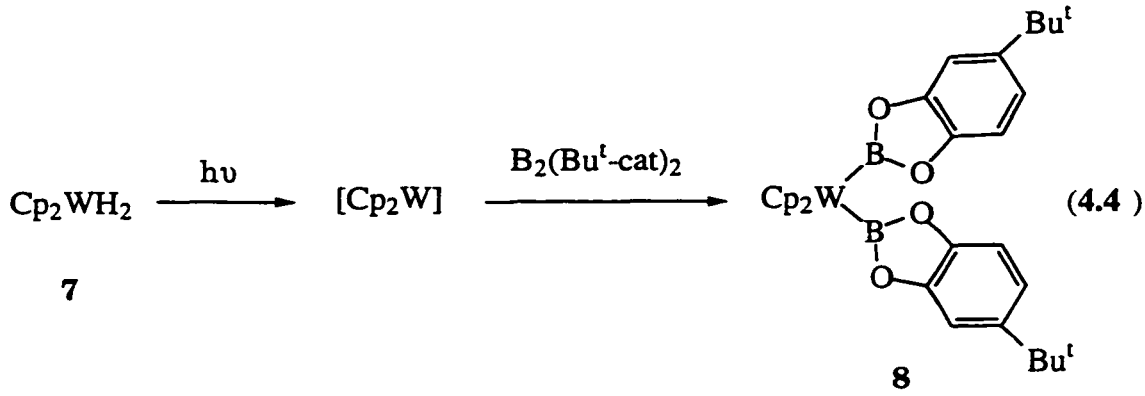
However, it has been demonstrated by us[3b] and others[3d,15] that Pt(0) phosphine complexes such as $[Pt(PPh_3)_2(\eta^2\text{-}C_2H_4)]$ (**5**) or $[Pt(PPh_3)_4]$ can react with not only B_2cat_2 analogs but also with B_2pin_2 (Reaction **4.3**). Nevertheless, the different reactivity was also obvious in that **2a** and **2b** can react readily with **5** upon mixing in toluene at ambient temperature where **5** does not react completely with **2d** in $CDCl_3$ or C_6D_6 after 12 hours. Other Pt(II) bis(boryl) complexes were obtained in a similar fashion from $[Pt(diphos)(\eta^2\text{-}C_2H_4)]$ where diphos is a chelating phospine ligand.



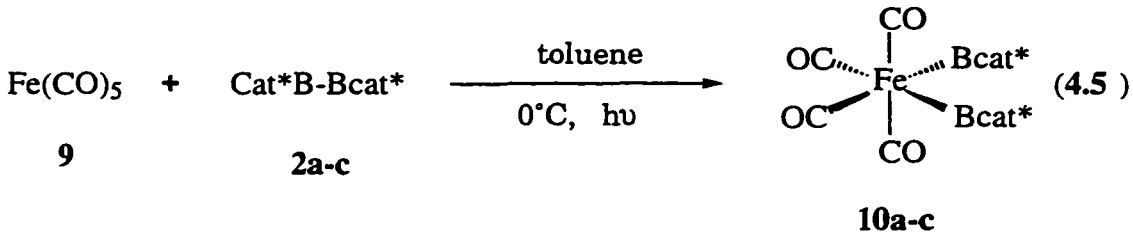
5 **2a:** B_2cat_2 **2b:** $B_2(4\text{-}Bu^t\text{-}cat)_2$ **2d:** B_2pin_2 **6a,b,d** (**4.3**)

B-B oxidative additions are not only restricted to Rh(I) and Pt(0) complexes. Very recently, Hartwig *et al.* have observed[16] oxidative addition of B_2cat_2 or $B_2(4\text{-}Bu^tcat)_2$ to $[Cp_2W]$ and $[Fe(CO)_4]$ fragments (Reactions **4.4**, **4.5**). These electronically

and coordinately unsaturated species were generated by UV irradiation with the loss of H_2 and CO, respectively.



7 **8** (**4.4**)



9 **2a-c** **10a-c** (**4.5**)

4.1.3 Other Routes to Metal Bis(boryl) Complexes

$[Fe(CO)_4(Bcat^*)_2]$ complexes (**10a-c**) could also be synthesized from the reactions of $Na_2[Fe(CO)_4]$ (**11**) with 2 equivalents of ClBcat* at 20°C in toluene (Reaction **4.6**).[16c] It was reported that the reactions needed to be conducted in hydrocarbon solvents. The yields of these reactions depended heavily on the purity of the metal dianion and the amount of THF contained in the solid Collman reagent, since the presence of THF lead to significant decomposition of the products. Previously,[17] reactions involving $Na_2[Fe(CO)_4]$ were reported to yield only $[Fe(CO)_4]_3$ as the predominant product. The real factor which THF played here is not clear yet, but we

have also observed in numerous cases that THF solvent can cause the decomposition of many other transition metal boryl complexes.

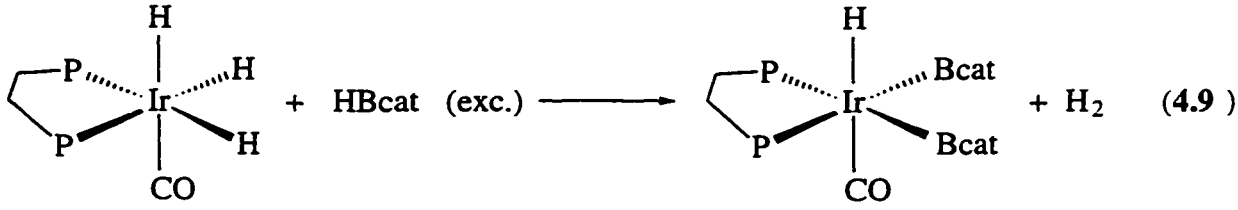
$$Na_2[Fe(CO)_4] + ClBcat^* \rightarrow [Fe(CO)_4(Bcat^*)_2] + 2\,NaCl \qquad (4.6)$$

Although Rh(III) bis(boryl) complex $[Rh(PPh_3)_2Cl(Bcat)_2]$ (**3a**) can be obtained very easily from the oxidative addition of B_2cat_2 to Wilkinson's catalyst, it was actually firstly reported from the reaction of $[Rh(PPh_3)_3Cl]$ with excess HBcat.[18] The HBcat oxidative addition product $[Rh(PPh_3)_2HClBcat]$ (**12**) can react further with HBcat to generate this bis(boryl) product with the elimination of H_2 gas. (Reaction **4.8**).

$$Rh(PPh_3)_3Cl + HBcat \rightarrow Rh(PPh_3)_2HClBcat + PPh_3 \qquad (4.7)$$

$$Rh(PPh_3)_2HClBcat + HBcat \rightarrow Rh(PPh_3)_2Cl(Bcat)_2 + H_2 \qquad (4.8)$$

Likewise, $[IrH(Bcat)_2(CO)(dppe)]$ (dppe = $Ph_2PCH_2CH_2PPh_2$) (**13**) was also observed by NMR spectroscopy in the reaction of *fac*-$[IrH_3(CO)(dppe)]$ (**14**) with excess HBcat[19] (Reaction **4.9**).



(4.9)

There were several early reports on the synthesis of Co bis(boryl) complexes by Schmid and Nöth, although none were prepared via B-B oxidative addition, and none were well characterized. Thus, these authors reported [20-22] that the reaction of Y_2BX with $[Co(dppe)_2(H)]$ (**15**) gave the 19-electron Co(II) bis(boryl) complexes *trans*-$[Co(dppe)_2(BR_2)_2]$ (**16**) (Reaction **4.10**). Compounds given by the formula, $[Co(Me_2P$-

o-C_6H_4-$PMe_2)_2(BR_2)_2$] (R = Ph, $R_2 = C_{12}H_8$)[21] (**17**) were also reportedly prepared by similar routes.

$$2\ Y_2BX + Co(dppe)_2(H) \rightarrow \textit{trans}\text{-}Co(dppe)_2(BR_2)_2 + Co(dppe)_2X_2 + H_2 \qquad \textbf{(4.10)}$$

X = Cl, Br, I; Y = Br, I, Ph; $Y_2B = Ph_2B$, PhClB; $Y_2B = C_{12}H_8B$

Utilizing these cobalt "boryl transfer reagents" they claimed to have prepared two Ni(II) bis(boryl) compounds [$Ni(dppe)_n(BPh_2)_2$] (n = 1, 2) (**18**) (Reaction **4.11**).

$$Co(dppe)_2(BPh_2)_2 + Ni(dppe)_nBr_2 \rightarrow Co(dppe)_2Br_2 + Ni(dppe)_n(BPh_2)_2$$

$$n = 1, 2 \qquad \textbf{(4.11)}$$

The interest in these Co(II)-bis(boryl) derivatives resulted from the unique reactivity displayed in σ-bond metathesis reactions, which were used to prepare several metal boryl derivatives that were virtually inaccessible by other routes about 30 years ago.

In recent years, σ-bond metathesis reactions are no longer an uncommon phenomenon with transition metal boryl complexes. Thus, the Rh(III) bis(boryl) complexes [$Rh(PPh_3)_2Cl(Bcat)_2$] (**3a**) reacts with other diboron reagent such as $B_2(Bu^t_2cat)_2$ (**2c**) affording unsymmetrical metal bis(boryl) [$Rh(PPh_3)_2Cl(Bcat)(BBu^t_2cat)$] (**19**) and mixed diboron compound catB-$B(Bu^t_2cat)$ (**2g**) (Reaction **4.12**). This reaction was proposed to proceed through the σ-bond metathesis mechanism.[23]

$$Rh(PPh_3)_2Cl(Bcat)_2 + B_2(Bu^t_2cat)_2 \rightarrow Rh(PPh_3)_2Cl(Bcat)(Bu^t_2cat) + catB\text{-}B(Bu^t_2cat) \qquad \textbf{(4.12)}$$

Nonetheless, treating [$Pt(PPh_3)_2(Bpin)_2$] (**6d**) with B_2cat_2 gave only [$Pt(PPh_3)_2(Bcat)_2$] (**6a**) and B_2pin_2 (Reaction **4.13**). Neither mixed Pt (II) bis(boryl) [$Pt(PPh_3)_2(Bpin)(Bcat)$] nor mixed diboron compound pinB-Bcat was detected, which implies the reversibility of the B-B oxidative addition [3g] rather than the above-mentioned σ-bond metathesis mechanism.

$$Pt(PPh_3)_2(Bpin)_2 + B_2cat_2 \rightarrow Pt(PPh_3)_2(Bcat)_2 + B_2pin_2 \quad (4.13)$$

4.1.4 Our Objectives

In this chapter, the B-B oxidative addition to some low valent group 9 metal (Co, Rh, Ir) complexes with PMe_3 ligand will be examined. Trimethylphospine is the smallest and yet one of the most electron rich ligands in the phosphine family, thus, the resulting metal boryl complexes are expected to be important as model compounds not only for the catalytic activity studies but also for theoretical calculations.

4.2 Results and Discussion

4.2.1 B-B oxidative Addition to [Co(PMe$_3$)$_4$]

B_2cat_2 (**2a**) underwent a facile reaction with the Co(0) complex [Co(PMe$_3$)$_4$][24] (**20**) when they ware mixed in THF yielding the yellow, formally Co(II), 17-electron complex [Co(PMe$_3$)$_3$(Bcat)$_2$] (**21**) in 60% yield (Reaction **4.14**).

$$Co(PMe_3)_4 + B_2cat_2 \rightarrow Co(PMe_3)_3(Bcat)_2 + PMe_3 \qquad (\mathbf{4.14})$$

Consistent with the complex being paramagnetic, no resonances were observed in either the $^{11}B\{^1H\}$ or $^{31}P\{^1H\}$ NMR spectra of **21**. Elemental analysis was consistent with the presence of three PMe$_3$ ligands in addition to the two Bcat groups. Single crystals suitable for X-ray diffraction were grown from hexane. This compound crystallized in an orthorhombic system, space group Pbca, a = 17.127(5), b = 15.303(4), c = 20.545(6) Å, U = 5385(2) Å^3. The molecular structure of **21** is shown in Figure **4.1**. The Co1 - B1 distance = 1.945(11) and Co1 - B2 = 1.970(11) Å. The Co-P distances, which average 2.214(3) Å, (Co1 - P1 = 2.203(3), Co1 - P2 = 2.233(3) and Co1 - P3 = 2.205(3) Å) show a small variation with Co1 - P2 being 0.03 Å longer than the other two which are quite similar. It seems likely that the slight lengthening of the Co1-P2 bond is due to the fact that the PMe$_3$ group involving P2 is more sterically hindered than the other two PMe$_3$ groups.

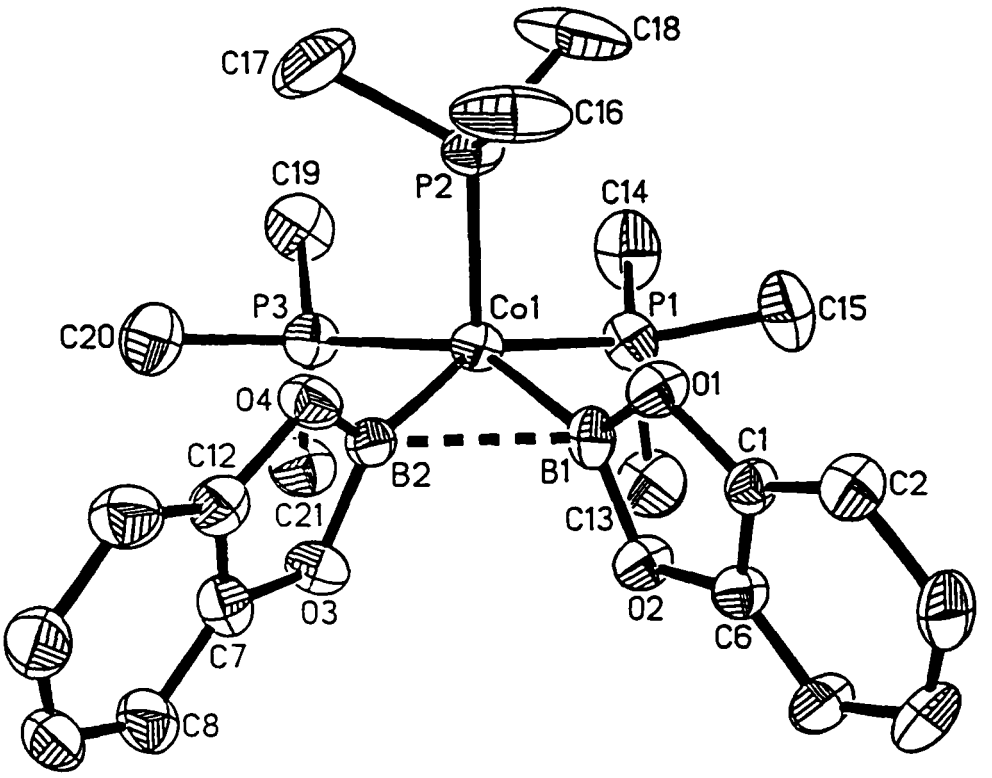


Figure 4.1 Projection of the molecular structure of **21** showing the atom numbering scheme and illustrating the distorted square-pyramidal description of the coordination environment. Hydrogen atoms are omitted for clarity. Selected bond distances (Å) and angles (°) for 21: Co(1) - B(1) = 1.945(11), Co(1) - B(2) = 1.970(11), Co(1) - P(1) = 2.203(3), Co(1) - P(2) = 2.233(3), Co(1) - P(3) = 2.205(3), B(1) - O(1) = 1.422(12), B(1) - O(2) = 1.426(12), B(2) - O(3) = 1.428(12), B(2) - O(4) = 1.437(12), B(1) - Co(1) - B(2) = 67.9(4), P(1) - Co(1) - P(2) = 104.3(1), P(1) - Co(1) - P(3) = 104.0(1), P(1) - Co(1) - B(1) = 89.0(3), P(1) - Co(1) - B(2) = 148.8(3), P(2) - Co(1) - P(3) = 101.1(1), P(2) - Co(1) - B(1) = 100.5(3), P(2) - Co(1) - B(2) = 100.4(3), P(3) - Co(1) - B(1) = 151.3(3) and P(3) - Co(1) - B(2) = 89.4(3).

Of particular interest is the B1 - Co1 - B2 angle of 67.9(4)° which gives rise to a B1 - B2 separation of only 2.185 Å. Although a small B1 - Pt1 - B2 angle of 77.1(2)° has been observed[3b] (77.8(7)° in ref.(15)) in the solid-state structure of *cis*-[$Pt(PPh_3)_2(Bcat)_2$] (**6a**), none as small as 67.9° has been found previously. The B-B bond distance[13] in B_2cat_2 of 1.678(3) Å is at the short end of the usual range for a B-B bond,[25] and the B-B separation in **21** is only 0.507 Å longer than this value suggesting the possibility of some remaining B-B interaction. Thus, the B1-B2 separation in **21** is only 0.212 Å longer than that for the peripheral B4'-B1 bond in decaborane(14) which was shown[26] to be 1.973 Å from a neutron diffraction study of $^{11}B_{10}{}^2H_{14}$ carried out at -160°C. The sum of the angles about B1 (359.3°) and B2 (359.5°) in **21** indicate clearly a trigonal planar environment about each boron, yet conjugation with the catecholato π-system will introduce electron density into the boron p_z-orbitals. The angles between the Co1 - B1 - B2 plane and B1 - O1 - O2 (88.8°) and B2 - O3 - O4 (86.5°) planes are quite similar, thus the two Bcat π-systems are facing each other with the closest approach being that of the two boron p_z-orbitals.

It is possible to describe the overall structure as a distorted square pyramid with P2 at the apical site and Co1 lying 0.0427 Å above the least-squares plane defined by P1, P3, B1 and B2 (deviations of these four atoms are 0.015, -0.015, -0.024 and 0.024 Å respectively). However, the close approach of the two boron atoms suggests the possibility that the $(Bcat)_2$ unit should be considered as a single ligand. Interestingly, the geometry of the [$Co(PMe_3)_3$] fragment in **21** (Figure **4.2**, top) is quite similar to that found in the Co(I) complex [$Co(PMe_3)_3Cl$] (**22**) which has been structurally characterized previously[27] at room temperature, and in this study[28], at 200 K (Figure **4.2**, bottom). The two structures of **22** are similar, and as the present one is more accurate, it is included here and used in the following discussion. In compound **22**, the Co1 and Cl1 atoms lie on a crystallographic 3-fold axis so that there is only one unique PMe_3 group.

The Co1 - P1 distance of 2.232(1) Å is only 0.018 Å longer than the average value in **21**, whereas the P - Co - P angles in **22** are all 104.5(1)° which is quite similar to the average P - Co - P angle of 103.1(1)° in **21**. Thus, complex **21** could be considered to have a distorted tetrahedral geometry in which the two boryl ligands occupy a single coordination site.[29] The degree of interaction between the two Bcat groups is not clear at this time; however, complex **21** may be viewed as lying part way along an oxidative addition reaction coordinate, with the possibility of some B-B interaction still of being present.

The reactivities of this novel Co(II) bis(boryl) complex have not been fully examined yet. However, when **21** was treated with $[Rh(PMe_3)_4]Cl$ (**23**) in hot hexane, a new Rh(I) boryl complex $[Rh(PMe_3)_4Bcat]$ (**24**) was generated which was characterized spectroscopically (see Section **4.2.3**).

$$Co(PMe_3)_3(Bcat)_2 + 2\ [Rh(PMe_3)_4]Cl \rightarrow Co(PMe_3)_3Cl_2 + 2\ Rh(PMe_3)_4Bcat \quad (\mathbf{4.15})$$

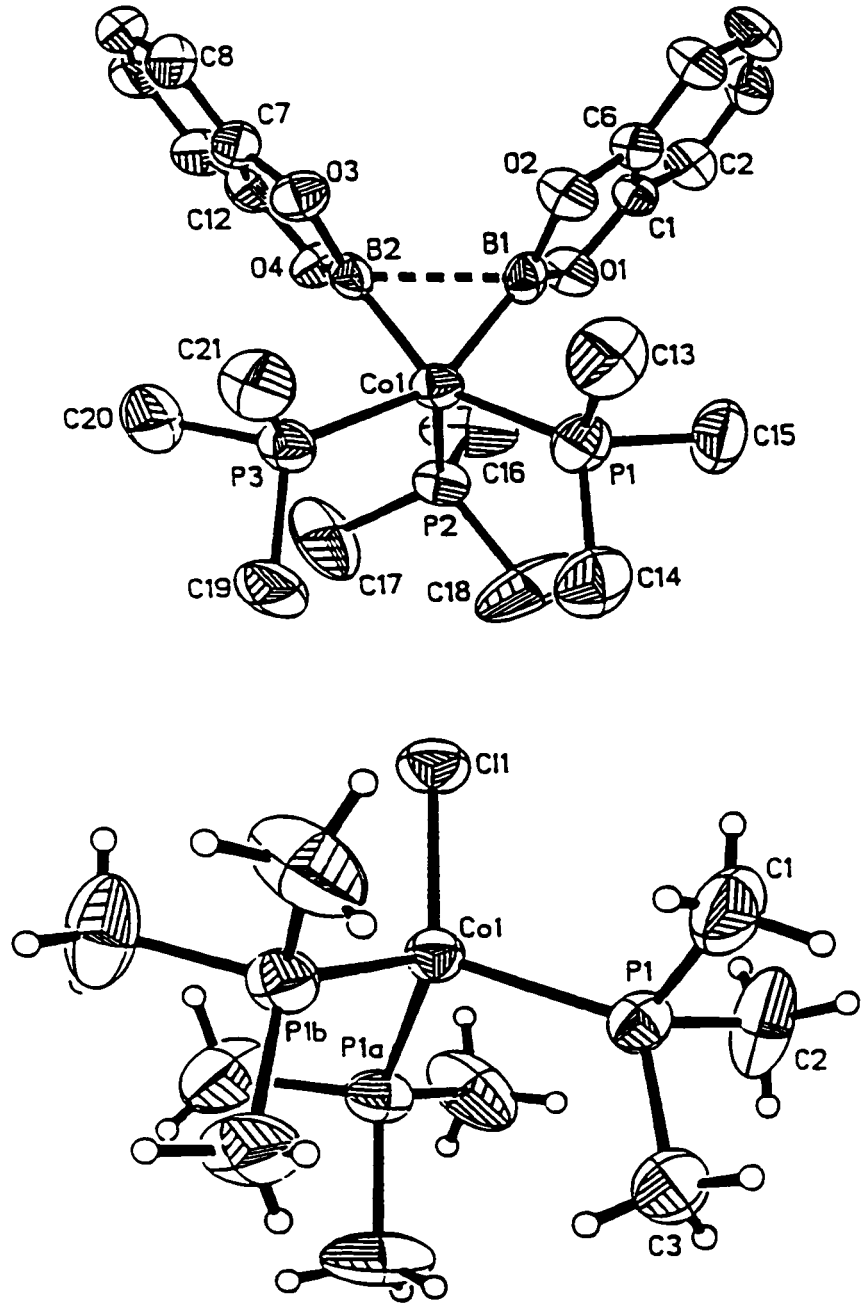
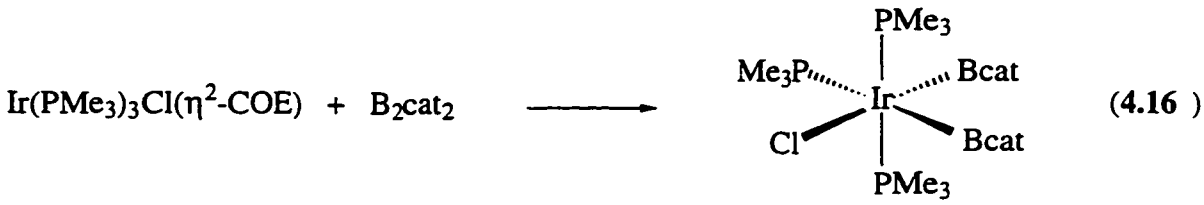


Figure 4.2 Projection of the molecular structure of **21** (top) illustrating the distorted tetrahedral description of the coordination environment. Projection of the molecular structure of **22** (bottom) with hydrogen atoms omitted for clarity. Selected bond distances (Å) and angles (°) for **22**: Co(1) - P(1) = 2.232(1), Co(1) - Cl(1) = 2.226(2), Cl(1) - Co(1) - P(1) = 114.1(1) and P(1) - Co(1) - P(1A) = 104.5(1).

4.2.2 B-B Oxidative Addition to [Ir(PMe$_3$)$_3$Cl(COE)]

Addition of B_2cat_2 to a THF solution of [Ir(PMe$_3$)$_3$Cl(COE)] (COE = *cis*-cyclooctene, **25**) at room temperature results in complete conversion (90% isolated yield) to the iridium bis(boryl) complex [Ir(PMe$_3$)$_3$Cl(Bcat)$_2$] (**26**) (Reaction **4.16**). The solution structure of **26** was established by ^{1}H, ^{13}C{^{1}H}, ^{31}P{^{1}H} and ^{11}B{^{1}H} NMR spectroscopy, and its solid state structure was confirmed by a single-crystal X-ray diffraction study on crystals grown by layering hexane over a CH_2Cl_2 solution.



(**4.16**)

The ^{31}P{^{1}H} NMR spectrum of **26** displays a doublet at -40.9 ppm ($^2J_{p-p}$ = 27.5 Hz) and a broad peak at -50.8 ppm in 2:1 ratio (Figure **4.3**). The latter broad signal clearly indicates that one phosphine ligand is *trans* to a boryl group and the resonance is influenced by the boron nucleus (^{11}B, spin 3/2, 80.4% natural abundance; ^{10}B, spin 3, 19.6% natural abundance) as the resonance of the spin 1/2 nucleus in the *trans* position will display significant broadening due to quadrupolar coupling.[30] The ^{11}B{^{1}H} NMR spectrum (Figure **4.4**) clearly displays two well separated resonances at 32.6 and 41.7 ppm, respectively, in which the first signal is consistent with a Bcat group *trans* to chloride as shown in other Ir(III) boryl complexes [Ir(PMe$_3$)$_3$(Cl)(H)(Bcat)] (**27**) (δ 32.8 ppm)[31] and [Ir(PEt$_3$)$_3$(Cl)(H)(Bcat)] (**28**) (δ 33.5 ppm),[32] while the other resonance at 41.7 ppm is quite close to the value of δ 44.7 ppm in an iridium tris(boryl) complex *fac*-[Ir(PEt$_3$)$_3$(Bcat)$_3$] (**29**) [33] in which the boryl groups are all *trans* to the phosphine ligands.

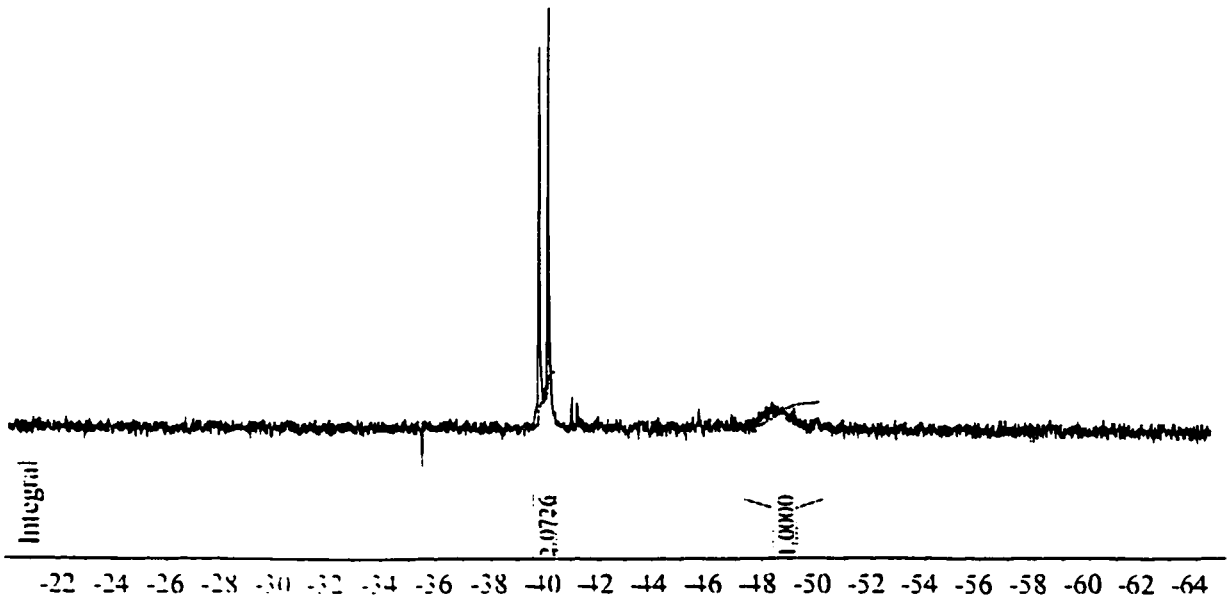


Figure 4.3 $^{31}P\{^{1}H\}$ NMR spectrum of **26** in $CDCl_3$

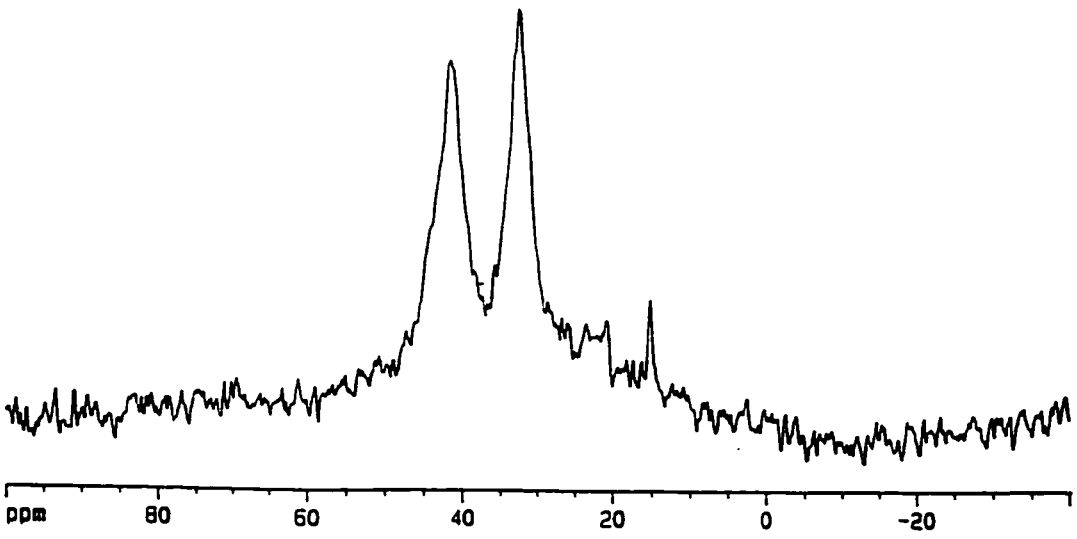


Figure 4.4 $^{11}B\{^{1}H\}$ NMR spectrum of **26** in $CDCl_3$

Also in the ^1H NMR spectrum, four sets of catecholate proton resonances are observed at (7.07, 6.76), (7.12 and 6.83) ppm, and six carbon resonances are observed at (110.53, 120.7, 149.84), (115.58, 120.76 and 150.03) ppm in $^{13}C\{^1H\}$ NMR spectrum in $CDCl_3$. From these results, the structure of **26** can be assigned unambiguously as *mer-cis*-$[Ir(PMe_3)_3Cl(Bcat)_2]$, with one boryl group *trans* to chloride and the other *trans* to the unique trimethylphosphine ligand.

The structure of **26** is further confirmed by single crystal X-ray diffraction (Figure **4.5**) The molecular structure of **26** consists of an octahedral arrangement with *mer* phosphine ligands. The two catecholatoboryl groups are mutually *cis* with an unusually large B-Ir-B angle of 91.6 (2)° *vide supra.* The two BO_2 planes of these boryl moieties are essentially perpendicular to one another. The boron *trans* to chloride has a iridium-boron distance of 2.024(6) Å, which is the same within statistical error as that in the compound *mer*-$[Ir(PMe_3)_3Cl(H)(Bcat)]$ (**27**) (2.023(10)Å) which was produced through the oxidative addition of the H-B bond in HBcat to **25**. [31] The other iridium-boron bond distance is 2.080(6) Å which is very close to the value of 2.093(7) Å in *fac*-$[Ir(PMe_3)_3H_2(BC_8H_{14})]$ (**29**) which was prepared from the reaction of $[Ir(PMe_3)_4H]$ with 9-BBN dimer and in which the BC_8H_{14} boryl group is *trans* to PMe_3. [32] These two Ir-B bond distances are in accordance with the fact that PMe_3 has a larger *trans* influence than Cl. For further comparison, the Ir-B bond in *trans*-$[Ir(PPh_3)_2Cl(CO)(H)(Bcat)]$ (**30**) is 2.045(5) Å where boron is *trans* to chloride.[33] Crabtree *et al.* reported [34] a novel Ir(IV) boryl complex $[Ir(PMe_3)_3(biphBF)Cl]BPh_4$ (**31**) prepared by the reaction of $[Ir(PMe_3)_3Cl(biph)]$ (biph = biphenyl-2,2-diyl) with $NOBF_4$. The molecular structure of $[Ir(PMe_3)_3(biphBF)Cl]^+$ was determined and the Ir-B bond distance was found to be 2.00(1) Å. The boryl group is *trans* to a phosphine ligand in this complex but unfortunately, the structure is not very accurate.

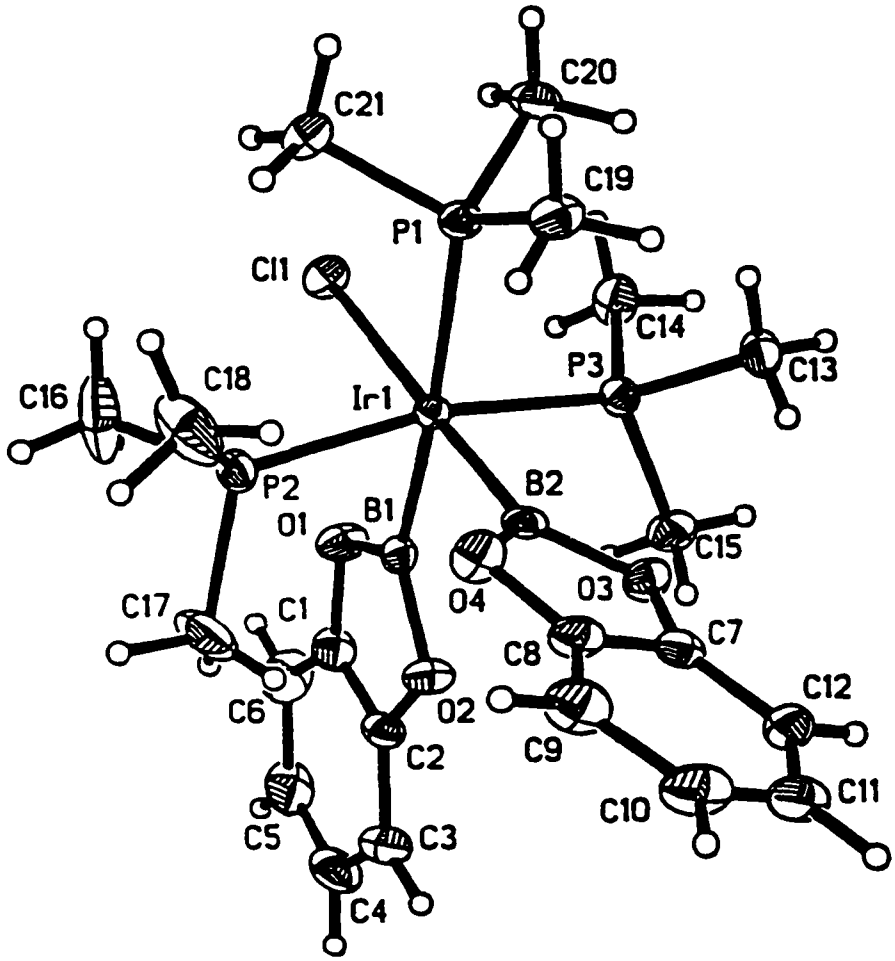


Figure 4.8. A view of the molecular structure of *mer-cis*-[Ir(PMe_3)$_3$Cl(Bcat)$_2$], (**26**) with thermal elipsoids at 50% probability. Selected bond distances (Å) and angles (°) for **26**: Ir(1) - B(1) = 2.080(6), Ir(1) - B(2) = 2.024(6), Ir(1) - P(1) = 2.3989(13), Ir(1) - P(2) = 2.3286(14), Ir(1) - P(3) = 2.3224(13), Ir(1) - Cl(1) = 2.5348(13), B(1) - Ir(1) - B(2) = 91.6(2), Cl(1)-Ir(1)-B(1) = 90.6(2), Cl(1)-Ir(1)-B(2) = 177.7(2), P(1) - Ir(1) - P(2) = 96.83(5), P(1) - Ir(1) - P(3) = 94.39(5), P(1) - Ir(1) - B(1) = 172.2(2), P(1) - Ir(1) - B(2) = 96.1(2), P(2) - Ir(1) - P(3) = 168.37(5), P(2) - Ir(1) - B(1) = 83.6(2), P(2) - Ir(1) - B(2) = 87.9(2), P(3) - Ir(1) - B(1) = 85.7(2) and P(3) - Ir(1) - B(2) = 87.9(2).

Among the Ir-P bond distances in complex **26**, the two mutually *trans* phosphine groups have Ir-P distances of 2.3286(14) and 2.3224(13) Å respectively, which are very similar to the two *trans* Ir-P distances in compound **27** (2.307(2) and 2.304(2) Å). However, the PMe_3 group *trans* to Bcat in **26** has a significantly longer Ir-P distance of 2.3989(13)Å while the PMe_3 group *trans* to hydride in complex **27** displays an Ir-B bond distance of only 2.351(2) Å. This suggests that the Bcat boryl group has a larger *trans* influence than PMe_3 and even hydride ligands, at least in this octahedral system.

Among recent structurally characterized metal bis(boryl) complexes, the above-discussed $[Co(PMe_3)_3(Bcat)_2]$ (**21**) is a paramagnetic compound with a distorted square pyramidal structure or it can be viewed as a distorted tetrahedron with the two boryl ligands occupying a single coordination site, while all Pt(II) bis(boryl) compounds, *cis*-$[Pt(PR_3)_2(Bcat)_2]$ (**6**), are four coordinate,[3b,3d,15] and Rh(III) bis(boryl) $[Rh(PPh_3)_2Cl(Bcat)_2]$ (**3a**) has a five coordinate, distorted square-pyramid configuration with one boryl group *trans* to Cl, the other *trans* to the vacant site.[13] The latter compound is fluxional in solution, giving only one broad signal in $^{11}B\{^1H\}$ NMR. Thus, compound **26**, *mer-cis*-$[Ir(PMe_3)_3Cl(Bcat)_2]$ is the first structurally characterized Ir bis(boryl) compound, and the first metal bis(boryl) complex with two distinct boryl group environments in solution.

4.2.3 B-B Oxidative Addition to [$Rh(PMe_3)_4Me$]

4.2.3.1. Syntheses of Rh(I) Boryl and Rh(III) Tris(boryl) Complexes

In order to study the reactivity of the M-B bond in low-valent, electron-rich, late metal boryl complexes, and to examine the reversibility of the B-B bond oxidative addition process, we sought to prepare a Rh(I) boryl complex. The only example of such a species to have been reported[22] is the poorly characterized species [$Rh(PPh_3)_3(BBr_2)$] (**32**), which was apparently obtained from the reaction of "[$Co(dppe)_2(BBr_2)_2$]" with [$Rh(PPh_3)_3Cl$]. Utilizing our newly prepared [$Co(PMe_3)_3(Bcat)_2$] (**21**) complex, we have observed the formation of the novel Rh(I) boryl complex [$Rh(PMe_3)_4(Bcat)$] (**24**) by $^{31}P\{^1H\}$ and $^{11}B\{^1H\}$ NMR spectroscopies. However, it could not be easily isolated and unambiguously identified. Our previous attempts to prepare Rh(I)-Bcat compounds directly *via* reactions of phosphine-Rh(I)-hydride and allyl precursors (e.g. [$Rh(PMe_3)_4H$] or [(dippe)Rh(η^3-2-Me-allyl)] (dippe = $^iPr_2PCH_2CH_2P^iPr_2$)) with HBcat[35,36] resulted in the formation of compounds such as $[Rh(PMe_3)_4]^+$, $[Rh(PMe_3)_4(H)_2]^+$ and the zwitterion [(dippe)Rh(η^6-catBcat)]. We reasoned that reaction of B_2cat_2 (**2a**) with [$Rh(PMe_3)_4Me$] (**33**) however, would likely lead to [$Rh(PMe_3)_4(Bcat)$] *via* oxidative addition of the B-B bond followed by rapid reductive elimination of MeBcat (**34**) (Reaction **4.17**), and the reactivities of other diboron compounds can also be tested.

$$\underset{\mathbf{33}}{Rh(PMe_3)_4Me} + \underset{\mathbf{2a}}{B_2cat_2} \xrightarrow[-PMe_3]{} \underset{\mathbf{35}}{Rh(PMe_3)_3(Me)(Bcat)_2}$$

$$\xrightarrow[-MeBcat\ (\mathbf{34})]{+PMe_3} \underset{\mathbf{24}}{Rh(PMe_3)_4(Bcat)} \qquad (\mathbf{4.17})$$

Indeed, when this reaction was conducted using a 1:1 molar ratio of **33:2a** in heptane, **24** and **34** were formed rapidly as evidenced by ^{1}H, $^{11}B\{^{1}H\}$, $^{13}C\{^{1}H\}$, and $^{31}P\{^{1}H\}$ NMR spectroscopy. The $^{11}B\{^{1}H\}$ spectrum in C_6D_6 showed a broad peak at δ 49.0 ppm which was assigned to the resulting Rh(I) mono(boryl) product **24** and a sharp peak at δ 35.2 ppm which was consistent with the presence of MeBcat [37] (Figure **4.6**). The presence of **34** in solution was confirmed additionally by ambient temperature vacuum transfer of all volatiles to a separate vessel and subsequent examination of these by GC/MS, which showed a peak at MS m/z 134 (M^+) with the expected isotope pattern. The isolated yields of **24** were 92-99%, but the material always contained a small amount (ca. 2% by NMR) of $[Rh(PMe_3)_4H]$ ($^{31}P\{^{1}H\}$, δ -18.86 (d, J_{Rh-P} 146)) due to its considerable moisture sensitivity. In one case, when the reaction was performed in C_6F_6, **24** free of $[Rh(PMe_3)_4H]$ was obtained.

Compound **24** is fluxional in solution as evidenced by the appearance of one doublet (-21.88 ppm, J_{Rh-P} = 137 Hz) in the room temperature $^{31}P\{^{1}H\}$ NMR spectrum which displays a sharp doublet of doublets (-22.03 ppm, J_{Rh-P} = 157, $^{2}J_{P-P}$ = 48 Hz, 3P) and a broader overlapped doublet of quartets (-13.21 ppm, J_{Rh-P} = 91, $^{2}J_{P-P}$ = 48 Hz, 1P) at 193 K (Figure **4.7**). The low temperature limiting spectrum indicates a trigonal bipyramidal geometry with the Bcat ligand occupying an axial site.

This structure was confirmed by single-crystal X-ray diffraction. Crystal data for (**24**): $C_{18}H_{40}BO_2P_4Rh$, M = 526.10, monoclinic, $P2_1/c$, a = 16.7763(12), b = 9.8236(7), c = 16.3714(12)Å, β = 103.728(2)°. A view of the molecular structure of **24** with selected bond distances and angles is given in Figure **4.8**. That the Bcat group prefers an axial rather than equatorial site suggests[37] strongly that it is a strong σ-donor and a poor π-acceptor (cf. $[(PMe_3)_4Rh(C{\equiv}CPh)]$)[38]; if Bcat were a strong π-acceptor, it would be expected to occupy an equatorial site and to lie perpendicular to the equatorial plane in such a d^8-ML_4-Bcat complex in order to maximize Rh→B π-bonding.

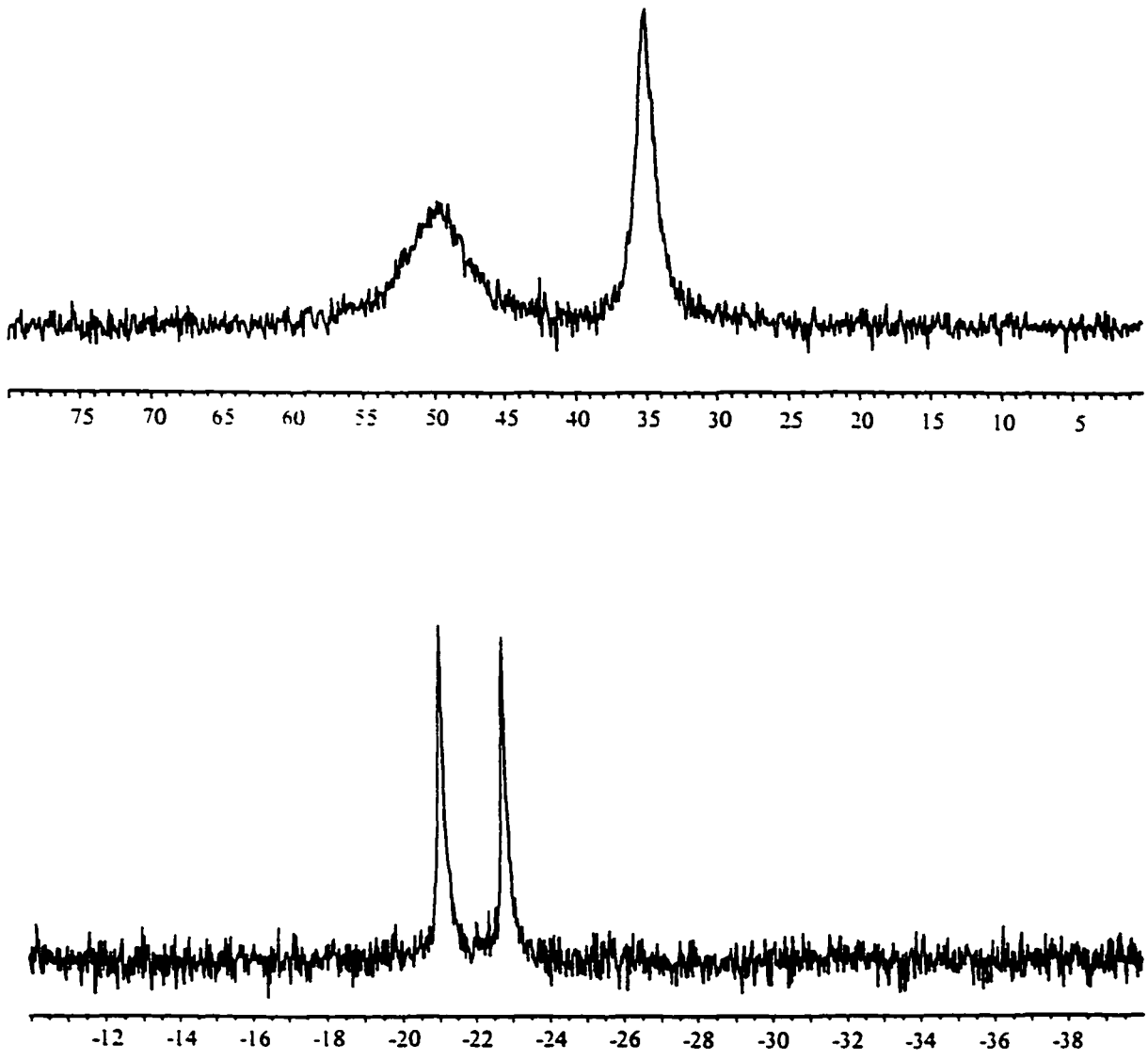


Figure 4.6 $^{11}B\{^1H\}$ and $^{31}P\{^1H\}$ spectra of $[Rh(PMe_3)_4Me] + B_2cat_2$ in C_6D_6

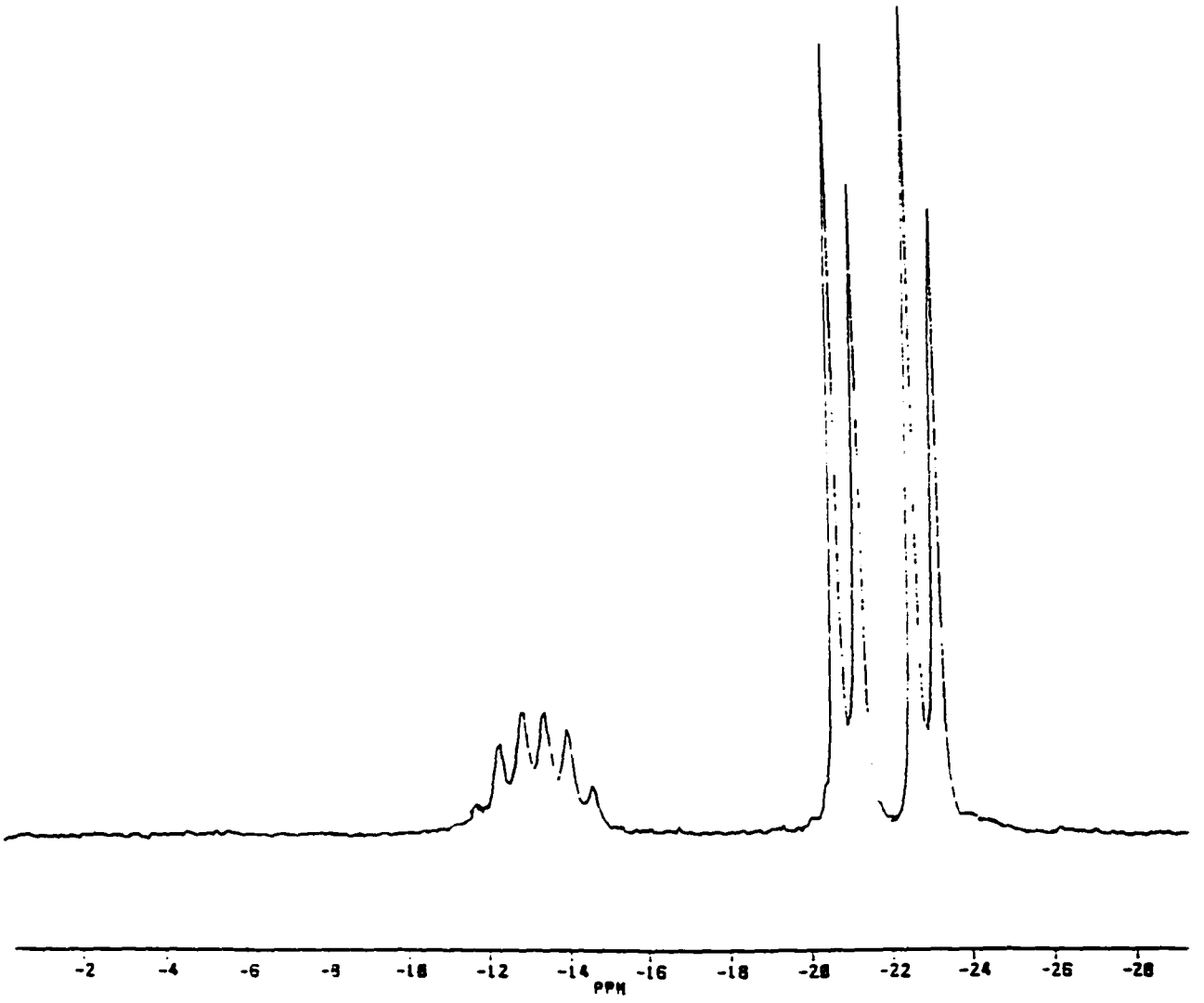


Figure 4.7 $^{31}P\{^{1}H\}$ spectrum of $Rh(PMe_3)_4(Bcat)$ at 193K

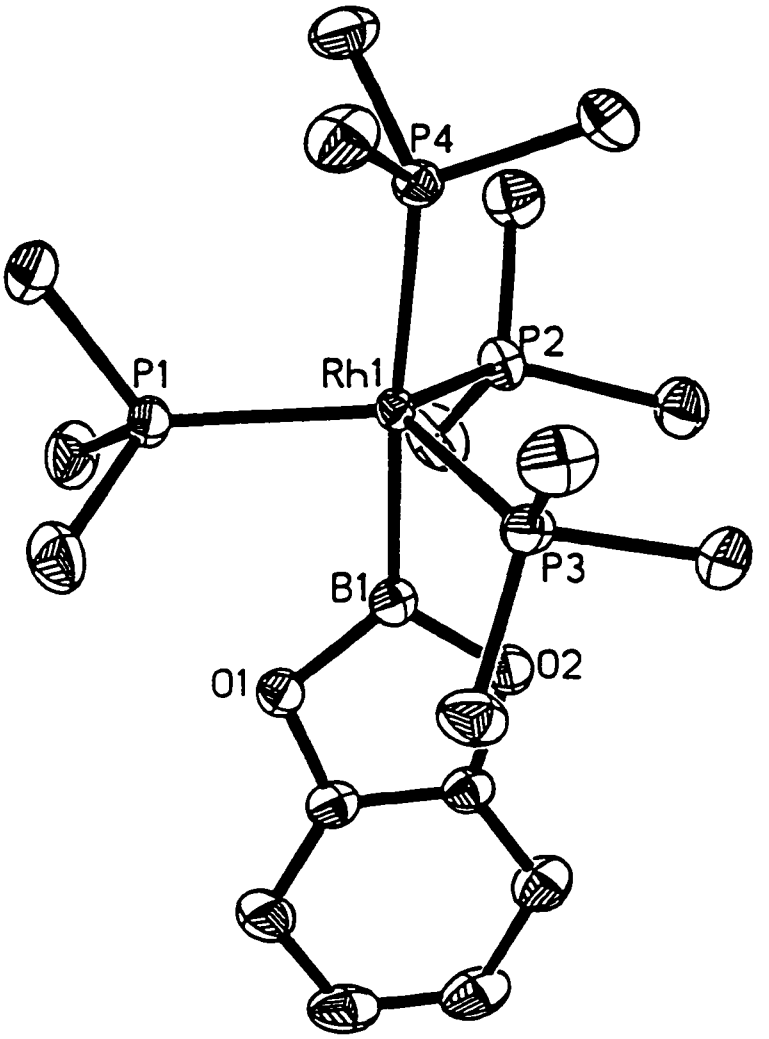


Figure 4.8. A view of the molecular structure of [Rh(PMe$_3$)$_4$(Bcat)] (**24**) with thermal elipsoids at 50% probability and H atoms omitted for clarity. Selected bond distances (Å) and angles (°): Rh(1)-B(1) = 2.047(2), Rh(1)-P(1) = 2.3049(6), Rh(1)-P(2) = 2.2891(6), Rh(1)-P(3) = 2.3096(6), Rh(1)-P(4) = 2.3404(6), B(1)-Rh(1)-P(1) = 87.32(7), B(1)-Rh(1)-P(2) = 83.07(7), B(1)-Rh(1)-P(3) = 80.39(7), B(1)-Rh(1)-P(4) = 174.74(7), P(4)-Rh(1)-P(1) = 97.30(2), P(4)-Rh(1)-P(2) = 96.74(2), P(4)-Rh(1)-P(3) = 95.09(2), P(1)-Rh(1)-P(2) = 119.53(2), P(1)-Rh(1)-P(3) = 119.51(2), P(2)-Rh(1)-P(3) = 117.30(2).

Reaction of **33** with two equiv. of **2a** generates the unusual tris(boryl) complex *fac*-[$Rh(PMe_3)_3(Bcat)_3$] (**36**) in quantitative yield with loss of one PMe_3 group and formation of **34** (Reaction **4.18**).

$$\underset{\mathbf{33}}{Rh(PMe_3)_4Me} + \underset{\mathbf{2a}}{B_2cat_2} \xrightarrow[\text{-MeBcat (34)}]{} \underset{\mathbf{24}}{Rh(PMe_3)_4(Bcat)}$$

$$\xrightarrow[\text{-}PMe_3]{+B_2cat_2} \underset{\mathbf{36}}{\textit{fac}\text{-}Rh(PMe_3)_3(Bcat)_3} \qquad (\mathbf{4.18})$$

The $^{31}P\{^1H\}$ NMR spectrum of the reaction products in C_6D_6 showed a broad doublet at δ -26.2 ppm corresponding to the Rh(III) tris(boryl) product [$Rh(PMe_3)_3(Bcat)_3$] as well as a sharp peak at δ -62.0 ppm for free PMe_3. The broad doublet did not sharpen even at 193K, which implies that all PMe_3 ligands are *trans* to Bcat. The $^{11}B\{^1H\}$ spectrum showed the characteristic peak for MeBcat at 35.1 ppm and one broad peak at δ 46.8 (Figure **4.9**). Compound **36** was obtained nearly quantitatively when **33** and 2 equiv. of **2c** were placed in heptane and stirred for 2 hours at room temperature. The resulting white precipitate was collected with sufficient purity. (Anal. Calcd for $C_{27}H_{39}B_3O_6P_3Rh$: C, 47.15; H, 5.71. Found: C, 47.80; H, 5.88.)

The only previously reported[39] tris(boryl) complexes are several [(η^6-arene)Ir(Bcat)$_3$] (**37**) derivatives formed in the reaction of [(η^5-Indenyl)Ir(η^2-COE)$_2$] (COE = cyclooctene) with ≥5 equiv. of HBcat in arene solvents. One such complex was found to react with 3 equiv. of PEt_3 with loss of arene yielding *fac*-[$Ir(PEt_3)_3(Bcat)_3$] (**38**) analogous to **36**. While two examples of **37** were structurally characterized, **38** was identified only by multinuclear NMR spectroscopy, and thus **36** represents the first structurally characterized phosphine or Rh containing tris(boryl) complex.

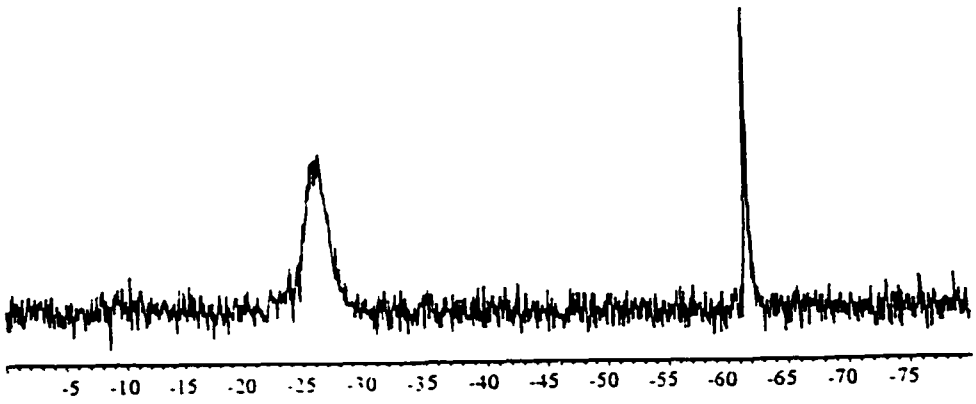


Figure 4.9a $^{31}P\{^{1}H\}$ NMR spectrum of $[Rh(PMe_3)_4Me] + 2\ B_2cat_2$ in C_6D_6

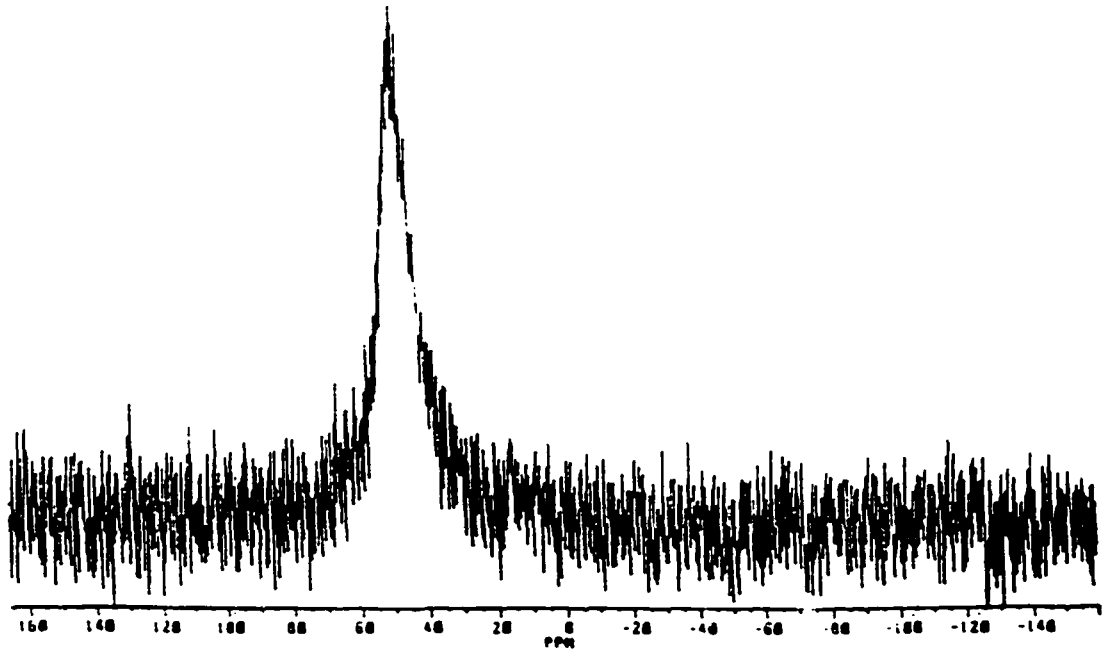


Figure 4.9b $^{11}B\{^{1}H\}$ NMR spectrum of $[Rh(PMe_3)_3(Bcat)_3]$ in C_6D_6

Single crystals suitable for X-ray diffraction were grown from toluene. The compound crystalizes in the triclinic space group $P\bar{1}$ with 0.5 mole of disordered toluene molecules in the lattice. Crystal data for (**36**): $C_{27}H_{39}B_3O_6P_3Rh \cdot 0.5C_7H_8$, M = 733.90 a = 9.4861(9), b = 11.5356(11), c = 17.8907(18)Å, α = 73.055(3), β = 83.211(2), γ = 68.390(2)°, V = 1741.0(3)Å^3. A view of the molecular structure of **36** with selected bond distances and angles is presented in Figure **4.10**. The *fac*-arrangement of the three Bcat groups is evidence once again of their very strong *trans*-influence which is most likely a reflection of their strong σ-donating ability. In fact, there are, as yet, no well characterized bis- or tris(boryl) complexes in which two boryl groups occupy mutually *trans*-coordination sites. The only case reported in the literature were Nöth's poorly characterized Co(II) bis(boryl) complexes such as *trans*-[Co(dppe)$_2$(BR$_2$)$_2$].[21]

In order to examine the possibility that the second B-B bond oxidative addition (**24** → **36**) might be reversible, **36** was reacted with one equiv. of **33** in the presence of one drop (excess) of PMe_3 giving **24** + **34** in quantitative yields (Reaction **4.19**). The simplest pathway consistent with (Reaction **4.19**) is the reductive elimination of B_2cat_2 from **36** to give the transient complex [$(PMe_3)_3Rh(Bcat)$] which is rapidly trapped by PMe_3 forming one equiv. of **24**, the free B_2cat_2 then reacting with **33** as in (Reaction **4.17**) to give a second equiv. of **24** and one equiv. of **34**.

$$\underset{\mathbf{36}}{\textit{fac}\text{-}Rh(PMe_3)_3(Bcat)_3} + \underset{\mathbf{33}}{Rh(PMe_3)_4Me} + PMe_3 \longrightarrow 2\,\underset{\mathbf{24}}{Rh(PMe_3)_4(Bcat)} + \underset{\mathbf{34}}{MeBcat} \qquad \textbf{(4.19)}$$

From the above studies, it would appear that Bcat group has a strong σ-donor ability, strong *trans*-influence, and relatively poor π-acceptor ability, and that the reaction of $[Rh(PMe_3)_4Me]$ with B_2cat_2 provides a simple route to the novel electron-rich Rh(I) boryl complex $[Rh(PMe_3)_4(Bcat)]$.

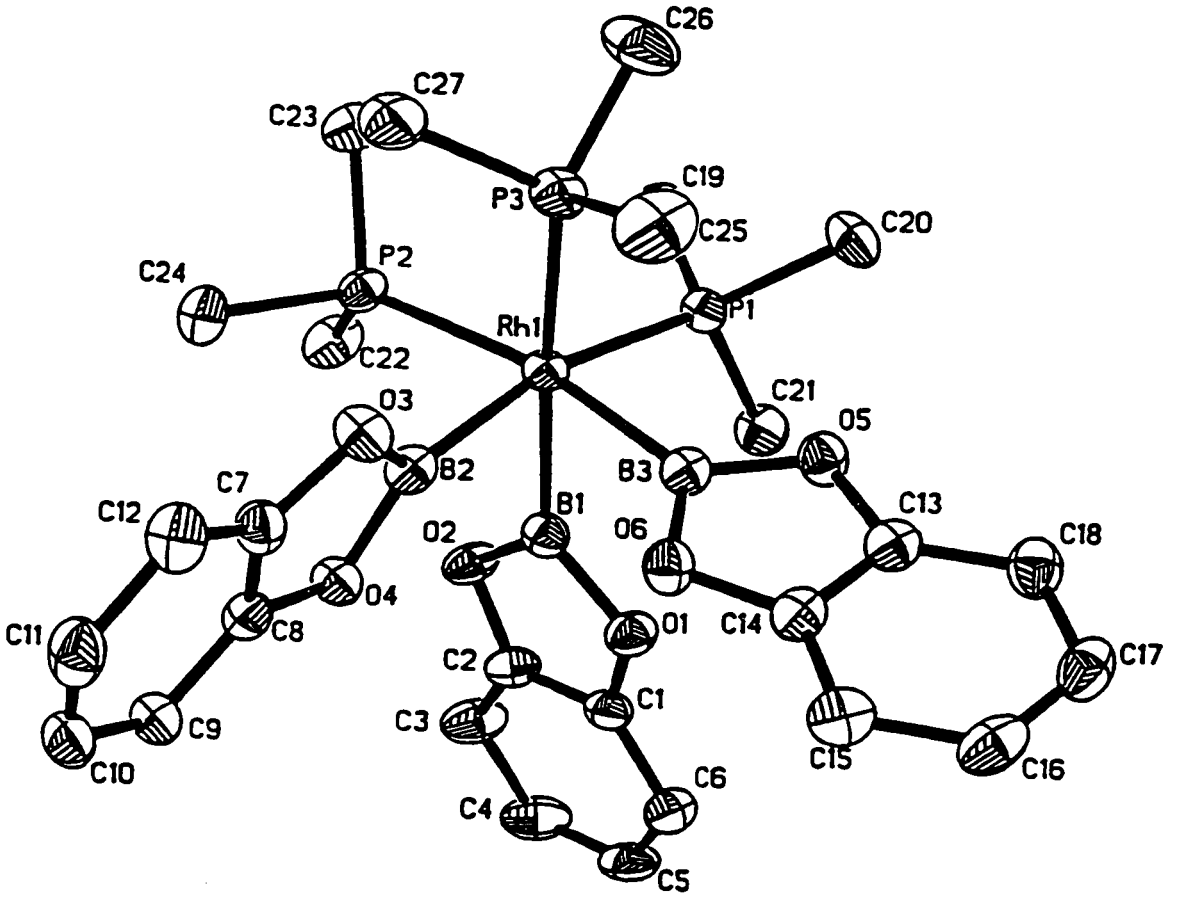


Figure 4.10. A view of the molecular structure of $[Rh(PMe_3)_3(Bcat)_3]$ (**36**) with thermal ellipsoids at 50% probability and H atoms omitted for clarity. Selected bond distances (Å) and angles (°): Rh(1)-B(1) = 2.055(4), Rh(1)-B(2) = 2.053(4), Rh(1)-B(3) = 2.061(4), Rh(1)-P(1) = 2.3913(8), Rh(1)-P(2) = 2.3906(9), Rh(1)-P(3) = 2.3920(9), B-Rh-B = 79.34(14) - 82.05(14), P-Rh-P = 94.42(3) - 99.69(3), *cis*-B-Rh-P = 86.80(10) - 95.49(10), *trans*-B-Rh-P = 166.82(10) - 169.72(11).

4.2.3.2. Reactions with Other Boron Compounds

4.2.3.2.1. With $B_2(4\text{-}Bu^t\text{-}cat)_2$ and $B_2(3,5\text{-}Bu^t_2\text{-}cat)_2$

The reaction of $B_2(4\text{-}Bu^t\text{-}cat)_2$ (**2b**) with $[Rh(PMe_3)_4Me]$ (1:1) in hexane proceeded essentially in the same manner as that of B_2cat_2 yielding $[Rh(PMe_3)_4[B(4\text{-}Bu^t\text{-}cat)]]$ (**39**) and $MeB(4\text{-}Bu^t\text{-}cat)$ (**40**), but with relatively more $[Rh(PMe_3)_4H]$ (18% by NMR) (Reaction **4.20**) showing in the NMR spectrum. As $MeB(4\text{-}Bu^t\text{-}cat)$ is a solid at room temperature ($^{11}B\{^1H\}$ δ 35.3 ppm), vacuum distillation could not remove **40** from $[Rh(PMe_3)_4B(4\text{-}Bu^t\text{-}cat)]$, thus, an yellow oily solid mixture of **39** + **40** resulted. The $^{31}P\{^1H\}$ NMR spectrum of **39** showed a slightly broader doublet at -21.93 ppm ($^1J_{Rh\text{-}P}$ 139 Hz), similar to that of $[Rh(PMe_3)_4(Bcat)]$. Also, they both showed the same $^{11}B\{^1H\}$ signal at 49.5 ppm.

$$Rh(PMe_3)_4Me + B_2(4\text{-}Bu^t\text{-}cat)_2 \rightarrow Rh(PMe_3)_4B(4\text{-}Bu^t\text{-}cat) + MeB(4\text{-}Bu^t\text{-}cat) \quad (\mathbf{4.20})$$

When $[Rh(PMe_3)_4Me]$ was treated by 2 equivalents of $B_2(3,5\text{-}Bu^t_2\text{-}cat)_2$ (**2c**) in hexane, the Rh(III) bis(boryl) complex $[Rh(PMe_3)_3\{B(3,5\text{-}Bu^t_2\text{-}cat)\}_3]$ (**41**) precipitated rapidly which was isolated in 77% yield as a white solid (Reaction **4.21**). Compound **41** was characterized by ^1H, $^{11}B\{^1H\}$, $^{13}C\{^1H\}$, and $^{31}P\{^1H\}$ NMR spectroscopy. The $^{31}P\{^1H\}$ NMR spectrum was better resolved than that for $[Rh(PMe_3)_3(Bcat)_3]$, yet the doublet at -25.9 ppm (-26.2 ppm for **36**) was still broad. The $^{11}B\{^1H\}$ NMR spectrum also displayed a very broad peak at 43.8 ppm (46.8 ppm for **36**). This reaction showed no obvious difference in the terms of reaction rate compared with that of B_2cat_2.

$$Rh(PMe_3)_4Me + 2\ B_2(3,5\text{-}Bu^t_2\text{-}cat)_2 \rightarrow Rh(PMe_3)_3(B(3,5\text{-}Bu^t_2\text{-}cat))_3 + PMe_3 + MeB(3,5\text{-}Bu^t_2\text{-}cat) \quad (\mathbf{4.21})$$

4.2.3.2.2. With B_2pin_2 and B_2neop_2

B_2pin_2 (**2d**) and B_2neop_2 (**2e**) exhibited the same reactivities toward [$Rh(PMe_3)_4Me$], resulting in the the production of Rh(I) mono(boryl) complexes [$Rh(PMe_3)_4Bpin$] (**42**) and [$Rh(PMe_3)_4Bneop$] (**43**), respectively (Reactions **4.22** and **4.23**). However, no corresponding Rh(III) tris(boryl) complexes in the forms of either [$Rh(PMe_3)_3(Bpin)_3$] or [$Rh(PMe_3)_3(Bneop)_3$] were observed when [$Rh(PMe_3)_4Me$] was treated with even 3 equiv of B_2pin_2 or 2.5 equiv of B_2neop_2 in C_6D_6. This observation implies that alkoxy diboron compounds **2d** and **2e** can only react with [$Rh(PMe_3)_4Me$] to form the corresponding Rh(I) mono(boryl) complexes [$Rh(PMe_3)_4Bpin$] or [$Rh(PMe_3)_4Bneop$]. However, the subsequent B-B addition to these resulting Rh(I) mono(boryl) complexes is ineffective under the above experimental conditions.

$$Rh(PMe_3)_4Me + B_2pin_2 \rightarrow Rh(PMe_3)_4(Bpin) + MeBpin \qquad (4.22)$$

$$Rh(PMe_3)_4Me + B_2neop_2 \rightarrow Rh(PMe_3)_4(Bneop) + MeBneop \qquad (4.23)$$

The $^{31}P\{^1H\}$ NMR spectrum of [$Rh(PMe_3)_4Me$] + 3 B_2pin_2 in C_6D_6 was very clean, with only a doublet at -22.0 ppm (J_{Rh-P} = 145.7 Hz) ([$Rh(PMe_3)_4(Bpin)$]), no free PMe_3 could be observed. (Figure **4.11**). The $^{11}B\{^1H\}$ NMR spectrum exhibited a broad peak for [$Rh(PMe_3)_4(Bpin)$] at 44.3 ppm and a sharp peak for MeBpin at 33.7 ppm along with excess B_2pin_2 at 31.9 ppm and some B_2pin_3 at 22.4 ppm. The presence of B_2pin_3 was due to the fact that the starting material of B_2pin_2 was not very pure, ca. 10% B_2pin_3 was present in the sample. Under the same conditions, however, the reaction of [$Rh(PMe_3)_4Me$] + 2.5 B_2neop_2 did not give a very clean $^{31}P\{^1H\}$ spectrum. In addition to the expected peak for [$Rh(PMe_3)_4(Bneop)$] at -20.9 ppm (d, J_{Rh-P} = 146.5Hz), [$Rh(PMe_3)_4H$] (δ -18.9, d, J_{Rh-P} = 146.5) was also present in ca. 8% yield (Figure **4.12**).

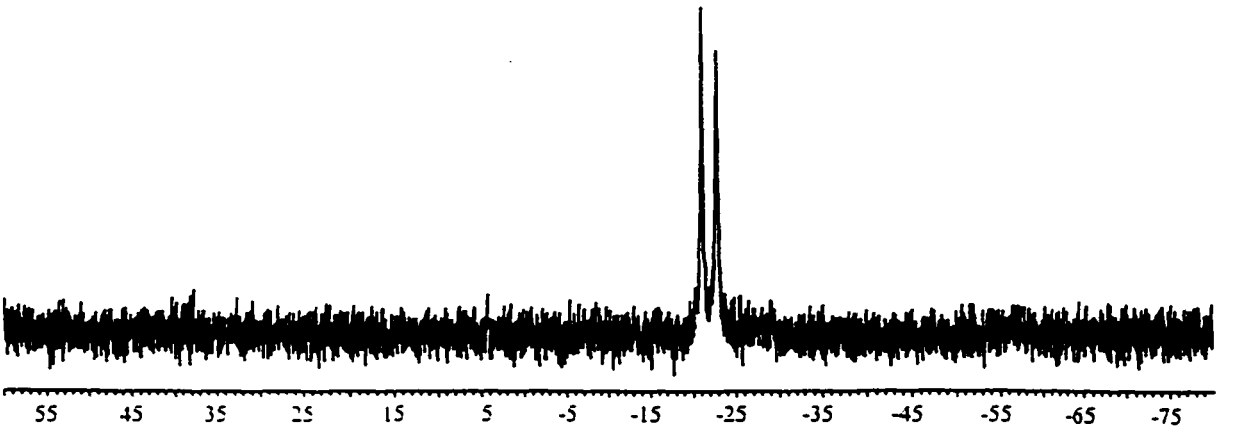


Figure 4.11 $^{31}P\{^{1}H\}$ NMR spectrum of $[Rh(PMe_3)_4Me]$ + 3 B_2pin_2 in C_6D_6

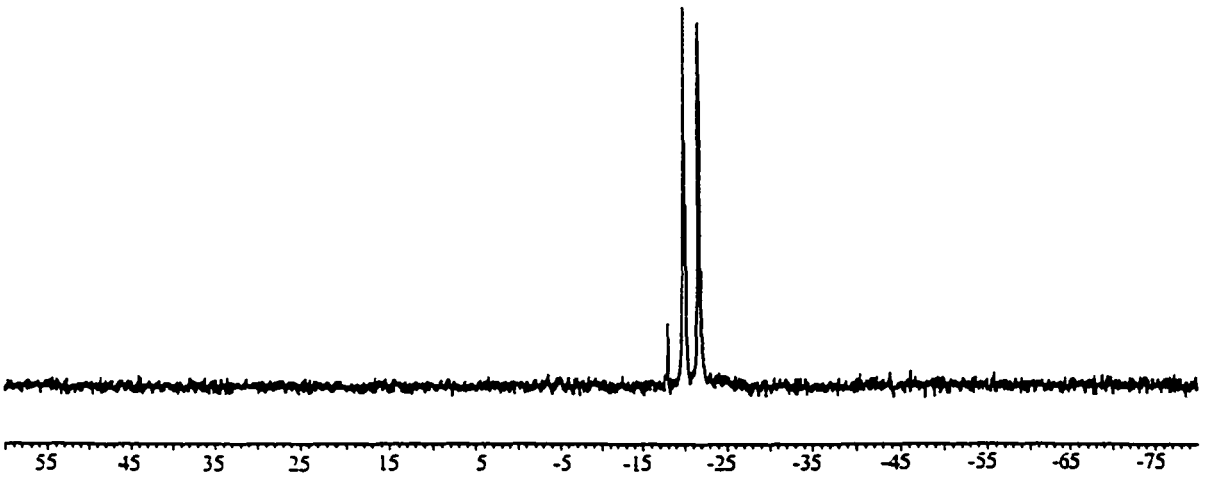


Figure 4.12 $^{31}P\{^{1}H\}$ NMR spectrum of $[Rh(PMe_3)_4Me]$ + 2.5 B_2neop_2 in C_6D_6

The $^{11}B\{^1H\}$ NMR spectrum showed the product peak at 42.5 ppm and MeBneop at 30.1 ppm along with excess B_2neop_2 at 28.2 ppm. Again, small impurity peaks at 19.8 (presumably B_2neop_3) and 17.4 ppm were also apparent in the spectrum.

In an attempt to prepare a mixed boryl Rh(III) tris(boryl) complex in the form of $[Rh(PMe_3)_3(Bneop)(Bcat)_2]$, $[Rh(PMe_3)_4Me]$ was reacted with one equivalent of B_2neop_2 firstly in hexane, then another molar equivalent of B_2cat_2 was added into the reaction solution (Reaction **4.24**). Some white precipitate was isolated in 53% yield based on the expected product $[(PMe_3)_3Rh(Bneop)(Bcat)_2]$. However, ^1H, $^{11}B\{^1H\}$ and $^{31}P\{^1H\}$ NMR spectroscopy all demonstrated that the resulting white solid was $[Rh(PMe_3)_3(Bcat)_3]$; the expected mixed tris(boryl) complexes were not obtained. This suggests that there may exist a redistribution reaction from $[(PMe_3)_3Rh(Bneop)(Bcat)_2]$ into $[Rh(PMe_3)_3(Bcat)_3]$ and other complexes. If we assume that the stoichiometry from B_2cat_2 to $[Rh(PMe_3)_3(Bcat)_3]$ follows $B_2cat_2 \rightarrow 0.5\ [Rh(PMe_3)_3(Bcat)_3]$, then the yield of $[Rh(PMe_3)_3(Bcat)_3]$ from the above process would be better calculated as ca. 104%, which is reasonably close to what might be expected as $[Rh(PMe_3)_3(Bcat)_3]$ is essentially insoluble in hexane.

$$Rh(PMe_3)_4(Bneop) + B_2cat_2 \rightarrow Rh(PMe_3)_3(Bneop)(Bcat)_2 + PMe_3 \quad (\mathbf{4.24})$$

This process was replicated in C_6D_6 and monitored by NMR. Thus, the $^{31}P\{^1H\}$ spectrum showed only a broad doublet at -26.5 ppm cf. $[Rh(PMe_3)_3(Bcat)_3]$ (δ -26.2 ppm). A broad peak for PMe_3 at -61.3 ppm (Figure **4.13**) was observed indicating the formation of Rh(III) tris(boryl) complexes. It aslo implies that there might exist a fast exchange process between the free PMe_3 and those on the Rh(III) tris(boryl) complexes. In its $^{11}B\{^1H\}$ spectrum, there was a broad peak at 46.4 ppm (46.6 ppm for

[$Rh(PMe_3)_3(Bcat)_3$]) and a sharp peak for MeBneop at 29.9 ppm. Though the spectra could not necessarily differentiate different Rh(III) tris(boryl) species, the results certainly indicate that B-B oxidative addition of B_2cat_2 to [$Rh(PMe_3)_4(Bneop)$] occurs in the same fashion as it does to [$Rh(PMe_3)_4(Bcat)$]. On the other hand, in another trial when B_2cat_2 and B_2neop_2 (1:1) were added to [$Rh(PMe_3)_4Me$] in the reverse order as before, the second diboron reagent B_2neop_2 showed no reactivity at all toward the resulting [$Rh(PMe_3)_4(Bcat)$] as evidenced by $^{31}P\{^1H\}$ and $^{11}B\{^1H\}$ NMR. Its $^{31}P\{^1H\}$ spectrum only exhibited a doublet at -21.9 ppm (J_{Rh-P} = 147.8 Hz) which was assigned to [$Rh(PMe_3)_4(Bcat)$], and there was no free PMe_3 present (Figure **4.14**). In another separate experiment, when [$Rh(PMe_3)_4Me$] was added to an equal molar mixture solution of B_2cat_2 and B_2neop_2 (1:1) in C_6D_6, again, little difference could be observed in the $^{31}P\{^1H\}$ and $^{11}B\{^1H\}$ spectra from the second trial, only [$Rh(PMe_3)_4(Bcat)$] was generated, there was no indication of the formation of any Rh(III) tris(boryl) complexes. If B_2neop_2 had some reaction with [$Rh(PMe_3)_4Me$] to produce [$Rh(PMe_3)_4(Bneop)$] in the first place, then the same situation as trial one would follow, and some Rh(III) tris(boryl) complexes would have been formed. However, this is not the case. On the other hand, reaction (**4.23**) seems not to be reversible, so we may rationalize from the above argument that although both B_2cat_2 and B_2neop_2 can react with [$Rh(PMe_3)_4Me$] to produce the corresponding Rh(I) mono(boryl) complexes, the reaction rates are probably different, with B_2cat_2 having a significantly faster reaction rate than B_2neop_2.

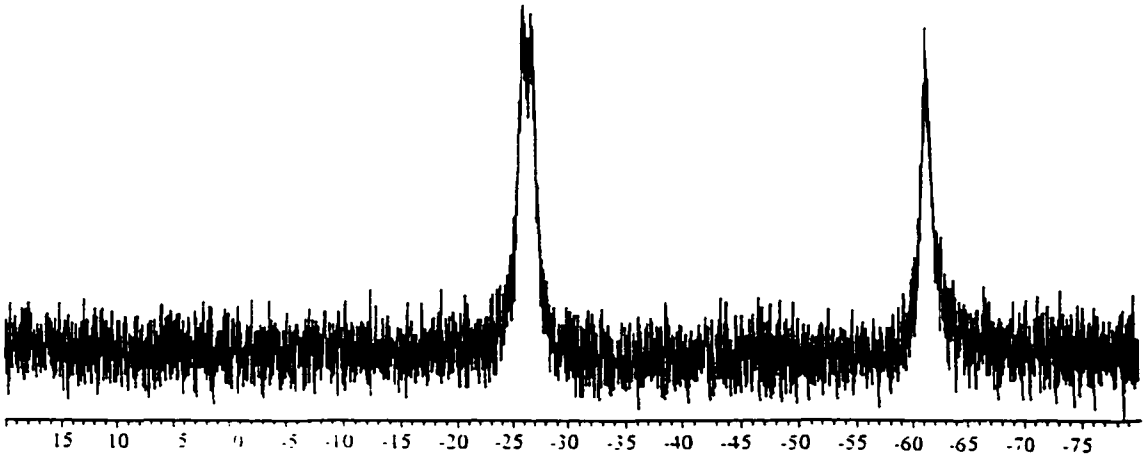


Figure 4.13 $^{31}P\{^{1}H\}$ NMR spectrum of $[Rh(PMe_3)_4Me]$ + B_2neop_2 +B_2cat_2 (1:1:1) in C_6D_6

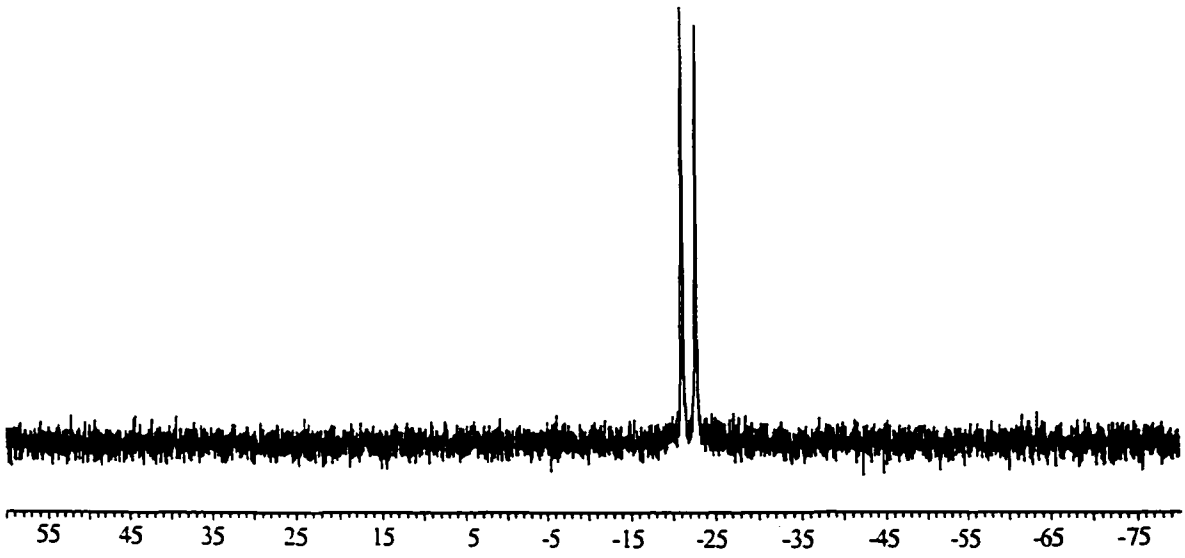


Figure 4.14 $^{31}P\{^{1}H\}$ NMR spectrum of $[Rh(PMe_3)_4Me]$ + B_2cat_2 +B_2neop_2 (1:1:1) in C_6D_6

4.2.3.2.3. With MeBcat

When two equivalents of [$Rh(PMe_3)_4Me$] (50mg, 0.12 mmol) was added to one equivalent of B_2cat_2 (14 mg, 0.06 mmol) in C_6D_6, the formation of [$Rh(PMe_3)_4(Bcat)$] was found as expected. However, no extra [$Rh(PMe_3)_4Me$] was detected in the solution, nor was the other would-be product MeBcat as in reaction (**4.17**). One possible assumption is that MeBcat may have reacted with the other equivalent of [$Rh(PMe_3)_4Me$]. However, the following idealized reaction (**4.25**) is very unlikely to occur.

$$Rh(PMe_3)_4Me + MeBcat \xrightarrow[-PMe_3]{} [Rh(PMe_3)_3(Me)_2(Bcat)]$$

$$\xrightarrow[-\ Me\text{-}Me]{+PMe_3} Rh(PMe_3)_4(Bcat) \qquad (\mathbf{4.25})$$

Actually, in spite of the fact that the ease of oxidative cleavage of B-C bond to form various functional groups is the dominant theme of organoborane chemistry,[40] B-C bond oxidative addition by transition metal complexes is not common. On the other hand, in this system of 2 [$Rh(PMe_3)_4Me$] / B_2cat_2, we have noticed the generation of a somewhat larger amount of yellow precipitate than usual (17 mg). This kind of yellow precipitate itself, indeed, has been observed on several occasions when reaction (**4.18**) was performed in various solvents such as hexane, heptane, benzene and toluene. It was originally believed to be the minor decomposition product of [$Rh(PMe_3)_4(Bcat)$], and was not taken seriously due to its negligible amount. Nevertheless, by dissolving the collected precipitated substance in CD_3CN, we observed a broad peak of $^{31}P\{^1H\}$ NMR spectrum at -12.8 ppm as the dominant signal which corresponded to a $[Rh(PMe_3)_4]^+$ cation signal similar to that of $[Rh(PMe_3)_4]^+Cl^-$ (**44**).[41] The $^{11}B\{^1H\}$ spectrum showed a main peak at 14.7 ppm ($Bcat_2^-$ signal) and two small peaks at 12.3 and 8.25 ppm, respectively. The ^1H spectrum was not very clean either, but one obvious feature was

that there was one broad peak upfield at -0.37 ppm which could be interpreted as a CH_3 group attached to a tetracoordinated boron center. Based on the above analysis, the reaction between $[Rh(PMe_3)_4Me]$ and MeBcat can now be seen simply as MeBcat abstracting the methyl group from $[Rh(PMe_3)_4Me]$ and thus forming $[Rh(PMe_3)_4]^+[Me_2Bcat]^-$ (**45**):

$$Rh(PMe_3)_4Me + MeBcat \rightarrow [Rh(PMe_3)_4]^+[Me_2Bcat]^- \quad (\mathbf{4.26})$$

When the reaction of $[Rh(PMe_3)_4Me]$ with pure MeBcat was also performed in hexane, the same precipitate was obtained in 96% yield if based on the complete formation of (**45**). However, single crystals were obtained from this substance in CD_3CN, and X-ray diffraction revealed that the structure was $[Rh(PMe_3)_4]^+[Bcat_2]^-$ (**46**) (Figure **4.15**). Again, there was some disproportion reaction from $[Me_2Bcat]^-$ to $[Bcat_2]^-$ and another anion (probably $[Me_4B]^-$). While compound **45** has not been completely characterized, further work is obviously needed to confirm its identity.

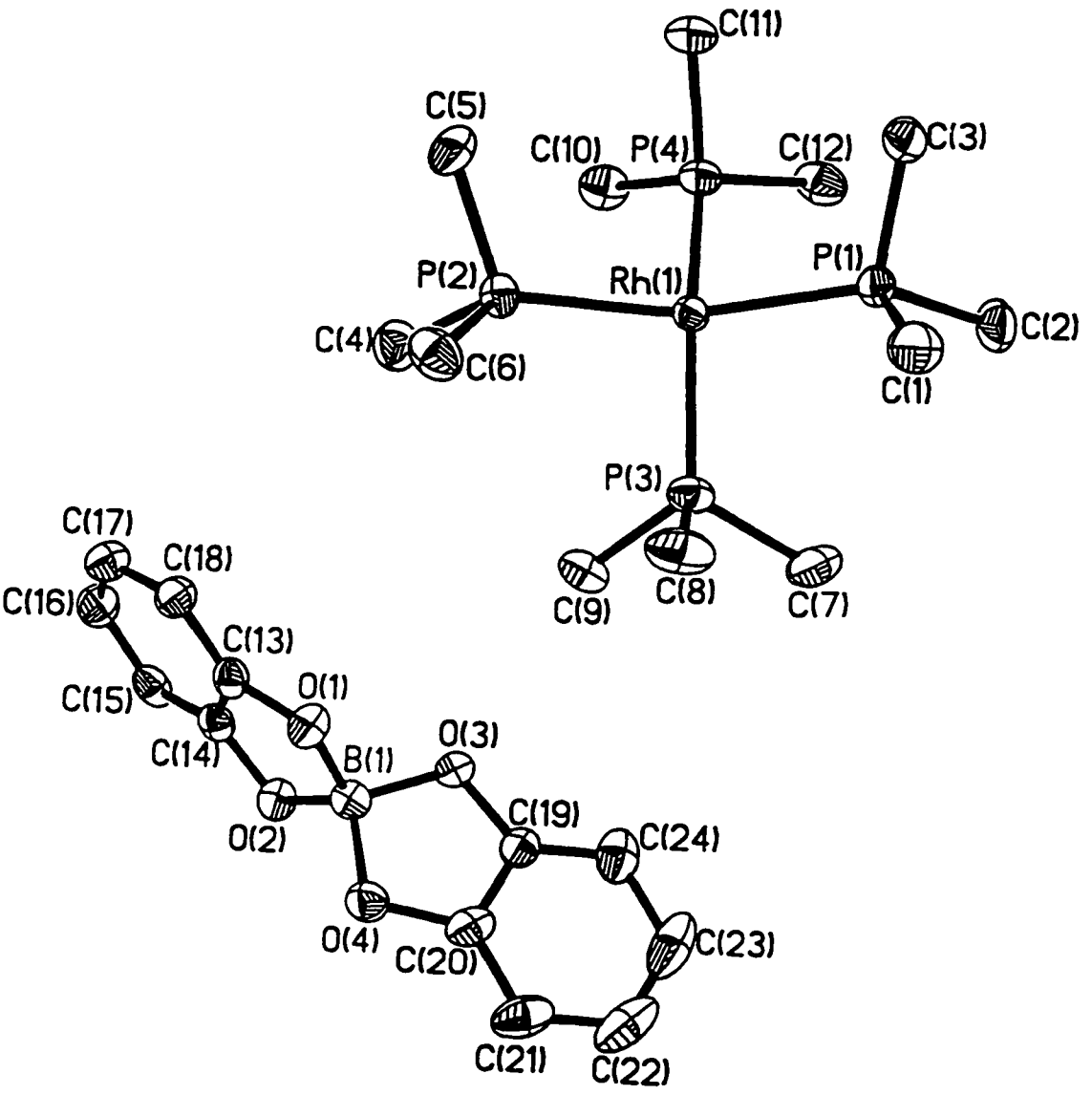


Figure 4.15 A view of the molecular structure of $[Rh(PMe_3)_4]^+[Bcat_2]^-$ (**46**) with thermal ellipsoids at 50% probability and H atoms omitted for clarity. Selected bond distances (Å) and angles (°): Rh(1)-P(1) = 2.3071(8), Rh(1)-P(2) = 2.2969(8), Rh(1)-P(3) = 2.3083(8), Rh(1)-P(4) = 2.2928(8), B(1)-O(1) = 1.472(4), B(1)-O(2) = 1.492(4), B(1)-O(3) = 1.493(4), B(1)-O(4) = 1.475(4), P(1)-Rh(1)-P(2) = 151.29(3), P(1)-Rh(1)-P(3) = 93.93(3), P(1)-Rh(1)-P(4) = 92.66(3), P(3)-Rh(1)-P(4) = 155.77(3), O(1)-B(1)-O(2) = 104.8(3), O(3)-B(1)-O(4) = 104.8(3), O(1)-B(1)-O(3) = 112.0(3), O(1)-B(1)-O(4) = 113.0(3)

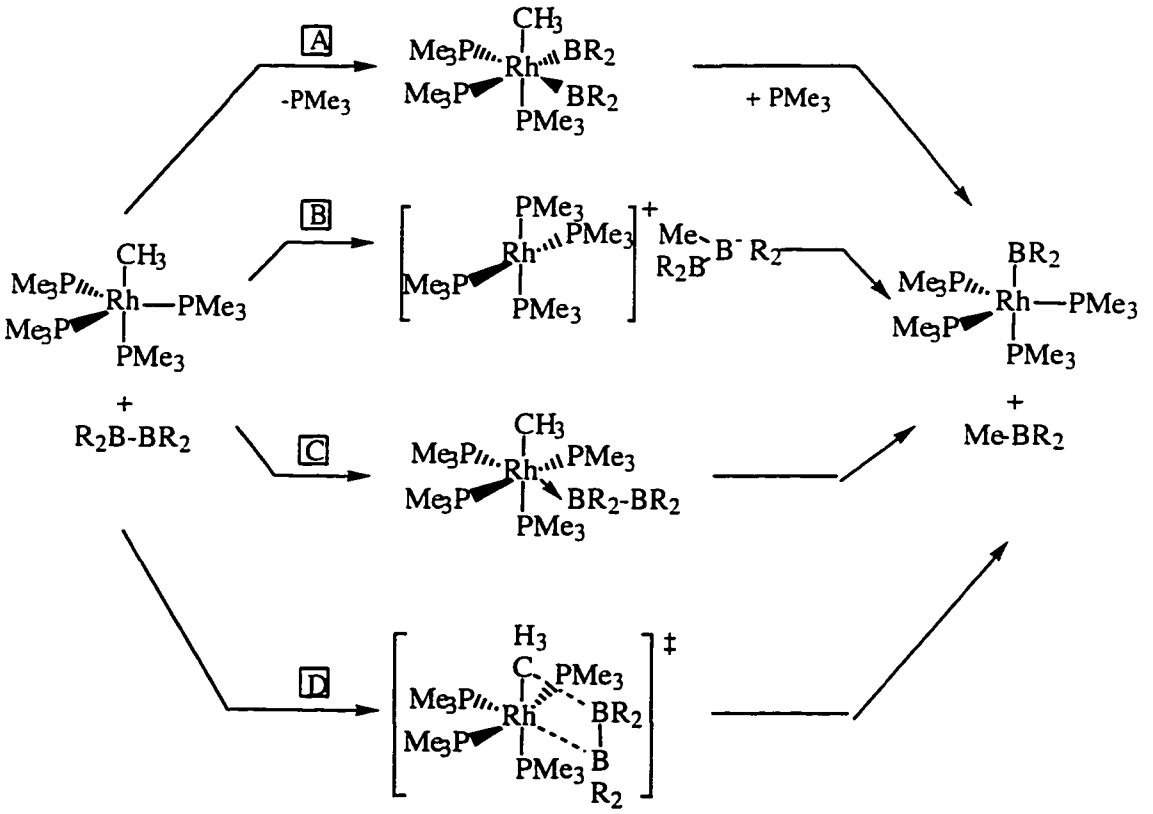
4.2.3.3. Mechanistic Consideration

In summary, we have discussed various reactions involving [$Rh(PMe_3)_4Me$] and related Rh boryl complexes with some organoboranes. They are presented as the following (Table **4.1**):

Table 4.1 Reactions between [$Rh(PMe_3)_4Me$] and rhodium boryl complexes with some organoboranes

	Reactants	Products
1	[$Rh(PMe_3)_4Me$] + B_2cat_2	[$Rh(PMe_3)_4(Bcat)$] + MeBcat
2	[$Rh(PMe_3)_4Me$] + $B_2(Bu^t\text{-cat})_2$	[$Rh(PMe_3)_4B(Bu^tcat)$]+ $MeB(Bu^tcat)$
3	[$Rh(PMe_3)_4Me$] + B_2pin_2	[$Rh(PMe_3)_4(Bpin)$] + MeBpin
4	[$Rh(PMe_3)_4Me$] + B_2neop_2	[$Rh(PMe_3)_4(Bneop)$] + MeBneop
5	[$Rh(PMe_3)_4(Bcat)$] + B_2cat_2	[$Rh(PMe_3)_3(Bcat)_3$] + PMe_3
6	[$Rh(PMe_3)_4(Bneop)$] + B_2cat_2	[$Rh(PMe_3)_3(Bcat)_3$] + ···· + PMe_3
7	[$Rh(PMe_3)_4Me$] + 2 $B_2(Bu^t_2\text{-cat})_2$	[$Rh(PMe_3)_3(B(Bu^t_2\text{-cat}))_3$] + PMe_3 + $MeB(Bu^t_2\text{-cat})$
8	[$Rh(PMe_3)_4(Bpin)$] + B_2pin_2	no reacton
9	[$Rh(PMe_3)_4(Bneop)$] + B_2neop_2	no reaction
10	[$Rh(PMe_3)_4(Bcat)$] + B_2neop_2	no reaction
11	[$Rh(PMe_3)_4Me$] + MeBcat	[$Rh(PMe_3)_4$][Me_2Bcat]
12	[$Rh(PMe_3)_4Me$] +[$Rh(PMe_3)_3(Bcat)_3$] + PMe_3	[$Rh(PMe_3)_4(Bcat)$] + MeBcat

Inspecting the above reactions, we can very easily notice that, unlike B_2cat_2 and its more sterically hindered analogs **2b-c**, the alkoxy diboron reagents B_2pin_2 and B_2neop_2 failed to react with Rh(I) boryl complexes to generate the Rh(III) bis(boryl) oxidative addition products. On the other hand, they did show reactivities toward $[Rh(PMe_3)_4Me]$ to yield Rh(I) mono(boryl) complexes, which means that they could undergo oxidative addition to $[Rh(PMe_3)_4Me]$, if the reaction follows the pathway depicted in (**4.17**). However, in the latter process, there was no formal change in the oxidation state of Rh between reactant and product. So, in addition to the oxidative addition and reductive elimination pathway **A**, there might be other reaction pathways by which $[Rh(PMe_3)_4Me]$ reacts with diboron compounds **2a-e** (Scheme **4.1**).



Scheme 4.1 Possible reaction pathways for $[Rh(PMe_3)_4Me]$ and B_2R_4

Pathway **B** involves the transfer of the methyl group to the diboron compounds to form a $[Rh(PMe_3)_4]^+$ cation intermediate with a noncoordinated borate counterion $[MeBR_2(BR_2)]^-$. When MeBcat, instead of any diboron compounds, reacted with $[Rh(PMe_3)_4Me]$, $[Rh(PMe_3)_4]^+[Me_2BR_2]^-$ was presumably the resulting product. Pathway **C** depicts the coordination of an electron rich Rh(I) center to one of the boron atom in B_2R_4. Diboron compounds would act as eletrophiles, followed by methyl and boryl group exchange. It has been calculated that the bond dissociation energies (BDEs) of B-B and B-C bonds are very similar (H_2B-BH_2, 445.9 kJ mol^{-1}; H_2B-CH_3, 443.8 kJ mol^{-1}),[42] but the metal-boron bond strength is greater than that of the corresponding metal-methyl for the late transition metal complexes.[43, 44] Pathway **D** involves the formation of a four-centered transition state with the simultaneous weakening of B-B and Rh-C bonds. Although this σ-bond metathesis mechanism is more characteristic of high-valent early transition metal complexes, for example, in early metal-catalyzed hydroboration reactions,[45] it has also been observed in the reaction of HBcat with a low-valent $CpRu(PPh_3)_2Me$ complex[46] (see also reference 23).

In our rhodium system, B_2cat_2 has unambiguously added oxidatively to $[Rh(PMe_3)_4(Bcat)]$ and $[Rh(PMe_3)_4(Bneop)]$ to form the corresponding Rh(III) tris(boryl)complexes. Pathway **A** is, thus, very likely to account for the reaction between $[Rh(PMe_3)_4Me]$ and various diboron compounds, since $[Rh(PMe_3)_4Me]$ has a very similar structure as that of $[Rh(PMe_3)_4(Bcat)]$.[47] When the yellow solution of $[Rh(PMe_3)_4Me]$ was added dropwise to the colorless solution of B_2cat_2, the yellow color could be seen to disappear immediately upon the mixing, and some white precipitate could be observed when $[Rh(PMe_3)_4Me]$ was added to $B_2(3,5\text{-}Bu^t_2\text{-}cat)_2$ in hexane. This white species may be the oxidative addition intermediates $[Rh(PMe_3)_3(Me)(BR_2)_2]$. However, no such intermediate was observed by NMR spectroscopy because it also disappears very rapidly. However, when $[Rh(PMe_3)_4Me]$ was added into B_2pin_2 or

B_2neop_2, no obvious such color change was observed, which may imply that B-C reductive elimination is extremely fast.

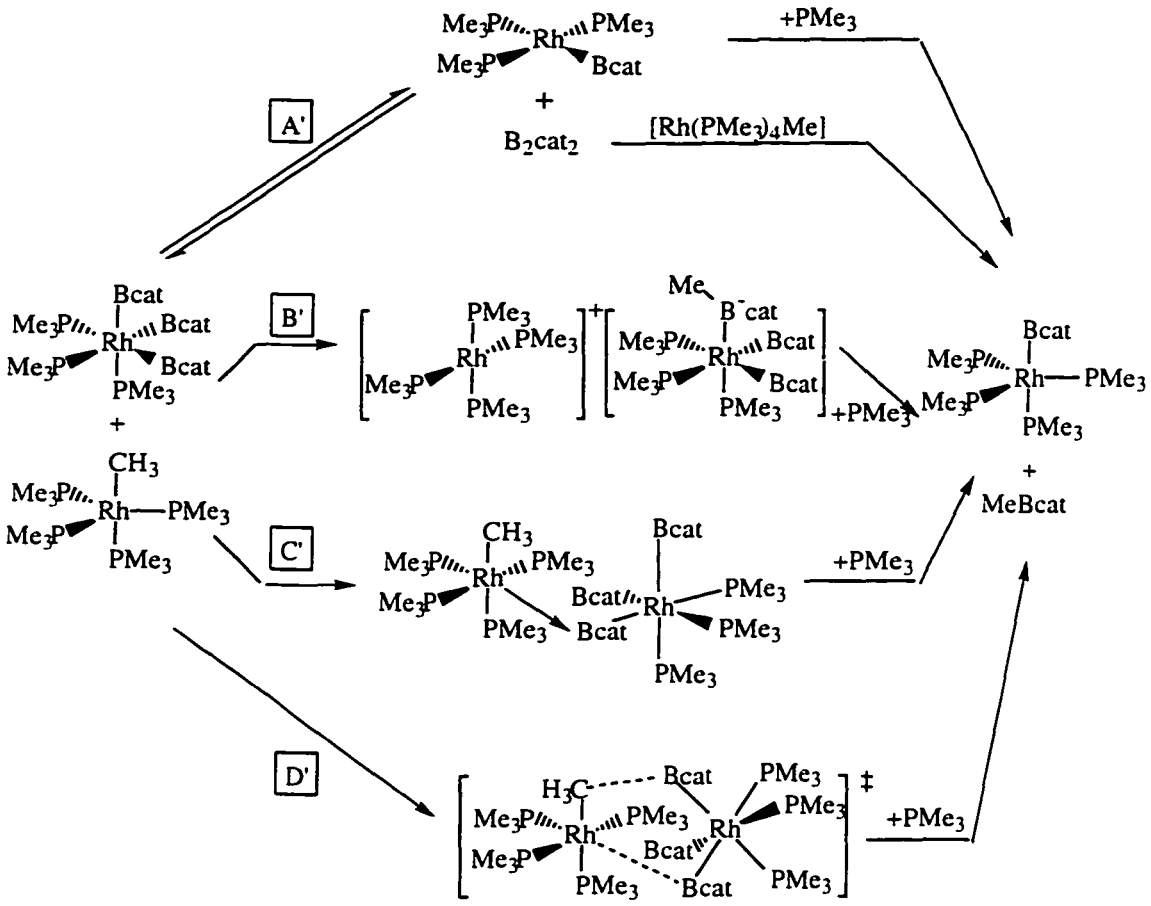
While the reaction of $[Rh(PMe_3)_3(Bcat)_3]$ with $[Rh(PMe_3)_4Me]$ is very likely following our previous assumption that $[Rh(PMe_3)_3(Bcat)_3]$ underwent a reversible B-B reductive elimination passway, a similar result was obtained when $[Rh(PMe_3)_3Cl_2(Bcat)]$ (**47**) was treated with $[Rh(PMe_3)_4Me]$ in the presence of PMe_3. MeBcat and $[Rh(PMe_3)_4]Cl$ were found to be the reaction products (Reaction **4.27**). In addition, ClBcat (**48**) reacted readily with $[Rh(PMe_3)_4Me]$ to generate $[Rh(PMe_3)_4]Cl$ and MeBcat. Reaction (**4.27**) could also be explained as the result of Cl-Bcat reductive elimination from **47**.

$$Rh(PMe_3)_3Cl_2(Bcat) + Rh(PMe_3)_4Me + PMe_3 \rightarrow 2\,[Rh(PMe_3)_4]Cl + MeBcat \qquad (\mathbf{4.27})$$

As a matter of fact, B-B reductive elimination has been observed on several occasions[3g] including the following reaction (**4.28**):[18]

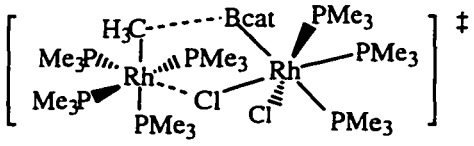
$$Rh(PPh_3)_2Cl(Bcat)_2 + ArNC \rightarrow Rh(PPh_3)_2Cl(ArNC) + B_2cat_2 \qquad (\mathbf{4.28})$$

While we favor a reductive elimination pathway, some possible alternatives are depicted in Scheme **4.2**.



Scheme 4.2 Possible reaction pathways for $[Rh(PMe_3)_3(Bcat)_3]$ and $[Rh(PMe_3)_4Me]$

Likewise, one plausible mechanism for the reaction of $[Rh(PMe_3)_3Cl_2(Bcat)]$ with $[Rh(PMe_3)_4Me]$ may follow pathway D' which involves the bridging Cl and methyl transition state.



In conclusion, in addition to the oxidative addition - reductive elimination pathway, there may exist other pathways in the reactions of $[Rh(PMe_3)_4Me]$. It is too early at this stage to state exactly how these reactions proceed.

4.3. Experimental

4.3.1. General Procedures

Reactions and NMR sample preparations were performed under a dry nitrogen atmosphere using glove box techniques. THF was freshly distilled from sodium benzophenone ketyl, toluene from sodium metal, hexane and heptane from Na/K alloy, and CH_2Cl_2 from CaH_2 under a N_2 atmosphere. NMR solvents were distilled from CaH_2 ($CDCl_3$, CD_3CN) or Na metal (C_6D_6) following three freeze/pump/thaw cycles. NMR spectra were recorded on Bruker AC 200 (^1H at 200 MHz, ^{13}C at 50 MHz, ^{31}P at 81 MHz) or AMX 500 (^1H at 500 MHz, ^{11}B at 160 MHz) spectrometers. The ^1H chemical shifts were referenced to the internal standard tetramethylsilane (TMS) and ^{13}C chemical shifts were referenced to the solvent resonances as an internal standard. The ^{31}P and ^{11}B chemical shifts were referenced to the external standards 85% H_3PO_4 and $F_3B{\cdot}OEt_2$ respectively. The ^{11}B NMR spectrum was obtained using a background subtraction routine to remove resonances due to borosilicate glass in the NMR probe and NMR tube. This was accomplished by recording the spectrum of an NMR tube containing the same volume of pure solvent and with identical acquisition parameters to those of the sample and by subtracting this background FID from that of the sample. Coupling constants are reported in Hz. Multiplicities are reported as (br) broad, (s) singlet, (d) doublet, (vt) virtual triplet, and (m) multiplet. Elemental analyses were obtained from M-H-W Laboratories, Phoenix, Arizona, and at the University of Newcastle, England.

GC/MS analyses were performed on a Hewlett-Packard 5890 Series II/5971A MSD instrument equipped with an HP 7673A autosampler and a fused silica column (30 m x 0.25 mm x 0.25 mm, cross-linked 5% phenylmethyl silicone). The following operating conditions were used: injector, 260°C; detector, 280°C; oven temperature was

ramped from 70°C to 260°C at the rate of 20°C/min. UHP grade helium was used as the carrier gas.

4.3.2. Experimental Precedures

Synthesis of $[Co(PMe_3)_3(Bcat)_2]$ (21) A scintillation vial was charged with $[Co(PMe_3)_4]$ (**20**) (100 mg, 0.275 mmol), B_2cat_2 (65 mg, 0.277 mmol) and THF (4 mL) resulting in a brown solution. After stirring at room temperature over night, the solution lightened to a yellow-brown color, and the solvent was removed *in vacuo* yielding 150 mg of a brown solid. Recrystallization from hot hexane gave 92 mg of yellow crystals of **21** in 60% yield. Anal. Calcd. for $C_{21}H_{35}B_2CoO_4P_3$: C 48.00, H 6.67; Found: C 48.23, H 6.55.

Reaction of $[Co(PMe_3)_3(Bcat)_2]$ with $[Rh(PMe_3)_4]Cl$ The compounds $[Co(PMe_3)_3(Bcat)_2]$ (50 mg, 0.095 mmol) and $[Rh(PMe_3)_4]Cl$ (101 mg, 0.23 mmol) were mixed in the solid state, then 20 mL of hexane was added. The reaction mixture was allowed to stir at 60°C for 6 h, then cooled to room temperature, resulting in some yellow precipitate and a yellow solution. Upon filtration, 48 mg of the yellow solid $[Co(PMe_3)_3Cl_2]$ was obtained. $^{31}P\{^1H\}$ NMR (81 MHz, 25°C in C_6D_6), δ: -15.08 (br). The yellow filtrate was collected and stripped to dryness *in vacuo*, yielding 103 mg (103%) of a yellow solid with slightly brown tint. Selected NMR data: $^{31}P\{^1H\}$ NMR (81 MHz, 25°C in C_6D_6), δ: -21.85 (d, J_{Rh-p} = 138.7 Hz, $Rh(PMe_3)_4(Bcat)$), -18.82 (d, J_{Rh-p} =146.0 Hz, $Rh(PMe_3)_4H$). $^{11}B\{^1H\}$ NMR (160 MHz, 25°C in C_6D_6), δ: 49.1 (br, $Rh(PMe_3)_4(Bcat)$).

Synthesis of $[Ir(PMe_3)_3Cl(Bcat)_2]$ (26) A solution of B_2cat_2 (84mg, 0.35 mmol) in 2 mL of THF was added to a solution of $[Ir(PMe_3)_3Cl(COE)]$ (200 mg, 0.35 mmol) in 10 mL of THF. The solution turned almost colorless immediately. After stirring for 1 h, the

solvent was removed under reduced pressure and the colorless residue was washed with hexane, dried *in vacuo* to yield 220 mg (90%) of complex **26.** $^{31}P\{^{1}H\}$ NMR (81 MHz, 25°C in C_6D_6), δ: -40.9 (d, $^{2}J_{P\text{-}P}$ = 27.5 Hz, 2P, *trans* PMe_3), -50.8 (br, PMe_3). $^{11}B\{^{1}H\}$ NMR (160 MHz, 25°C in C_6D_6), δ: 41.7 (br, Bcat), 32.6 (br, Bcat). ^{1}H NMR (500 MHz, 25°C in $CDCl_3$), δ: 1.15 (d, $^{2}J_{P\text{-}H}$ = 7.5 Hz, 9H, PMe_3), 1.48 (vt, $^{2}J_{P\text{-}H}$ = 3.7 Hz, 18H, PMe_3), 7.12, 6.83 (AA'BB', 4H, Bcat), 7.07, 6.76 (AA'BB', 4H, Bcat). $^{13}C\{^{1}H\}$ NMR (50 MHz, 25°C in C_6D_6), δ: 17.73 (d, $J_{P\text{-}C}$ = 26 Hz, PMe_3), 19.52 (dvt, $^{1}J_{P\text{-}C}$ = 19Hz, $^{3}J_{P\text{-}C}$ = 4.5 Hz, PMe_3), 110.86 (s), 121.24 (s), 150.65 (s, Bcat), 111.86(s), 121.45 (s, Bcat). In C_6D_6, the two resonances due to the inequivalent C-O groups of the two Bcat ligands are coincident. $^{13}C\{^{1}H\}$ NMR (50 MHz, 25°C in $CDCl_3$), δ: 18.06 (dm, $J_{P\text{-}C}$ = 26 Hz, PMe_3), 19.57(dvt, $J_{P\text{-}C}$ = 19.5 Hz, $J_{P\text{-}C}$ = 4.2 Hz, PMe_3), 110.53(s), 120.71 (s) 149.84 (d, $J_{P\text{-}C}$ = 2.6 Hz, Bcat), 111.58 (s), 120.76 (s), 150.03 (s, Bcat). Anal. calcd. for $C_{21}H_{35}B_2ClIrO_4P_3$: C 36.36, H 5.09; found C 37.07, H 5.11.

Synthesis of [$Rh(PMe_3)_4$(Bcat)] (24) In a scintillation vial, compounds [$Rh(PMe_3)_4Me$] (200 mg, 0.474 mmol) and B_2cat_2 (113 mg, 0.475 mmol) were added with 10 mL of heptane. The reaction mixture was allowed to stir over night, resulting in a nearly completely clear yellow solution. After filtration, the filtrate was collected and was stripped to dryness *in vacuo*. A pale yellow solid (230 mg, yield 92%) was collected as the product **24**. $^{31}P\{^{1}H\}$ NMR (81 MHz, 25°C in C_6D_6), δ: -21.88 (d, $J_{Rh\text{-}P}$ = 137 Hz, PMe_3), $^{31}P\{^{1}H\}$ NMR (81 MHz, 193 K in C_6D_6), δ: -22.03 (dd, $J_{Rh\text{-}P}$ = 157, $^{2}J_{P\text{-}P}$ = 48 Hz, 3P), -13.21 (dq, $J_{Rh\text{-}P}$ = 91, $^{2}J_{P\text{-}P}$ = 48 Hz, 1P); $^{11}B\{^{1}H\}$ NMR (150 MHz, 25°C in C_6D_6), δ: 49.0 (br); ^{1}H NMR (200 MHZ, 25°C in C_6D_6), δ: 7.11 (m, 2H), 6.86 (m, 2H), 1.28 (s, 36H); $^{13}C\{^{1}H\}$NMR (50 MHZ, 25°C in C_6D_6), δ: 150.6, 120.8, 110.7 (cat), 26.9 (br, PMe_3). For MeBcat: $^{11}B\{^{1}H\}$ δ 35.2 (s); ^{1}H δ 6.99 (m, 2H), 6.79 (m. 2H), 0.46 (s, 3H); MS-EI m/z 134 (M^+) with expected isotope pattern.

Synthesis of [Rh(PMe$_3$)$_3$(Bcat)$_3$] (36) A solution of [Rh(PMe$_3$)$_4$Me] (100 mg, 0.237 mmol) in 2 mL of hexane was added dropwise to a suspension of B_2cat_2 (114 mg, 0.479 mmol) in 6 mL of hexane with stirring. The yellow color disappeared immediately upon the first part of addition. With the last several drops, the color did not disappear as quickly, but ca. 5 min after the completion of addition, the solution was colorless with a large amount of white precipitate. Stirring was continued for 2 h. The solid was filtered and washed with hexane, yielding 155 mg (95.1%) of white powder. NMR spectroscopic data for (**36**) in C_6D_6: $^{31}P\{^1H\}$ δ -26.2 (br); $^{11}B\{^1H\}$ δ 46.8 (br); ^1H: δ 6.98 (m, 2H), 6.73 (m, 2H), 1.19 (dd, $^4J_{Rh-H}$ = 1.8, $^3J_{P-H}$ = 3.6 Hz, 9H); $^{13}C\{^1H\}$: δ 150.4, 120.9, 111.2 (cat), 22.5 (dd, $^3J_{Rh-C}$ = 8.5, $^2J_{P-C}$ = 18.7 Hz, PMe$_3$).

Reaction of [Rh(PMe$_3$)$_3$(Bcat)$_3$] with [Rh(PMe$_3$)$_4$Me)] A solution of [Rh(PMe$_3$)$_4$Me] (42 mg, 0.1 mmol) in 1 mL of hexane was added to a suspension of [Rh(PMe$_3$)$_3$(Bcat)$_3$] (69 mg, 0.1 mmol) in 5mL of hexane, and a drop of PMe$_3$ was also added. The reaction mixture was allowed to stir at room temperature for 3 h, becoming almost clear brown-yellow with a small amount of yellow precipitate. About 0.5 mL of solution was removed and placed in an NMR tube to which 2 drops of C_6D_6 was added. $^{31}P\{^1H\}$ NMR spectrum showed very clean Rh(PMe$_3$)$_4$Bcat peaks at δ -21.88 (d, J_{Rh-P} = 137 Hz) along with a broad peak for PMe$_3$ at δ -62.24 ppm. $^{11}B\{^1H\}$: δ 49.21 (br, Rh(PMe$_3$)$_4$Bcat) and 35.00 (s, MeBcat) in a ratio of ca. 2:1. The solid was removed by filtration, and the filtrate was stripped to dryness *in vacuo*, yielding 108 mg (theoretically, 105 mg) of yellow solid as crude **24.**

Reaction of [Rh(PMe$_3$)$_4$Me] with B$_2$(4-Bu^t-cat)$_2$ A solution of [Rh(PMe$_3$)$_4$Me] (100 mg, 0.237 mmol) in 2 mL of hexane was added dropwise to a solution of B$_2$(4-Bu^t-cat)$_2$ (83 mg, 0.237 mmol) in 2 mL of hexane. Some white cloudy precipitate was generated right upon mixing, which disappeared rapidly. After the addition was complete, the solution was allowed to stir for 1 h at room temperature, resulting in a pale yellow

solution with minimal yellow precipitate. After filtration, the solvent was removed *in vacuo*, yielding 140 mg of yellow oily solid. NMR spectroscopic data for **39** in C_6D_6: $^{31}P\{^1H\}$ δ -21.9 (d, J_{Rh-p} = 138.7 Hz); $^{11}B\{^1H\}$ δ 49.5 (br); ca. 18% $[Rh(PMe_3)_4H]$ was also present: $^{31}P\{^1H\}$ δ -19.0 (d, J_{Rh-p} = 146.1 Hz); MeB(4-Bu^t-cat): $^{11}B\{^1H\}$ δ 35.3 (s).

Synthesis of $[Rh(PMe_3)_3(B(3,5\text{-}Bu^t_2\text{-}cat))_3]$ (41). A solution of $[Rh(PMe_3)_4Me]$ (20 mg, 0.047 mmol) in 2 mL of hexane was added dropwise to a solution of $B_2(3,5\text{-}Bu^t_2\text{-}cat)_2$ (44 mg, 0.095 mmol) in 3 mL of hexane, and some white solid precipitated readily. After stirring for 1 h, the solid was collected, yielding 37 mg (77%) of white product **41**. $^{31}P\{^1H\}$ NMR (C_6D_6) δ 25.89 (br); $^{11}B\{^1H\}$ NMR (C_6D_6) δ 43.8 (br); ^1H NMR (C_6D_6) δ 1.21 (s, 27H, Bu^t), 1.28 (s, 27H, PMe_3), 1.37 (s, 27H, Bu^t), 7.03 (d, J_{H-H} = 1.2 Hz, 3H), 7.31 (d, J_{H-H} = 1.2 Hz, 3H).

NMR reaction of $[Rh(PMe_3)_4Me]$ with B_2pin_2. Compounds $[Rh(PMe_3)_4Me]$ (25 mg, 0.06 mmol) and B_2pin_2 (45 mg, 0.18 mmol) were mixed and dissolved in 1 mL of C_6D_6, and a pale yellow solution was obtained. This was allowed to stir at room temperature for 1 h, and then was transferred into an NMR tube. Selected NMR data: $^{31}P\{^1H\}$ NMR (C_6D_6) δ -22.00 (d, J_{RhP} = 145.7 Hz, $[Rh(PMe_3)_4(Bpin)]$; $^{11}B\{^1H\}$ NMR (C_6D_6) δ 44.3 (br, $[Rh(PMe_3)_4(Bpin)]$), 33.7 (s, MeBpin).

NMR reaction of $[Rh(PMe_3)_4Me]$ with B_2neop_2. Compounds $[Rh(PMe_3)_4Me]$ (25 mg, 0.06 mmol) and B_2neop_2 (27 mg, 0.12 mmol) were dissolved in 1 mL of C_6D_6, resulting in a pale yellow solution, which was allowed to stir at room temperature for 1 h, and was then transferred into an NMR tube. Selected NMR data: $^{31}P\{^1H\}$ NMR (C_6D_6) δ -20.90 (d, J_{RhP} = 146.5 Hz, $[Rh(PMe_3)_4(Bneop)]$), -18.86 (d, J_{RhP} = 146.5 Hz, $[Rh(PMe_3)_4H]$); $^{11}B\{^1H\}$ NMR (C_6D_6) δ 43.1 (br, $[Rh(PMe_3)_4(Bneop)]$), 30.1 (s, MeBneop).

NMR reaction of [Rh(PMe$_3$)$_4$Me] / B$_2$cat$_2$ / B$_2$neop$_2$ (1:1:1). Compounds [Rh(PMe$_3$)$_4$Me] (25 mg, 0.06 mmol) and B$_2$cat$_2$ (14 mg, 0.06 mmol) were dissolved in 1 mL of C_6D_6, and an yellow solution was obtained, which was allowed to stir at room temperature for 30 min. Then a solution of B$_2$neop$_2$ (13 mg, 0.06 mmol) of in 0.5 mL of C_6D_6 was added. No obvious color change was observed. After stirring for 1 h, the solution was transferred into an NMR tube. Selected NMR data: $^{31}P\{^1H\}$ NMR (C_6D_6) δ -21.92 (d, J_{Rh-P} = 137.8 Hz, [Rh(PMe$_3$)$_4$(Bcat)]); $^{11}B\{^1H\}$ NMR (C_6D_6) δ 49.5 (br, [Rh(PMe$_3$)$_4$(Bcat)]), 34.9(s, MeBcat), 30.0 (s, MeBneop), 28.0 (br, B$_2$neop$_2$).

NMR reaction of [Rh(PMe$_3$)$_4$Me] / B$_2$neop$_2$ / B$_2$cat$_2$ (1:1:1). Compounds [Rh(PMe$_3$)$_4$Me] (25 mg, 0.06 mmol) and B$_2$neop$_2$ (13 mg, 0.06 mmol) were mixed and dissolved in 1 mL of C_6D_6, yielding a pale yellow solution. After stirring for 30 min, a solution of B$_2$cat$_2$ (14 mg, 0.06 mmol) in 1 mL of C_6D_6 was added. The resulting solution turned almost colorless, and was allowed to stir for 1 h, after which it was transferred into an NMR tube. Selected NMR data: $^{31}P\{^1H\}$ NMR (C_6D_6) δ -26.48 (br d, [Rh(PMe$_3$)$_3$(Bcat)$_3$]), -61.32 (br, PMe$_3$); $^{11}B\{^1H\}$ NMR (C_6D_6) δ 46.4 (br, [Rh(PMe$_3$)$_3$(Bcat)$_3$]), 29.9 (s, MeBneop).

Reaction of [Rh(PMe$_3$)$_4$Me] / B$_2$neop$_2$ / B$_2$cat$_2$ (1:1:1). Compounds [Rh(PMe$_3$)$_4$Me] (100 mg, 0.24 mmol) and B$_2$neop$_2$ (53 mg, 0.24 mmol) were mixed and then dissolved in 2 mL of hexane, yielding a pale yellow solution, which was allowed to stir over night. Then the solution was added into a suspension of B$_2$cat$_2$ (56 mg, 0.024 mmol) in 3 mL of hexane. The solution turned almost colorless, and more white solid was precipitated. The reaction was allowed to stir for 5 h, the solid was collected by filtration and washed with hexane thoroughly, and dried *in vacuo*, yieling 85 mg of white powder. Selected NMR data: $^{31}P\{^1H\}$ NMR (C_6D_6) δ -26.48 (br d, [Rh(PMe$_3$)$_3$(Bcat)$_3$]); $^{11}B\{^1H\}$ NMR (C_6D_6) δ 46.4 (br, [Rh(PMe$_3$)$_3$(Bcat)$_3$]); ^1H NMR (C_6D_6) δ 1.20 (dd, $^4J_{Rh-H}$ = 1.8 Hz, $^3J_{P-H}$ = 3.6 Hz, 9H), 6.73 (m, 2H), 6.93 (m, 2H).

NMR reaction of [Rh(PMe$_3$)$_4$Me] / (B_2cat_2 + B_2neop_2) (1:1:1). Compound [Rh(PMe$_3$)$_4$Me] (25 mg, 0.06 mmol) in 1 mL of C_6D_6 was added into a solution of B_2cat_2 (14 mg, 0.06 mmol) and B_2neop_2 (13 mg, 0.06 mmol) in 1 mL of C_6D_6, a yellow solution was obtained, which was allowed to stir at room temperature for 1 h, during which no obvious color change was observed. Then, the solution was transferred into an NMR tube. Selected NMR data: $^{31}P\{^1H\}$ NMR (C_6D_6) δ -21.92 (d, J_{Rh-P}= 137.6 Hz, [Rh(PMe$_3$)$_4$(Bcat)]); $^{11}B\{^1H\}$ NMR (C_6D_6) δ 49.8 (br, [Rh(PMe$_3$)$_4$(Bcat)]), 34.9(s, MeBcat), 29.9 (s, MeBneop), 28.0 (br, B_2neop_2).

Reaction of [Rh(PMe$_3$)$_4$Me] with B_2cat_2 (2:1). Compounds [Rh(PMe$_3$)$_4$Me] (50 mg, 0.12 mmol) and B_2cat_2 (14 mg, 0.06 mmol) along with 1 mL of C_6D_6 were charged into a scintillation vial, and the solution was allowed to stir at room temperature over night, yielding a yellow solution with some yellow precipitate. The precipitate was collected by filtration and washed thoroughly with hexane, then dried *in vacuo*, yielding 17 mg (52%) of yellow solid. Selected NMR data for the filtrate: $^{31}P\{^1H\}$ NMR (C_6D_6) δ -21.95 (d, J_{Rh-P} = 139.0 Hz, [Rh(PMe$_3$)$_4$(Bcat)]); $^{11}B\{^1H\}$ NMR (C_6D_6) δ 50.4 (br, [Rh(PMe$_3$)$_4$(Bcat)]). The solid was dissolved in CD_3CN. Selected NMR data: $^{31}P\{^1H\}$ NMR (CD_3CN) δ -12.92 (br, $[Rh(PMe_3)_4]^+$); $^{11}B\{^1H\}$ NMR (CD_3CN) δ 14.7 (br, $(Me_2Bcat)^-$, or $Bcat_2^-$), 12.3, 8.3; ^1H NMR (CD_3CN) δ -0.37 (s, CH_3-B^-), 1.42 (s, PMe_3), 6.18(m, cat), 6.52 (s, $Bcat_2^-$).

Reaction of [Rh(PMe$_3$)$_4$Me] with MeBcat. Compound [Rh(PMe$_3$)$_4$Me] (84 mg, 0.2 mmol) in 3 mL of hexane was added into a solution of MeBcat (32 mg, 0.24 mmol) in 10 mL of hexane. The solution rapidly turned cloudy upon additon, which was allowed to stir at room temperature over night. The yellow precipitate was then collected, yielding 98 mg (96%) of yellow solid. Selected NMR data: $^{31}P\{^1H\}$ NMR (CD_3CN) δ -12.74 (br, $[Rh(PMe_3)_4]^+$); $^{11}B\{^1H\}$ NMR (CD_3CN) δ 14.4 (br, $(Me_2Bcat)^-$, or $Bcat_2^-$),

12.3; ^{1}H NMR (CD_3CN) δ -0.35 (s, CH_3-B^-), 1.42 (s, PMe_3), 6.37(m, cat), 6.62 (s, $Bcat_2^-$).

Reaction of [Rh(PMe$_3$)$_4$Me] with [Rh(PMe$_3$)$_3$Cl$_2$(Bcat)]. Compound [$Rh(PMe_3)_4Me$] (25mg, 0.059 mmol) in 1 mL of toluene was added to a solution of [$Rh(PMe_3)_3Cl_2(Bcat)$] (30 mg, 0.058 mmol) in 1 mL of toluene. Some orange solid precipitated rapidly. The mixture was allowed to stir at room temperature for 1 h, resulting in an orange solution with some orange precipitate. A drop of PMe_3 was then added and more precipitate was produced. After stirring for another hour, The solid was collected by filtration, yielding 46 mg (90%) of [$Rh(PMe_3)_4$]Cl as a yellow powder. Selected NMR data: $^{31}P\{^1H\}$ NMR (CD_3CN) δ -12.41 (br, $[Rh(PMe_3)_4]^+$); ^{1}H NMR (CD_3CN) δ 1.41 (s, PMe_3). NMR data for filtrate: $^{11}B\{^1H\}$ NMR (C_6D_6/toluene) δ 35.2 (s, MeBcat); $^{31}P\{^1H\}$ NMR (C_6D_6/toluene) δ –60.66 (s, PMe_3).

4.3.3. Molecular Structure Determinations

4.3.3.1 Work at Waterloo

Structures of **21**, **22** were determined at the University of Waterloo. The data sets were collected at 295 K on a Siemens R3m/V diffractometer using graphite monochromated Mo Kα radiation (0.71073 Å) and ω scan methods with variable scan rates. Background measurements were made at the beginning and end of each scan for a total time equal to a quarter the scan time. Data were corrected for Lorentz and polarization effects and absorption (face-indexed numerical). The structures were solved by direct methods and refined by full-matrix least-squares methods using Siemens SHELXTL PLUS (VMS) software, with anisotropic thermal parameters for all non-hydrogen atoms and isotropic thermal parameters for hydrogen atoms. The function

minimized was $\sum w (|F_o|-|F_c|)^2$. The atomic scattering factors were taken from the International Tables Vol. 4.

4.3.3.1 Work at Newcastle, England

Structures of **24**, **26**, **36**, and **46** were determined at the University of Newcatle, England. Crystallographic data were collected at low temperature on a Siemens SMART CCD area-detector diffractometer using graphite-monochromated MoK_α radiation (λ = 0.71073 Å) and ω scan methods. The single crystal was mounted on a glass fiber with a coating of perfluoropolyether oil, cell parameters were refined from the observed setting angles and detector spot positions for selected reflections and intensities were measured from a series of frames each covering a 0.3° oscillation in ω. Absorption correction was carried out using a semi-empirical method from ω-scans, based on sets of equivalent reflections measured at different azimuthal angles.

The structure was solved by direct methods (SHELXS) (15), and refined by full-matrix least-squares techniques. The refinement was on F^2 of all independent reflections, to minimize $\sum\omega(F_o^2 - F_c^2)^2$, with weighting $\omega^{-1} = \sigma^2(F_o^2) + (aP)^2/bP$, where $P = (F_o^2 + 2F_c^2)/3$; the refined isotropic extinction parameter χ is defined such that F_c is multiplied by $(1 + 0.001\chi F_c^2 \lambda^3/\sin 2\theta)^{-1/4}$. Anisotropic displacement parameters were refined for all non-hydrogen atoms (16), and isotropic hydrogen atoms were constrained to ride on their parent carbon atoms with fixed bond lengths and idealized bond angles. Programs were standard Siemens control and integration software, versions 4 and 5 of SHELXTL, and local programs.

4.4. References

1. For reviews, see: (a) Burgess, K.; Ohlmeyer, M. J., *Chem. Rev.*, **1991**, 91, 1179. (b) Burgess, K.; van der Donk, W. in "Encyclopedia of Inorganic Chemistry", King, R. B. (ed.), John Wiley & Sons, **1994**, Vol. 3, p. 1420-1426. (c) Beletskaya, I; Pelter, A., *Tetrahedron*, **1997**, *53*, 4957.

2. For review on asymmetric metal-catalyzed hydroboration, see: Burgess, K., in "Advanced Asymmetric Synthesis", Stephenson, G. R. (Ed.), Chapman & hall, London, **1996**, p. 181-211.

3. (a) Baker, R. T.; Nguyen, P.; Marder, T. B.; Westcott, S. A., *Angew. Chem. Int. Ed. Engl.*, **1995**, *34*, 1336. (b) Lesley, G.; Nguyen, P.; Taylor, N. J.; Marder, T. B.; Scott, A. J.; Clegg, W.; Norman, N. C., *Organometallics*, **1996**, *15*, 5137. (c) Lawson, Y. G.; Lesley, M. J. G.; Marder T. B.; Norman, N. C.; Rice, C. R. *Chem. Commun.* **1997**, 2051. (d) Marder T. B.; Norman, N. C.; Rice, C. R. *Tetrahedron Lett.* in the press. (e) Ishiyama, T; Matsuda, N; Miyaura, N.; Suzuki, A., *J. Am. Chem. Soc.*, **1993**, *115*, 11018. (f) Ishiyama, T; Matsuda, N; Murata, M; Ozawa, F; Suzuki, A.; Miyaura, N., *Organometallics*, **1996**, *15*, 713. (g) Ishiyama, T; Yanmamoto, M.; Miyaura, N., *Chem. Commun*, **1996**, 2073. (h) Ishiyama, T; Yanmamoto, M.; Miyaura, N., *Chem. Commun*, **1997**, 689. (i) Iverson, C. N.; Smith, III, M. R., *Organometallics*, **1996**, *15*, 5155. (j) Iverson, C. N.; Smith, III, M. R., *Organometallics*, **1997**, *16*, 2757. (k) Cui, Q.; Musaev, D. G.; Morokuma, K., *Organometallics*, **1997**, *16*, 1355.

4. (a) Siginome, M.; Nakamura, H.; Ito, Y., *Chem. Commun*, **1996**, 2777. (b) Siginome, M.; Nakamura, H.; Ito, Y., *Angew. Chem. Int. Ed. Eng.* **1997**, *36*, 2516. (c) Onozawa, S. -Y.; Hatanaka, Y.; Tanaka, M.*Chem. Commun*, **1997**, 1229.

5. (a) Onozawa, S.; Hatanaka, Y.; Sakakura, T.; Shimada, S.; Tanaka, M., *Organometallics*, **1996**, *15*, 5450. (b) Onozawa, S. -Y.; Hatanaka, Y.; Choi, N.; Tanaka, M., *Organometallics*, in the press.

6. Ishiyama, T; Nishijima, K.; Miyaura, N.; Suzuki, A., *J. Am. Chem. Soc.*, **1993**, *115*, 7219.

7. (a) Ishiyama, T; Matsuda, N; Miyaura, N., *J. Org. Chem.*, **1995**, *60*, 7508. (b) Ishiyama, T; Itoh, T.; Kitano, Miyaura, N., *Tetrahedron Lett.* **1997**, *38*, 3447.

8. (a) Waltz, K. M.; He, X.; Muhoro, C.; Hartwig, J. F., *J. Am. Chem. Soc.*, **1995**, *117*, 11357. (b) Hartwig, J. F., *Science*, **1997**, *277*, 211.

9. Schmid, G. *Angew. Chem. Int. Ed. Engl.*, **1970**, *9*, 819.

10. Männig, D.; Nöth, H., *Angew. Chem. Int. Ed. Engl.*, **1985**, *24*, 878.

11. Kono, H.; Ito, K.; Nagai, Y., *Chem. Lett.*, **1975**, 1095.

12. Hewes, J. D.; Kreimendahl, C. W.; Marder, T. B.; Hawthorne, M. F., *J. Am. Chem. Soc.*, **1984**, *106*, 5757.

13. Nguyen, P.; Lesley, G.; Taylor, T. J.; Marder, T. B.; Pickett, N. L.; Clegg, W.; Elsegood, M. R. J.; Norman, N. C., *Inorg. Chem.*, **1994**, *33*, 4623.

14. (a) Brotherton, R. J.; McCloskey, A. J.; Boone, J. L.; Manasevit, H. M., *J. Am. Chem. Soc.*, **1960**, *82*, 6245. (b) Brain, P. T.; Downs, A. J.; Maccallum, P.; Rankin, D. W. H.; Robertson, H. E.; Forsyth, G. A., *J. Chem. Soc., Dalton Trans.*, **1991**, 1195.

15. Iverson, C. N.; Smith, III, M. R., *J. Am. Chem. Soc.*, **1995**, *117*, 4403.

16. (a) Hartwig, J. F.; He, X., *Angew. Chem. Int. Ed. Engl.*, **1996**, *35*, 315. (b) Hartwig, J. F.; He, X., *Organometallics*, **1996**, *15*, 5350. (c) He, X.; Hartwig, J. F., *Organometallics*, **1996**, *15*, 400.

17. Nöth, H.; Schmid, G., *Angew. Chem. Int. Ed. Engl.*, **1963**, *2*, 623.

18. Baker, R. T.; Calabrese, J. C.; Westcott, S. A.; Nguyen, P.; Marder T. B., *J. Am. Chem. Soc.*, **1993**, *115*, 4367.

19. Cleary, B. P.; Eisenberg, R., *Organometallics.*, **1995**, *14*, 4525.

20. Schmid, G.; Nöth, H., *Z. Naturforsch.*, **1965**, *20b* 1008.

21. Schmid, G.; Nöth, H., *Chem. Ber.*, **1967**, *100*, 2899.

22. Schmid, G., *Chem. Ber.*, **1969**, *102*, 191.

23. Marder, T. B.; Norman, N. C.; Rice, C. R.; Robbins, E. G., *Chem. Commun.*, **1997**, 53.

24. (a) Klein, H.F., *Angew. Chem. Int. Ed. Engl.*, **1971**, *10*, 343. (b) Klein ,H.F.; Karsch, H.H. ,*Chem. Ber.*, **1975**, *108*, 944.

25. Moezzi, A.; Olmstead, M.M.; Power, P.P., *J. Chem. Soc., Dalton Trans.*, **1992**, 2429.

26. Tippe, A.; Hamilton, W. C., *Inorg. Chem.*, **1969**, *8*, 464.

27. Jones, R.A.; Stuart, A.L.; Atwood, J.L.; Hunter, W.E.; *J. Cryst. Spectrosc.*, **1983**, *13*, 273.

28. Crystal data for **22**: $C_9H_{27}ClCoP_3$, crystal size = 0.11{100} mm (distance from a common center), M = 322.6, cubic, space group $Pa\bar{3}$, a = 15.345(2) Å, U =

3613.4(16) Å^3, Z = 8, D_c = 1.186 g cm^{-3}, μ = 13.37 cm^{-1} , F(000) = 1360, R = 0.0361, R_w = 0.0322 for 52 parameters and 632 unique observed [F > 6.0σ(F)] data ($2\theta_{max}$ = 50°), $w^{-1} = \sigma^2(F)$, measured at 200 K.

29. For studies of metal complexes of the $(\eta^2\text{-}B_2H_5)^-$ ligand see, for example: Coffy, T. J., Medford, G.; Plotkin, J.; Long, G. J.; Huffman, J. C.; Shore, S. G., *Organometallics*, **1989**, *8* , 2404, and references therein. These complexes, which can be regarded as containing the protonated $(\eta^2\text{-}B_2H_4)^{2-}$ ligand (isoelectronic with ethylene) have three center B-M-B bonds. In $[Fe(\eta^5\text{-}C_5H_5)(CO)_2(\eta^2\text{-}B_2H_5)]$, for example, the Fe-B distances average 2.217(3) Å and the B-B distance is 1.773(8) Å, i.e. the M-B distance is considerably longer and the B-B distance shorter than that in **21**.

30. Harris, R. K. In "Nuclear Magnetic Resonance Spectroscopy", Longman Scientific and Technical: Essex, U. K. **1986**.

31. Knorr, J. R.; Merola, J. S., *Organometallics*. **1990**, *9*, 3008.

32. Westcott, S. A.; Marder, T. B.; Baker, R. T.; Calabrese, J. C., *Can. J. Chem.*, **1993**, *71*, 930.

33. Baker, R. T.; Ovenall, D. W.; Calabrese, J. C.; Westcott, S. A.; Taylor, N. J.; William, I. D.; Marder, T. B., *J. Am. Chem. Soc*. **1990**, *112*, 9399.

34. Lu, Z.; Jun, C.; de Gala, S. R.; Sigalas, M.; Eisenstein, O. ; Crabtree, R. H., *J. Chem. Soc. Chem. Commun.* **1993**, 1877.

35. Westcott, S.A.; Taylor, N.J.; Marder, T.B.; Baker, R.T.; Jones, N.L.; Calabrese, J.C. *J. Chem. Soc., Chem. Commun.* **1991**, 304.

36. Westcott, S.A.; Blom, H.P.; Marder, T.B.; Baker, R.T.; Calabrese, J.C. *Inorg. Chem.* **1993**, *32*, 2175.

37. Rossi, A.R.; Hoffmann, R. *Inorg. Chem.* **1975**, *14*, 2899.

38. Zargarian, D.; Chow, P.; Taylor, N.J.; Marder, T.B. *J. Chem. Soc., Chem. Commun.* **1989**, 540.

39. Nguyen, P.; Blom, H.P.; Westcott, S.A.; Taylor, N.J.; Marder, T.B. *J. Am. Chem. Soc.* **1993**, *115*, 9329.

40. Matteson, D.S., "Sterodirected Synthesis with Organoboranes", **1995**, Springer, Berlin, pp 2-15.

41. Jones, R.A.; Mayor Real, F.; Wilkinson, G.; Galas, A.M.R.; Hursthouse, M.B.; Malik, K.M.A. *J. Chem. Soc., Dalton Trans*, **1980,** 511.

42. Sana, M.; Leroy, G; Wilante, C., *Organometallics*, **1992**, *11*, 781.

43. Rablen, P. R.; Hartwig, J. F.; Nolan, S. P., *J. Am. Chem. Soc.* **1994**, *116*, 4121.

44. Musaev, D. G.; Morokuma, K., *J. Phys. Chem.*, **1996**, *100*, 6509.

45. (a) Harrison, K.N.; Marks, T.J., *J. Am. Chem. Soc.* **1992**, *114*, 9220. (b) He, X.; Hartwig, J.F., *J. Am. Chem. Soc.* **1996**, *118*, 1696. (c) Pereira, S.; Srebnik, M., *Organometallics*, **1995**, *14*, 3127. (d) Lantero, D. R.; Ward, D. L.; Smith, III, M. R. *J. Am. Chem. Soc.* **1997**, *119*, 9699.

46. Hartwig, J. F.; Bhandari, S.; Rablen, P. R., *J. Am. Chem. Soc.* **1994**, *116*, 1839.

47. (a) Thorn, D.L., *Organometallics*, **1985**, *4*, 192. (b) Price, R.T.; Anderson, R.A.; Muetterties, E.L., *J. Organomet. Chem.*, **1989**, *376*, 407.

Chapter 5

Reactions between B_2cat_3 and Rh(I) Complexes: New Homogeneous Catalysts for the Diboration of Alkenes

5.1 Introduction

It has been known for more than 40 years that the B-B bonds in B_2X_4 diboron compounds (X = Cl, Br)[1,2] can add readily to unsaturated hydrocarbons to afford bis(dihaloboryl) organic compounds, which can then be converted easily to other important derivatives. In 1954, Schlesinger and co-workers[3] firstly reported that 1,2-bis(dichloroboryl)ethane was obtained in quantitative yield *via* stereospecific *syn* addition of B_2Cl_4 to ethylene at -80°C. Subsequent work has shown that B_2Cl_4 can also add to alkynes,[4] dienes,[5] aromatic compounds (benzene and naphthalene[6]), and a variety of vinyl-containing inorganic (or organometallic) compounds.[7] Figure **5.1** illustrates the generally accepted mechanism for this type of conventional diboration reactions.[4c,6c,8] The filled π-orbitals of the organic fragment are presumed to interact with the empty p-orbitals on the diboron compound giving rise to a four-centered transition state, which is followed by homolytic B-B bond cleavage to yield the corresponding diborated product.

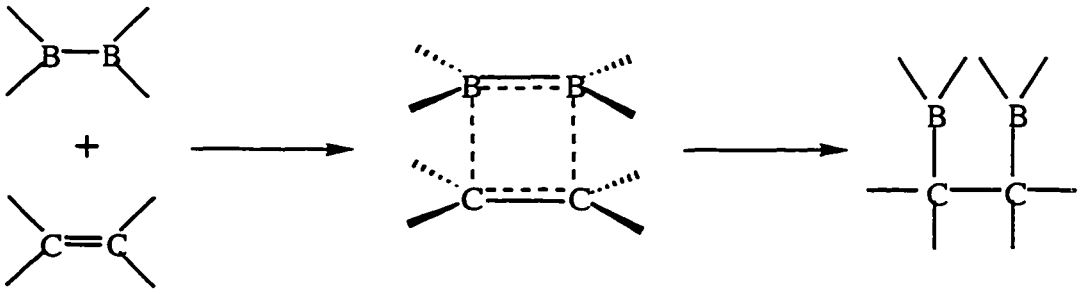


Figure 5.1 Mechanism for uncatalyzed diboration of alkenes.

However, some theoretical calculations on the reaction of B_2H_4 with ethylene[9a] and acetylene[9b] suggested that a three-center π-complex is preferred over the four-center one as an intermediate (Figure **5.2**). In the transition state, the π system donates some electronic charge to *one* of the boron atoms instead of both atoms.

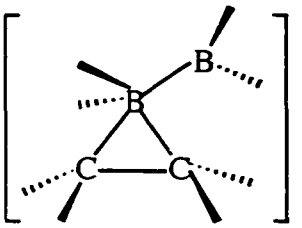


Figure 5.2 Three-center π-complex intermediate.

Despite the high reactivity of B_2X_4 compounds, difficulties in the preparation and handling of these hazardous reagents have precluded their widespread use in organic synthesis. Other hetero-atom substituted diboron compounds such as $B_2(OR)_4$ (**1**) and $B_2(NR_2)_4$ (**2**) are much more stable. However, they fail to add to carbon-carbon multiple bonds under normal conditions.[10] In the past 10 years or so, considerable progress has been made toward transition-metal catalyzed hydroboration (H-B) reactions,[11] as has some understanding of transition metal boryl (M-B) chemistry,[12,13] and eventually, transition metal catalyzed diboration (B-B) reactions.

In 1993, while working on Rh catalyzed alkene hydroboration reactions,[14] researchers in our group discovered[15] that a novel Rh(III) bis(boryl) complex $[Rh(PPh_3)_2Cl(Bcat)_2]$ (**3**) was formed slowly (days) *via* reaction of $[Rh(PPh_3)_2(\mu\text{-}Cl)]_2$ (**4**) with excess of HBcat (cat = 1,2-$O_2C_6H_4$). It was found that the rapid formation of the H-B oxidative addition product $[Rh(PPh_3)_2(Cl)(H)(Bcat)]$ (**5**) was followed by a slow second step reaction with loss of H_2, resulting in **3**. (Reactions **5.1**, **5.2**)

$$[Rh(PPh_3)_2(\mu\text{-}Cl)]_2 + 2\ HBcat \rightarrow 2\ [Rh(PPh_3)_2(Cl)(H)(Bcat)] \qquad (\mathbf{5.1})$$

$$[Rh(PPh_3)_2(Cl)(H)(Bcat)] + HBcat \rightarrow [Rh(PPh_3)_2(Cl)(Bcat)_2] + H_2 \quad (5.2)$$

It was observed that reaction of **3** with an alkene substrate such as 4-vinylanisole led to the formation of several organoboron products, including the 1,2-diborated product 4-$MeOC_6H_4CH(Bcat)CH_2(Bcat)$. Other species such as the dehydrogenative borylation product vinylboronate ester (*E*)-4-$MeOC_6H_4CH{=}CH(Bcat)$ and hydroboration product 4-$MeOC_6H_4CH(Bcat)CH_3$ were also present in the solution. This result clearly indicates that the C=C bond is capable of insertion into the M-B bond in the Rh(III) bis(boryl) complex **3**, and it also implies the existence of the competing B-C reductive elimination and β-hydride elimination pathways from the common alkene insertion intermediate. In the meantime, we have also demonstrated[17] that diboron compounds such as B_2cat_2 (**1a**)[16] and its analogs $B_2(4\text{-}Bu^t\text{-}cat)_2$ (**1b**) and $B_2(3,5\text{-}Bu^t{}_2\text{-}cat)_2$ (**1c**) undergo facile quantitative oxidative addition to complex **4**. Based on these two observations, it is highly plausible to believe that the addition of the more stable diboron compounds $B_2(OR)_4$ to unsaturated hydrocarbons could be achieved by employing certain transition metal complexes as catalysts.

5.1.1. Pt(0) Catalyzed Diboration of Alkynes

Shortly after our discovery of the alkene insertion into the metal boron bond, Suzuki and Miyaura reported[18] that $[Pt(PPh_3)_4]$ (**6**) could effectively catalyze the addition of B_2pin_2 (**1d**,[19] pin = $OCMe_2CMe_2O$) to alkynes. However, this catalyst was ineffective for alkenes, and the authors also stated that Wilkinson's catalyst, $[Rh(PPh_3)_3Cl]$ (**7**), was incapable of catalyzing the addition of **1d** to alkynes. Subsequent reports in this area by several research groups including Suzuki & Miyaura,[20] Smith,[21] and our group[22] demonstrated that B_2cat_2 (**1a**) and $B_2(OMe)_4$ (**1e**) are also suitable for Pt(0) catalyzed diboration of alkynes. The B-B oxidative addition product

cis-[$Pt(PPh_3)_2(B(OR)_2)_2$] (**8a,d**) has been shown to play an important role in the catalytic cycle, which can also be readily generated through the reactions of $B_2(OR)_4$ with [$Pt(PPh_3)_2(\eta\text{-}C_2H_4)$] (**9**).[22, 23] Various alkynes or 1,3-butadiynes undergo diboration or tetraboration reactions in high yield under mild conditions by employing a catalytic amount of either **6**, **9** or Pt(II) bis(boryl) complexes **8**.

The Pt(0) catalyzed alkyne diboration reactions can also tolerate a broad range of functionality such as carbon-carbon double bond, chloro, epoxy, ester, cyano, and ketones, etc. It is not surprising to see their swift applications in organic synthesis. For instance, Kraft and Tochtermann reported[24] in 1994 the synthesis of a 12-membered ring compound (Z)-(±)-5,6-dimethylcyclododec-5-en-1-ol (**11**), a cedarwood fragrance substance, where the key reaction step is the diboration of the intermediate cycloalkynone (**10**) (Figure **5.3**).

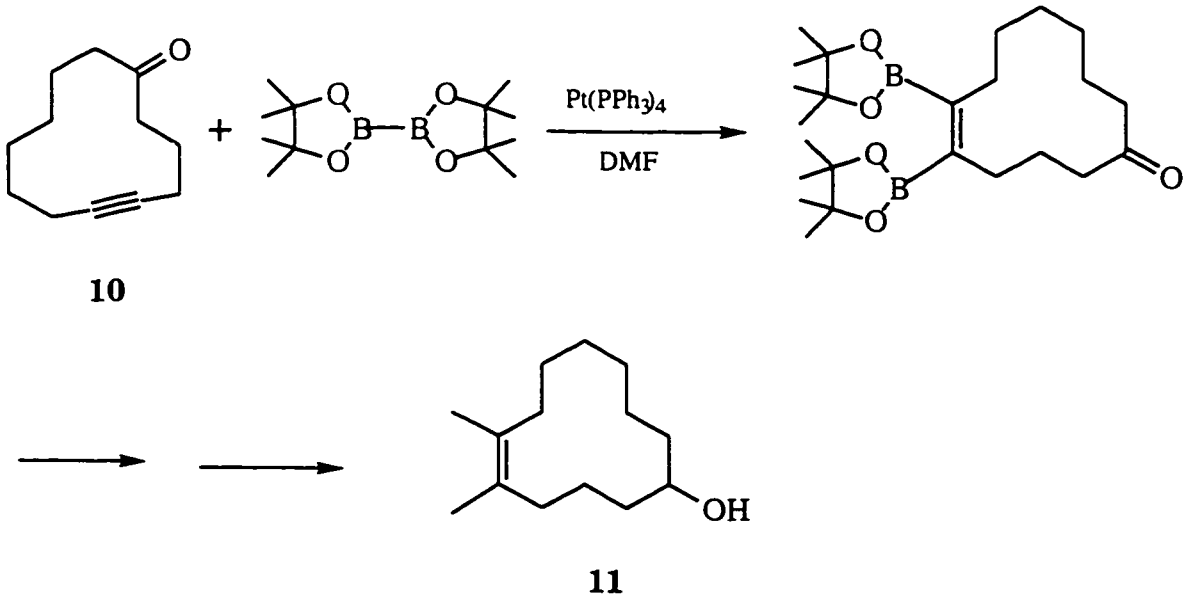


Figure 5.3 Synthesis of (Z)-(±)-5,6-dimethylcyclododec-5-en-1-ol (**11**).

Likewise, Siebert and co-workers[25] recently reported that diboration of catB-C≡C-Bcat (**12**) by **1a** in the presence of 6.2 mol% **9** led to the formation of the novel tetraborylethene compound $(catB)_2C{=}C(Bcat)_2$ (**13**) in 50% yield. A compound of this

type ($C_2(BF_2)_4$) was only obtained previously through a gas-phase reaction of carbon and B_2F_4.[26] In addition, following Miyaura and Suzuki's procedure, Brown and Armstrong[27] diborated a variety of internal alkynes. The resulting *cis*-bis(boryl)alkenes **14** were then coupled with 1.5 equiv of organohalide catalyzed by $[Pd(PPh_3)_2Cl_2]$ to give predominantly the monoaddition product **15**, which then underwent another Suzuki coupling reaction[28] with resin-bound aryl iodide to generate the final tetrasubstituted ethylene compounds **16** captured on the solid support. This method provides a general route to a number of antiestrogenic triphenylethylene derivatives[29] such as tamoxifen, [30] which is used to treat breast cancer.

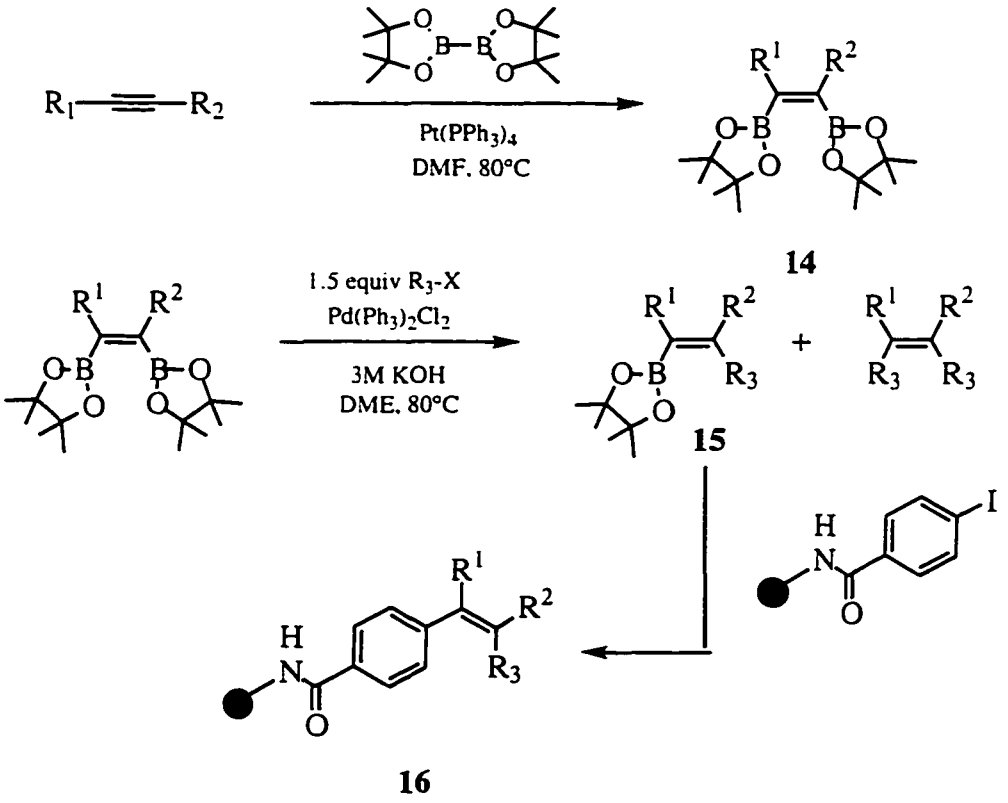
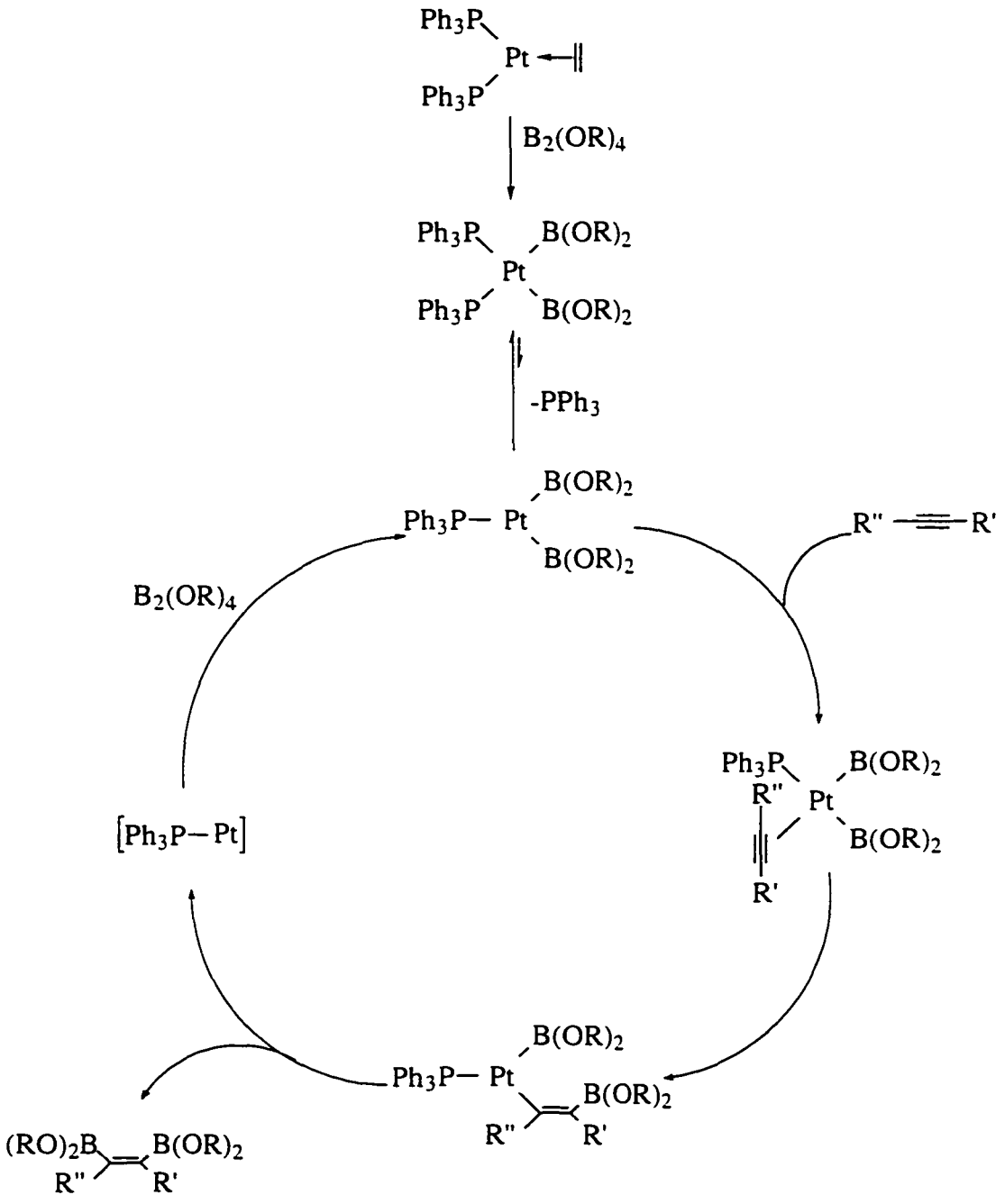


Figure 5.4 Synthesis of tetrasubstituted ethylenes on solid support.

The proposed catalytic cycle for Pt(0) catalyzed diboration of alkynes follows fundamentally the common process with a group 10 transition metal. (Scheme **5.1**) It is initiated by oxidative addition of the B-B bond to the metal center Pt(0), followed by the coordination of the alkyne to Pt(II) and migratory insertion into one of the Pt-B bonds. Reductive elimination of a B-C bond then gives the diborated product and regenerates the catalyst. Experimental[21,22] and theoretical[31] studies all suggested that the phosphine dissociation step is critical to the reaction. It has been demonstrated[21,22] that catalysts with only two phosphine ligands (**8a**, **8d**, and **9**) exhibited higher activity than [$Pt(PPh_3)_4$], while Pt(II) bis(boryl) complexes with chelating phosphines showed extremely low ([Pt(dppb)$(Bcat)_2$], **17**) or no catalytic activity at all ([Pt(dppe)$(Bcat)_2$], **18**). The catalytic reactions were greatly hampered when additional PPh_3 was added to catalyst **9**.



Scheme 5.1 Proposed catalytic cycle for diboration of alkynes.

5.1.2. Pt(0) Catalyzed Diboration of Alkenes

The complex [$Pt(PPh_3)_4$] was also able to catalyze the diboration reactions of alka-1,3-dienes to yield selectively the 1,4-diborated products[32] (Figure **5.4**). For instance, when isoprene (1.5 equiv.) was allowed to react with **1d** at 80°C for 16 h in the presence of 3 mol% of **6** in toluene, (*Z*)-1,4-bis(pinicolatoboryl)but-2-ene was obtained as the sole product in 93% yield. However, diboration of alkenes with Pt complexes was not successful until very recently when Miyaura [33] applied phosphine free Pt(0) complexes toward this task.

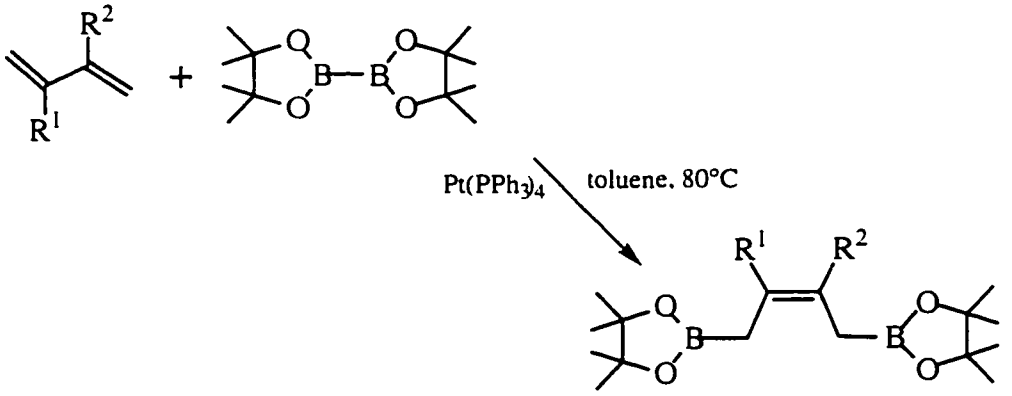
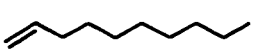
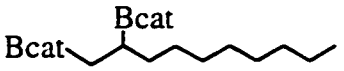
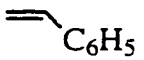
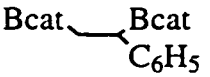
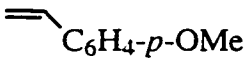
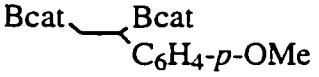
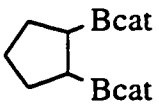
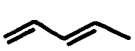
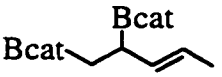


Figure 5.5 [$Pt(PPh_3)_4$]-catalyzed diboration of 1,3-alkenes

It became clear from the mechanistic analysis on the Pt(0) catalyzed diboration of alkynes that phosphine dissociation is a critical step in the catalytic pathway. Both Smith[21] and our group[22] concluded that catalyst precursors with fewer and monodentate phosphine ligands exhibit higher activity. Therefore, Miyaura [33] reported very recently that the phosphine free Pt(0) complex, [$Pt(dba)_2$] (dba = dibenzylideneacetone, **19**) was able to catalyze the addition of **1d** to various aliphatic and aromatic terminal alkenes at 50°C in toluene. Cyclic alkenes with internal strain were also diborated similarly with good yields (Table **5.1**). However, attempts in the diboration of other internal alkenes such as stilbene and 2-methylpropene were unsuccessful. It is interesting to note that in

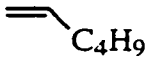
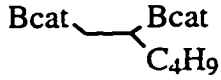
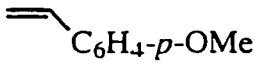
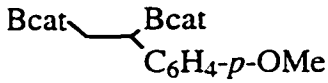
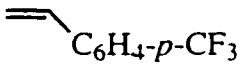
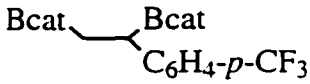
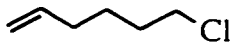
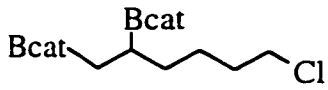
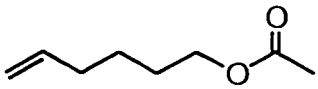
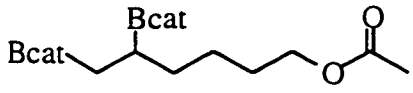
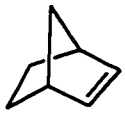
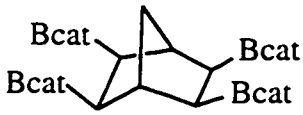
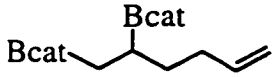
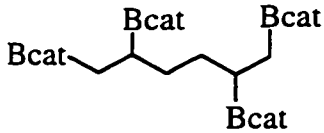
Entry 6, the catalyst [Pt(dba)$_2$] gives formation of the 1,2-addition product only with certain conjugated dienes such as penta-1,3-pentene, whereas, [Pt(PPh$_3$)$_4$] generates the 1,4-addition product at 80°C as shown earlier. This allows one to apply different catalysts to the diboration of dienes for various purposes. It is important to notice that the reported isolated yields were based on the diboron reagent **1d**, to which 1.5 equivalents of alkene (3.0 equiv of 4-vinylanisole in entry 3) were added for the reactions. These results, nevertheless, have certainly indicated the right direction for the search for more efficient diboration catalysts.

Table 5.1 Pt(dba)$_2$-catalyzed diboration of alkenes

Entry	Olefin	Product	%yield
1			82
2			86
3			76
4			85
5			85
6			82

Almost simultaneously, Smith et al.[34] independently came to the same conclusion employing phosphine free Pt(0) catalysts for the diboration of alkenes. Instead, they utilized the base-free Pt compounds [$Pt(COD)_2$] (COD = 1,5-cycloocta-di-ene, **20**) and [$Pt(NBE)_3$] (NBE = norbornadiene, **21**) which were reported by Stone and co-workers[35] 20 years ago, and higher diboration reactivities were observed (Table **5.2**). Again, even these catalysts failed to diborate non-strained internal alkenes. These findings are, indeed, big breakthroughs toward the metal catalyzed diboration of alkenes, however, further work is apparently needed for internal alkene substrates.

Table 5.2 $Pt(COD)_2$ or $Pt(NBE)_2$-catalyzed diboration of alkenes

Entry	Olefin	Product	%yield
1			84
2			95
3			90
4			95
5			85
6			88
7			93
8			89
9			82
10			87

5.1.3. Pd(0) Catalyzed Cross-Coupling Reactions between Arylhalides and Diboron Compounds

Recently, there has been a growing interest in both academic and industrial laboratories in the tetra(alkoxy) diboron compounds, particularly, B_2cat_2 (**1a**) and B_2pin_2 (**1d**). These diboron reagents exhibit good stability, and they can be prepared in large quantities through the reaction of $B_2(NMe_2)_4$ (**2a**) with corresponding diols (Figure **5.6**). Very recently, B_2pin_2 became commercially available[36] from two chemical companies, Frontier Scientific Inc., Utah (www.Frontiersci.com), and Callery Chemical Co., Pennsylvania (callery.info.MSAnet.com). It is clear that research on the application of these diboron compounds in organic synthesis will be greatly enhanced in the near future.

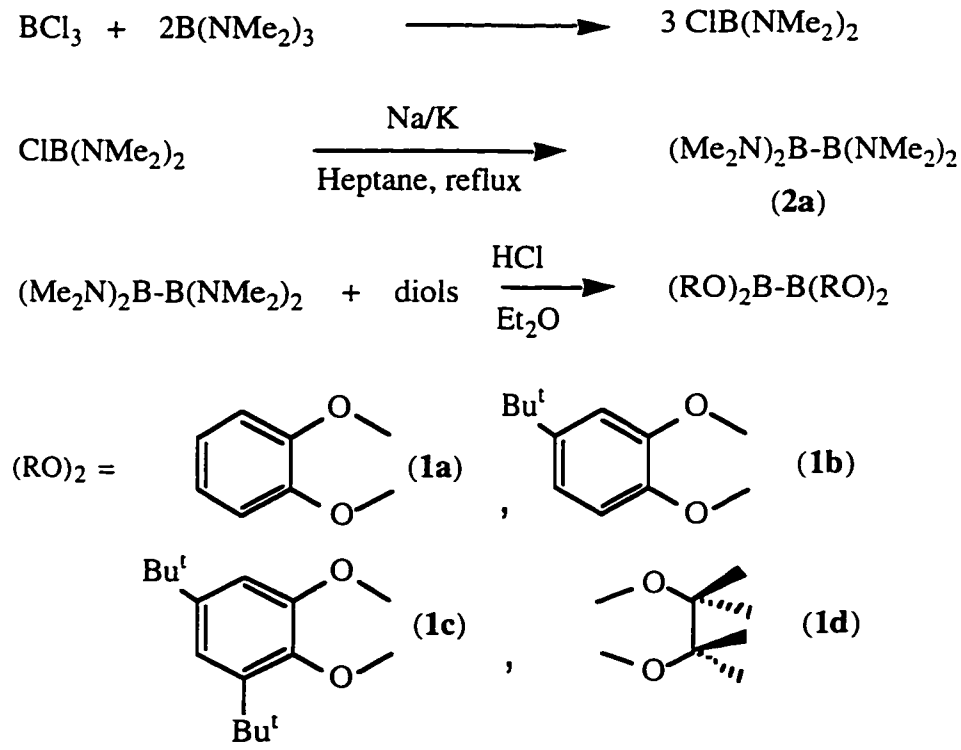


Figure 5.6 Synthesis of diboron compounds **1a-d.**

In addition to the Pt(0) catalyzed diboration reaction with alkynes, dienes, and alkenes, Miyaura[37] also reported that diboron compound such as **1d** can undergo Pd(0)

catalyzed cross-coupling reactions with haloarenes, which provides a novel direct route to arylboronic esters without using Grignard or other metal-mediated reagents. Subsequent application of this reaction includes : solid-phase Suzuki coupling reactions, [27, 38] one pot biaryl synthesis via *in situ* boronate formation, [39] and so on (Figure **5.7**).

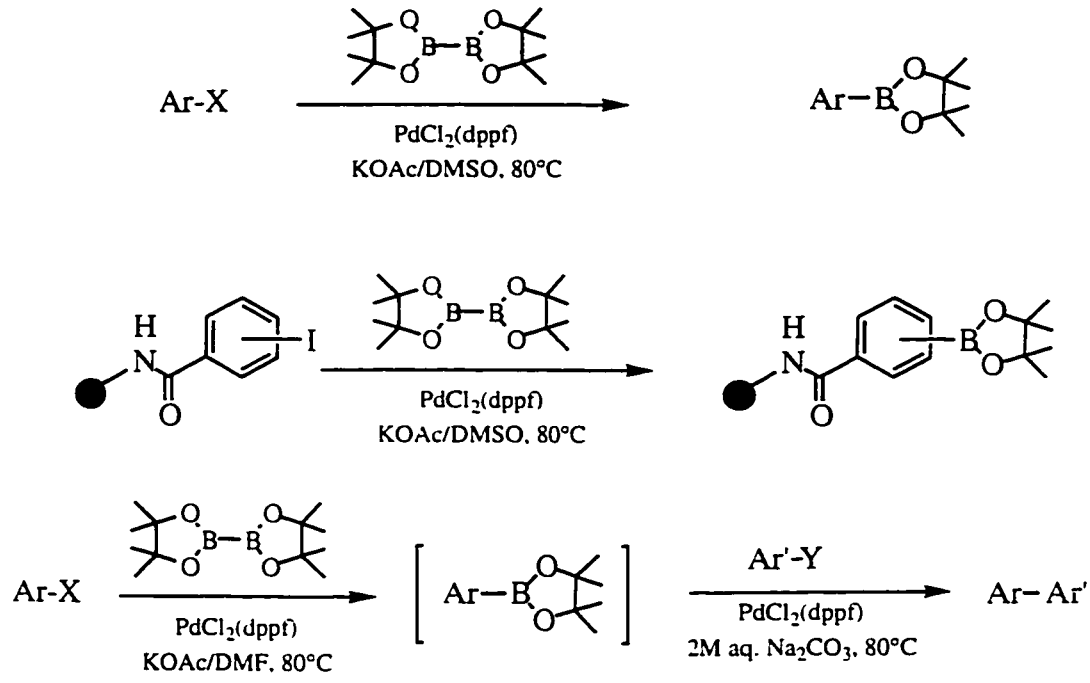
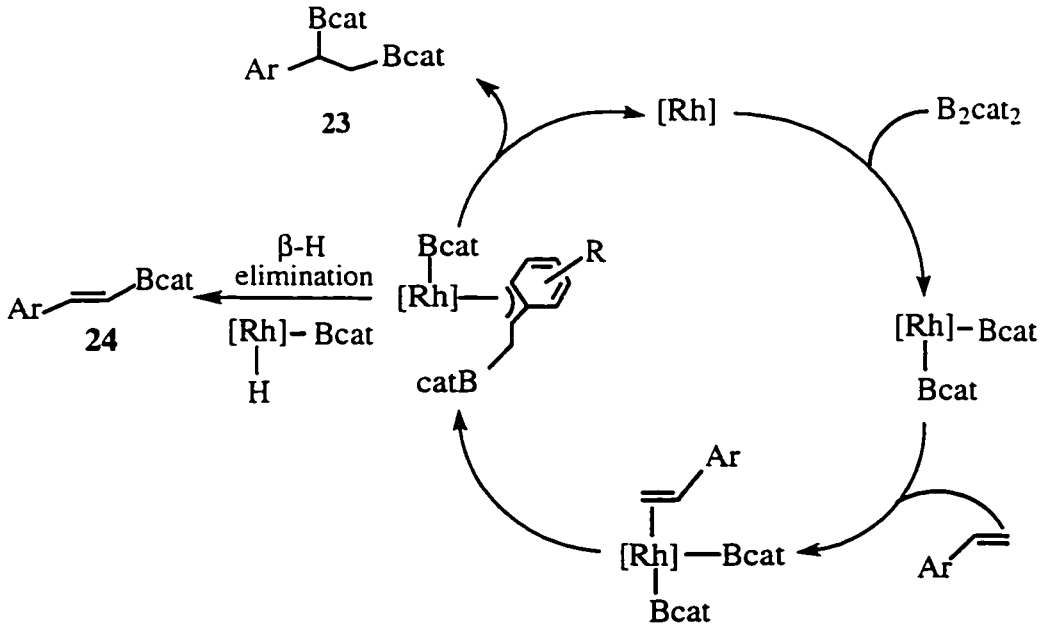


Figure 5.7 Pd(0)-catalyzed cross-coupling of **1d** with arylhalides

5.1.4. Rh(I) Catalyzed Diboration of Alkenes

We have had a long-standing interest in the Rh-catalyzed diboration of alkenes. Stoichiometric reaction between the Rh(III) bis(boryl) complex $[Rh(PPh_3)_2(Cl)(Bcat)_2]$ and 4-vinylanisole ($MeO\text{-}C_6H_4\text{-}CH{=}CH_2$, **22**) gave the corresponding 1,2-bis(boronate) ester (**23**) along with other species. We reported[40] for the first time in 1995, that catalytic diboration of **22** by **1a** was achieved by a number of rhodium complexes. However, the biggest drawback of these Rh catalytic systems is that the selectivity of this reaction suffers heavily from the competing β-H elimination pathway as already observed at the

previous stoichiometric reaction. With typical rhodium hydroboration catalysts such as [$Rh(PPh_3)_3Cl$], only 10% of the desired product **23** was observed (see Table **5.3**). We assumed that the proposed mechanism resembled that of Rh(I) catalyzed hydroboration or Pt(0) catalyzed diboration reactions. It is initiated by oxidative addition of B-B bond to Rh(I) center, followed by coordination of the alkene and migratory insertion into one of the Rh-B bonds, and subsequent B-C reductive elimination affords the diborated product **23** (Scheme **5.2**). However, the competing β-H elimination reaction from the Rh(III) β–borylalkyl intermediate complicates the catalytic cycle (Scheme **5.3**). As a result, subsequent reactions such as hydroboration, hydrogenation, dehydrogenative borylation as well as diboration give rise to an array of by-products. We have also successfully terminated the β-H elimination by using $Au(PEt_3)Cl$/dcpe as a catalyst, which gives exclusively 1,2-diborated product. However, the higher selectivity is accompanied by much lower reactivity and stability. The reaction is probably too sluggish to act as a practical method for organic synthesis. Obviously, better catalysts are needed.

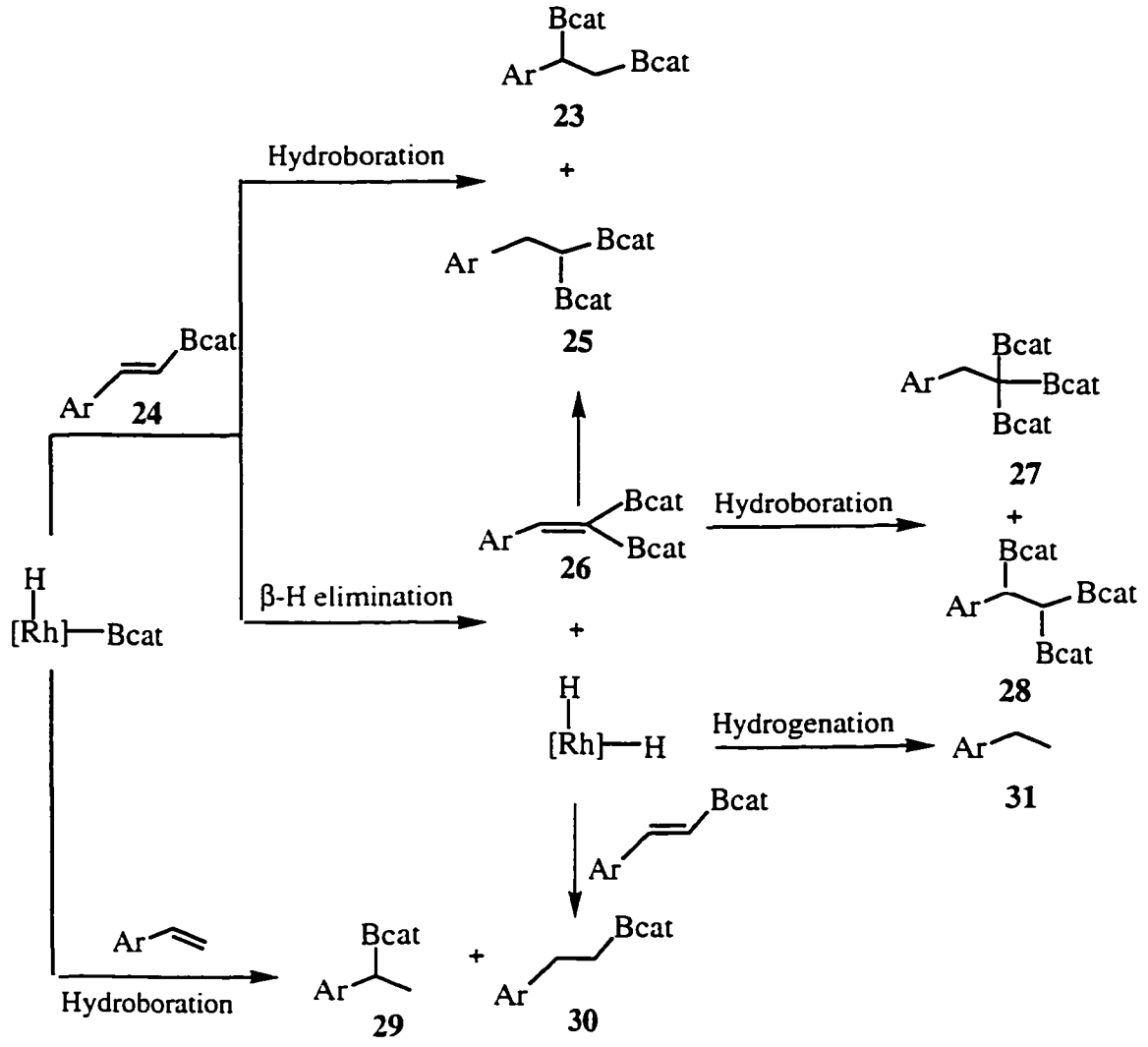


Scheme 5.2 Proposed catalytic cycle for Rh(I) catalyzed diboration of alkenes

Table 5.3 Transition metal catalyzed addition of B_2cat_2 (**1a**) to 4-vinylanisole.[a]

Entry	Catalyst	23	24	25	26	27	28	29	30	31
a	$RuCl_2(PPh_3)_4$[b]	-	42	13	7	-	-	2	25	11
b	$[Ir(\mu\text{-}Cl)(COE)_2]_2$[c]	21	35	1	-	-	-	14	27	2
c	$[Rh(\mu\text{-}Cl)(COE)_2]_2$	7	40	-	2	1	2	43	1	4
d	$RhCl(N_2)(PPr^i_3)_2$	8	20	36	5	9	-	10	12	-
e	$(\eta^6\text{-}Bcat_2)Rh(Dippe))$	10	34	31	-	3	-	20	-	2
f	$RhCl(PPh_3)_3$	11	31	1	1	4	1	50	1	1
g	$RhCl(PPh_3)_3$/10 PPh_3	13	14	1	3	28	7	30	3	1
h	$[Rh(COD)(DPPB)]BF_4$	26	35	5	-	-	-	32	1	1
i	$(\eta^6\text{-}Bcat_2)Rh(dppb)$	44	-	10	-	22	-	22	-	2
j	$AuCl(PEt_3)$/dcpe	**100**	-	-	-	-	-	-	-	-

[a]All reactions were carried out in THF at room temperature for 20 h in the presence of 4 mol% catalyst (**1a**/alkene/catalyst = 1.0/1.0/0.04). Product ratios determined by ^1H and ^{13}C NMR. [b]Reactions were complete after 40 hr. [c]Only 75% conversion due to catlayst deactivation. [d]Carried out 80°C for 48 h with 8 mol% catalyst. COE = cyclooctene, COD = 1,5-cyclooctadiene, DiPPE = 1,2-bis(diisopropylphosphino)ethane, DPPB = 1,4-bis(diphenylphosphino)butane.



Scheme 5.3 Possible products resulting from the β-H elimination pathway.

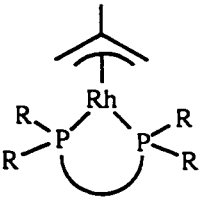
5.1.5 Our Objectives

While progress has been made very recently toward phosphine free Pt(0) catalysts for the diboration of alkenes, we turned our attention back to the Rh(I) system. We reasoned that: (1) Pt(0) catalysts still had no success for non-strained internal alkenes, but preliminary results in our group[41] indicated that certain rhodium complexes are capable of diborating 1,2-disubstituted alkenes. Moreover, with Rh phosphine catalysts, it should

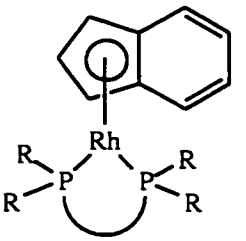
be possible to develop asymmetric catalytic diboration of alkenes and other substrates. (2) Instead of trying to avoid the β-H elimination pathway in these systems, we may be able to take advantage of this fact to develop a way of pursuing the dehydrogenative borylation reactions. In fact, preliminary results in our lab demonstrated that when **1d** and 1-octene (1:1) along with 2 mol% $[Rh(PPh_3)_2(CO)Cl]$ (**32**) were heated at 80°C for 3 days in toluene/acetonitrile (3:1), 72% of the novel 1,1-bis(pinacolboryl)oct-1-ene was observed.[42] (3) Previous studies on Rh-catalyzed *hydroboration* reactions[14c, 14b] indicated that competing β-H elimination pathway could be avoided by use of a rhodium complex with a chelating bis(phosphine) ligand. Among various Rh catalysts that we had screened earlier, the best selectivity for diboration of 4-vinylanisole was obtained with the zwitterionic complex $[(\eta^6\text{-}Bcat_2)Rh(dppb)]$ (dppb = 1,4-bis(diphenylphosphino) butane, **33g**). This complex has initially been demonstrated to be an extremely efficient *hydroboration* catalyst.[42] Even though its result on the *diboration* of 4-vinylanisole is not yet satisfactory (44% diborated product), perhaps fine tuning of the bis(phosphine) ligand could lead to much better catalyst.

Complex **33g** belongs to a family of zwitterionic Rh(I) complexes $[(\eta^6\text{-}Bcat_2)RhL_2]$ (**33**) where the RhL_2 fragment coordinates to one of the arene rings of the $[B(cat)_2]^-$ anion. The only previously isolated and well characterized complex in this series is $[(\eta^6\text{-}Bcat_2)Rh(Dippe)]$ (Dippe = 1,2-bis(diisopropylphosphino)ethane, **33n**), which was first obtained from the reaction of $[(\eta^3\text{-}2\text{-Me-allyl})Rh(Dippe)]$ (**34n**) with a large excess of HBcat (**35**).[43] Subsequent work in our lab demonstrated that complexes $[(\eta^5\text{-indenyl})Rh(P_2)]$ (**36**) and $[(acac)Rh(P_2)]$ (acac = acetylacetonate, **37**) were also able to lead to the formation of **33** in a similar fashion.[14b,42,44] These $(\eta^6\text{-}Bcat_2)RhL_2$ zwitterionic complexes are of great interest to us because they exhibit both extremely high catalytic activities and regio selectivities in catalytic *hydroborations* of alkenes.[42] Their formation was believed to involve the redistribution of catecholate groups from HBcat, but the exact mechanism is not yet clear . The reactions depend largely on the

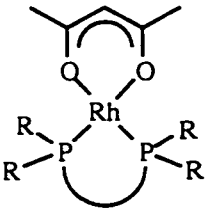
properties of the ancillary ligands L_2. In some cases, **33** was obtained as the sole Rh-containing product, but on other occasions, the products were too complicated to identify. Some special processes have to be applied to make a certain complex. For instance, in order to make **33g**, a stoichiometric hydroboration reaction has to be conducted in the presence of certain alkenes to secure a clean conversion. It is apparent that a more efficient and more general route to the preparation of these novel $[(\eta^6\text{-}Bcat_2)RhL_2]$ zwitterionic complexes is vividly required.



34



36

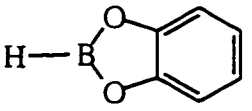


37

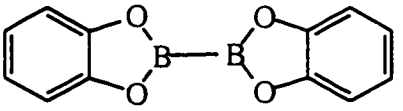
In this chapter, we will start with a brief description of the reactions between B_2cat_3 (tris(catecholato) diboron, **38**) and several types of Rh(I) complexes. We have found that the reaction of **38** and $[(acac)RhL_2]$ can afford the exclusive formation of $[(\eta^6\text{-}Bcat_2)RhL_2]$ complexes. Their synthesis and molecular structures with various ancillary ligands have been studied, and finally, these complexes have been applied as catalysts for the diboration of alkenes.

5.2 Results and Discussion

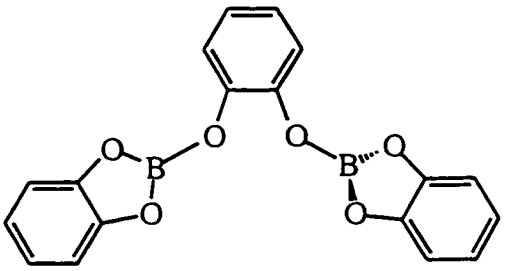
In the preceding chapter, we have described reactions between the electron rich Rh(I) complex [$Rh(PMe_3)_4Me$] (**39**) and the diboron compound B_2cat_2 (**2a**) and its analogs **2b-2f**. This complex has also shown reactivity toward the hydroboron reagent HBcat (**35**), [45] the haloboron reagent ClBcat (**40**), and even the alkylboron compound MeBcat (**41**) (see chapter 4). Can it react with the structural related compound B_2cat_3?



35



2a



38

5.2.1 B_2cat_3 and Its Reactions with Low Valent Rh(I) Complexes

B_2cat_3 (**38**) is a very closely related compound to the above Bcat containing reagents. As a matter of fact, it has its presence in numerous transition metal catalyzed hydroboration (HBcat) or diboration (B_2cat_2) experiments as an undesired side product. This is not surprising, since even pure HBcat decomposes slightly at room temperature to give B_2cat_3 as one product (Reaction **5.3**), and the commercially available HBcat product (solution in THF) decomposes more rapidly, forming B_2cat_3 and H_3B•THF adduct.[45] Therefore, HBcat samples, either neat or as THF solutions, need to be stored at low temperature, and special care should be taken when **35** is distilled *in vacuo* from its

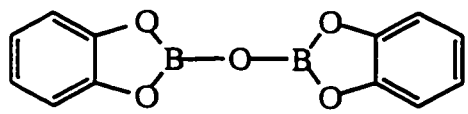
THF solution in order to avoid elevated operating temperatures which lead to decomposition. We have also studied stoichiometric reactions between **35** and certain nucleophiles which are often present in the metal-catalyzed hydroboration or diboration processes.[45] For instance, PPh_3 promotes HBcat degradation ($t_{1/2}$ = 4 h) to $H_3B{\bullet}PPh_3$ and **38**, other bulky phosphines afford analogous products (Reaction **5.4**); Wilkinson's catalyst, $[Rh(PPh_3)_3Cl]$ also mediates the irreversible degradation of HBcat to mainly **38** and $[RhH_2Cl(PPh_3)_3]$ (Reaction **5.5**) to some extent. This process is largely assumed to be responsible for the hydrogenation side products in the Rh catalyzed hydroboration (HBcat) reactions.[14a]

$$3\ \text{HBcat} \rightleftharpoons B_2cat_3 + BH_3 \qquad \textbf{(5.3)}$$

$$3\ \text{HBcat} + PPh_3 \longrightarrow B_2cat_3 + H_3B{\bullet}PPh_3 \qquad \textbf{(5.4)}$$

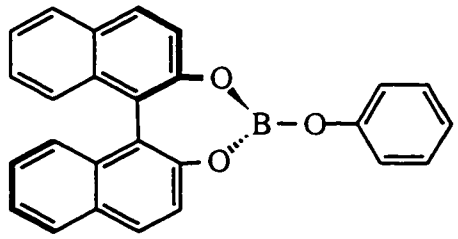
$$n\ \text{HBcat} + RhCl(PPh_3)_3 \longrightarrow B_2cat_3 + RhH_2Cl(PPh_3)_3 + \text{unidentified boron containing products} \qquad \textbf{(5.5)}$$

Like **35**, ClBcat also exhibits similar thermal and chemical stabilities (though not to the same extent), and B_2cat_3 is often one of the main degradation products.[42,46] The involvement of B_2cat_3 in the catalytic B_2cat_2 addition processes is not clear yet, and the question of whether B_2cat_3 is an intermediate in the degradation of B_2cat_2 is still under investigation. Usually, a resonance at *ca.* 23 ppm in the $^{11}B\{^1H\}$ NMR spectrum is observed, which is consistent with the signal of B_2cat_3. However, other species such as catB-O-Bcat (**42**) may also resonate in this region. Nevertheless, B_2cat_3 has always been related to the transition metal catalyzed H-Bcat and catB-Bcat addition reactions, and it has always been regarded as an unwelcome degradation product.

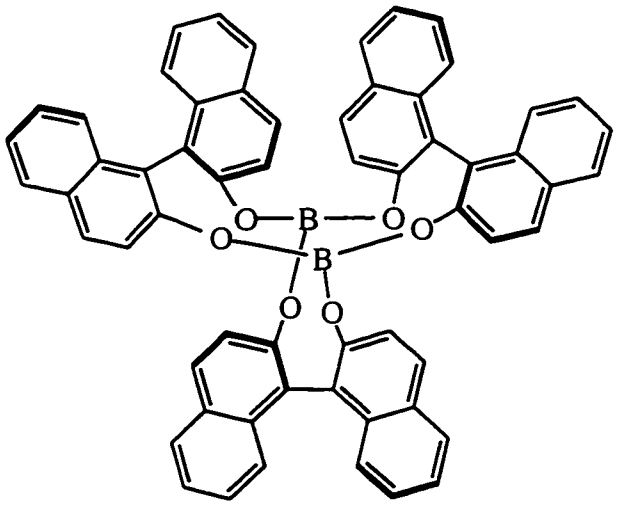


42

However, a triaryl borate compound like B_2cat_3 obviously presents an appreciable Lewis acidity on the boron atom which should find itself some positive applications. Similar compounds have been widely utilized as selective Lewis acid catalysts for Diels-Alder and aldo type reactions. For example, Yamamoto[47] has demonstrated that chiral boron compound **43** is a very efficient promoter for the aza Diels-Alder reaction of imines; Kaufmann[48] prepared the novel **38** analog $B_2(BINOL)_3$ (**44**) which exhibits a unique cyclic structure with a C_3-symmetry due to the large chelating β-binaphtholate ligands. Compound **44** shows excellent stereo- and enantio-selectivity toward the Diels-Alder reaction of methacrolein and cyclopentadiene.[48]



43



44

In the structure of B_2cat_3 (Figure **5.8**),[45] the two B-O bonds in the bridging catecholate group are somewhat shorter than the chelate B-O bond distance, averaging 1.352(4) vs 1.382(4) Å, respectively, the latter is essentially the same as that in B_2cat_2 (1.388 Å).[49] The two opposing chelate catecholate groups are nearly perpendicular to one another, presumably due to steric constrains imposed by the oxygen lone pairs. While the chelating catecholate groups are planar, the B-O vectors of the bridge from a dihedral angle of 4.94°.

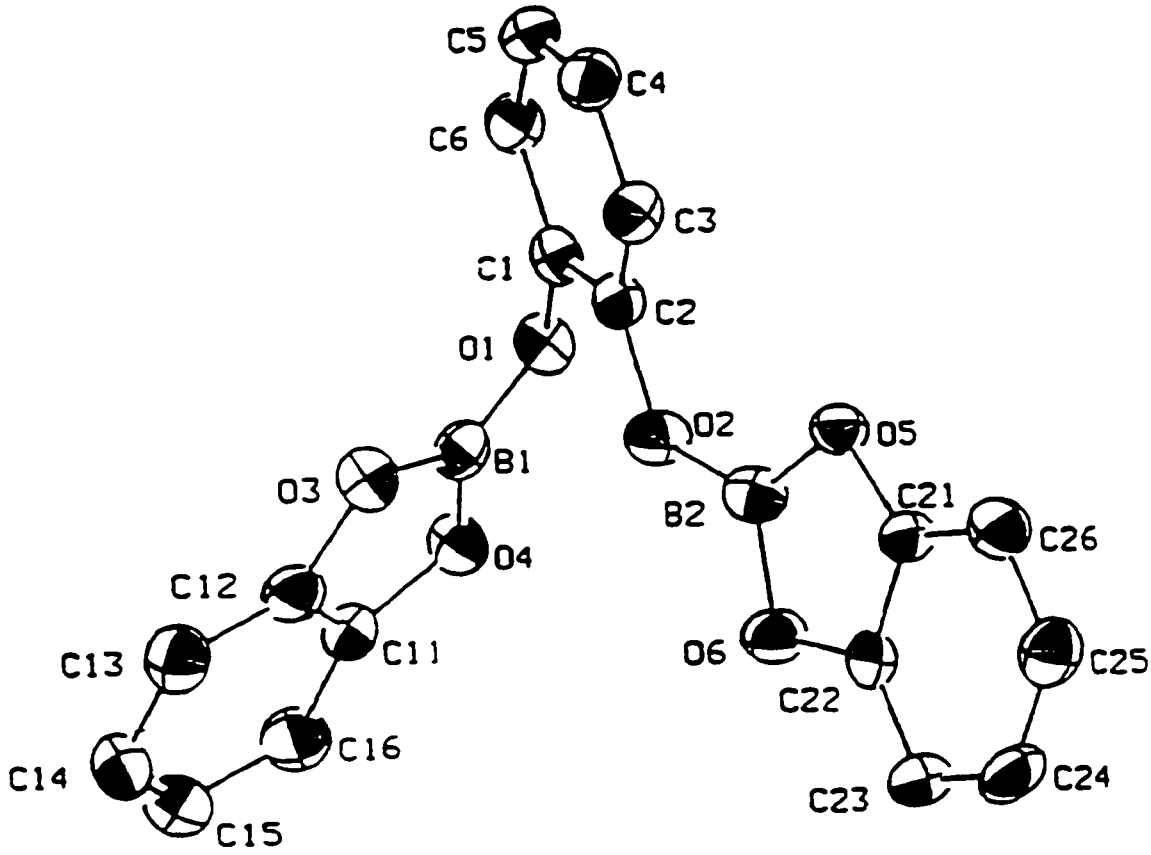


Figure 5.8 Crystal structure of B_2cat_3 (**38**), with 50% probability ellipsoids.

5.2.1.1 Reaction of B_2cat_3 and $[Rh(PMe_3)_4Me]$

When equal molar amounts of B_2cat_3 and $[Rh(PMe_3)_4Me]$ in C_6D_6 were mixed at room temperature, the orange ionic compound $[Rh(PMe_3)_4]^+[Bcat_2]^-$ (**45**) precipitated readily from the solution, MeBcat being the other product, which was characterized by $^{11}B\{^1H\}$, ^1H NMR spectroscopy and GC-MS. The reaction was rapid and quantitative, no other products were detected (Reaction **5.6**).

$$[Rh(PMe_3)_4Me] + B_2cat_3 \rightarrow [Rh(PMe_3)_4]^+[Bcat_2]^- + MeBcat \qquad (\mathbf{5.6})$$

The $^{31}P\{^1H\}$ NMR spectrum of $[Rh(PMe_3)_4][Bcat_2]$ in CD_3CN showed only one broad peak at *ca.* -13.30 ppm, however, in THF, a well resolved doublet is apparent at -14.30 ppm (d, $^1J_{Rh-P}$ = 131.6 Hz), which is consistent with that of other $[Rh(PMe_3)_4]^+$ salts.[50] The sharp singlet at 14.8 ppm in $^{11}B\{^1H\}$ NMR spectrum is very typical for a $[Bcat_2]^-$ anion.[45] This $Bcat_2^-$ anion also gives rise to just a singlet resonance (6.54 ppm) in the ^1H NMR spectrum in CD_3CN due to coincidental overlap of the two types of aromatic hydrogens.

Hydrogenation of $[Rh(PMe_3)_4][Bcat_2]$ in THF led readily to the formation of the colorless dihydride complex $[Rh(PMe_3)_4(H)_2][Bcat_2]$ (**46**). The $^{31}P\{^1H\}$ NMR spectrum in CD_3CN showed two doublets of triplets peaks at -22.35 (*trans* PMe_3) and -11.01 ppm (*cis* PMe_3) respectively, which is consistent with the *cis* disposition of the hydrides. The hydride resonance in CD_3CN appeared as a pseudo doublet of quintets at -10.69 ppm. Crystals suitable for X-ray diffraction were obtained by diffusion of a layer of heptane into a THF solution of **46**. The structure consists of well-separated anions and cations (Figure **5.9**). The cation displayed a pseudooctahedral configuration with the Rh-H distance being 1.49(6) Å, and the H-Rh-H angle being 88(4)°.

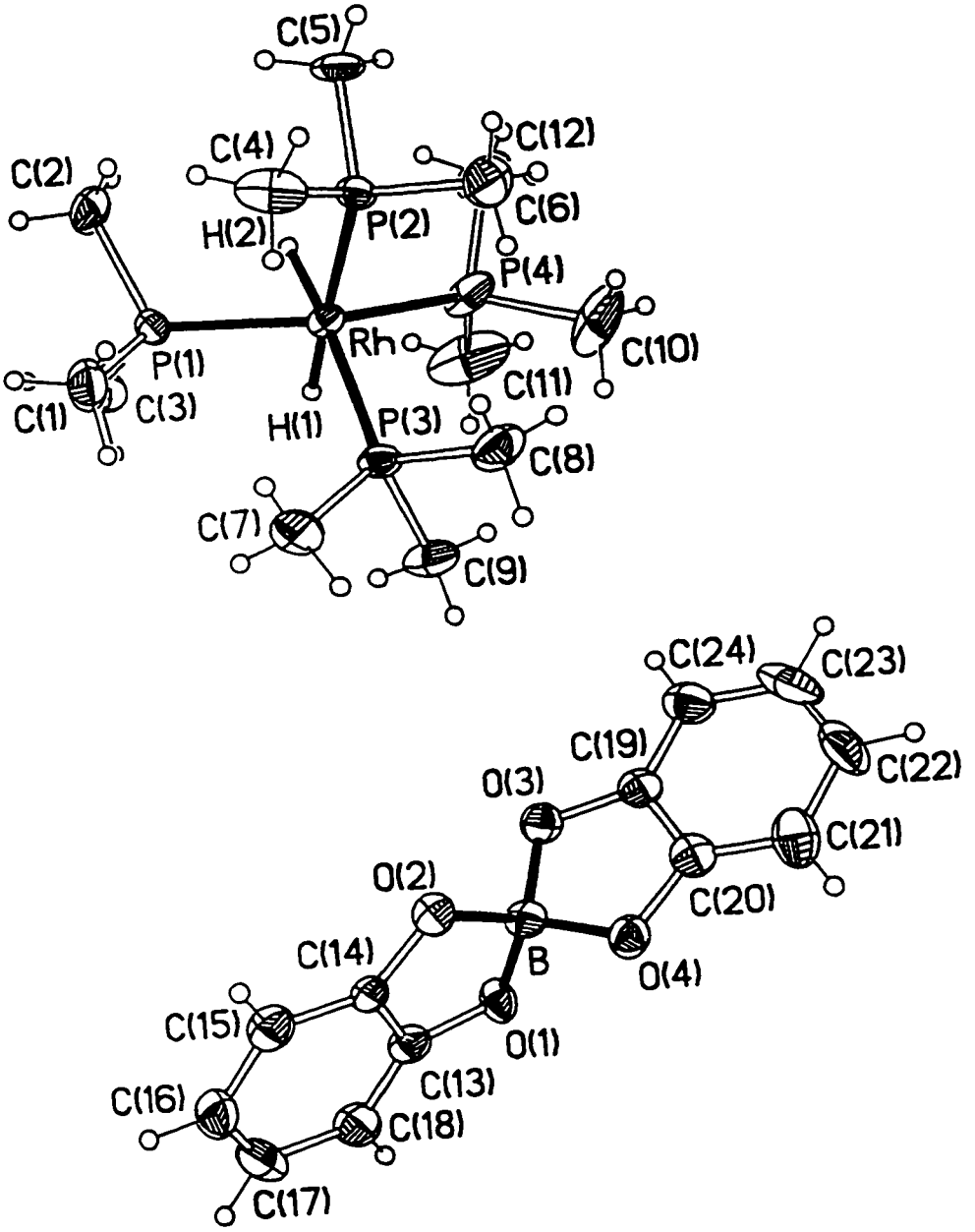
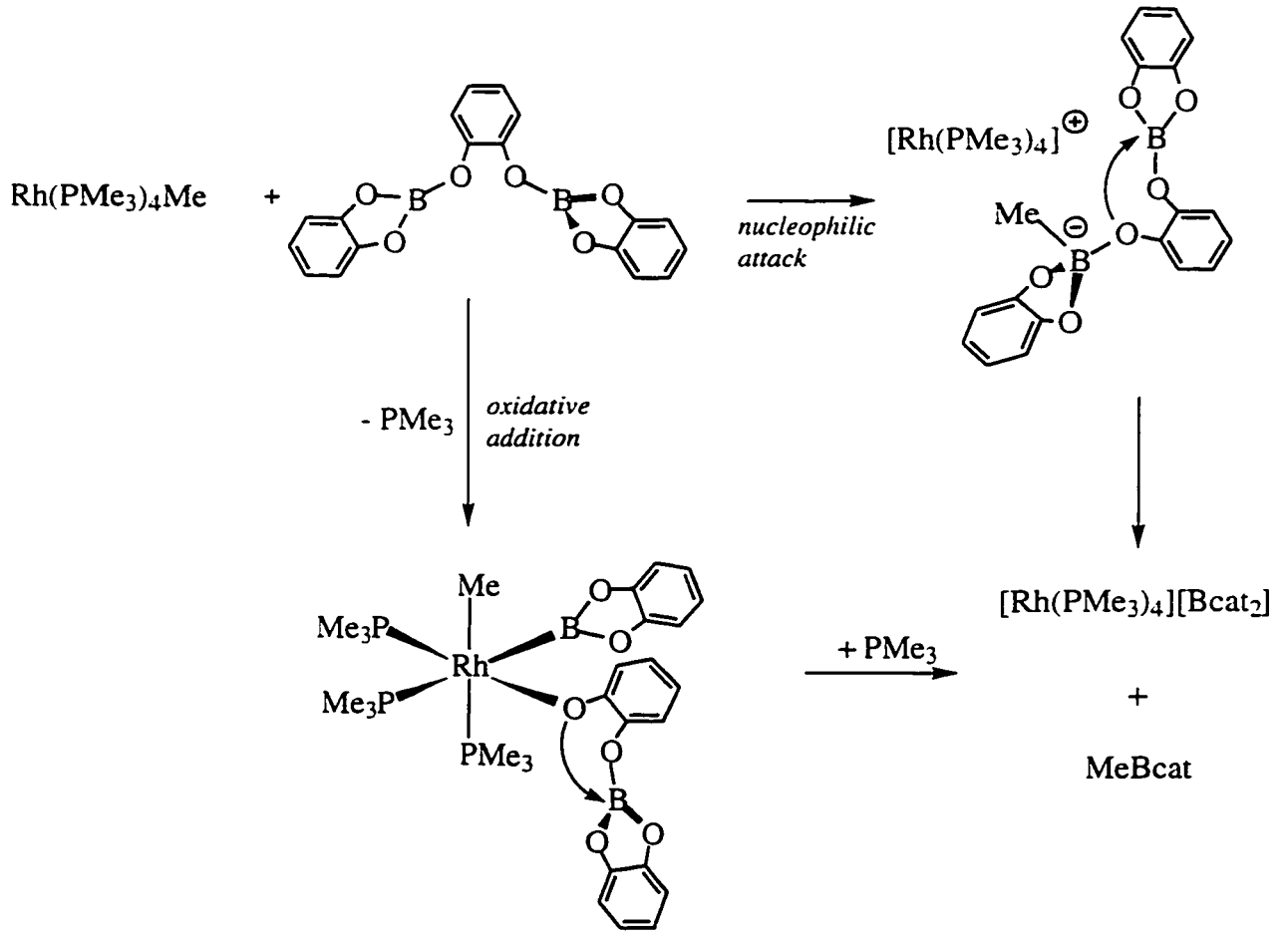


Figure 5.9 Molecular structure of $[Rh(PMe_3)_4(H)_2][Bcat_2]$ (**46**) with 50% probability ellipsoids.

There are two possible ways to rationalize the result of the reaction between B_2cat_3 and $[Rh(PMe_3)_4Me]$. First, despite of the high stability of the B-O bond, there may still exist the possibility that B_2cat_3 undergoes B-O oxidative addition to the metal center, followed by reductive elimination of MeBcat. However, it is more likely that $[Rh(PMe_3)_4Me]$ facilitates nucleophilic attack of Me on one of the boron atoms in B_2cat_3, followed by methyl transfer and $Bcat_2^-$ acts as a leaving group to generate MeBcat and $[Rh(PMe_3)_4][Bcat_2]$.



Reactions between B_2cat_3 and the simple organic lithium reagents MeLi and C_6H_5-C≡CLi were also performed. Accordingly, they both gave $Li[Bcat_2]$ and MeBcat

or C_6H_5-C≡C-Bcat respectively (Reactions **5.7** & **5.8**). In this respect, B_2cat_3 can be an alternative source for the synthesis of organoboranes. In comparison with the haloboron starting materials such as ClBcat or BrBcat, B_2cat_3 is less expensive and more stable making it easier to use. In addition, the final acidifying workup step encountered in the synthesis *via* other borates $B(OR)_3$ can be simply eliminated because the facile leaving of the $[Bcat_2]^-$ group ensures the release of free organoboron compound (Reaction **5.9**).

$$MeLi + B_2cat_3 \longrightarrow Li[Bcat_2] + MeBcat \qquad (\mathbf{5.7})$$

$$C_6H_5\text{-}C{\equiv}C\text{-}Li + B_2cat_3 \longrightarrow Li[Bcat_2] + C_6H_5\text{-}C{\equiv}C\text{-}Bcat \qquad (\mathbf{5.8})$$

$$MeLi + B(OR)_3 \longrightarrow Me\text{-}B(OR)_3^- \xrightarrow{HCl} Me\text{-}B(OR)_2 \qquad (\mathbf{5.9})$$

5.2.1.2. Reaction of B_2cat_3 and $CpRh(PMe_3)_2$

In order to investigate the possibility of B_2cat_3 being a useful boron source for the synthesis not only of organoboranes but also transition metal boryl complexes, the reaction between B_2cat_3 and $[CpRh(PMe_3)_2]$ (**47**) was performed. When a red solution of **47** in C_6D_6 was added dropwise to an equal molar solution of B_2cat_3 in C_6D_6, the red color disappeared rapidly, and a white precipitate with a slightly pink tint precipitated immediately from the solution. $^{31}P\{^1H\}$ and $^{11}B\{^1H\}$ NMR analysis on the colorless filtrate gave no identification of any phosphorus or boron containing species at all. The precipitate, on the other hand, was collected and dissolved in CD_3CN. In the $^{31}P\{^1H\}$ spectrum (Figure **5.10a**), in addition to the main doublet signal at 8.29 ppm ($^1J_{Rh\text{-}P}$ =

138.8 Hz), there was also another similar but sharper doublet resonance (*ca.* 20%) at 7.02 ppm ($^1J_{Rh-P}$ = 136.8 Hz). The later doublet can be assigned to the signal arising from $[CpRh(PMe_3)_2H](Bcat_2)$ when referenced to that of $[CpRh(PMe_3)_2H]PF_6$ (**48**)[51] which was obtained separately from the reaction of **47** with NH_4PF_6. In the $^{11}B\{^1H\}$ spectrum (Figure **5.10b**), two signals were observed with one sharp singlet at 15.13 ppm which is characteristic of a $[Bcat_2]^-$ anion and another broad peak at 43.35 ppm which falls in the region that most Rh(III) Bcat complexes appear. Therefore, from these observations, this precipitate can be tentatively identified as $[CpRh(PMe_3)_2(Bcat)][Bcat_2]$ (**49**) with some amount of $[CpRh(PMe_3)_2(H)][Bcat_2]$ (**50**). This was also verified from the ^1H NMR spectrum which exhibit two Cp signals at 5.62 and 5.46 ppm respectively, the latter is consistent with that of **50**. In addition to the singlet for $[Bcat_2]^-$ at 6.56 ppm, the Rh-Bcat multiplets at 7.06 and 7.22 ppm were apparent.

The resulting precipitate from this reaction is soluble in polar solvents such as CH_3CN, THF, and CH_2Cl_2, but it is not soluble in benzene, toluene, etc. The above spectroscopic data were obtained from a freshly prepared NMR sample in CD_3CN. However, when the same NMR sample was run again 24 h later, only peaks belonging to **50** could be observed. Other attempts in THF-d^8 or CD_2Cl_2 were also examined, but they gave even more complicated spectra. While the firm characterization of this product has not been accomplished yet, the above preliminary results have nonetheless indicated that electron rich Rh(I) complex can split B_2cat_3 to the [Bcat] and $[Bcat_2]$ fragments to form a direct Rh-B bond. This reaction most likely follows a nucleophilic attack pathway (Figure **5.11**).

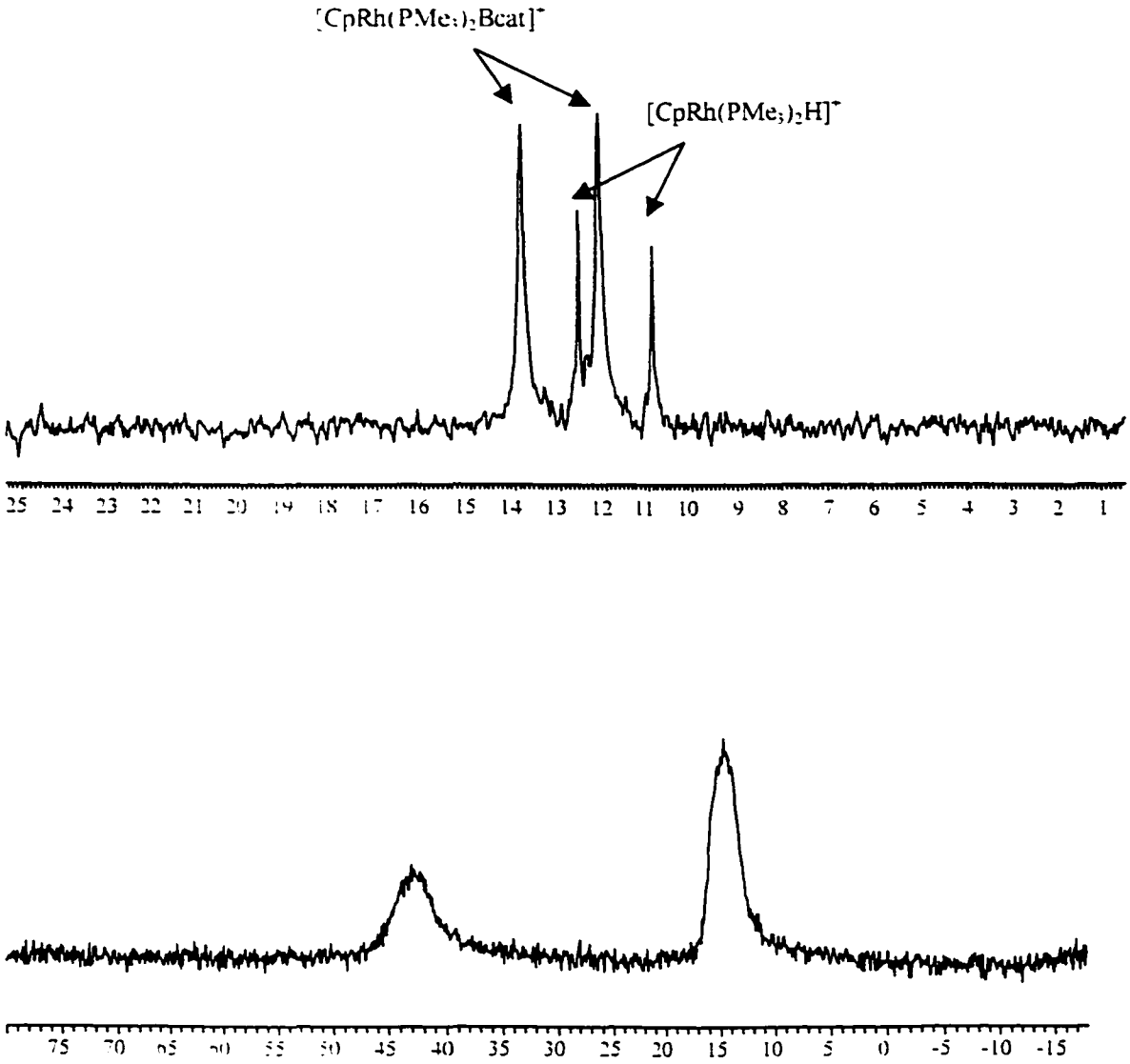


Figure 5.10 $^{31}P\{^1H\}$ and $^{11}B\{^1H\}$ NMR spectra of $CpRh(PMe_3)_2/B_2cat_3$ in CD_3CN

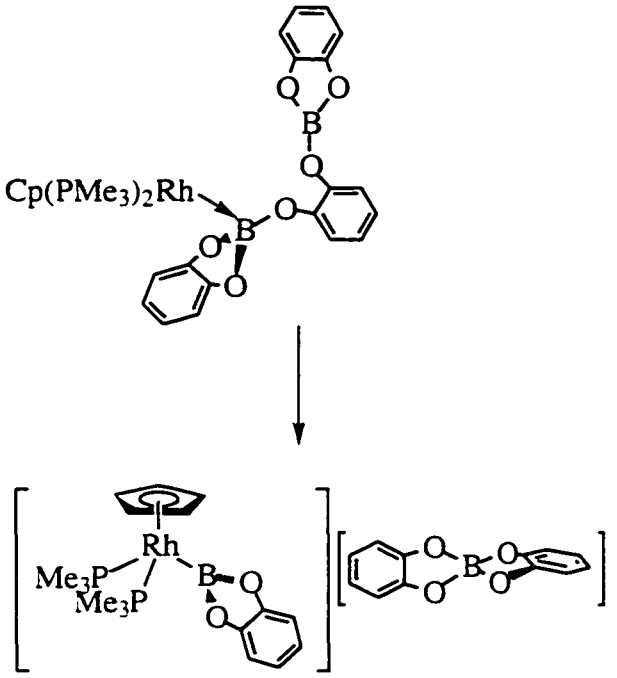
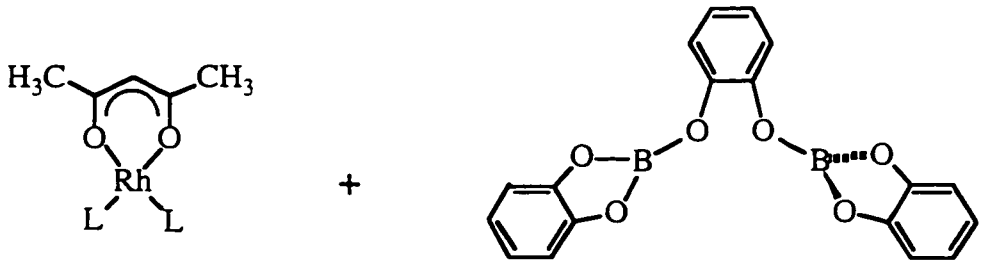


Figure 5.11 Reaction between [$CpRh(PMe_3)_2$] and B_2cat_3

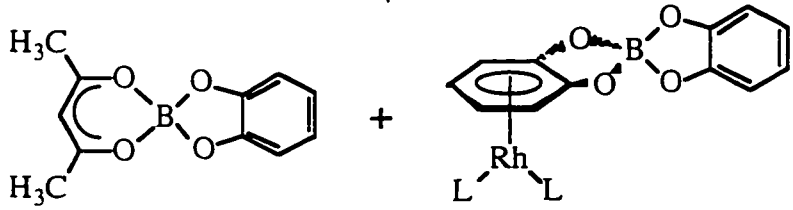
5.2.2 Synthesis of Zwitterionic Complexes [(η^6-$Bcat_2$)RhL_2]

So far, we have discussed the possibility of utilizing B_2cat_3 as a boron source for the synthesis of organoboranes and metal boryl complexes, which makes use of its Bcat fragment, with the other part $Bcat_2$ only acting as a counterion. Can we take advantage of this $Bcat_2$ fragment to make more meaningful compounds? The answer is obvious: we reasoned that the reaction between B_2cat_3 and [(acac)RhL_2] complexes could lead us to the synthesis of a series of (η^6-$Bcat_2$) bearing Rh(I) zwitterionic complexes [(η^6-$Bcat_2$)RhL_2] which was one of our long term goals. The reaction is illustrated as below (Reaction **5.11**).



38

37a, $L_2 = (\eta^2\text{-}C_2H_4)_2$ **37b**, $L_2 = (\eta^2\text{-COE})_2$
37c, $L_2 = \eta^4$-COD **37d**, $L_2 = (PPh_2Me)_2$
37e, L_2 =dppm **37f**, L_2 =dppe
37g, L_2 =dppp **37h**, L_2 =dppb
37i, L_2 =dppf **37j**, L_2 =dmpe
37k, L_2 =dcpe **37l**, L_2 =(R,R)-diop
37m, L_2 =R-tol-BINAP



51 **33a-m** (**5.11**)

5.2.2.1 Synthesis of $[(\eta^6\text{-Bcat}_2)RhL_2]$ Complexes

When one equiv. of B_2cat_3 in C_6D_6 was added to the solution of various $[(acac)RhL_2]$ complexes **37a-m** in C_6D_6, a yellow compound (acac)Bcat (**51**) and the corresponding zwitterionic complexes $[(\eta^6\text{-Bcat}_2)RhL_2]$ (**33a-m**) were generated readily. Compounds **33a-c** with η^2-olefin ligands are barely soluble in C_6D_6 so that they precipitated rapidly and were isolated as yellow or orange solids nearly quantitatively; others with phosphine ligands (**33d-m**) exhibited brown-reddish color. During the course

of the reactions, the color change could be observed immediately when the two reactants (B_2cat_3 and (acac)RhP_2) were mixed together, and the clean conversion was verified by $^{31}P\{^1H\}$ and $^{11}B\{^1H\}$ NMR spectroscopies (Figure **5.12**) as no other species were present. Generally, these deeply colored zwitterionic compounds [(η^6-$Bcat_2$)RhP_2] exhibit considerable solubility in C_6D_6 (except **33e** and **33i**), which makes the separation of them from **51** difficult. Nevertheless, pure samples were obtained by repeated recrystalization.

The driving force for these reactions is obviously the formation of (acac)Bcat (**51**), which is a very stable chelated four-coordinate borate compound. The 12e$^-$ [RhL_2] fragment, then is readily coordinated to one of the benzene rings in $Bcat_2^-$ to form an 18e$^-$ complex [(η^6-$Bcat_2$)RhL_2] (**33a-m**). Compound **51**, (acac)Bcat, in turn, can also be obtained readily through the reaction of B_2cat_3 with Na(acac) in toluene. It shows identical spectroscopic properties as those from reaction **5.11**.

The reaction depicted above appeared to be a direct and facile route to various [(η^6-$Bcat_2$)RhL_2] zwitterionic complexes. The starting materials [(acac)RhL_2] are very easily obtained. For instance, **37a-c** are commercially available, alternatively, they can be very easily prepared from the reactions of Na(acac) with the corresponding [$RhCl_2$(alkene)]$_2$ dimers in toluene.[52] Substitution reactions between [(acac)Rh(COE)$_2$] (**37b**) and various phosphine ligands gave very clean [(acac)Rh(P)$_2$] complexes as evidenced by $^{31}P\{^1H\}$ NMR spectra. Although it has been stated[52,53] that the substitution of COD in [(hfac)Rh(COD)] (hfac = hexafluoroacetylacetonate) by chelating phosphine ligands is always accompanied by the generation of some [Rh(P^P)$_2$]$^+$(hfac)$^-$, the displacement of COE in **37b** by the above phosphines is extremely clean, and no special procedure such as dropwise addition of bis(phosphine) ligands at low temperature as stated in ref. 53 is necessary to make the appropriate [(acac)Rh(P)$_2$] compounds.

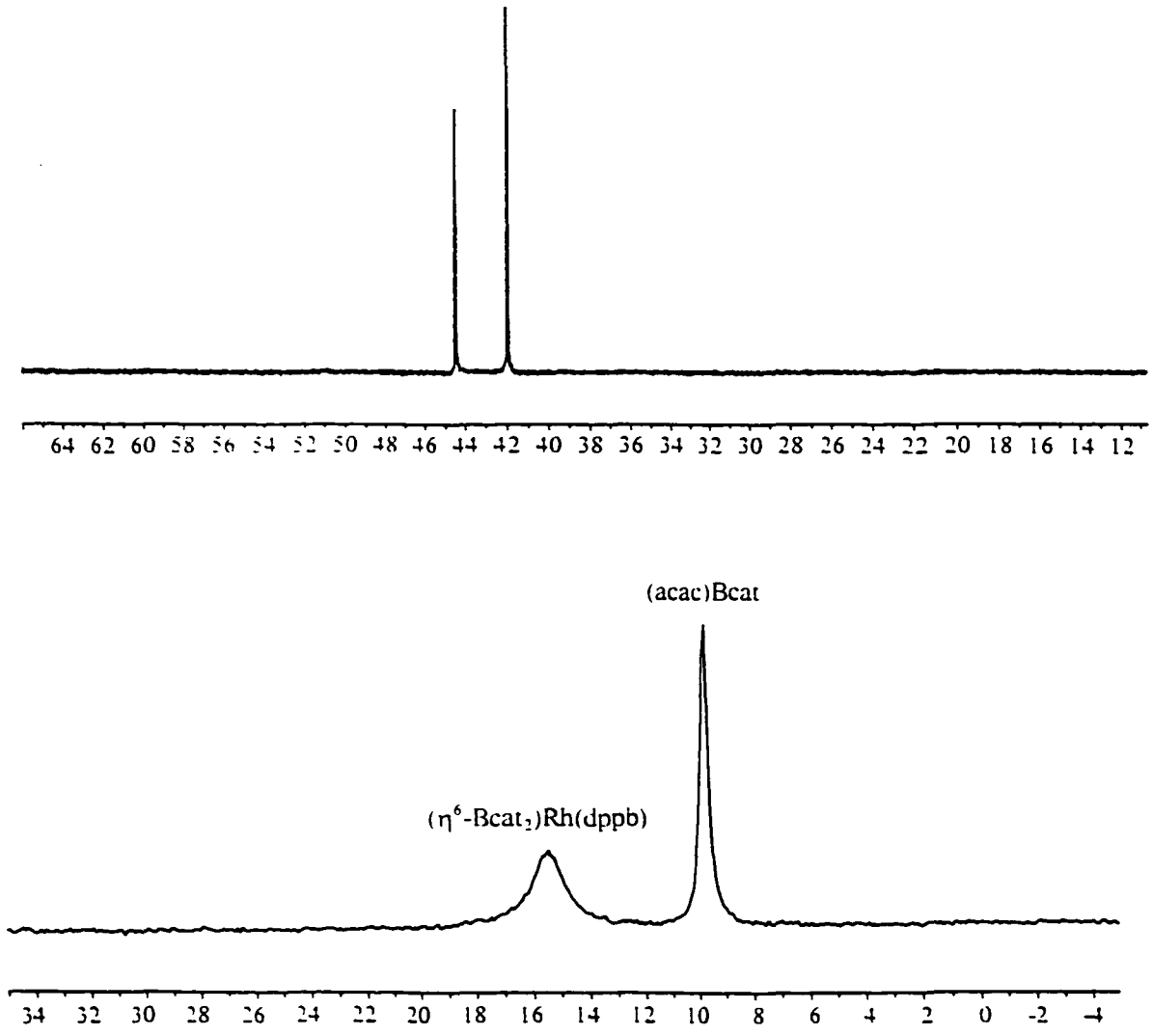


Figure 5.12 $^{31}P\{^1H\}$ and $^{11}B\{^1H\}$ NMR spectra for reaction of [(acac)Rh(dppb)] and B_2cat_3

5.2.2.2 Spectroscopic Properties of $[(\eta^6\text{-Bcat}_2)RhL_2]$ Complexes

The $^{11}B\{^1H\}$ NMR spectrum of **51**, (acac)Bcat, displayed a peak at 9.8 ppm which is very typical for a four-coordinate boron atom. In the $[(\eta^6\text{-Bcat}_2)RhL_2]$ complexes, the $^{11}B\{^1H\}$ NMR resonances in C_6D_6 all shifted down-field compared to the isolated $[Bcat_2]^-$ anion (*ca.* 14.5 ppm) due to the coordination by the RhL_2 moiety. They appeared in the range of 15-17 ppm, and broader peaks were apparent, but, when some of these complexes were placed in polar solvents, such as THF or CH_2Cl_2, a negligible shift was observed. For instance, the resonance for $[(\eta^6\text{-Bcat}_2)Rh(dppb)]$ (**33h**) in C_6D_6 is at 15.5 ppm, but it appears at 14.7 ppm in C_6D_6/THF and at 14.1 ppm in C_6D_6/CH_2Cl_2, respectively, although all the peaks were broad and identical $^{31}P\{^1H\}$ NMR spectra were observed in the above three solvents. However, in CD_3CN, it showed a sharp $^{11}B\{^1H\}$ NMR resonance at 14.2 ppm and entirely different $^{31}P\{^1H\}$ NMR signals were exhibited, which suggests that the solvent molecules CD_3CN probably coordinate to the metal center, and that $Bcat_2^-$ dissociates, at least to some extent, from the coordination sphere and only acts only as a counterion, $[Rh(dppb)(CD_3CN)_n]^+[Bcat_2]^-$. No attempts were made to identify this species, but in another experiment, when **33b** was dissolved in CD_3CN, the resulting product $[Rh(COE)_2(CD_3CN)_n]^+[Bcat_2]^-$ were verified by $^{11}B\{^1H\}$, ^1H, and $^{13}C\{^1H\}$ NMR spectroscopies. The dissociation of the π–bound arene ligand by coordinating solvents has also been observed in the structurally related analogs $[(\eta^6\text{-BPh}_4)RhL_2]$ (**52**).[54] One of the consequences of the easy displacement of $(\eta^6\text{-Bcat}_2)$ by nucleophiles has been shown by the fact that mixing of **33b** or **33c** with one equiv. of dppb in either C_6D_6 or THF did not lead to the formation of complex $[(\eta^6\text{-Bcat}_2)Rh(dppb)]$ at all.

Table 5.4 $^{31}P\{^{1}H\}$ and $^{11}B\{^{1}H\}$ NMR data[a] for [(acac)RhP_2] and [(η^6-$Bcat_2$)RhP_2]

No.	Ligand	(acac)RhP_2 (**37**)		(η^6-$Bcat_2$)RhP_2 (**33**)		
		^{31}P, δ	$^{1}J_{Rh-P}$	^{31}P, δ	$^{1}J_{Rh-P}$	^{11}B, δ
d	$(PPh_2Me)_2$	37.8	192.5	28.8	208.8	15.8
e	dppm	-18.7	163.7	-23.0	184.6	15.8
f	dppe	70.6	195.1	75.8	213.3	15.8
g	dmpe	52.0	190.1	49.7	209.7	15.4
h	dcpe	92.2	193.8	98.9	208.9	15.3
i	dppp	38.1	180.7	28.7	195.6	16.0
j	dppb	49.4	187.9	43.2	206.5	15.5
k	diop	39.1	189.0	31.2	208.3	15.7
l	dppf	52.9	199.5	45.9[b]	220.5[b]	14.9[b]
m	tol-BINAP	53.3	189.2	47.9	191.8	15.4

[a] in C_6D_6; [b] in THF-d_8.

The $^{31}P\{^{1}H\}$ NMR resonances of **33 d-m** are shifted down field compared to the free ligands. They are also mostly deshielded compared with the starting materials [(acac)Rh(P)$_2$] except when P_2 = dppe and dcpe (Table **5.4**). The nonchelate complex **33d**, [(η^6-Bcat$_2$)Rh(PPh$_2$Me)$_2$] exhibits a resonance at δ 28.8 ppm, while the analogous bis(phosphine) complexes [(η^6-Bcat$_2$)Rh{(Ph$_2$P)$_2$(CH$_2$)$_n$}] (n =1-4) exhibit resonances at -23.0, 75.8, 28.7 and 43.2 ppm, respectively. Such chemical shift differences between the bidentate bis(phosphine) ligands and the monodentate phosphine containing complexes are generally realized to be a function of the presence or absence of chelation and the chelate ring size.[55] The ring contribution Δ_R can be calculated for the above chelating phosphines Ph$_2$(CH$_2$)$_n$PPh$_2$ on the basis of $\Delta\delta$ = 56.8 for PPh$_2$Me (δ = 28.0) and [(η^6-Bcat$_2$)Rh(PPh$_2$Me)$_2$] (δ = 28.8). So the Δ_R values are -57.2 for n =1, 32.3 for n = 2, -10.8 for n = 3, and 1.4 for n = 4 (Table **5.5**), which follow the typical pattern in that the 4-membered ring (as in **33e**) is very shielded and the 5-membered ring (i.e. **33f**) is deshielded. The same calculations can be carried out to the respective [(acac)Rh(P$_2$)] compounds, and the same pattern is followed.

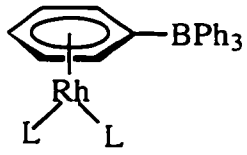
Table 5.5 "Ring contributions", Δ_R to ^{31}P chemical shifts in [(η^6-Bcat$_2$)Rh(P$_2$)].

Complex	δ ([(η^6-Bcat$_2$)RhL$_2$])	δ (free L)	$\Delta\delta$ [a]	Δ_R [b]
(η^6-Bcat$_2$)Rh(PPh$_2$Me)$_2$	28.8	-28.0	56.8	
(η^6-Bcat$_2$)Rh(dppm)	-23.0	-22.6	-0.4	-57.2
(η^6-Bcat$_2$)Rh(dppe)	75.8	-13.3	89.1	32.3
(η^6-Bcat$_2$)Rh(dppp)	28.7	-17.3	46.0	-10.8
(η^6-Bcat$_2$)Rh(dppb)	43.2	-15.0	58.2	1.4

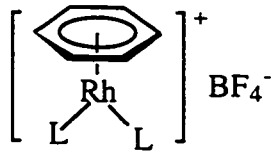
[a] $\Delta\delta$ = δ ([(η^6-Bcat$_2$)RhL$_2$]) - δ (free L);

[b] Δ_R = $\Delta\delta$ ((η^6-Bcat$_2$)Rh(P^P)) - $\Delta\delta$ ((η^6-Bcat$_2$)Rh(PPh$_2$Me)$_2$).

In the above [(η^6-Bcat$_2$)Rh(P$_2$)] complexes, the chemically equivalent ^{31}P nuclei give rise to doublets with $^1J_{Rh\text{-}P}$ between 185 to 220 Hz, which are all larger by about 20 Hz than the corresponding $^1J_{Rh\text{-}P}$ values in [(acac)Rh(P)$_2$] complexes (see Table **5.4**). This suggests that a stronger Rh-P interaction results when Rh is π-coordinated to Bcat$_2$. The structurally related η^6-tetraphenylborate complexes of the general form of [(η^6-BPh$_4$)RhL$_2$] (**52**) with L = P(OR)$_3$ [56] and L$_2$ = R$_2$P(CH$_2$)$_2$PR$_2$,[54,57] R$_2$P(CH$_2$)$_4$PR$_2$,[58] R$_2$P(η^5-C$_5$H$_4$)Fe(η^5-C$_5$H$_4$)PR$_2$ [59] as well as R$_2$PCH$_2$SbR$_2$ [60] have been reported, as have ionic η^6-arene complexes of [(η^6-arene)RhL$_2$]$^+$X$^-$ (**53**) with various phosphine ligands.[61] With the same phosphine ligand, the zwitterionic complexes [(η^6-Bcat$_2$)Rh(dppb)] (**33j**) and [(η^6-BPh$_4$)Rh(dppb)] [58] both exhibit larger Rh-P coupling constant values (206 and 200 Hz, respectively) than that of [(η^6-C$_6$H$_5$CH$_3$)Rh(dppb)]$^+$BF$_4^-$ (198 Hz), [61c] furthermore, the $^1J_{Rh\text{-}P}$ value in [(η^6-Bcat$_2$)Rh(dppb)] is larger than that in [(η^6-BPh$_4$)Rh(dppb)]. For [(η^6-Bcat$_2$)Rh(dppf)] (**33l**) $^1J_{Rh\text{-}P}$ = 220 Hz, and for [(η^6-BPh$_4$)Rh(dppf)] $^1J_{Rh\text{-}P}$ = 212 Hz.[58]



52



53

Both ^{1}H and ^{13}C{^{1}H} NMR spectra of complexes [(η^6-Bcat$_2$)RhL$_2$] displayed two sets of distinctive resonances for the η^6-coordinated and non-bonded catecholate

benzene rings (Table **5.6**). The spectra were recorded in C_6D_6 or, as otherwise stated, in THF-d_8. No reference spectra have been recorded on isolated $(Bcat_2)^-$ salts in C_6D_6 due to their poor solubilities in nonpolar solvents. Perhaps, a compound such as $(Bu^n{}_4N)(Bcat_2)$ would be soluble in C_6D_6, but this has not yet been proposed. Instead, resonances for $[Rh(PMe_3)_4](Bcat_2)$ (**45**) in CD_3CN are taken for comparison. The isolated $(Bcat_2)^-$ anion in **45** gives rise to only a singlet ^1H signal at 6.54 ppm and three $^{13}C\{^1H\}$ resonances at 108.79, 118.29 and 152.97 ppm, respectively. However, in the zwitterionic complexes $[(\eta^6\text{-}Bcat_2)RhL_2]$, the coordinated catecholate protons clearly display an AA'BB' spin pattern at higher field, while the uncoordinated catecholate protons give rise to overlapped multiplets at either roughly the same field or lower field. Although rigorous comparison would not be appropriate here because different solvents were applied to obtain the NMR spectra (i.e. CD_3CN, THF-d_8, or C_6D_6), the data in Table **5.5** nonetheless indicate that two distinct chemical environments are experienced by the two catecholate groups in the coordinated $(Bcat_2)^-$ anion. Inspection of these data also shows that the chemical shifts of each set of protons of both the coordinated and uncoordinated benzene rings is strongly affected by the nature of the ancillary ligands in the Rh coordination sphere. The smaller upfield shift of the coordinated catecholate protons in $[(\eta^6\text{-}Bcat_2)Rh(C_2H_4)_2]$ (**33a**) and $[(\eta^6\text{-}Bcat_2)Rh(COD)]$ (**33c**) with respect to $[(\eta^6\text{-}Bcat_2)Rh(phosphine)_2]$ (**33d-l**) is consistent with their poorer σ-donor and higher π-acceptor ability of the alkene ancillary ligands.

Table 5.6 Chemical shifts [δ(ppm), C_6D_6] of catecholate protons and carbons in some Rh(η^6-$Bcat_2$) complexes.[a]

Complex	H η^6-(cat)	H free-(cat)	C η^6-(cat)	C free-(cat)
(η^6-$Bcat_2$)Rh(η^2-C_2H_4)$_2$[b]	5.70 (m), 7.02 (m)	6.51 (m)	90.21, 94.37 (d, J_{Rh-C} =4.2), 141.48	109.32; 118.88, 119.01; 152.23, 152.51
(η^6-$Bcat_2$)Rh(COD) [b]	5.63 (m), 6.94 (m)	6.49 (m)	90.19, 93.66 (d, J_{Rh-C} =4.2), 140.10	109.23; 118.73, 118.86; 152.33, 152.58
(η^6-$Bcat_2$)Rh(PPh_2Me)$_2$	4.60 (m), 5.25 (m)	7.16 (m)	86.51, 90.89, 143.37	109.03, 109.96; 118.73, 119.16; 152.74
(η^6-$Bcat_2$)Rh(dppm)	4.74 (m), 6.28 (m)	6.60 (m), 6.76 (m)	87.02 (d, J_{Rh-C} =3.2), 87.87, 140.96	109.58, 112.09; 118.31, 122.31; 151.90
(η^6-$Bcat_2$)Rh(dppe)	4.50 (m), 5.70 (m)	6.85 (m)	86.81, 89.08, 142.76	108.89, 109.92; 118.66, 118.96; 152.66
(η^6-$Bcat_2$)Rh(dppp)	4.79 (m), 4.97 (m)	6.84 (m)	86.42(d, J_{Rh-C} =3.2), 91.79(d, J_{Rh-C} =3.1), 143.83	108.99, 109.65; 118.94, 152.49, 152.89
(η^6-$Bcat_2$)Rh(dppb)	4.59 (m), 4.96 (m)	6.84 (m), 7.03 (m)	87.90, 91.13, 144.05	108.62, 109.70; 118.62, 118.93; 152.77, 152.90
(η^6-$Bcat_2$)Rh(dppf) [b]	5.89 (m), 6.01 (m)	7.29 (m)	88.59, 92.00, 144.62	108.65, 108.65; 118.01, 118.23; 152.79, 153.02

[a] Isolated $(Bcat_2)^-$ in [Rh(PMe_3)$_4$]($Bcat_2$) (in CD_3CN): ^1H, δ: 6.54 (s); $^{13}C\{^1H\}$, δ:108.79, 118.29, 152.97;

[b] In THF-d_8.

The assignment of the carbon resonances to each catecholate group in complexes [(η^6-$Bcat_2$)RhL_2] was verified by ^1H-^{13}C coupled 2D HMQC NMR spectroscopy (Figure **5.13**). The coordination of the benzene ring in $Bcat_2^-$ to Rh also causes an upfield shift of the carbon atom resonances, again, smaller shifts being seen for the complexes with alkenes as ancillary ligands (i.e. **33a**, **33c**). Small ^{13}C-^{103}Rh coupling with $^1J_{C\text{-}Rh}$ between 3.1 to 4.1 Hz for the coordinated catecholate benzene ring has been observed on some occasions, which may be further split by coupling with ^{31}P, however, negligible couplings were seen in other cases. There were reports on the C-Rh coupling of [(η^6-BPh_4)RhL_2] complexes (**52**) in the magnitude of 2.3-3.1 Hz,[54,58] but no such data on the [(η^6-arene)RhL_2]$^+X^-$ complexes were reported.[61c] This situation may largely depend on how well the spectra were processed. The chemical shifts of the uncoordinated catecholate carbons are only weakly affected by the coordination of the other benzene ring to Rh (see, Table **5.5**); however, essentially each carbon atom in this non-bound catecholate group has its distinctive resonance, which is notably different from the [(η^6-BPh_4)RhL_2] complexes. The coordination of the RhL_2 moiety to $Bcat_2$ breaks down its symmetry.

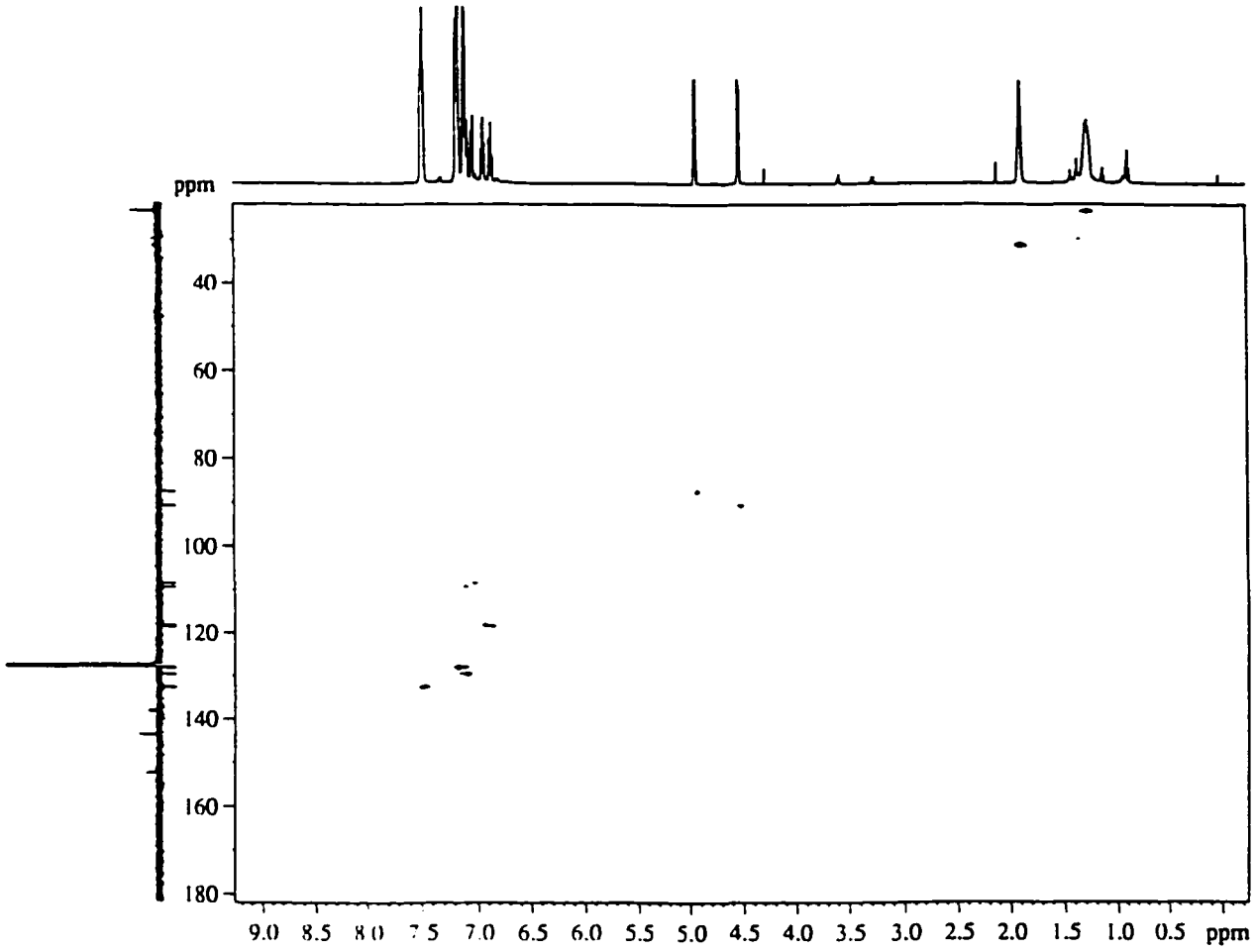


Figure 5.13 $^{1}H\{^{13}C\}$ 2D HMQC NMR spectrum of [(η^6-$Bcat_2$)Rh(dppb)] in C_6D_6.

5.2.2.3 Crystal Structures of $(\eta^6\text{-Bcat}_2)RhL_2$ Complexes

Crystals of $[(\eta^6\text{-Bcat}_2)RhL_2]$ complexes suitable for X-ray crystal structure analysis were obtained by several different means. Those of the complex $[(\eta^6\text{-Bcat}_2)$ Rh(dppm)] (**33e**) were grown directly from the reaction mixture of [(acac)Rh(dppm)] and B_2cat_3 in C_6D_6, while single crystals of complexes $[(\eta^6\text{-Bcat}_2)$Rh(dppe)] (**33f**) and $[(\eta^6\text{-Bcat}_2)$Rh(dppb)] (**33j**) were obtained from the corresponding $[(acac)RhL_2]/B_2cat_3$ reaction mixture solutions in toluene. Meanwhile, crystals of $[(\eta^6\text{-Bcat}_2)Rh(COE)_2]$ (**33b**) and $[(\eta^6\text{-Bcat}_2)$Rh(COD)] (**33c**) were grown by recrystallizing the pure samples from toluene, and finally, $[(\eta^6\text{-Bcat}_2)$Rh(dppf)] from THF-d_8. It is very interesting to note that, in the case of $[(\eta^6\text{-Bcat}_2)$Rh(dppe)] (**33f**), the single crystal obtained from the reaction mixture of [(acac)Rh(dppe)] and B_2cat_3 in toluene actually contains both the product molecules **33f** and (acac)Bcat, **51** in the lattice!

$$(acac)Rh(dppe) + B_2cat_3 \rightarrow (\eta^6\text{-Bcat}_2)Rh(dppe) + (acac)Bcat$$

This gives a unique example of how crystallography can not only characterize the compounds but also elucidate the reaction itself! Single crystals of **51**, (acac)Bcat [62] were also obtained both directly from its pure samples by recrystallization from toluene, and from the filtrate solution of $[(acac)Rh(COE)_2]$ (or [(acac)Rh(COD)]) and B_2cat_3 in C_6D_6. The crystallographic data for **51** and the above six $[(\eta^6\text{-Bcat}_2)RhL_2]$ complexes are depicted in Table **5.7**.

Table 5.7. Crystal data, structure solution and refinement for (acac)Bcat and complexes $[(\eta^6\text{-Bcat}_2)\text{Rh}(\text{L})_2]$.

	(acac)Bcat	L = (COE)	L_2 = COD	L_2 = dppm	L_2 = dppe	L_2 = dppb	L_2 = dppf
Formula	$C_{11}H_{11}BO_4$	$C_{28}H_{36}BO_4Rh$	$C_{20}H_{20}BO_4Rh$	$C_{37}H_{30}BO_4P_2Rh$ C_6D_6	$C_{38}H_{32}BO_4P_2Rh$ $C_{11}H_{11}BO_4$	$C_{40}H_{36}BO_4P_2Rh$	$C_{46}H_{36}BF_4O_4 \cdot 1.5$ C_4H_8O
MW	218.01	550.29	438.08	798.42	946.30	756.35	992.41
Crystal system	Monoclinic	Monoclinic	Orthorhombic	Orthorhombic	Triclinic	Monoclinic	Monoclinic
Space group	$P2_1/n$	$P2_1/c$	Pbca	$P2_12_12_1$	$P\bar{1}$	Cc	$P2_1/c$
a(Å)	10.0477(8)	12.6347(8)	12.6156(6)	13.2932(7)	9.5240(5)	9.8773(10)	11.3622(4)
b (Å)	8.3713(7)	9.9506(7)	16.0659(8)	15.2327(8)	12.2197(7)	19.497(2)	22.794(9)
c (Å)	12.4749(10)	20.5217(13)	16.9313	17.8046(10)	19.0770(11)	17.4641(18)	17.8086(7)
α (deg)	90	90	90	90	78.731(2)	90	90
β (deg)	95.493(2)	106.873(2)	90	90	79.657(2)	93.533(3)	96.552(2)
γ (deg)	90	90	90	90	86.664(2)	90	90
V ($Å^3$)	1044.47(15)	2469.0(3)	3431.7(3)	3605.3(3)	2141.4(2)	3356.9(6)	4579.2(3)
Z	4	4	8	4	2	4	4

	(acac)Bcat	L = (COE)	L_2 = COD	L_2 = dppm	L_2 = dppe	L_2 = dppb	L_2 = dppf
d_{calc} (g cm^{-3})	1.386	1.480	1.696	1.471	1.468	1.497	1.440
Crystal size (mm)	0.70 x 0.40 x 0.36	0.38 x 0.14 x 0.04	0.60 x 0.38 x 0.35	0.36 x 0.18 x 0.16	0.18 x 0.16 x 0.04	0.54 x 0.20 x 0.20	0.54 x 0.30 x 0.04
Crystal color	Pale Yellow	Yellow	Yellow	Orange	Orange	Red	Yellow-orange
Temperature (K)	160(2)	160(2)	160(2)	160(2)	160(2)	160(2)	160(2)
μ (mm^{-1})	0.068	0.724	1.019	0.606	0.530	0.647	0.796
F (000)	456	1144	1776	1624	972	1552	2040
Reflections for cell refinement	5245(θ range 2.04 to 28.36°)	11452(θ range 2.07to 28.53°)	15045 (θ range 1.74 to 28.54°)	22102(θ range 1.76 to 28.40°)	10778(θ range 2.17 to 28.85°)	8242 (θ range 2.06 to 28.29°)	19335(θ range 1.78 to 28.37°)
θ range	2.49 to 28.39°	1.68 to 24.99°	2.38 to 28.44°	2.29 to 28.46°	1.84 to 28.85°	2.09 to 28.38°	1.46 to 28.48°
Index ranges	-13≤ h ≤ 8,	-11 ≤ h ≤ 16,	-16 ≤ h ≤ 16,	-17 ≤ h ≤ 16,	-12≤ h ≤ 12,	-13≤ h ≤ 12,	-13≤ h ≤ 14,
	-10≤ k ≤ 10,	-12 ≤ k ≤ 11,	-16 ≤ k ≤ 21,	-20≤ k ≤ 19,	-16 ≤ k ≤ 16,	-25≤ k ≤ 23,	-29 ≤ k ≤ 28,
	-16 ≤ l ≤ 11	-25 ≤ l ≤ 26	-21 ≤ l ≤ 10	-22 ≤ l ≤ 22	-24 ≤ l ≤ 25	-23 ≤ l ≤ 13	-23 ≤ l ≤ 23
Refl measd	6401	12600	19596	26554	16039	10544	36273
Independent refl	2387(R_{int}= 0.0243)	4326(R_{int}= 0.0251)	4045(R_{int}= 0.0501)	8415(R_{int}= 0.0251)	9776(R_{int}= 0.0297)	5259(R_{int}= 0.0282)	10572(R_{int}= 0.0525)
Refl with I>2σ(I)	2060	3853	3356	7960	8220	4931	7660

	(acac)Bcat	L = (COE)	L_2 = COD	L_2 = dppm	L_2 = dppe	L_2 = dppb	L_2 = dppf
Weighting parameters a, b	0.0608, 0.3153	0.928, 3.0376	0.0363, 0.000	0.0236, 0.2153	0.0222, 2.7878	0.0248, 0.000	0.0584, 1.6623
No. of parameters	148	308	248	461	561	434	587
GOF on F^2	1.074	1.051	0.998	1.068	1.123	1.005	1.046
Final R indices [$I>2\sigma(I)$]	R1 = 0.0404	R1 = 0.0271	R1 = 0.0265	R1 = 0.0212	R1 = 0.0555	R1 = 0.0252	R1 = 0.0441
	wR2 = 0.1116	wR2 = 0.0636	wR2 = 0.0631	wR2 = 0.461	wR2 = 0.0954	wR2 = 0.0512	wR2 = 0.1025
R indices (all data)[a]	R1 = 0.0464	R1 = 0.0323	R1 = 0.0351	R1 = 0.0244	R1 = 0.0710	R1 = 0.0290	R1 = 0.0749
	wR2 = 0.1160	wR2 = 0.0665	wR2 = 0.0657	wR2 = 0.0473	wR2 = 0.1005	wR2 = 0.0523	wR2 = 0.1153
Extinction coeff.	0.014(3)	0.00040(12)	0.00227(18)	0.00004(13)		0.00044(6)	0.00035(12)
Largest shift/esd	0.000	0.002	0.000	0.005	0.001	0.002	0.240
Largest diff. peak and hole (e $Å^{-3}$)	0.284, -0.230	1.172, -0.406	0.507, -0.912	0.279, -0.250	1.031, -0.782	0.417, -0.432	0.904, -0.963

[a] $R = \Sigma(|F_O|-|F_C|)/\Sigma(|F_O|)$, $wR = \{\Sigma[w(F_o^2-F_c^2)^2]/\Sigma[w(F_o^2)^2]\}^{1/2}$, $GOF = S = \{\Sigma[w(F_o^2-F_c^2)^2]/(n-p)\}^{1/2}$ for n reflections and p parameters in the refinement.

The accompanying product **51**, (acac)Bcat crystallizes in the monoclinic space group, $P2_1/n$ (Figure **5.14**). The boron atom adopts a tetrahedral arrangement. The chelating O-B-O angle in the Bcat moiety (107.27°) is wider than that of the isolated $Bcat_2^-$ anion in the structure of $[Rh(PMe_3)_4](Bcat_2)$ (**45**, 104.8°). As a result of forming the six-membered chelating ring with the acetylacetonate moiety, the other intra-ring O-B-O angle in (acac)B is even larger, being 109.68°, a value close to the ideal sp^3 tetrahedral coordination angle. Accordingly, the mean B-O bond distance in the Bcat fragment of **51** (1.467 Å) is slightly shorter than that in $Bcat_2^-$ (1.485 Å in **45**), while those in the (acac)B fragment of **51** are slightly longer, averaging 1.493 Å.

In the crystal structures of the zwitterionic complexes $[(\eta^6\text{-}Bcat_2)RhL_2]$ (**33b**, **c**, **e**, **f**, **j**, **l**), the Rh atom is directly bonded, *via* π-interaction, to one of the catecholate benzene rings of the $Bcat_2^-$ anion. Selected structural features are listed in Table **5.8**. Again, complex $[Rh(PMe_3)_4](Bcat_2)$ (**45**) is taken as a reference for the structure of the isolated $Bcat_2^-$ group in the solid state. The only previously reported structure of an η^6-$Bcat_2$ complex is $[(\eta^6\text{-}Bcat_2)Rh(Dippe)]$ which was reported by our group in 1993.[43]

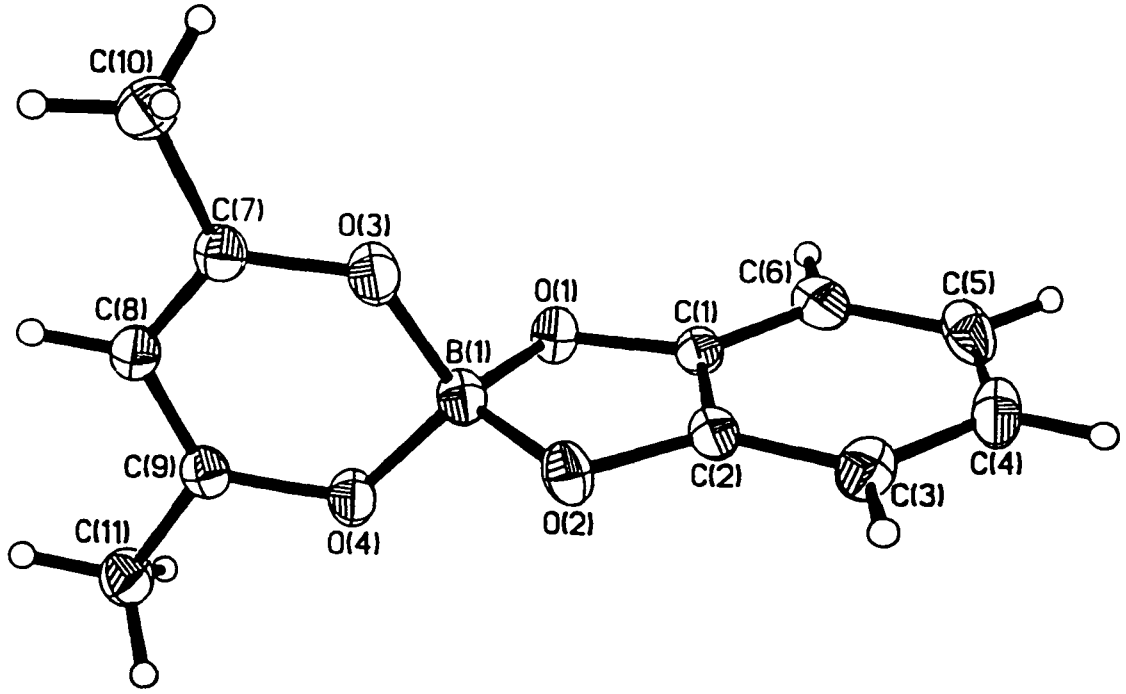


Figure 5.14 Molecular structure of (acac)Bcat (**51**), with 50% probability ellipsoids.

Table 5.8 Selected structural features of the complexes $[(\eta^6\text{-Bcat}_2)RhL_2]$ and $[Rh(PMe_3)_4](Bcat_2)$.

Complex	Rh-L [a] [Å]	L-Rh-L [b] [°]	B-O (η^6-cat) [Å]	B-O (free-cat) [Å]	O-B-O [c] (η^6-cat) [°]	O-B-O [c] (free-cat) [°]	(O-B-O) [d] dihedral angle [°]
$(\eta^6\text{-Bcat}_2)Rh(COE)_2$ **(33b)**	2.041, 2.069	97.7	1.504, 1.505	1.456, 1.466	102.8	106.7	89.9
$(\eta^6\text{-Bcat}_2)Rh(COD)$ **(33c)**	2.012, 2.022	86.7	1.504, 1.505	1.458, 1.466	103.3	106.5	89.6
$(\eta^6\text{-Bcat}_2)Rh(dppm)$ **(33e)**	2.213, 2.233	72.9	1.503, 1.506	1.461, 1.463	103.2	106.3	88.2
$(\eta^6\text{-Bcat}_2)Rh(dppe)$ **(33f)**	2.203, 2.227	83.8	1.484, 1.502	1.458, 1.483	103.4	105.9	89.5
$(\eta^6\text{-Bcat}_2)Rh(dppb)$ **(33j)**	2.223, 2.254	93.2	1.500, 1.513	1.453, 1.478	102.8	105.9	89.7
$(\eta^6\text{-Bcat}_2)Rh(dppf)$ **(33l)**	2.227, 2.258	96.0	1.494, 1.504	1.458, 1.473	103.1	106.1	89.7
$[Rh(PMe_3)_4](Bcat_2)$ **(45)**			1.472, 1.492	1.475, 1.493	104.8	104.8	90.0

[a, b] For coordinated double bonds, the mid-points are used; [c] Intra-ring angles; [d] Dihedral angle between the two OBO planes.

Table 5.8 Selected structural features of the complexes $[(\eta^6\text{-Bcat}_2)\text{RhL}_2]$ and $[\text{Rh}(\text{PMe}_3)_4](\text{Bcat}_2)$.

Complex	Rh-L [a] [Å]	L-Rh-L [b] [°]	B-O (η^6-cat) [Å]	B-O (free-cat) [Å]	O-B-O [c] (η^6-cat) [°]	O-B-O [c] (free-cat) [°]	(O-B-O) [d] dihedral angle [°]
$(\eta^6\text{-Bcat}_2)\text{Rh(COE)}_2$ **(33b)**	2.041, 2.069	97.7	1.504, 1.505	1.456, 1.466	102.8	106.7	89.9
$(\eta^6\text{-Bcat}_2)\text{Rh(COD)}$ **(33c)**	2.012, 2.022	86.7	1.504, 1.505	1.458, 1.466	103.3	106.5	89.6
$(\eta^6\text{-Bcat}_2)\text{Rh(dppm)}$ **(33e)**	2.213, 2.233	72.9	1.503, 1.506	1.461, 1.463	103.2	106.3	88.2
$(\eta^6\text{-Bcat}_2)\text{Rh(dppe)}$ **(33f)**	2.203, 2.227	83.8	1.484, 1.502	1.458, 1.483	103.4	105.9	89.5
$(\eta^6\text{-Bcat}_2)\text{Rh(dppb)}$ **(33j)**	2.223, 2.254	93.2	1.500, 1.513	1.453, 1.478	102.8	105.9	89.7
$(\eta^6\text{-Bcat}_2)\text{Rh(dppf)}$ **(33l)**	2.227, 2.258	96.0	1.494, 1.504	1.458, 1.473	103.1	106.1	89.7
$[\text{Rh}(\text{PMe}_3)_4](\text{Bcat}_2)$ **(45)**			1.472, 1.492	1.475, 1.493	104.8	104.8	90.0

[a, b] For coordinated double bonds, the mid-points are used; [c] Intra-ring angles; [d] Dihedral angle between the two OBO planes.

The complex [(η^6-Bcat$_2$)Rh(COE)$_2$] (**33b**) crystallizes as yellow needles, and has the usual half-sandwich geometry (Figure **5.15**). Besides the η^6-Bcat$_2$ group, the Rh atom is bonded to two ancillary η^2-COE ligands. The C-C double bond length in both COE groups is 1.406 (4) Å. The distances from Rh to the carbon atoms in these double bonds range from 2.138 (2) to 2.193 (2) Å, its distance to the mid-points of the double bonds being 2.041(2) and 2.069 (2) Å, respectively. The double bond mid-points are also used for the calculation of the L-M-L coordination angle to the Rh center by the two COE ligands, which is 97.7°. The distance of Rh to the mean plane of the benzene ring is 1.878 Å, while the separation between Rh and the ring centroid **X** is 1.882(2) Å. The Rh···**X** direction and the perpendicular to the ring are not coincident, forming an angle of 4.1°. This value can be used as a convenient measurement of the ring slippage from the ring center (see Table **5.7**). Examination of the six Rh-C distances also indicates that the catecholate benzene ring is not symmetrically coordinated, as they vary from 2.264 (2) to 2.411 (2) Å. The Rh atom slips slightly away from the ring center toward the C(4) and C(5) edge (see Figure **5.15**). A mean plane calculation through the carbon atoms shows that they are not coplanar, the average deviation from planarity being 0.0063 Å. The coordination of the Rh(COE)$_2$ moiety to the ring also results in profound changes in other parts of the Bcat$_2$ group. The coordinated catecholate shows longer C-O bonds as well as O-B bonds than the other one because of the electron-donation from the benzene ring to the metal. The two intra-ring chelating O-B-O angles are no longer identical for the coordinated and free catecholates (102.8 and 106.7°, respectively). In contrast, a value of 104.8° is observed for isolated Bcat$_2^-$ in **45**). Accordingly, slightly wider B-O-C angles are found for the η^6-coordinated catecholate (108.18 and 108.41° *vs.* 106.02 and 106.42°), but the dihedral angle between the two OBO planes remains close to 90° (89.9° in **33b**). The uncoordinated catecholate benzene ring also deviates slightly from planarity, but to a lesser extent, the mean deviation for the six carbon atoms being 0.0030 Å.

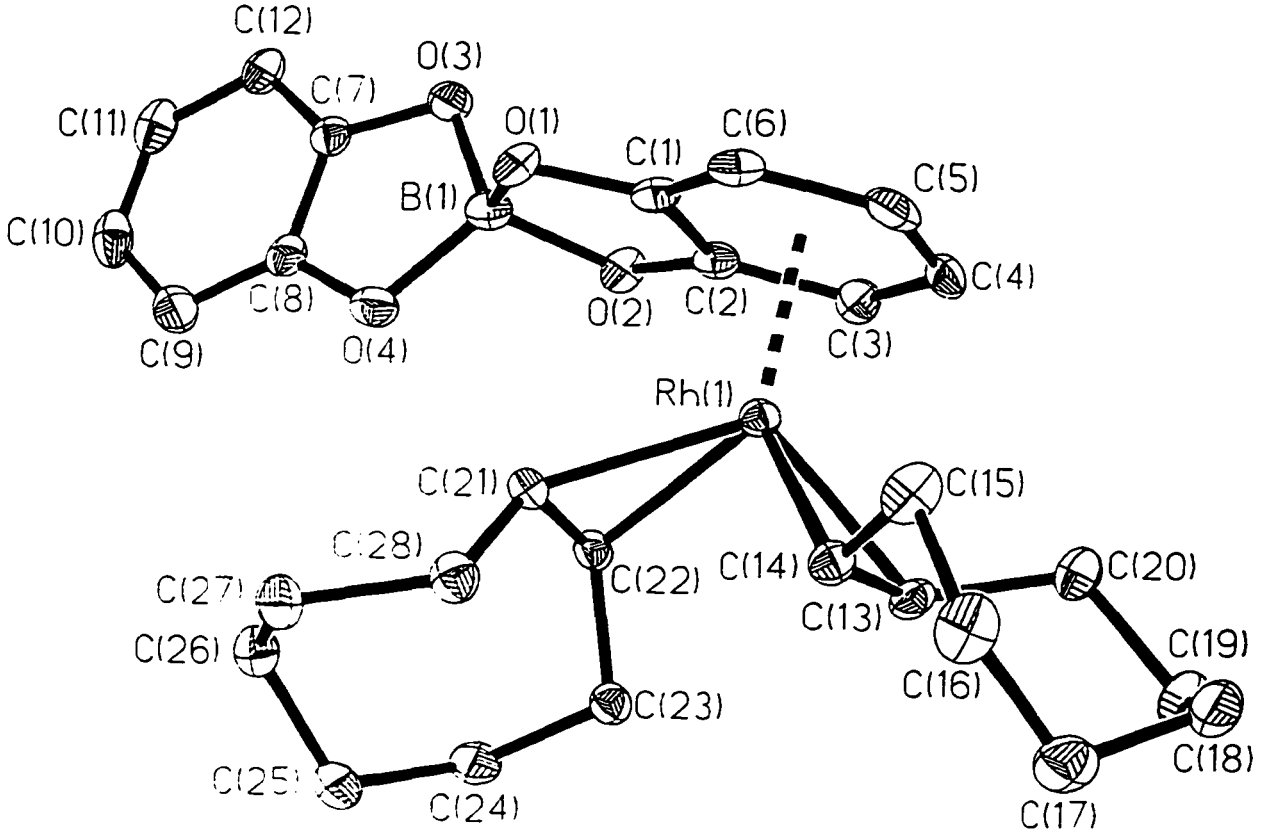


Figure 5.15 Molecular structure of $[(\eta^6\text{-Bcat}_2)\text{Rh(COE)}_2]$ (**33b**), with 50% probability ellipsoids.

In the structure of [(η^6-Bcat$_2$)Rh(COD)] (**33c**, Figure **5.16**), the C-C double bonds length is 1.400 (3) Å in the ancillary η^4-COD ligand. It shows similar distances from Rh to the coordinated double bonds as in **33b**, being 2.012 and 2.022 Å to their mid-points. In comparison to the bis(COE) complex **33b**, the (C=C)-Rh-(C=C) angle (86.7°) in **33c** is apparently smaller due to the chelating coordination of COD to Rh. Furthermore, the distance from Rh to the η^6-coordinated benzene ring is notably shorter, with the distances from Rh to the ring centroid and to the mean plane being 1.841 and 1.838 Å, respectively (1.882 and 1.878 Å for **33b**). The corresponding ring slippage criterion for **33c** is calculated as 3.4° which is less severe compared to **33b** (4.1°). While both **33b** and **33c** have basically the same coordination sphere at the metal center, the Rh atom interacts more strongly with the η^6-catecholate unit in **33c**. Obviously, these differences are mainly due to the chelate effect of the COD ligand, but, probably more importantly, there is less steric repulsion between the smaller COD ligand and the Bcat$_2$ group in **33c**. In line with these differences, the coordinated catecholate benzene ring in **33c** displays more non-planar character, the mean deviation of the six carbon atoms from planarity is calculated to be 0.0239 Å (0.0063 for **33b**), no such difference is observed for the other uncoordinated ring.

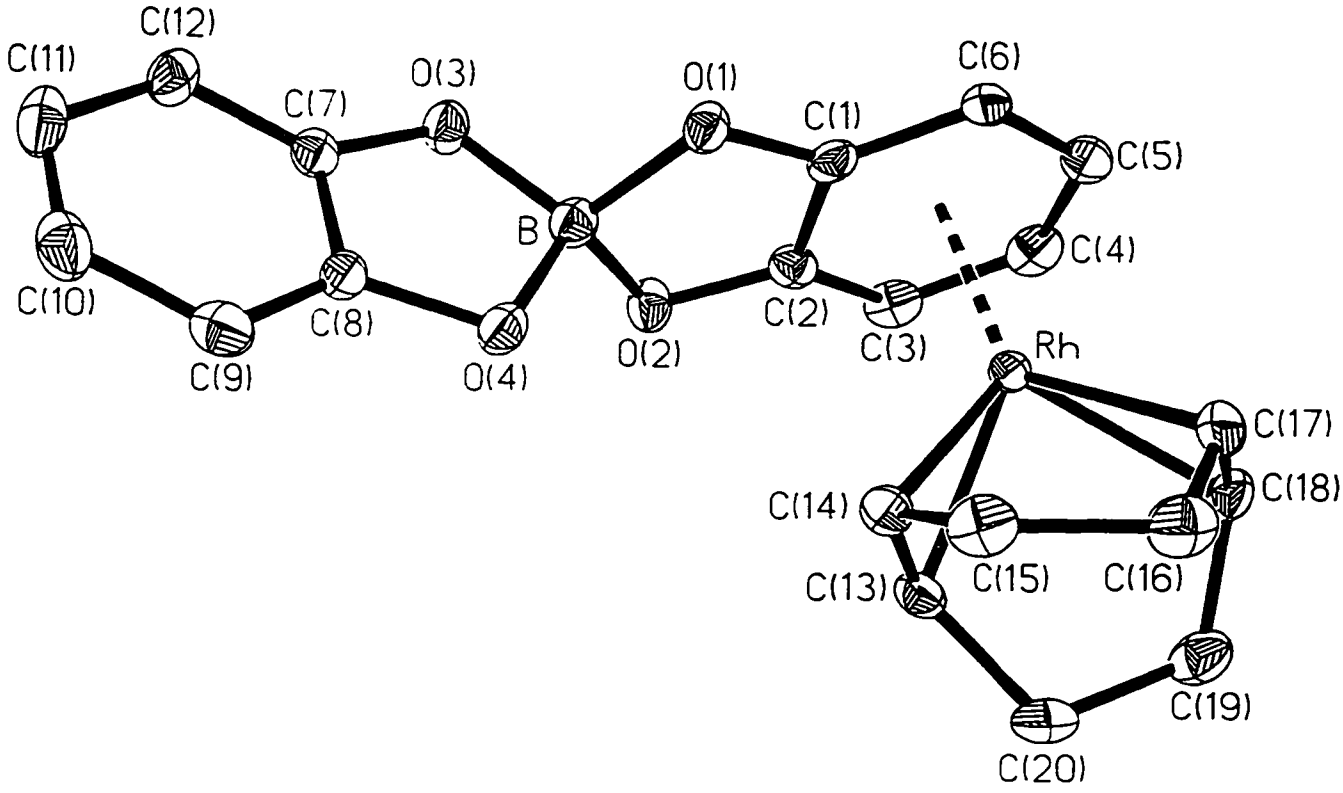


Figure 5.16 Molecular structure of $[(\eta^6\text{-Bcat}_2)\text{Rh(COD)}]$ (**33c**), with 50% probability ellipsoids.

The complex [(η^6-Bcat$_2$)Rh(dppm)] (**33e**, Figure **5.17**) crystallizes as orange blocks from C_6D_6 with incorporation of one solvent molecule in the lattice. The coordination of the Rh atom by the chelating phosphine dppm results in a notably small P-Rh-P angle (72.9°). The Rh-P bonds are 2.213 and 2.233 Å, respectively. The Rh atom is slightly further away from the η^6-catecholate benzene ring than in **33c** as evidenced by the fact that the Rh-C distances range from 2.2445 to 2.4243 Å, and that the distances of Rh to the ring centroid and to the mean plane are 1.879 and 1.973 Å, respectively (1.841 and 1.838 Å for **33c**). From an electronic point of view, the displacement of the alkene ligand such as COD by phosphines will likely result in a slight weakening of the Rh·····ring interaction because of the stronger π-accepting properties of the alkene ligands. However, these distances may be also dominated by steric factors, as they are essentially the same as those in **33b**. Similar deviations of the η^6-Bcat$_2$ group from the ideal D_{2d} symmetry of the free Bcat$_2^-$ anion are observed in complex **33e** as described above for **33b** and **33c** (see Table **5.8**), and noteworthy differences in this structure can be seen from at least two aspects. First, while the coordinated catecholate benzene ring in **33e** deviates from planarity (mean deviation 0.0066 Å), it is the uncoordinated catecholate group that is less planar (mean deviation 0.0105 Å). Second, the dihedral angle between the two OBO planes deviates the most from being perpendicular (88.2°), whereas in the other compounds, the angles are all close to 90°. Of course, the most striking feature in this compound is the very small P-Rh-P angle so that the metal center is most "popped-up" from the chelating bucket.

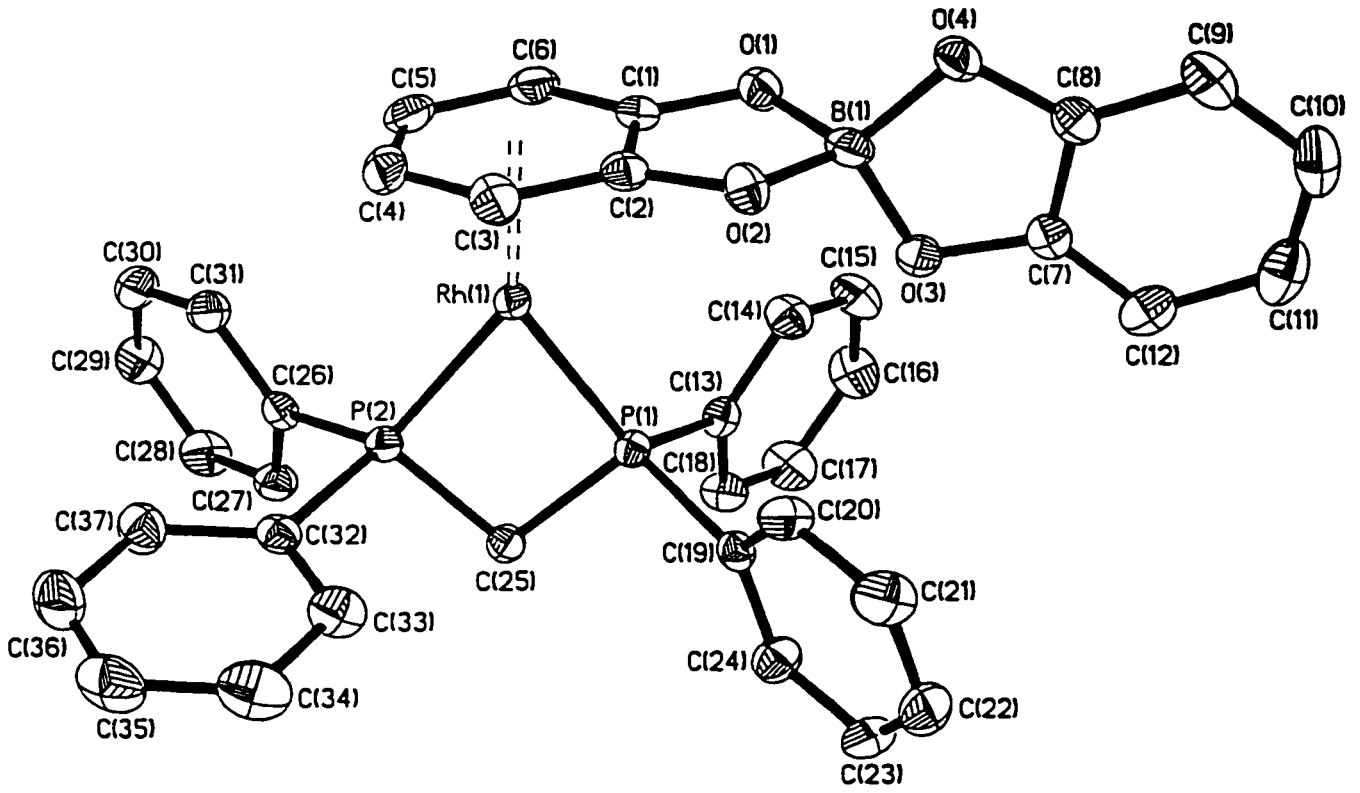


Figure 5.17 Molecular structure of $[(\eta^6\text{-Bcat}_2)\text{Rh(dppm)}]$ (**33e**), with 50% probability ellipsoids.

The crystal of complex [(η^6-Bcat$_2$)Rh(dppe)] (**33f**, Figure **5.18**) actually incorporates one molecule of (acac)Bcat per molecule of the Rh complex. No significant differences were observed between the structures of **51** in this crystal and on its own. They are not identical, obviously, but the differences appear to be minimal. In the structures of [(η^6-Bcat$_2$)Rh(dppe)], [(η^6-Bcat$_2$)Rh(dppb)] (**33j**, Figure **5.19**), and [(η^6-Bcat$_2$)Rh(dppf)] (**33l**, Figure **5.20**), the P-Rh-P angles are opened to 83.8, 93.2, and 96.0°, respectively with increasing length on the bidentate phosphine backbones. Lengthening Rh-P bond distances are expected with the increasing P-Rh-P angles in these complexes, except that in **33f**, the five-membered chelate ring configuration may be more favorable for the Rh-P interaction than the strained four-membered ring in **33e**. The distances of Rh to the coordinated catecholate benzene mean plane, on the other hand, follow an increasing order as the ancillary ligands go from dppm to dppb (1.873 to 1.918, accordingly), and more significant ring slippages are also observed (4.5 to 9.0°). The ferrocenyl bridge in **33l**, naturally provides a wider spacer, but it gives less flexibility to the backbone compared with the -$(CH_2)_n$- chains in the other three structures. A shorter Rh to ring distance and less ring slippage are observed for **33l** when compared with **33j** (L_2 = dppb). Other selected structural data for these complexes are illustrated in Table **5.7**.

In summary, the crystal structure study of the zwitterionic complexes [(η^6-Bcat$_2$)RhL_2] reveals that these compounds adapt a half-sandwich geometry in the solid state. The properties of the ancillary ligand(s) L_2 can effect prominently not only the properties of the metal center but also the geometry of the Bcat$_2$- unit in the molecules. We can foresee that the reactivity of the metal center can be easily fine-tuned by the selection of different L_2 ligands.

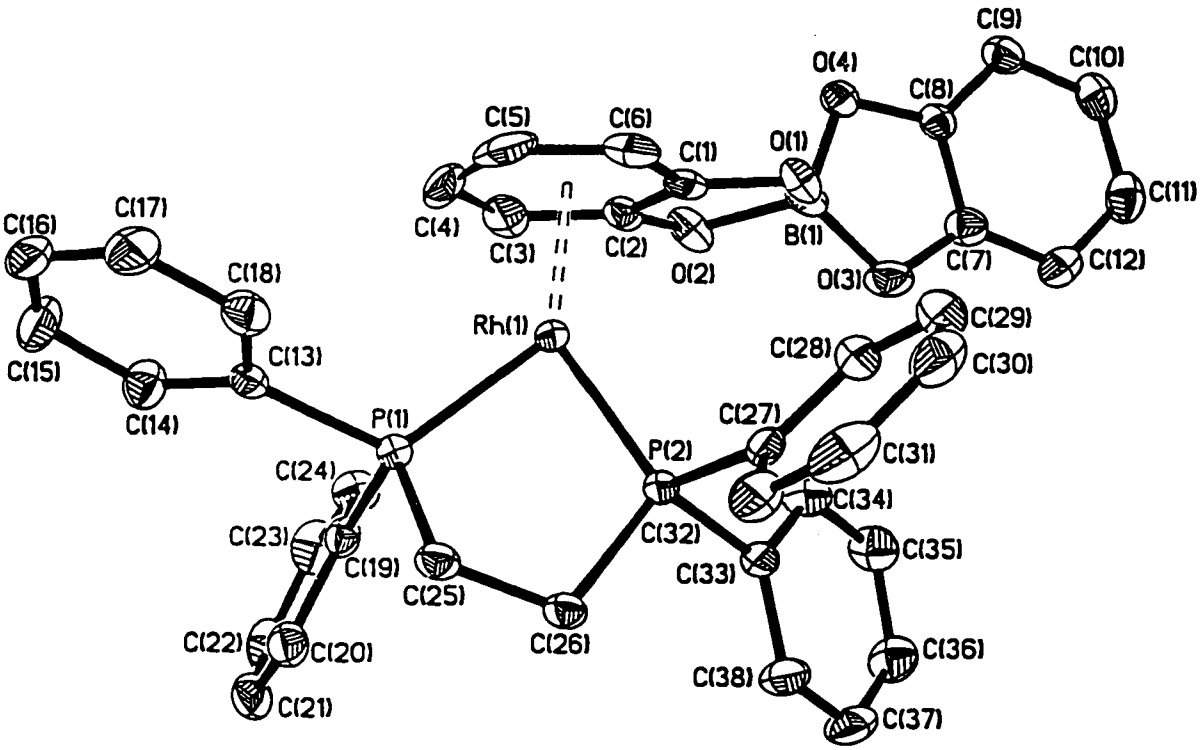


Figure 5.18 Molecular structure of $[(\eta^6\text{-Bcat}_2)\text{Rh(dppe)}]$ (**33e**), with 50% probability ellipsoids.

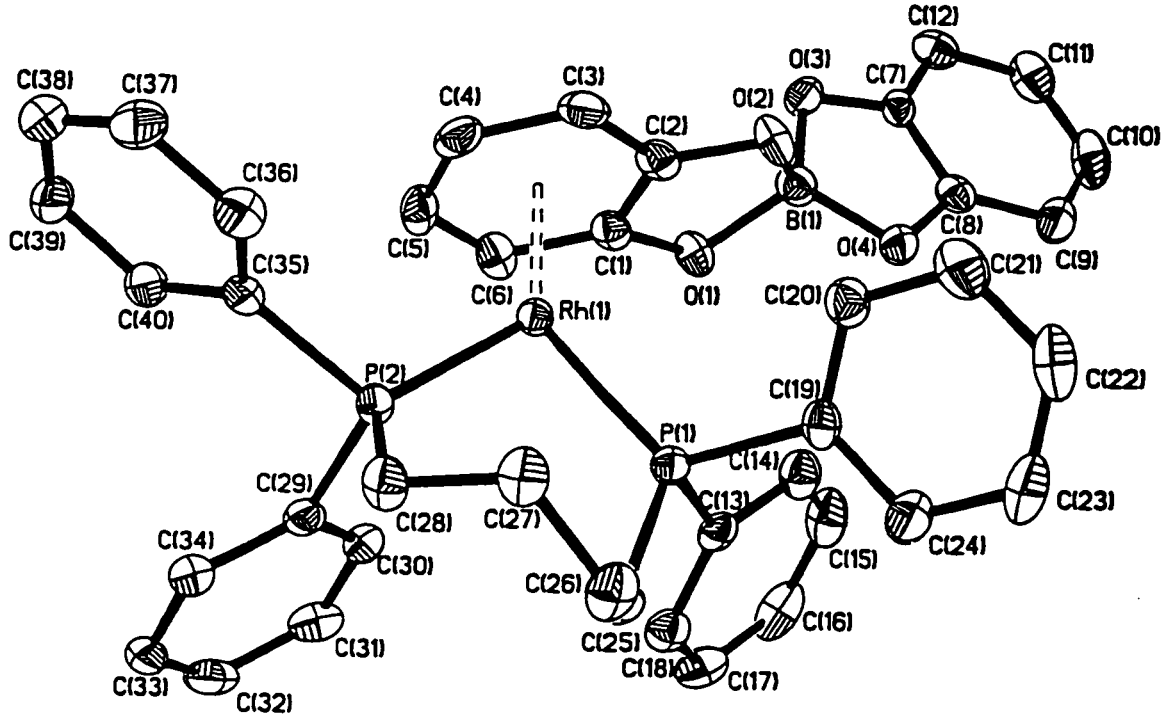


Figure 5.19 Molecular structure of $[(\eta^6\text{-Bcat}_2)\text{Rh(dppb)}]$ (**33j**), with 50% probability ellipsoids.

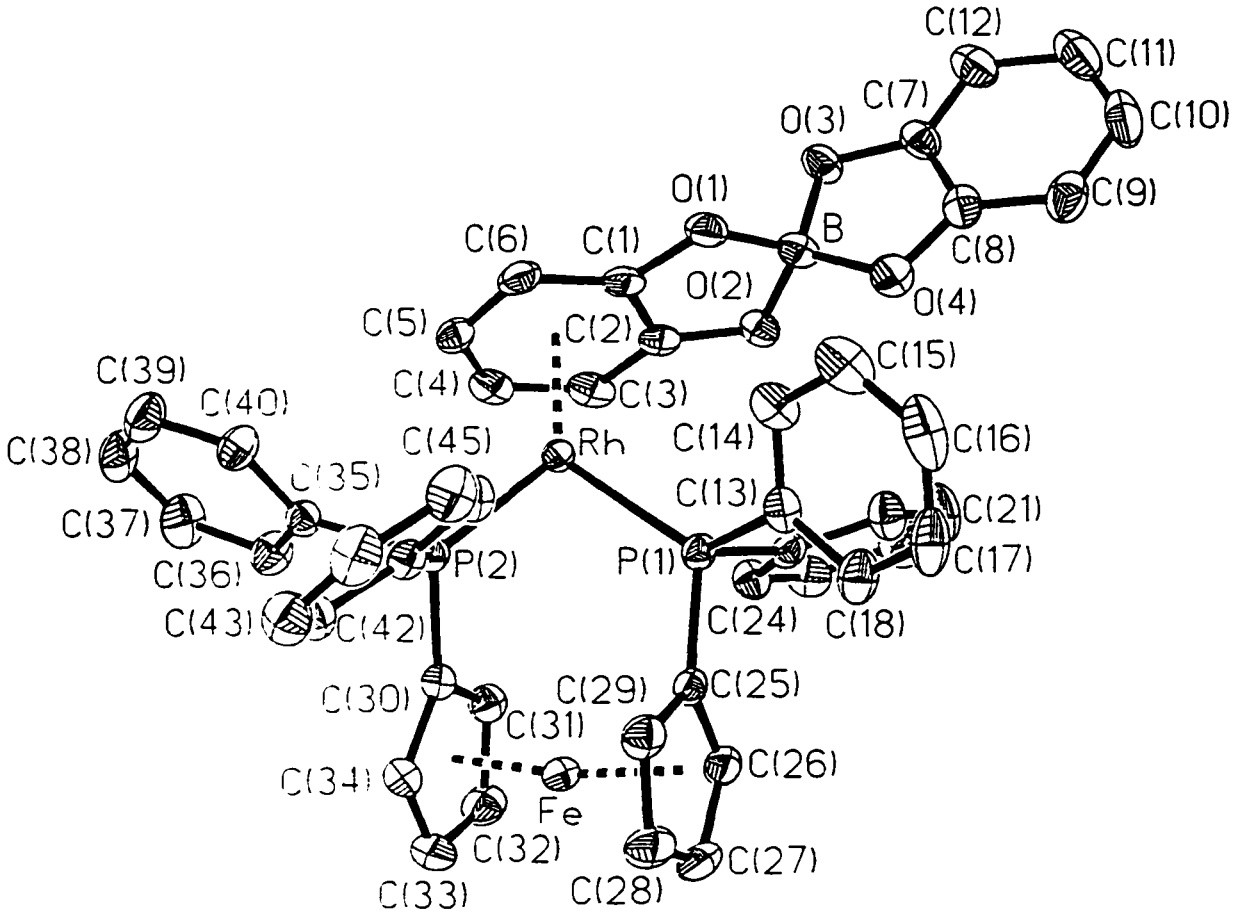


Figure 5.20 Molecular structure of $[(\eta^6\text{-Bcat}_2)\text{Rh(dppf)}]$ (**33l**), with 50% probability ellipsoids.

5.2.3 Catalytic Diborations of Alkenes

About five years ago, the Rh(I) zwitterionic complex [(η^6-$Bcat_2$)Rh(dppb)] (**33j**) was first generated and identified in our research group, and it has been demonstrated to be an excellent hydroboration catalyst.[14b] The clean synthesis of **33j** and many of its analogs, however, has not previously been entirely straightforward, although several [(acac)RhL_2] (**37**) complexes have been shown to react with excess of HBcat to provide the zwitterions under catalytic conditions. Our new results on the facile reactions between **37** and B_2cat_3, as described above, clearly indicate that various complexes **33** can be generated readily by mixing **37** with 1 equiv. of B_2cat_3 in solution. Not only phosphine containing complexes (**33 d-m**), but alkene coordinated compounds (**33 a-c**) were easily obtained, which could not be prepared from previous reactions involving HBcat. As stated earlier, pure complexes **33** can be isolated by precipitation or recrystallization from the other product (acac)Bcat. However, since the above conversion is rapid and quantitative, and (acac)Bcat is likely inert in most of the catalytic processes investigated, it would be even more convenient to utilize just the [(acac)RhL_2]/B_2cat_3 mixture as *in situ* catalyst precursors.

5.2.3.1 Effectiveness of the [(acac)RhL_2]/B_2cat_3 Catalyst Systems

To this end, three parallel experiments were performed to test the effectiveness of this [(acac)RhL_2]/B_2cat_3 system. Thus, the addition of HBcat to 4-vinylanisole in THF-d_8 at room temperature was catalyzed separately by (i) [(acac)Rh(dppb)]; (ii) [(η^6-$Bcat_2$)Rh(dppb)]; and (iii) [(acac)Rh(dppb)] /B_2cat_3 with the same loading of Rh (VA / HBcat / catalyst = 1.0 / 1.05 / 0.02). Essentially identical results were obtained in all the trials, i.e. within 30 min, the hydroboration gave over 99% of the internal H-B addition product, which is consistent with our original report.[14c] Then, [(acac)Rh(dppb)]/B_2cat_3

(4 mol%) was also applied to the catalytic hydroboration (HBcat, 150 %) of the hindered alkene 2,3-dimethylbut-2-ene in THF-d_8. The reaction was successful, but it took 80 h to complete instead of 24 h as in the initial report.[14c] Recently, there has been some argument on prolonged hydroboration reactions such as this current case, as the decomposition of HBcat to BH_3 might play a major role in the process, that is, BH_3 readily adds to alkene to afford R-BH_2, followed by HBcat and R-BH_2 exchange resulting in the R-Bcat product. Since, in the above reaction, there are no regio isomers present, it is difficult to tell whether the outcome of the reaction is due to conventional H-BH_2 addition or metal-catalyzed H-Bcat addition. In fact, by adding 4 mol% of BH_3•THF instead of the Rh catalyst to the reaction solution, clean hydroboration was also observed within 7 days. During the course of 2 days, the ^1H NMR spectrum indicated that *ca.* 50% of the alkene was converted, and ca. 21% of the alkene formed R-BH_2. However, when the reaction was catalyzed by [(acac)Rh(dppb)] /B_2cat_3, it reached *ca.* 92% conversion in 2 days, and the R-BH_2 product was negligible. Therefore, from this comparison, we might conclude that the metal catalysis is the dominant factor in this reaction.

5.2.3.2 B_2cat_2 Addition to 4-Vinylanisole

With a series of catalyst precursors in hand, we were ready to apply the [(acac)RhL_2]/B_2cat_3 system to the catalytic addition of B_2cat_2 to 4-vinylanisole which we have been studying in the group for several years. We foresaw that fine tuning of the properties of the ancillary ligand(s) L_2 might have a profound impact on the catalytic reactivity of these [(η^6-$Bcat_2$)RhL_2)] catalysts.

The reactions of 4-vinylanisole with B_2cat_2 were performed in THF-d_8 at room temperature for 20 h, and 4 mol % of the [(acac)RhL_2]/B_2cat_3 catalyst precursors were

employed. The results are shown in Table **5.9**. As we have experienced earlier, a host of products are observed to different extents with each catalyst. Their structures are illustrated in Figure **5.21.**

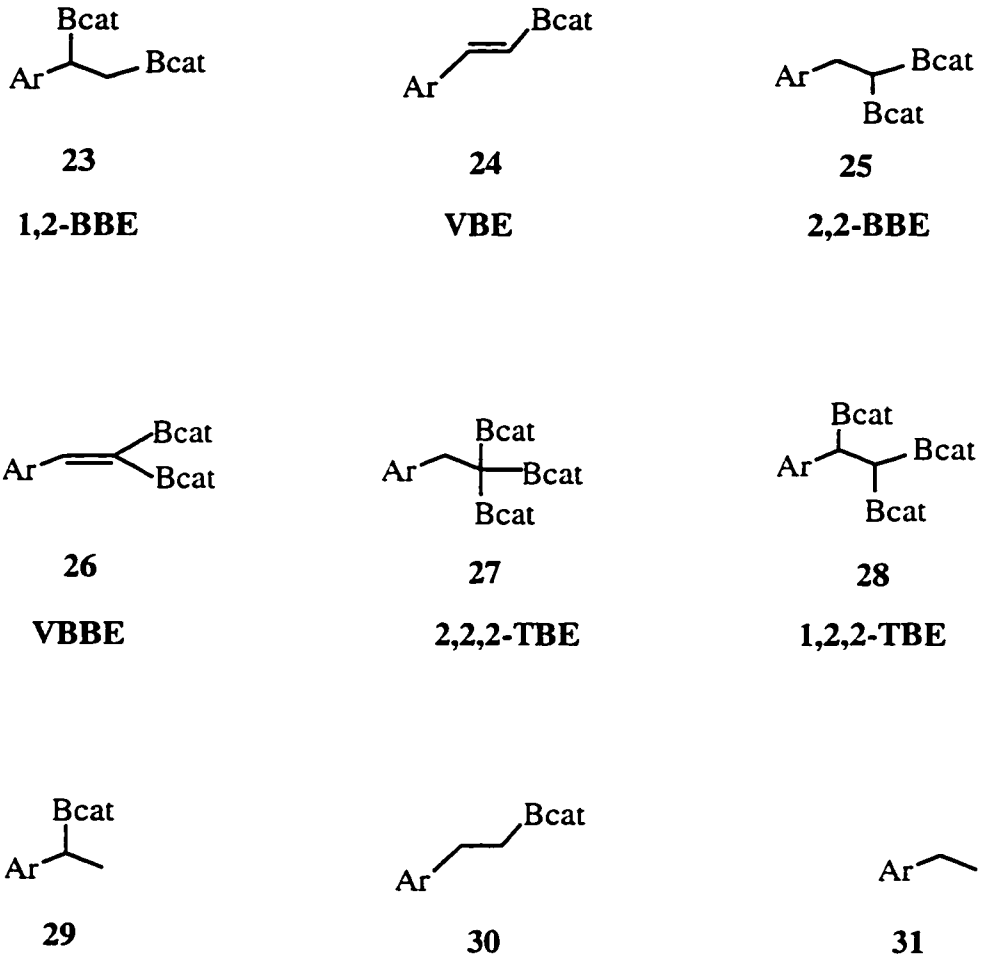


Figure 5.21 Products obtained from the addition of B_2cat_2 to 4-vinylanisole.

Table 5.9 Catalyzed Addition of B_2cat_2 (**1a**) to 4-Vinylanisole.[a]

Entry	Catalyst	23	24	25	26	27	28	29	30	31
1	(η^6-Bcat$_2$)Rh(COE)$_2$	10	30	5	5	-	5	33	5	7
2	(η^6-Bcat$_2$)Rh(COD)	29	17	3	3	-	14	31	-	3
3	(η^6-Bcat)Rh(PPh$_2$Me)$_2$	14	-	13	-	36	-	36	-	1
4	(η^6-Bcat$_2$)Rh(dppm)	**89**	-	2	-	2	2	2	3	-
5	(η^6-Bcat$_2$)Rh(dppe)	47	-	11	-	16	4	19	1	2
6	(η^6-Bcat$_2$)Rh(dppp)	50	-	30	-	10	-	10	-	-
7	(η^6-Bcat$_2$)Rh(dppb)	40	8	12	-	13	-	25	-	2
8	(η^6-Bcat$_2$)Rh(dppf)	44	11	6	-	11	-	27	-	1

[a]All reactions were carried out in THF-d_8 at room temperature for 20 h in the presence of 4 mol% catalyst (**1a**/alkene/catalyst = 1.0/1.0/0.04). Product ratios determined by ^{1}H and ^{13}C NMR.

dppm = bis(diphenylphosphino)methane, dppe = 1,2-bis(diphenylphosphino)ethane, dppp = 1,3-bis(diphenylphosphino)propane, dppb = 1,4-bis(diphenylphosphino)butane, dppf = 1,1'-bis(diphenylphosphino)ferrocene, COD = 1,5-cyclooctadiene, COE = cyclooctene.

The above results indicate that: (1) in contrast to the successful conduct of phosphine free Pt catalysts on the diboration of alkenes, the phosphine-free Rh catalysts [(η^6-$Bcat_2$)Rh(COE)$_2$] and [(η^6-$Bcat_2$)Rh(COD)] are unsuitable (Entries 1 and 2). Complexes with phosphine ligands (Entries 3 to 8), in turn, give essentially only four products. In comparison to other Rh catalysts we have tested earlier as seen in table **5.3**, the [(η^6-$Bcat_2$)RhP_2] catalyst systems, in general, exhibit the highest selectivity. (2) Chelating phosphines give much better results than monodentate ones. The catalyst [(η^6-$Bcat_2$)Rh(PPh_2Me)$_2$] was chosen as the model compound to compare with the bis(phosphine) analogs. The product mixture from this catalyst consists of only *ca.* 14% of the desired product 1,2-bis(boronate) ester (1,2-BBE, **23**). The remaining products include 2,2-bis(boronate) ester (2,2-BBE, **25**, 13%), and significant amounts of 2,2,2-tris(boronate) ester (2,2,2-TBE, **27**, 36%) and internal alkylboronate ester (**29**, 36%), all of which presumably arise from the competing β-H elimination process (*vide infra*). However, the chelating bis(phosphine)s in other catalysts have largely depressed this side reaction process, and higher 1,2-BBE yields were observed (over 40%). This chelating effect is also apparent between ligands COE and COD in Entries 1 and 2 (10% *vs* 29% of 1, 2-BBE, respectively). (3) Among the series of bis(phosphine) ligands with different backbones, i.e., Ph_2P-$(CH_2)_n$-PPh_2 (n = 1-4) and Ph_2P-(η^5-C_5H_4)Fe(η^5-C_5H_4)-PPh_2, the least "bucketed" ligand dppm shows an outstanding selectivity toward the diboration of 4-vinylanisole (89% of 1,2-BBE). There appears to be a general trend of decreasing selectivity with increasing P-Rh-P angle in the structures of [(η^6-$Bcat_2$)Rh(P_2)] catalysts. One interesting question is what the coordination modes of the $Bcat_2^-$ anion to the metal will be in all stages of the catalysis. A complete dissociation from the metal seems very unlikely as catalysts [(η^6-$Bcat_2$)Rh(dppb)] (**33j**) and [Rh(COD)(dppb)]BF_4 exhibit very different reactivity (Table **5.3**, entries h and i). While detailed mechanistic studies have not yet been performed, the differences in results using ligands from dppm to dppf suggest at least the following two points. First, the results of the crystal structure

analysis have already revealed that the coordination geometry at the Rh center in [(η^6-$Bcat_2$)Rh(P_2)] is largely determined by the steric factors of the chelating phosphines. When L_2 = dppm, the Rh atom is least shielded, in other words, it is mostly accessible by the reactants. Recently, Leitner and co-workers[53] have proposed a so-called AMS (the accessible molecular surface) model which they used to correlate the ligand steric effects to the observed catalytic activities of [(hfac)Rh(P_2)] (hfac = hexafluoroacetylacetonate) complexes on the hydrogenation of CO_2 to formic acid.[63] In the sense of this AMS concept, the catalyst [(η^6-$Bcat_2$)Rh(dppm)] (**33e**) surely contains the highest accessible surface, which might account for its best selectivity. Second, the single CH_2 linkage between the two PPh_2 groups in dppm builds up the highest rigidity to the coordination chelate ring. It does not allow any variation in the P-Rh-P angle. However, with other rather "spring-like" or "rotator-like" $(CH_2)_n$ or ferrocenyl bridges, the geometry of the chelate rings in [(η^6-$Bcat_2$)Rh(P_2)] catalysts are naturally more flexible, and thus may have some effect on the selectivities these catalysts present in the reactions.

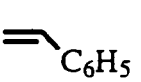
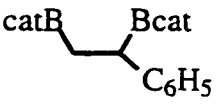
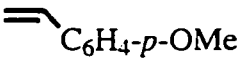
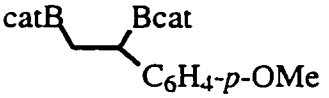
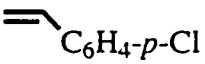
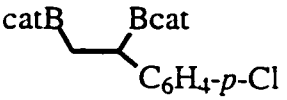
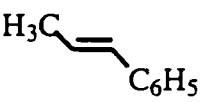
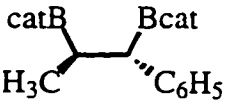
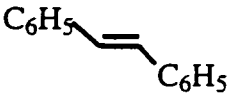
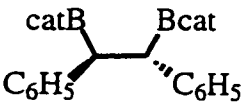
In conclusion, by applying a series of [(η^6-$Bcat_2$)Rh(P_2)] catalysts for the diboration of 4-vinylanisole by B_2cat_2, much improved results have been observed with chelating phosphine (η^6-$Bcat_2$)Rh complexes compared to other structural types of Rh catalysts we have screened before. To our delight, we finally found that at least one Rh phosphine catalyst, [(η^6-$Bcat_2$)Rh(dppm)] (**33e**) can diborate 4-vinylanisole very cleanly.

5.2.3.3 Catalyzed Diboration of Other Alkenes Using [(acac)Rh(dppm)]/B_2cat_3

To test the generality of this [(η^6-$Bcat_2$)Rh(dppm)] catalyst, various alkene substrates have been reacted with B_2cat_2 in the presence of 4 mol% of a mixture of [(acac)Rh(dppm)] and B_2cat_3, which act as the precursors to the zwitterionic catalyst [(η^6-$Bcat_2$)Rh(dppm)]. The reactions were performed in THF-d_8 at room temperature

and were monitored by ^1H NMR for completion, and the yields were verified by high field ^1H and $^{13}C\{^1H\}$ NMR. Selected results are illustrated in Table **5.10**.

Table 5.10 [(acac)Rh(dppm)]/B_2cat_3-catalyzed diboration of alkenes[a]

Entry	Olefin	Product	Time (h)	%yield
1			1[b]	69
2			1	89
3			1[b]	79
4			1	100
5			30	>95
6			56	>95

[a] All reactions were carried out in THF-d_8 at room temperature in the presence of 4 mol% catalyst [(acac)Rh(dppm)]/B_2cat_3, product yields determined by ^1H and ^{13}C NMR spectroscopy;

[b] Reaction completed within 1 h, the exact reaction time was not recorded.

The diboration of 4-vinylanisole was complete within 1 h giving 89% of the desired 1,2-diborated product as determined by *in situ* NMR. In comparison to the phosphine-free Pt(0) catalysts (Tables **5.1** & **5.2**), [(η^6-Bcat$_2$)Rh(dppm)] is very similar to [Pt(COD)$_2$] or [Pt(NBE)$_2$][34] but superior to [Pt(dba)$_2$][33] in terms of reactivity for the 4-vinylanisole. Likewise, both styrene and 4-chlorostyrene were effectively diborated, giving 69% and 79% 1,2-BBE respectively (Entries 1 and 3). The lower yield with styrene is due to the large amount of 1,1-vinylbis(boronate) ester (VBBE, **26**, 22%) in the products. The reactions were found to be complete within 1 h. However, as the reactions were not monitored before 1 h, it is possible that some or all were complete in a shorter time and that there may be different reactivities as a function of para substituents; Miyaura[33] indicated that 4-vinylanisole reacted more slowly than styrene.

As with the above mentioned Pt(0) catalysts, [(η^6-Bcat$_2$)Rh(dppm)] also afforded rapid and extremely clean diboration of the cyclic alkene norbornene (Entry 4). While both Miyaura[33] and Smith[34] failed to diborate any unstrained internal alkenes, [(η^6-Bcat$_2$)Rh(dppm)], however, was able to catalyze the addition of B$_2$cat$_2$ to *trans*-β-methylstyrene (Entry 5) and *trans*-stilbene (Entry 6). The reactions are notably slower (30 and 56 h); however, only minimal amounts of side products were detected by NMR. Noting that these reactions were conducted at room temperature, they would not be regarded as being particularly sluggish reactions. The diborated product from *trans*-stilbene was readily crystallized from the reaction medium (THF-d$_8$) as colorless plates, and its structure has been determined by X-ray crystallography (Figure **5.22**). Consistent with *cis*-addition, the product has the expected D, L rather than *meso* form. It is also interesting that there is a THF-d$_8$ molecule wedged between the two boron atoms with an O-B distance of 2.664 Å but this distance is rather long for coordination and thus it is best regarded as being a solvent of crystallization. The catecholate groups in the compound stack parallel to another with a *ca.* 3.5 Å interplanar distance.

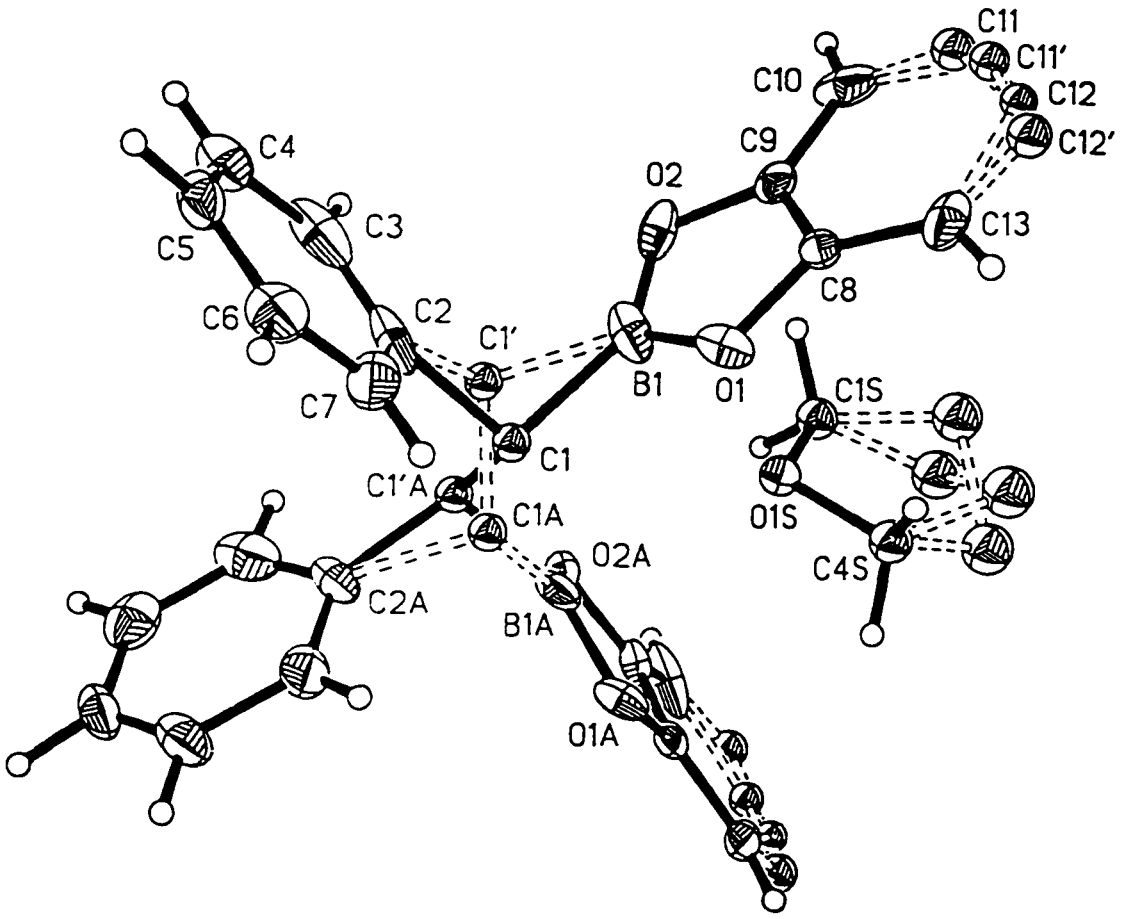


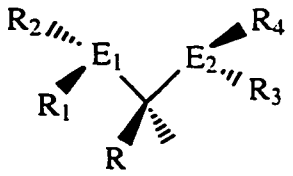
Figure 5.22 Molecular structure of the product of diboration of *trans*-stilbene, with 50% probability ellipsoids.

5.3 Conclusions

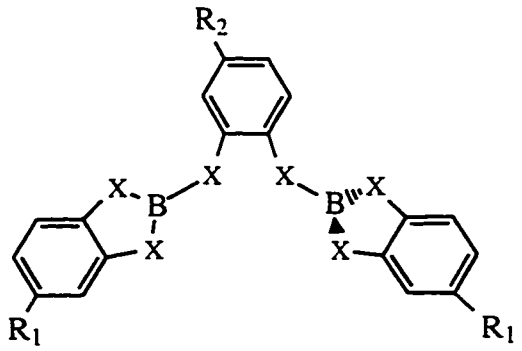
In this chapter, we have shown that, instead of being regarded as an undesired waste substance, B_2cat_3 can be utilized as a convenient source for the synthesis of organoboron compounds and possibly even metal boryl complexes. More importantly, the facile reactions between B_2cat_3 and low valent Rh(I) $[(acac)RhL_2]$ complexes provide a direct and general route to the novel zwitterionic complexes $[(\eta^6\text{-}Bcat_2)RhL_2]$ with a variety of ancillary ligands.

Crystallographic studies on the $[(\eta^6\text{-}Bcat_2)RhL_2]$ complexes indicate that the coordination environment at the metal center as well as the conformation of the coordinated $Bcat_2^-$ anion are dominated by the steric effects of the ancillary ligands. These complexes exhibit very different catalytic activities toward the diborations of alkenes with the variation of phosphine ligands. The catalyst $[(\eta^6\text{-}Bcat_2)Rh(dppm)]$ has demonstrated outstanding reactivities as well as selectivities in the diboration reactions. The catalyzed diboration of unstrained internal alkenes has been realized for the first time.

Further variation in the structure of the bis(phosphine) ligands can be investigated with the $[(\eta^6\text{-}Bcat_2)RhL_2]$ complexes. The small bite angle with dppm seems critical to the reactivity. Other analogs, even chiral bis(phosphine)s based on dppm can be applied to the reaction in order to achieve even better results or asymmetric synthesis. On the other hand, the $\eta^6\text{-}Bcat_2$ fragment can be easily derivatized from the corresponding B_2cat_3 analogs shown below. Moreover, the reaction between B_2cat_3 and $[(acac)RhL_2]$ may be more general in that ligands other than acac may prove applicable.



E_1, E_2 = P, As, Sb;
R = H, CH_3;
R_1-R_4 = aryl, alkyl.



X = O, S;
R_1, R_2 = H, alkyl.

Finally, experimental results have demonstrated that zwitterionic complexes [(η^6-$Bcat_2$)RhL_2] represent a series of efficient hydroboration and diboration catalysts. With a wealth of catalytic chemistry on the related [(η^6-BPh_4)RhL_2] complexes for comparison, we believe that [(η^6-$Bcat_2$)RhL_2] can also find broader applications in homogeneous catalysis.

5.4 Experimental

5.4.1 General Procedures

Reactions were performed under a dry nitrogen atmosphere using glove box techniques. THF was freshly distilled from sodium benzophenone ketyl, and heptane from sodium metal under an N_2 atmosphere. NMR solvents were distilled from CaH_2 (CD_3CN) or Na metal (C_6D_6) following three freeze/pump/thaw cycles. [$Rh(PMe_3)_4Me$]was prepared by established methods. [64] NMR spectra were recorded on a Bruker AC 200 (^1H at 200 MHz, ^{13}C at 50 MHz, ^{31}P at 81 MHz) spectrometer. The ^1H and ^{13}C chemical shifts were referenced to the solvent resonances as an internal standard. The ^{31}P and ^{11}B chemical shifts were referenced to the external standards 85% H_3PO_4 and $F_3B{\cdot}OEt_2$ respectively. The ^{11}B NMR spectrum was obtained using a background subtraction routine to remove resonances due to borosilicate glass in the NMR probe and NMR tube. This was accomplished by recording the spectrum of an NMR tube containing the same volume of pure solvent and with identical acquisition parameters to those of the sample and by subtracting this background FID from that of the sample. Coupling constants are reported in Hz. Multiplicities are reported as (br) broad, (s) singlet, (d) doublet, (vt) virtual triplet, and (m) multiplet.

5.4.2 Synthesis

[$Rh(PMe_3)_4$][$Bcat_2$] The compound B_2cat_3 (164 mg, 0.474 mmol) was dissolved in 100 mL of heptane at 40°C, and then a solution of [$Rh(PMe_3)_4Me$] (200 mg, 0.474 mmol) in 3 mL of heptane was added dropwise with stirring. A voluminous orange precipitate formed immediately. The reaction was stirred for for 1 h at 40°C and another hour at room temperature. The orange solid was filtered and washed thoroughly with

toluene and heptane, respectively, and dried *in vacuo*, yielding 293 mg (98%) orange solid. Recrystallization from THF gave 246 mg of flaky orange crystals. $^{31}P\{^{1}H\}$ NMR (CD_3CN) δ -12.74 (br. s); $^{31}P\{^{1}H\}$ NMR (C_6D_6/THF (1:10)), δ -14.30 (d, $^{1}J_{Rh-P}$ = 131.6 Hz); $^{11}B\{^{1}H\}$ NMR (C_6D_6/THF (1:10)), δ: 14.7 (s, $Bcat_2$); ^{1}H NMR (CD_3CN), δ 6.54 (s, 8H, $Bcat_2$), 1.41 (s, 36H, PMe_3). $^{13}C\{^{1}H\}$ NMR (CD_3CN), δ 20.65 (s, PMe_3), 108.79 (s), 118.29(s), 152.97 (s).

$[Rh(PMe_3)_4H_2][Bcat_2]$ H_2 gas was bubbled into a solution of $[Rh(PMe_3)_4][Bcat_2]$ (100 mg, 0.158 mmol) in 10 mL of THF for about 10 minutes. The solution turned colorless very quickly. By layering this solution with 15 mL of heptane, 95 mg (95%) of colorless crystals were obtained. $^{31}P\{^{1}H\}$ NMR (81 MHz, 25°C in CD_3CN), δ: -11.01 (dt, 2P, $^{1}J_{Rh-P}$= 96.4, $^{2}J_{p-p}$ =27 Hz, 2 PMe_3), -22.35 (dt, 2P, $^{1}J_{Rh-P}$ = 85.7, $^{2}J_{p-p}$ = 27 Hz, 2 PMe_3), $^{11}B\{^{1}H\}$ NMR (64 MHz, 25°C in CD_3CN), δ: 14.7 (s, $Bcat_2$). ^{1}H NMR (200 MHz, 25°C in CD_3CN), δ: 6.53 (s, 8H, $Bcat_2$), 1.46 (pseudo dt, 36H, $^{3}J_{Rh-H}$ = 11.5 Hz, PMe_3), -10.69 (pseudo dq, 2H, $^{2}J_{P-H}$ (*trans*)= 136.6, $^{2}J_{P-H}$ (*cis*) = $^{1}J_{Rh-H}$ = 14.8 Hz, Rh-H). $^{13}C\{^{1}H\}$ NMR (50 MHz, 25°C in CD_3CN), δ: 22.04 (t, PMe_3), 25.46 (t, PMe_3), 108.77 (s, $Bcat_2$), 118.49 (s, $Bcat_2$), 152.97 (s, $Bcat_2$).

(acac)Bcat A solution of B_2cat_3 (284 mg, 0.82 mmol) in 2 mL of THF was added to a solution of Na(acac) (100 mg, 0.82 mmol) in 10 mL of THF, resulting in a yellow solution. After stirring at room temperature for 1 h, the solvent was removed *in vacuo*, and the yellow residue was extracted with toluene, leaving 200 mg of a white solid of $Na[Bcat_2]$ (98%). The yellow toluene solution was stripped to dryness *in vacuo*, yielding 154 mg of yellow crystals (87%). $^{11}B\{^{1}H\}$ NMR spectrum (C_6D_6): δ 9.82; ^{1}H NMR spectrum (C_6D_6): δ 1.28 (s, 6H, CH_3), 4.69 (s, 1H, *CH*), 6.83 (m, 2H, C_6H_4), 7.07 (m, 2H, C_6H_4); $^{13}C\{^{1}H\}$ NMR spectrum (C_6D_6): δ 23.14 (s, CH_3), 101.43 (s, *C*H), 109.99 (s, cat), 120.17(S, cat), 151.60 (s, cat), 190.89 (s, *C*=O).

(acac)Rh(COD) The compounds $[RhCl(COD)]_2$ (800 mg, 1.62 mmol) and Na(acac) (400 mg, 3.28 mmol) were mixed in the solid state, then 20 mL of heptane and 30 mL of toluene were added, and the mixture was allowed to stir for 4 h at 50°C, then the solid was removed by filtration. The filtrate was concentrated to dryness *in vacuo,* and the crude product was extracted by heptane, yielding 1.01 g of yellow solid (99%). ^1H NMR (C_6D_6) δ: 1.77 (s, 6H, CH_3), 1.60 (m, 4H, CH_2), 2.26 (m, 4H, CH_2), 4.27 (br. s, 4H, =CH), 5.13 (s, 1H, CH). $^{13}C\{^1H\}$ NMR (C_6D_6) δ: 27.3 (s, CH_2), 30.55 (s, CH_3), 76.20 (d, CH), 99.70 (s, CH), 186.58 (s, C=O).

(η^6-Bcat$_2$)Rh(η^2-C_2H_4)$_2$ A solution of (acac)Rh(η^2-C_2H_4)$_2$ (50 mg, 0.19 mmol) in 0.5 mL of C_6D_6 was added dropwise to a solution of B_2cat_3 (67 mg, 0.19 mmol) in 1 mL of C_6D_6, and a clear yellow solution was obtained at first, but *ca.* 2 min. later, a large amount of yellow precipitate formed. The mixture was allowed to stir for 2 h. The solid was filtered and washed thoroughly with benzene and hexane, and dried *in vacuo,* yielding 71 mg (95%) of pale yellow solid. $^{11}B\{^1H\}$ NMR (THF-d_8) δ: 14.87 (s, η^6-Bcat$_2$); ^1H NMR (THF-d_8) δ: 2.71 (br. s, 8H, =CH_2), 5.70 (m, 2H, η^6-$C_6H_4O_2$), 6.51 (m, 4H, $C_6H_4O_2$), 7.02 (m, 2H, η^6-$C_6H_4O_2$); $^{13}C\{^1H\}$ NMR (THF-d^8) δ: 53.27 (d, $^1J_{Rh\text{-}C}$ = 12.30 Hz, C_2H_4), 90.21 (s, η^6-$C_6H_4O_2$), 94.37 (d, $^1J_{Rh\text{-}C}$ = 4.2 Hz, η^6-$C_6H_4O_2$), 109.32 (s, $C_6H_4O_2$), 118.88 (s, $C_6H_4O_2$), 119.01 (s, $C_6H_4O_2$), 141.48 (s, η^6-$C_6H_4O_2$), 152.23 (s, $C_6H_4O_2$), 152.51 (s, $C_6H_4O_2$).

(η^6-Bcat$_2$)Rh(COE)$_2$ 33b was obtained in a similar fashion from (acac)Rh(COE)$_2$; yield 96%. This compound is very insoluble in C_6D_6, its existence in the filtrate solution could not be detected by either $^{11}B\{^1H\}$ or ^1H NMR spectrum. $^{11}B\{^1H\}$ NMR in toluene, δ: 16.0, $^{11}B\{^1H\}$ (in THF-d_8) 15.4 (s, η^6-Bcat$_2$); no good ^1H or $^{13}C\{^1H\}$ NMR spectra were obtained in C_7H_8 due to its poor solubility. In THF-d_8, it also gave a complicated ^1H NMR spectrum. A sample in CD_3CN, however, gave rather the presumably displaced compound $[Rh(COE)_2(CD_3CN)_2][Bcat_2]$. $^{11}B\{^1H\}$ NMR

spectrum in CD_3CN, δ: 14.8 (s); ^1H NMR spectrum (CD_3CN), δ: 1.48 (br s, 16H, CH_2), 2.07 (br m, 8H, CH_2), 4.83 (m, 4H, CH), 6.54 (s, 8H, $Bcat_2^-$); $^{13}C\{^1H\}$ spectrum (CD_3CN), δ: 26.9 (CH_2), 27.7 (CH_2), 30.7 (CH_2), 103.9 (br, CH), 108.8 (s, CH), 118.3 (s, CH)), 152.9 (s, CO). Nevertheless, a good analysis for $(\eta^6\text{-}Bcat_2)Rh(COE)_2$ was obtained from the solid, calcd. for $C_{28}H_{36}BO_4Rh$: C, 61.11; H, 6.59. Found: C, 60.92; H, 6.38.

$(\eta^6\text{-}Bcat_2)Rh(COD)$ 33c was obtained in a similar fashion from (acac)Rh(COD); yield 87%. $^{11}B\{^1H\}$ NMR spectrum (THF-d_8) δ: 14.78 (s, η^6-$Bcat_2$); ^1H NMR spectrum (THF-d_8) δ: 2.10 (m, 4H, CH_2), 2.31 (m, 4H, CH_2), 4.35 (br. s, 4H, CH), 5.63 (m, 2H, η^6-$C_6H_4O_2$), 6.49 (m, 4H, $C_6H_4O_2$), 6.94 (m, 2H, η^6-$C_6H_4O_2$); $^{13}C\{^1H\}$ NMR (THF-d_8) δ: 32.47 (s, CH_2), 78.33 (d, $^1J_{Rh\text{-}C}$ = 3.3 Hz, CH), 90.19 (s, η^6-$C_6H_4O_2$), 93.66 (d, $^1J_{Rh\text{-}C}$ = 4.2 Hz, η^6-$C_6H_4O_2$), 109.23 (s, $C_6H_4O_2$), 118.73 (s, $C_6H_4O_2$), 118.86 (s, $C_6H_4O_2$), 141.10 (s, η^6-$C_6H_4O_2$, 152.33 (s, $C_6H_4O_2$), 152.58 (s, $C_6H_4O_2$).

$(\eta^6\text{-}Bcat_2)Rh(PPh_2Me)_2$ $^{31}P\{^1H\}$ NMR spectrum (C_6D_6): δ 28.82 (d, $^1J_{Rh\text{-}P}$ = 208.8 Hz) ; $^{11}B\{^1H\}$ NMR spectrum (C_6D_6) δ: 15.84 (s, η^6-$Bcat_2$); ^1H NMR spectrum (C_6D_6) δ: 1.47 (m, 6H, PMe_3), 4.60 (m, 2H, η^6-$C_6H_4O_2$), 5.25 (m, 2H, η^6-$C_6H_4O_2$), 6.93-7.01 (ov m, 12 H, C_6H_5), 7.16 (m, 4H, $C_6H_4O_2$), 7.32-7.40 (m, 8H, C_6H_5); $^{13}C\{^1H\}$ NMR spectrum (C_6D_6) δ: 17.2 (t, J = 17.2 Hz, P-CH_3), 86.51 (s, η^6-$C_6H_4O_2$), 90.89 (s, η^6-$C_6H_4O_2$), 109.03 (s, $C_6H_4O_2$), 109.96 (s, $C_6H_4O_2$), 118.74 (s, $C_6H_4O_2$), 119.16 (s, $C_6H_4O_2$), 128.18 (t, $J_{P\text{-}C}$ = 5.5, C_6H_5), 129.81 (br s, C_6H_5), 132.58 (t, $J_{P\text{-}C}$ = 5.1, C_6H_5), 137.74 (vt, $J_{P\text{-}C}$ = 24.0, C_6H_5), 143.37 (s, η^6-$C_6H_4O_2$), 152.74 (s, $C_6H_4O_2$).

(acac)Rh(dppm) $^{31}P\{^1H\}$ NMR spectrum (C_6D_6): δ -18.66 (d, $^1J_{Rh\text{-}P}$ = 163.7 Hz) ; ^1H NMR spectrum (C_6D_6): δ 1.95 (s, 6H, CH_3), 3.58 (td, $^3J_{Rh\text{-}H}$ = 2.29 Hz, $^2J_{P\text{-}H}$ = 10.29 Hz, 2H, CH_2), 5.41 (s, 1H, CH), 7.02 (m, 12H, C_6H_5), 8.01 (m, 8H, C_6H_5); $^{13}C\{^1H\}$ NMR (C_6D_6) δ: 28.08 (s, CH_3), 47.40 (t, $^1J_{P\text{-}C}$ = 12.66 Hz, CH_2) 99.54 (s, CH), 128.29

(d, $J_{P\text{-}C}$ = 4.55 Hz, C_6H_5), 129.53 (s, C_6H_5), 132.86 (t, $J_{P\text{-}C}$ = 6.02 Hz, C_6H_5), 136.49 (t, $J_{P\text{-}C}$ = 18.26 Hz, C_6H_5), 186.58 (s, *C*=O).

(η^6-Bcat$_2$)Rh(dppm) $^{31}P\{^1H\}$ NMR spectrum (C_6D_6): δ -22.97 (d, $^1J_{Rh\text{-}P}$ = 184.6 Hz); $^{11}B\{^1H\}$ NMR spectrum (C_6D_6): δ 15.76; ^1H NMR spectrum (C_6D_6): 3.62 (td, $^3J_{Rh\text{-}H}$ = 2.00 Hz, $^2J_{P\text{-}H}$ = 10.83 Hz, 2H, CH_2), 4.74 (m, 2H, η^6-$C_6H_4O_2$), 6.28 (m, 2H, η^6-$C_6H_4O_2$); 6.60 (m, 1H, $C_6H_4O_2$), 6.76 (m, 2H, $C_6H_4O_2$), 6.87-7.13 (ov m, 13H, $C_6H_4O_2$ and C_6H_5), 7.65 (m, 8H, C_6H_5). $^{13}C\{^1H\}$ NMR spectrum (THF-d_8) δ: 45.69 (t, $J_{P\text{-}C}$ = 25.9 Hz), 87.02 (d, $J_{Rh\text{-}C}$ = 3.2 Hz, η^6-$C_6H_4O_2$), 87.87 (br s, η^6-$C_6H_4O_2$), 109.58 (s, $C_6H_4O_2$), 112.09 (s, $C_6H_4O_2$), 118.31 (s, $C_6H_4O_2$), 122.31 (s, $C_6H_4O_2$), 129.20 (t, $J_{P\text{-}C}$ = 6.1 Hz, C_6H_5), 130.89 (br s, C_6H_5), 133.07 (t, $J_{P\text{-}C}$ = 6.1 Hz, C_6H_5), 136.86 (t, $J_{P\text{-}C}$ = 21.4 Hz, C_6H_5), 140.96 (s, η^6-$C_6H_4O_2$), 151.90 (s, $C_6H_4O_2$).

(η^6-Bcat$_2$)Rh(dppe) $^{31}P\{^1H\}$ NMR spectrum (C_6D_6): δ 75.80 (d, $^1J_{Rh\text{-}P}$ = 213.3 Hz); $^{11}B\{^1H\}$ NMR spectrum (C_6D_6): δ 15.75; ^1H NMR spectrum (C_6D_6): 1.65 (br, 4H, CH_2), 4.50 (m, 2H, η^6-$C_6H_4O_2$), 5.70 (m, 2H, η^6-$C_6H_4O_2$); 6.85 (m, 4H, $C_6H_4O_2$), 7.10 (m, 12H, C_6H_5), 7.52 (m, 8H, C_6H_5). $^{13}C\{^1H\}$ NMR spectrum (C_6D_6) δ 29.46 (t, CH_2), 86.81 (s, η^6-$C_6H_4O_2$), 89.08 (s, η^6-$C_6H_4O_2$), 108.89 (s, $C_6H_4O_2$), 109.72 (s, $C_6H_4O_2$), 118.66 (s, $C_6H_4O_2$), 118.96 (s, $C_6H_4O_2$), 128.66 (vt, C_6H_5), 130.40 (s, C_6H_5), 132.76 (vt, C_6H_5), 136.67 (vt, C_6H_5), 142.76 (s, η^6-$C_6H_4O_2$), 152.66 (s, $C_6H_4O_2$).

(η^6-Bcat$_2$)Rh(dppp) $^{31}P\{^1H\}$ NMR spectrum (C_6D_6): δ 28.67 (d, $^1J_{Rh\text{-}P}$ = 195.6 Hz); $^{11}B\{^1H\}$ NMR spectrum (C_6D_6): δ 15.96; ^1H NMR spectrum (C_6D_6): 1.38 (br, 2H, CH_2), 1.95 (br, 4H, CH_2), 4.79 (m, 2H, η^6-$C_6H_4O_2$), 4.97 (m, 2H, η^6-$C_6H_4O_2$); 6.84 (m, 4H, $C_6H_4O_2$), 7.08 (m, 12H, C_6H_5), 7.48 (m, 8H, C_6H_5); $^{13}C\{^1H\}$ NMR spectrum (C_6D_6) δ 27.84 (t, J = 19.4 Hz, P-CH_2), 30.15 (s, CH_2), 86.42 (d, $J_{Rh\text{-}C}$ = 3.1 Hz, η^6-$C_6H_4O_2$), 91.79 (d, $J_{Rh\text{-}C}$ = 3.1 Hz, η^6-$C_6H_4O_2$), 108.99 (s, $C_6H_4O_2$), 109.65 (s, $C_6H_4O_2$), 118.94 (s, $C_6H_4O_2$), 128.37 (vt, J = Hz, C_6H_5), 130.15 (br s, C_6H_5), 132.97

(vt, J = 6.2 Hz, C_6H_5), 136.40 (vt , J = 22.9 Hz, C_6H_5), 143.83 (s, η^6-$C_6H_4O_2$), 152.49 (s, $C_6H_4O_2$), 152.89 (s, $C_6H_4O_2$).

(η^6-Bcat$_2$)Rh(dppb) $^{31}P\{^1H\}$ NMR spectrum (C_6D_6): δ 43.22 (d, $^1J_{Rh-P}$ = 206.5 Hz); $^{11}B\{^1H\}$ NMR spectrum (C_6D_6): δ 15.48; ^1H NMR spectrum (C_6D_6): δ 1.28 (br, 4H, CH_2), 1.90 (br, 4H, CH_2), 4.59 (m, 2H, η^6-$C_6H_4O_2$), 4.96 (m, 2H, η^6-$C_6H_4O_2$); 6.84 (m, 2H, $C_6H_4O_2$), 7.03 (m, 2H, $C_6H_4O_2$), 7.14 (m, 12H, C_6H_5), 7.47 (m, 8H, C_6H_5); ^1H NMR spectrum ($CDCl_3$): δ 1.65 (br, 2H, CH_2), 2.31 (br, 4H, CH_2), 5.01 (m, 2H, η^6-$C_6H_4O_2$), 5.21 (m, 2H, η^6-$C_6H_4O_2$); 6.65 (m, 4H, $C_6H_4O_2$), 7.53 (m, 12H, C_6H_5), 7.60 (m, 8H, C_6H_5); $^{13}C\{^1H\}$ NMR spectrum (C_6H_6): δ 23.97 (s, CH_2), 31.76 (t, J = 15.9 Hz, P-CH_2), 87.90 (s, η^6-$C_6H_4O_2$), 91.13 (s, η^6-$C_6H_4O_2$), 108.62 (s, $C_6H_4O_2$), 109.70 (s, $C_6H_4O_2$), 118.62 (s, $C_6H_4O_2$), 118.93 (s, $C_6H_4O_2$), 128.13 (vt, J = 5.0 Hz, C_6H_5), 130.04 (br s, C_6H_5), 133.03 (vt, J = 5.8 Hz, C_6H_5), 138.59 (vt, J = 21.6 Hz, C_6H_5), 144.05 (s, η^6-$C_6H_4O_2$), 152.77 (s, $C_6H_4O_2$), 152.90 (s, $C_6H_4O_2$).

(acac)Rh(dppf) A solution of (acac)Rh(COE)$_2$ (100 mg, 0.24 mmol) in 10 mL of hexane was added dropwise to a solution of dppf (132 mg, 0.24 mmol) in 5 mL of toluene, resulting in a yellow solution. This was allowed to stir at room temperature for 2 h, during which time some yellow solid precipitated. The precipitate was collected by filtration and washed thoroughly with hexane, and then dried *in vacuo,* yielding 155 mg (87%) of yellow solid. $^{31}P\{^1H\}$ NMR spectrum (C_6D_6): δ 52.89 (d, $^1J_{Rh-P}$ = 199.5 Hz); ^1H NMR spectrum (C_6D_6): δ 1.50 (s, 6H, CH_3), 3.85 (m, 4H, C_5H_4), 4.32 (m, 4H, C_5H_4), 5.27 (s, 1H, CH), 7.09 (m, 12H, C_6H_5), 8.15 (m, 8H, C_6H_5), $^{13}C\{^1H\}$ NMR spectrum (C_6D_6): δ 27.1 (s, CH_3), 72.01 (s, C_5H_4), 72.81 (s, C_5H_4), 75.80 (vt, J = 4.6 Hz, C_5H_4), 99.7 (s, CH), 127.3 (vt, J = 4.5 Hz, C_6H_5), 129.04 (br s, C_6H_5), 135.33 (vt, J = 5.9 Hz, C_6H_5), 138.3 (vt, J = 20.3 Hz, C_6H_5), 184.34 (s, C=O).

(η^6-Bcat$_2$)Rh(dppf) A solution of B_2cat_3 (14 mg, 0.04 mmol) in 0.5 mL of C_6D_6 was added dropwise to a solution of (acac)Rh(dppf) (30 mg, 0.04 mmol) in 0.5 mL of C_6D_6, and the solution turned reddish brown immediately. After *ca.* 10 min, a large amount of orange-brownish solid precipitated. The precipitate was collected by filtration and washed thoroughly with benzene and hexane, and then dried *in vacuo*, yielding 33 mg (95%) of brown solid. $^{31}P\{^1H\}$ NMR spectrum (THF-d_8): δ 45.88 (d, $^1J_{Rh-P}$ = 220.5 Hz); $^{11}B\{^1H\}$ NMR spectrum (THF-d_8): δ 14.78; ^1H NMR spectrum (THF-d_8): δ 5.16 (br. s, 8H, C_5H_4), 5.89 (m, 2H, η^6-$C_6H_4O_2$), 6.01 (m, 2H, η^6-$C_6H_4O_2$); 7.29 (s, 4H, $C_6H_4O_2$), 8.20 (m, 12H, C_6H_5), 8.60 (m, 8H, C_6H_5). $^{13}C\{^1H\}$ NMR spectrum (THF-d_8): δ 73.43 (s, C_5H_4), 73.50 (s, C_5H_4), 76.88 (vt, J = 4.9 Hz, C_5H_4), 88.59 (s, η^6-$C_6H_4O_2$), 92.00 (s, η^6-$C_6H_4O_2$), 108.65 (s, $C_6H_4O_2$), 108.85 (s, $C_6H_4O_2$), 118.01 (s, $C_6H_4O_2$), 118.23 (s, $C_6H_4O_2$), 128.62 (vt, J = 5.4 Hz, C_6H_5), 130.76 (br s, C_6H_5), 134.85 (vt, J = 6.5 Hz, C_6H_5), 139.05 (vt, J = 23.2 Hz, C_6H_5), 144.62 (s, η^6-$C_6H_4O_2$), 152.79 (s, $C_6H_4O_2$), 153.02 (s, $C_6H_4O_2$) .

(η^6-Bcat$_2$)Rh(diop) $^{31}P\{^1H\}$ NMR spectrum (C_6D_6): δ 31.20 (d, $^1J_{Rh-P}$ = 208.3 Hz); $^{11}B\{^1H\}$ NMR spectrum (C_6D_6): δ 15.68 (br); ^1H NMR spectrum (C_6D_6): δ 1.22 (s, 6H, CH_3), 2.40 (br. m, 2H, CH_2), 2.89 (br. m, 2H, CH_2), 3.93 (br. t, 2H, CH), 4.75 (m, 4H, η^6-$C_6H_4O_2$), 6.85 (m, 4H, $C_6H_4O_2$), 7.06 (m, 12H, C_6H_5), 7.32 (m, 4H, C_6H_5), 7.63 (m, 4H, C_6H_5);

(η^6-Bcat$_2$)Rh(R-tol-BINAP) $^{31}P\{^1H\}$ NMR spectrum (C_6D_6): δ 45.00 (d, $^1J_{Rh-P}$ = 208.4 Hz); $^{11}B\{^1H\}$ NMR spectrum (C_6D_6): δ 16.15 (br).

(η^6-Bcat$_2$)Rh(dmpe) $^{31}P\{^1H\}$ NMR spectrum (C_6D_6): δ 49.66 (d, $^1J_{Rh-P}$ = 209.7 Hz); $^{11}B\{^1H\}$ NMR spectrum (C_6D_6): δ 15.39 (br).

(η^6-Bcat$_2$)Rh(dcpe) $^{31}P\{^1H\}$ NMR spectrum (C_6D_6): δ 96.85 (d, $^1J_{Rh-P}$ = 208.9 Hz); $^{11}B\{^1H\}$ NMR spectrum (C_6D_6): δ 15.32 (br); ^1H NMR spectrum (C_6D_6): δ 0.95-2.03

(ov m, 44H, C_6H_{11}), 4.99 (m, 2H, η^6-$C_6H_4O_2$), 6.31 (m, 2H, η^6-$C_6H_4O_2$), 6.75 (m, 2H, $C_6H_4O_2$), 6.86 (m, 2H, $C_6H_4O_2$).

(η^6-Bcat$_2$)Rh(PCy$_3$)(COE) $^{31}P\{^1H\}$ NMR spectrum (C_6D_6): δ 47.95 (d, $^1J_{Rh-P}$ = 191.8 Hz); $^{11}B\{^1H\}$ NMR spectrum (C_6D_6): δ 15.37 (br); ^1H NMR spectrum (C_6D_6): δ 1.10-1.73 (ov m, 42H, CH_2), 2.20 (br. d, 3H, CH), 2.68 (br, 2H, CH), 5.06 (m, 2H, η^6-$C_6H_4O_2$), 6.12 (m, 2H, η^6-$C_6H_4O_2$), 6.84 (m, 2H, $C_6H_4O_2$), 7.04 (m, 2H, $C_6H_4O_2$).

5.4.3 Catalysis

(acac)Rh(dppb)/B$_2$cat$_3$ Catalyzed Hydroboration of 4-Vinylanisole The compounds B_2cat_3 (7.0 mg, 0.02 mmol) and (acac)Rh(dppb) (13 mg, 0.02 mmol) were charged into a scintillation vial, then a solution of 4-vinylanisole (142 mg, 1.0 mmol) in 0.5 mL of THF-d_8 was added. The solution was stirred for 2 min to ensure that the solids were dissolved completely. To this solution, HBcat (125 mg, 0.25 mmol) in 0.5 mL of THF-d_8 was added. The reaction mixture was stirred at room temperature for 30 min, and then analyzed by high-field ^1H, $^{13}C\{^1H\}$ and $^{11}B\{^1H\}$ NMR spectroscopy.

MeO-C$_6$H$_4$-CH(Bcat)CH$_3$ (29) $^{11}B\{^1H\}$ NMR spectrum (THF-d_8): δ 34.6 (br); ^1H NMR spectrum (500 MHz, THF-d_8) δ 1.52 (d, J_{H-H} = 7.6 Hz, 3H, CH_3), 2.86 (q, J_{H-H} = 7.6 Hz, 3H, CH), 6.80 (m, 2H, phenyl H), 6.98 (m, 2H, catecholate H), 7.10-7.22 (ov m, 4H, phenyl H + catecholate H); $^{13}C\{^1H\}$ NMR (THF-d_8): δ 17.6 (CH_3), 55.4 (CH_3O), 123.0 (CH), 114.7 (CH), 123.3 (CH), 129.5 (CH), 136.3(C), 149.4(C), 158.9 (C). B-CH signal was not distinguishable due to overlapping with the signals of THF-d_8, however, it could be observed as a broad peak at 17.3 ppm in C_6D_6.

(acac)Rh(dppb)/B$_2$cat$_3$ catalyzed hydroboration of 2,3-dimethylbut-2-ene. This reaction was performed in a similar fashion, as above. Alkene/HBcat/catalyst =

1.0/1.5/0.02. Reaction was complete in 80 h. Selected spectroscopic data for $(CH_3)_2CH$-$C(CH_3)_2$(Bcat) in THF-d_8. $^{11}B\{^1H\}$ NMR spectrum: δ 36.6 (br); ^1H NMR spectrum: δ 0.93 (d, J_{H-H} = 6.9 Hz, 6H, CH_3), 1.14 (s, 6H, CH_3), 1.78 (m, J_{H-H} = 6.9 Hz, 1H, CH), 7.01 (m, 2H, catecholate H), 7.18 (m, 2H, catecholate H); $^{13}C\{^1H\}$ NMR spectrum: δ 19.1 (CH_3), 22.3 (CH_3), 27.9 (v br, B-C), 36.3 (CH), 112.6 (CH), 123.1(CH), 149.1(C).

General Procedure for the Catalyzed Diboration of 4-Vinylanisole The compounds B_2cat_3 (3.5 mg, 0.01 mmol) and various (acac)RhL_2 (0.01 mmol) were charged into a scintillation vial, followed by addition of 0.5 mL of THF-d_8 to dissolve them, and the solution was stirred to ensure that the solids dissolved completely. After stirring for 5 min, a solution of 4-vinylanisole (34 mg, 0.25 mmol) in 0.5 mL of THF-d_8 was added by pipette in. Then, B_2cat_2 (60 mg, 0.25 mmol) was added portionwise with a spatula. The reaction mixture was stirred at room temperature for 20 h and then analyzed by high-field ^1H, $^{13}C\{^1H\}$ and $^{11}B\{^1H\}$ NMR spectroscopy. Product distributions were verified by comparison of various typical resonances in the ^1H and $^{13}C\{^1H\}$ NMR spectra.

MeO-C_6H_4-CH(Bcat)-CH_2(Bcat) (23) $^{11}B\{^1H\}$ NMR spectrum (THF-d_8): δ 35.0 (br); ^1H NMR spectrum (500 MHz, THF-d_8) δ 1.81-1.86 (2nd order dd, 1H, CH_2Bcat), 2.10-2.16 (2nd order dd, 1H, CH_2Bcat), 3.25-3.29 (2nd order dd, 1H, CHBcat), 3.67 (s, 3H, OCH_3), 6.80 (m, 2H, phenyl H), 6.97-7.01 (ov m, 4H, catecholate H), 7.11-7.16 (ov m, 4H, catecholate H), 7.33 (m, 2H, phenyl H); $^{13}C\{^1H\}$ NMR spectrum (THF-d_8): δ 14.0 (br. s, CH_2Bcat), 24.8 (br. s, CHBcat), 55.1 (CH_3O), 112.2 (cat), 112.4 (cat), 114.1(phenyl), 122.2 (cat), 122.5 (cat), 128.7 (phenyl), 134.7 (phenyl), 148.1 (cat), 148.2 (cat), 157.8 (phenyl).

MeO-C_6H_4-CH=CH(Bcat) (24) ^1H NMR spectrum (THF-d_8): δ 3.76 (s, 3H, OCH_3), 6.30 (d, J_{H-H} = 8.43 Hz, 1H, CH), 6.94 (m, 2H, phenyl H), 7.05 (m, 2H, catecholate H), 7.25 (m, 2h, catecholate H), 7.54 (d, J_{H-H} = 8.43 Hz, 1H, CH).

MeO-C_6H_4-$CH_2CH(Bcat)_2$ (25) Selected ^1H NMR spectrum (THF-d_8): δ 2.12 (t, J_{H-H} = 8.0 Hz, 1H, C*H*(Bcat)$_2$), 3.29 (d, J_{H-H} = 8.0 Hz, 2H, C*H*$_2$), 3.64 (s, 3H, OC*H*$_3$).

MeO-C_6H_4-CH=C(Bcat)$_2$ (26) Selected ^1H NMR spectrum (THF-d_8): δ 8.37 (s, 1H, C*H*=C(Bcat)$_2$).

MeO-C_6H_4-CH_2C(Bcat)$_3$ (27) Selected ^1H NMR spectrum (THF-d_8): δ 3.69 (s, 3H, OC*H*$_3$), 3.81 (s, 2H, C*H*$_2$C(Bcat)$_3$).

MeO-C_6H_4-CH(Bcat)CH(Bcat)$_2$ (28) Selected ^1H NMR spectrum (THF-d_8): δ 2.71 (d, J_{H-H} = 12.3 Hz , 1H, C*H*(Bcat)$_2$), 3.61 (s, 3H, OC*H*$_3$), 3.73 (d, J_{H-H} = 12.3 Hz, 1H, C*H*(Bcat)CH(Bcat)$_2$).

General Procedure for (acac)Rh(dppm)/B_2cat_3 Catalyzed Diboration of Olefins. The compounds (acac)Rh(dppm) (6.0 mg, 0.01 mmol) and B_2cat_3 (3.5 mg, 0.01 mmol) were charged into a scintillation vial, followed by addition of 0.5 mL of THF-d_8, and the solution was stirred to ensure that the solids were dissolved completely. Five min later, a solution of olefin substrate (0.25 mmol) in 0.5 mL of THF-d_8 was added by pipette. Then, B_2cat_2 (60 mg, 0.25 mmol) was added portionwise with a spatula. The reaction mixture was stirred at room temperature, and its completion was monitored by ^1H NMR spectroscopy. Product distributions were verified by comparison of various typical resonances in the ^1H and $^{13}C\{^1H\}$ spectra.

C_6H_5-CH(Bcat)-CH_2(Bcat) $^{11}B\{^1H\}$ NMR spectrum (THF-d_8): δ 34.2 (br); ^1H NMR spectrum (500 MHz, THF-d_8) δ 1.82-1.87 (2nd order dd, 1H, C*H*$_2$Bcat), 2.14-2.20 (2nd order dd, 1H, C*H*$_2$Bcat), 3.32-3.37 (2nd order dd, 1H, C*H*Bcat), 6.97 (m, 4H, catecholate H), 7.14 (ov m, 5H, catecholate H + phenyl H), 7.23 (m, 2H, phenyl H), 7.38 (m, 2H, phenyl H); $^{13}C\{^1H\}$ spectrum (THF-d_8): δ 112.79 (CH), 112.98 (CH), 123.13 (CH),

123.27 (CH), 126.46 (CH), 128.78 (CH), 129.28 (CH), 144.47 (C), 149.41 (C), 149.43 (C).

C_6H_5-CH(Bcat)-$CH(CH_3)$(Bcat) $^{11}B\{^1H\}$ NMR spectrum (THF-d_8): δ 34.2 (br); ^1H NMR (500 MHz, THF-d_8) δ 1.11 (d, J_{H-H} = 7.5 Hz, 3H, C*H*$_3$), 2.31-2.38 (2nd order dq, 1H, C*H*(CH$_3$)(Bcat)), 3.04 (d, J_{H-H} = 11.6 Hz, 1H, C*H*Bcat), 6.98(m, 4H, catecholate H), 7.07-7.14 (ov m, 5H, catecholate H + phenyl H), 7.25 (m, 2H, phenyl H), 7.35 (m, 2H, phenyl H); $^{13}C\{^1H\}$ NMR spectrum (THF-d_8) δ 15.0 (CH_3), 112.9 (CH), 113.0 (CH), 123.2 (CH), 126.7 (CH), 129.3 (CH), 130.0 (CH), 141.7 (C), 149.2 (C), 149.3 (C).

4-Cl-C_6H_4-CH(Bcat)-CH_2(Bcat) $^{11}B\{^1H\}$ NMR spectrum (THF-d_8): δ 34.2 (br); ^1H NMR spectrum (500 MHz, THF-d_8) δ 1.80-1.87 (2nd order dd, 1H, C*H*$_2$Bcat), 2.13-2.19 (2nd order dd, 1H, C*H*$_2$Bcat), 3.32-3.36 (2nd order dd, 1H, C*H*Bcat), 7.00 (m, 4H, catecholate H), 7.14 (m, 4H, catecholate H), 7.25 (m, 2H, phenyl H), 7.37 (m, 2H, phenyl H); $^{13}C\{^1H\}$ spectrum (THF-d_8): δ 112.4 (CH), 112.9 (CH), 122.6 (CH), 122.7 (CH), 128.7 (CH), 129.8 (CH), 131.5 (C), 142.7 (C), 148.7 (C), 148.9 (C).

C_6H_5-CH(Bcat)-CH(Bcat)-C_6H_5 $^{11}B\{^1H\}$ NMR spectrum (C_6D_6): δ 34.5 (br); ^1H NMR (200 MHz, C_6D_6) δ 3.81 (s, 2H, C*H*), 6.30 (m, 4H, catecholate H), 6.85-7.03 (ov m, 10H, catecholate H + phenyl H), 7.20 (m, 4H, phenyl H); $^{13}C\{^1H\}$ NMR spectrum (C_6D_6) δ 35.1 (br), 112.5 (CH), 122.9 (CH), 126.1 (CH), 128.7(CH), 129.3 (CH), 140.2 (C), 148.6 (C).

Diboration of Norbornene $^{11}B\{^1H\}$ NMR spectrum (THF-d_8): δ 34.9 (br); ^1H NMR spectrum (500 MHz, THF-d_8) δ 1.37 (d, J_{H-H} = 10.0 Hz, 2H, C*H*$_2$), 1.47 (d, J_{H-H} = 11.5 Hz, 2H, C*H*$_2$), 1.69 (d, J_{H-H} = 7.0 Hz, 2H, C*H*$_2$), 1.82 (s, 2H, C*H*), 2.62 (s, 2H, C*H*), 6.91 (s, 8H, catecholate); $^{13}C\{^1H\}$ NMR (THF-d_8) δ 32.6 (CH_2), 39.1 (CH_2), 40.0 (CH), 112.6 (CH), 123.0 (CH), 149.2 (C). *C*-Bcat signal was not observed.

5.4.4 Molecular Structure Determinations

Data were collected at low temperature on a Siemens SMART CCD area-detector diffractometor using graphite-monochromated MoKα radiation (λ = 0.71073 Å) and ω scan methods. The single crystal was mounted on a glass fiber with a coating of perfluropolyether oil, cell parameters were refined from the observed setting angles and detector spot positions for selected reflections and intensities were measured from a series of frames each covering a 0.3° oscillation in ω. Absorption correction was semi-empirical from ω-scans, based on sets of equivalent reflections measured at different azimuthal angles.

The structures were solved by direct methods (SHELXS),[15] and refined by full-matrix least-squares techniques. The refinements were on F^2 of all independent reflections, to minimize $\sum\omega(F_o^2 - F_c^2)^2$, with weighting $\omega^{-1} = \sigma^2(F_o^2) + (aP)^2/ bP$, where $P = (F_o^2 + 2F_c^2)/3$; the refined isotropic extinction parameter χ is defined such that F_c is multiplied by $(1 + 0.001\chi F_c^2 \lambda^3/ \sin2\theta)^{-1/4}$. Anisotropic displacement parameters were refined for all non-hydrogen atoms,[16] and isotropic hydrogen atoms were constrained to ride on their parent carbon atoms with fixed bond lengths and idealized bond angles.

5.5 References

1. For reviews on diboron tetrahalide chemistry, see: (a) Urry, G. in *The Chemistry of Boron and Its Compounds*, Mutterties, E. L. (Ed.), Wiley: New York, **1967**, p. 325. (b) Massey, A. G. *Adv. Inorg. Chem Radiochem.* **1983**, *26*, 1. (c) Morrison, J. A. *Chem. Rev.* **1991**, *91*, 35.

2. Ahmed, L.; Castillo, J.; Saulys, D. A.; Morrison, J. A. *Inorg. Chem.* **1992**, *31*, 706.

3. Urry, G.; Kerrigan, J.; Parsons, T. D.; Schlesinger, H.I. *J. Am. Chem. Soc.* **1954**, *76*, 5299.

4. (a) Ceron, P.; Finch, A.; Frey, J.; Kerrigan, J.; Parsons, T.; Urry, G.; Schlesinger, H. I. *J. Am. Chem. Soc.* **1959**, *81*, 6368. (b) Chambers, C.; Holliday, A. K.; Walker, S. M. *Proc. Chem. Soc.* **1964**, 286. (c) Zeldin, M.; Gatti, A. R.; Wartik, T. *J. Am. Chem. Soc.* **1967**, *89*, 4217. (d) Siebert, W.; Hildenbrand, M.; Hornbach, P.; Karger, G. *Z. Naturforsch.* **1989**, *44b*, 1179.

5. (a) Zeldin, M.; Wartik, T. *J. Am. Chem. Soc.* **1966**, *88*, 1336. (b) Fox, W. B.; Wartik, T. *J. Am. Chem. Soc.* **1961**, *83*, 498.

6. (a) Zeldin, M.; Wartik, T. *J. Am. Chem. Soc.* **1966**, *88*, 1336. (b) Fox, W. B.; Wartik, T. *J. Am. Chem. Soc.* **1961**, *83*, 498.

7. (a) Coyle, T. D.; Ritter, J. J. *J. Organomet. Chem.* **1968**, *12*, 269. (b) Kotz, J. C.; Post, E. W. *Inorg. Chem.* **1970**, *9*, 1661.

8. (a) Holliday, A. K.; Massey, A. G. *J. Inorg. Nucl. Chem.* **1961**, *18*, 108. (b) Feeney, J.; Holliday, A. K.; Marsden, F. J. *J. Chem. Soc.* **1961**, 356. (c) Rudolph, R. W. *J. Am. Chem. Soc.* **1967**, *89*, 4216. (d) Coyle, T. D.; Ritter, J. J. *J. Am. Chem. Soc.* **1967**, *89*, 5739.

9. (a) Chadha, R.; Ray, N. K. *J. Phys. Chem.* **1982**, *86*, 3293. (b) Chadha, R.; Ray, N. K. *Theor. Chim. Acta*, **1982**, *86*, 3293.

10. Brotherton, R. J. in *Progress in Boron Chemistry*, Steinberg, H.; McCloskey, A.L. (Eds.), Macmillan: New York, **1964**, p 46.

11. For reviews on metal-catalyzed hydroboration reactions, see: (a) Burgess, K.; Ohlmeyer, M. J. , *Chem. Rev.*, **1991**, *91*, 1179. (b) Burgess, K.; van der Donk, W. in "Encyclopedia of Inorganic Chemistry", King, R. B. (Ed.), John Wiley & Sons, 1994, Vol. 3, P. 1420-1426. (c) Beletskaya, I; Pelter, A., *Tetrahedron*, **1997**, 53, 4957. (d) Burgess, K., in "Advanced Asymmetric Synthesis", Stephenson, G. R. (Ed.), Chapman & hall, London, **1996**, p. 181-211.

12. For review of early work on metal boryl chemistry, see: Schmid, G. *Angew. Chem. Int. Ed. Engl.*, **1970**, *9*, 819.

13. (a) Marder, T. B.; Norman, N. C., et al., *Chem. Rev.*, manuscript in preparation. (b) Wadepohl, H. *Angew. Chem. Int. Ed. Engl.* **1997**, *36*, 2441.

14. (a) Burgess, K.; van der Donk, W. A.; Westcott, S. A.; Marder, T. B.; Baker, R. T.; Calabrese, J. C. *J. Am. Chem. Soc.* **1992**, *114*, 9350. (b) Westcott, S. A.; Blom, H. P.; Marder, T. B.; Baker, R. T. *ibid.* **1992**, *114*, 8863. (c) Westcott, S. A.; Marder, T. B.; Baker, R. T.; *Organometallics*, **1993**, *12*, 975, and references therein.

15. Baker, R. T.; Calabrese, J. C.; Westcott, S. A.; Nguyen, P.; Marder, T. B. *J. Am. Chem. Soc.*, **1993**, *115*, 4367.

16. (a) Welch, C.N.; Shore, S.G. *Inorg. Chem.* **1968**, *7*, 225. (b) Brotherton, R.J.; Woods, W.G. U.S. Patent 3 009 941.

17. Nguyen, P.; Lesley, G.; Taylor, N. C.; Marder, T. B.; Pickett, N. L.; Clegg, W.; Elsegood, M. R. J.; Norman, N. C. *Inorg. Chem.*, **1994**, *33*, 4623.

18. Ishiyama, T.; Matsuda, N.; Miyaura, N.; Suzuki, A. *J. Am. Chem. Soc.*, **1993**, *115*, 11018.

19. Nöth, H. *Z. Naturforsch.* **1984**, *39b*, 1463.

20. Ishiyama, T; Matsuda, N; Murata, M; Ozawa, F; Suzuki, A.; Miyaura, N. *Organometallics*, **1996**, *15*, 713.

21. Iverson, C. N.; Smith, III, M. R. *Organometallics*, **1996**, *15*, 5155.

22. Lesley, G.; Nguyen, P.; Taylor, N. J.; Marder, T. B.; Scott, A. J.; Clegg, W.; Norman, N. C. *Organometallics*, **1996**,*15*, 5137.

23. Iverson, C. N.; Smith III, M. R. *J. Am. Chem. Soc.* **1995**, *117*, 4403.

24. Kraft, P.; Tochtermann, W. *Liebigs Ann. Chem.* **1994**, 827.

25. Maderna, A; Pritzkow, H.; Siebert, W., *Angew. Chem. Int. Ed. Engl.*, **1995**, *35*, 1501.

26. Dobson, J. E.; Tucker, P. M.; Stone, F.G.A.; Schaeffer, R., *J. Chem. Soc., A* **1969**, *12*, 1882.

27. Brown, S. D.; Armstrong, R. W., *J. Am. Chem. Soc.* **1996**, *118*, 6331.

28. For reviews, see: (a) Suzuki, A. *Acc. Chem. Res.* **1982**, *15*, 178. (b) Miyaura, N.; Suzuki, A. *Chem. Rev.* **1995**, *95*, 2457.

29. van den Koedijk, C. D.; Blankenstein, M. A.; Thissen, J. H. *Biochem. Pharmacol.* **1994**, *47*, 1927.

30. Harper, M. J. K.; Walpole, A. L. *Nature (London)* **1966**, *212*, 87.

31. Cui, Q.; Musaev, D. G.; Morokuma, K., *Organometallics* **1997**, *16*, 1355.

32. Ishiyama, T; Yanmamoto, M.; Miyaura, N., *Chem. Commun.* **1996**, 2073.

33. Ishiyama, T; Yanmamoto, M.; Miyaura, N., *Chem. Commun.* **1997**, 689.

34. Iverson, C. N.; Smith, III, M. R., *Organometallics*, **1997**, *16*, 2757.

35. Green, M.; Howard, J. A. K.; Spencer, J. L.; Stone, F. G. A. *J. Chem. Soc., Dalton Trans.* **1977**, 271.

36. (a) Chem. & Eng. News, Nov. 25, **1996**, p. 47. (b) Chem. & Eng. News, July 14, **1997**, p. 8.

37. Ishiyama, T; Murata, M..; Miyaura, N., *J. Org. Chem.* **1995**, *60*, 7508.

38. Piettre, S. R.; Baltzer, S. *Tetrahedron Lett.* **1997**, *38*, 1197.

39. Giroux, A.; Han, Y.; Prasit, P. *Tetrahedron Lett.* **1997**, *38*, 3841.

40. Baker, R. T.; Nguyen, P.; Marder, T. B.; Westcott, S. A., *Angew. Chem. Int. Ed. Engl.*, **1995**, *34*, 1336.

41. Nguyen, P., in Ph. D. Thesis, University of Waterloo, **1995**.

42. Souza, F. E. S., in M. Sc. Thesis, University of Waterloo, **1997**.

43. Westcott, S. A.; Marder, T. B.; Baker, R. T.; Jones, N. J.; Calabrese, J. C. *J. Chem. Soc., Chem. Commun.* **1991**, 304.

44. Blom, H. P., in M. Sc. Thesis, University of Waterloo, **1993**.

45. Westcott, S. A.; Blom, H. P.; Marder, T. B.; Baker, R. T.; Calabrese, J. C. *Inorg. Chem.*, **1993**, *32*, 2175.

46. Gerrard, W.; Lappert, M. F.; Mountfield, B. A. *J. Chem. Soc.* **1959**, 1529.

47. (a) Hattori, K; Yamamoto, H. *J. Org. Chem.* **1992**, *57*, 3264. (b) Hattori, K; Yamamoto, H. *Synlett* **1993**, *48*, 129. (d) Hattori, K; Yamamoto, H. *Synlett* **1993**, *49*, 1749.

48. Kaufmann, D.; Boese, R. *Angew. Chem., Int. Ed. Engl.*, **1990**, *29*, 545.

49. Clegg, W.; Elsegood, M. R. J.; Lawlor, F.; Norman, N. C.; Pickett, N. L.; Robins, E. G.; Scott, A. J.; Nguyen, P.; Taylor, N. J.; Marder, T. B. *Inorg. Chem.*, (in press)

50. Jones, R. A.; Mayor Real, F.; Wilkinson, G.; Galas, A. M. R.; Hursthouse, M. B. *J. Chem. Soc, Dalton Trans*, **1980**, 511.

51. Werner, H.; Feser, R.; Buchner, W. *Chem. Ber.* **1979**, *112*, 834.

52. (a) Duan, Z.; Hampden-Smith, M. J.; Duesler, E. N.; Rheingold, A. L. *Polyhedron*, **1994**, *13*, 609. (b) Fennis, P. J.; Budzelaar, P. H. M.; Frijins, J.H.G.; Orpen, A. G. *J. Organomet. Chem.*, **1990**, *393*, 287.

53. Angermund, K.; Baumann, W.; Dinjus, E.; Fornika, R.; Görls, H.; Kessler, M.; Krüger, C.; Leitner, W.; Lutz, F. *Chem. Eur. J.*, **1997**, *3*, 755.

54. Aresta, M.; Quaranta, E.; Tommasi, I. *New J. Chem.*, **1997**, *21*, 595.

55. Garrou, P. E. *Chem. Rev.* **1981**, *81*, 229.

56. (a) Nolte, M. J.; Gafner, G.; Haines, L. M. *J. Chem. Soc., Chem. Commun.* **1969**, 1406; (b) Schrock, R. R.; Osborn, *Inorg. Chem.* **1970**, *9*, 2339.

57. Albano, P.; Aresta, M.; Manassero, M. *Inorg. Chem.* **1980**, *19*, 1069;

58. Zhou, Z.; Facey, G.; James. B. R.; Alper, H. *Organometallics*, **1996**, *15*, 2496.

59. Longato, B.; Pilloni, G.; Graziani, R.; Casellato, U. *J. Organomet. Chem.* **1991**, *407*, 369.

60. Manger, M.; Wolf, J.; Laubender, M.; Teichert, M.; Stalke, D.; Werner, H. *Chem. Eur. J.* **1997**, *3*, 1442.

61. (a) Townsend, J. M.; Blount, J. F. *Inorg. Chem.* **1981**, *20*, 269. (b) Singewald, E. T.; Shi, X.; Mirkin, C. A.; Schofer, S. J.; Stern, C. L. *Organometallics* **1996**, *15*, 3062. (c) Singewald, E. T.; Slone, C. S.; Stern, C. L.; Mirkin, C. A.; Yap, G. P. A.; Liable-Sands, L. M.; Rheingold, A. L. *J. Am. Chem. Soc.* **1997**, *119*, 3048. (d) Slone, C. S.; Mirkin, C. A.; Yap, G. P. A.; Guzei, I. A.; Rheingold, A. L. *J. Am. Chem. Soc.* **1997**, *119*, 10743.

62. Shäfer, H.; Braun, O. *Naturwissenshaften*, **1952**, *39*, 280.

63. (a) Leitner, W. *Angew. Chem. Int. Ed. Engl.* **1995**, *34*, 2207. (b) Leitner, W. *Coord. Chem. Rev.* **1996**, *153*, 257. (c) Graf, E.; Leitner, W. *J. Chem. Soc., Chem. Commun.* **1992**, 623. (d) Leitner, W.; Dinjus, E.; Gassner, F. *J. Organomet. Chem.* **1994**, *475*, 257. (e) Gassner, F.; Leitner, W. *J. Chem. Soc., Chem. Commun.* **1993**, 1465. (f) Fornika, R.; Gorls, H. Seemann, B.; Leitner, W. *J. Chem. Soc., Chem. Commun.* **1995**, 1479. (g) Graf, E.; Leitner, W. *Chem. Ber.* **1996**, *129*, 91.

64. Zargarian, D.; Chow, O.; Taylor, N. J.; Marder, T. B. *J. Chem. Soc., Chem. Commun.* **1989**, 540.

Chapter 6

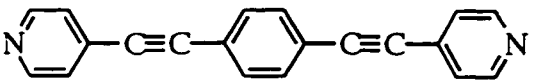
Conclusions and Future Work

In the work presented in this thesis, we have demonstrated applications of transition metal complexes in two very different fields: the synthesis of rigid-rod conjugated phenylacetylene derivatives as liquid crystal materials, and the catalytic diboration reactions of alkenes. The diborated products are of great potential importance as intermediates in organic synthesis and potentially as bidentate Lewis acid catalysts. Although just a dewdrop in the vast ocean of organometallic chemistry, our current work reflects well the applications of homogeneous catalysis in organic synthesis and material science studies,[1] and further investigations are merited.

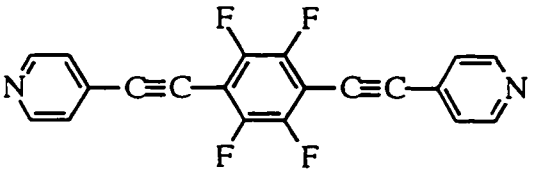
6.1 Pd/Cu Catalyzed Cross-Coupling Reactions of Arylhalides with Terminal Alkynes as a Route to Multifunctional Materials.

We have demonstrated the exceptional utility of the Pd/Cu catalyzed cross-coupling methodology to synthesize a series of symmetrically substituted 1,4-bis(*p*-R-phenylethynyl)acetylenes (BPEB's) and their partially and fully fluorinated derivatives. These compounds are highly fluorescent due to their π-conjugated molecular structure, but more importantly, they serve as an ideal system to explore the effect of soft interactions (i.e., charge distribution) and intermolecular interactions on calamitic liquid crystals. Extensive single crystal X-ray diffraction and liquid crystalline phase behavior studies on these molecules have demonstrated that intermolecular interactions, particularly the interactions between phenyl and perfluorophenyl units, have a profound influence on their molecular packing modes in the crystal structures and thus on their thermal properties.

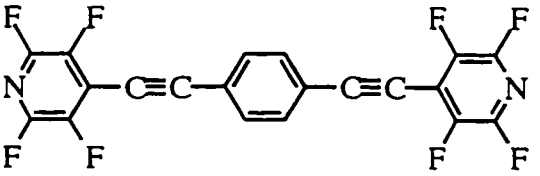
In addition to the above BPEB compounds, we have also prepared several 1,4-bis(pyridylethynyl)benzene analogs (**1a-c**). We reasoned that the introduction of the nitrogen atoms into the core structure might alter the charge distribution along the molecules and affect their crystal structures as well as their liquid crystalline phase behavior. We also wanted to investigate possible co-crystal formation among these molecules as well as in combination with the four parent BPEB's. However, no single crystal structure study on them has been conducted so far, and it remains a challenge to obtain suitable crystals for X-ray diffraction. Of special interest is the application of these molecules as bridging ligands in the construction of coordination molecular squares or boxes[2] and infinite coordination networks.[3] The complexes with fluorinated ligands, **1b** and **1c**, as well as the perfluorinated analog are expected to exhibit specific molecular recognition properties toward electron rich guest molecules.



1a



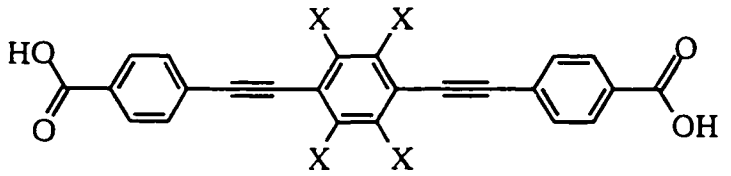
1b



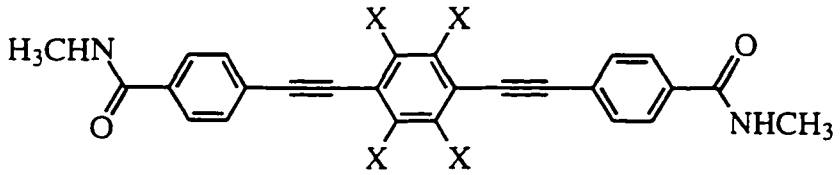
1c

We have also initiated an effort to add other functional end groups to the BPEB system to access versatile hydrogen bonding architectures. In compounds **2a-b** and **3a-b**, the -COOH and -CONHMe units are expected to facilitate the hydrogen bonding between molecules in crystals, as do OH groups in **4a-b**. Alternatively, molecules **5a-b**

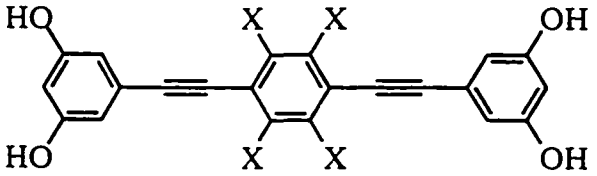
should form co-crystals with **4a-b** due to the complementary hydrogen bonding, or, in the asymmetric compounds **6a-b**, the molecules bear both hydrogen bonding donors and acceptors at the ends. Hydrogen bonding, being recognized as a master key in the contexts of molecular recognition, crystal engineering, or supramolecular chemistry,[4] should bring additional packing forces to these molecules in the crystal structures. It would be interesting to examine the respective hydrogen bonding and arene-arene (arene-perfluoroarene) interactions in the crystalline phase[5] and also their liquid crystalline phase behavior.



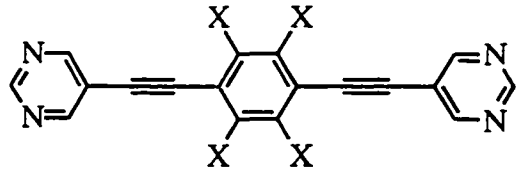
2a X = H, **2b** X = F



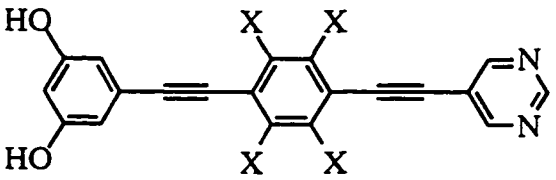
3a X = H, **3b** X = F



4a X = H, **4b** X = F

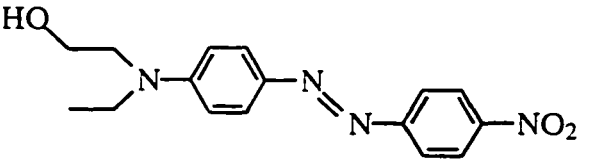


5a X = H, **5b** X = F



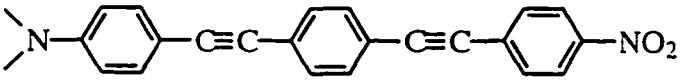
6a X = H, **6b** X = F

Due to their π-conjugated molecular structures, the unsymmetrically donor-acceptor substituted BPEB's are expected to exhibit large second order optical nonlinearities. Preliminary work in our laboratory by P. Nguyen[6] has demonstrated that this system can give very large first order molecular hyperpolarizabilities (β). Moreover, in comparison with the widely utilized chromophores such as disperse red 1 (**7**, DR1, $\mu\beta(0) = 500 \times 10^{-48}$ esu), the BPEB compound such as **8** ($\mu\beta(0) = 510 \times 10^{-48}$ esu) exhibit both higher thermal stability (K $_{271.7}$ S $_{290.1}$ N) and better transparency in the visible region (λ_{max} = 384 nm in $CHCl_3$), both of which are important factors with respect to practical applications. In continuation with this work, I have prepared the fluorinated analog **9** and compound **10** with an even stronger electron-withdrawing group $-CH=C(CN)_2$, and their nonlinear optical (NLO) properties as well as thermal properties are to be studied.



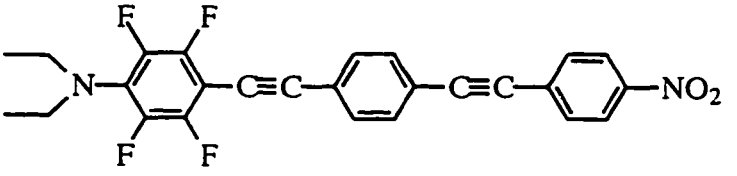
7

$\mu\beta(0) = 500 \times 10^{-48}$; $\lambda_{max} = 455$ nm

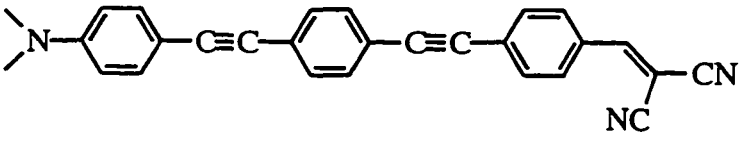


8

$\mu\beta(0) = 510 \times 10^{-48}$; $\lambda_{max} = 384$ nm



9



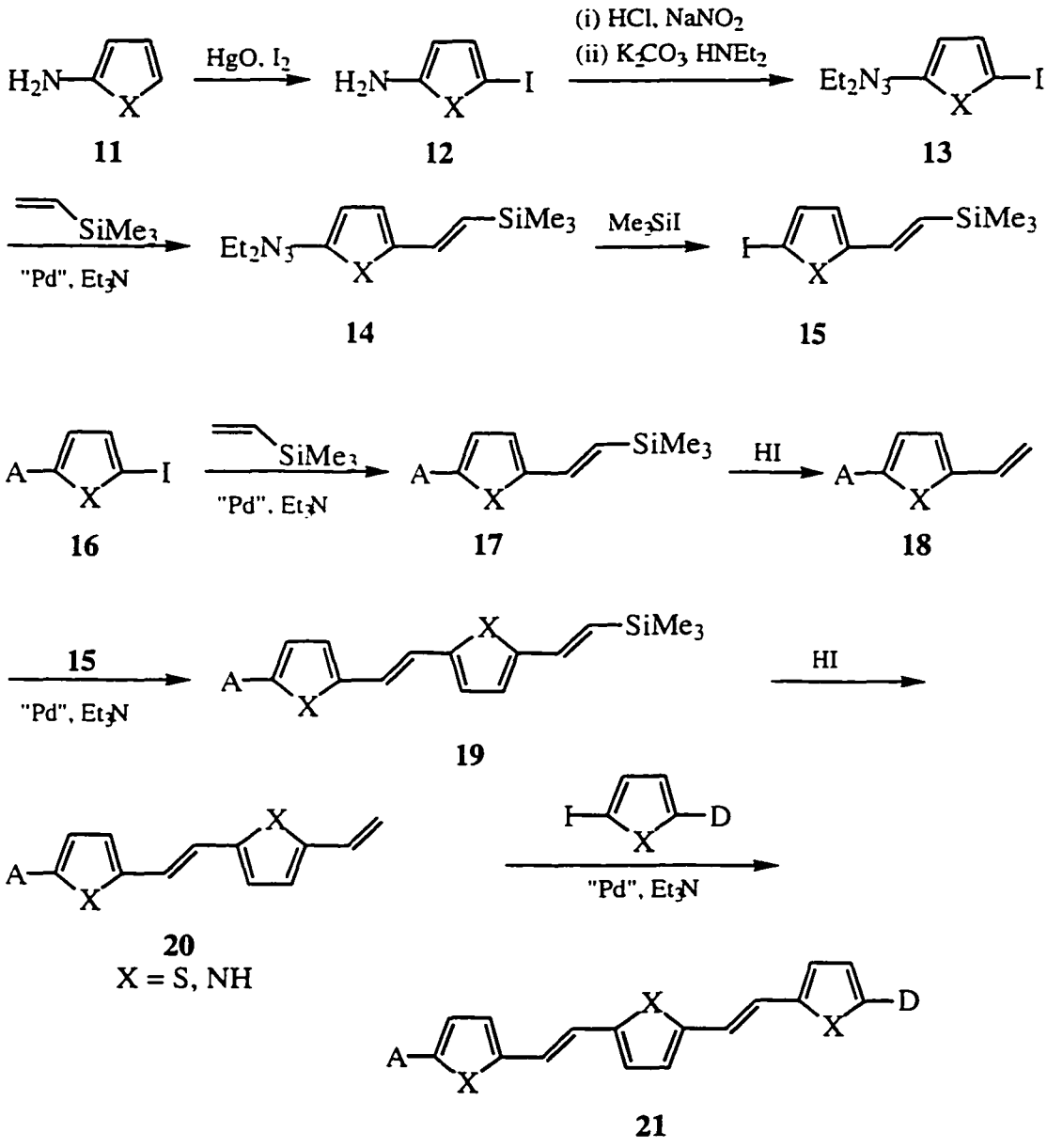
10

Over more than twenty years, there has been tremendous interest in the study of organic and polymeric nonlinear optical materials.[7] The subject of nonlinear optics is the study of interaction of laser with matter. For example, when an infrared laser with a wavelength of 1064 nm is passed into a second order nonlinear optical material, it emerges with a wavelength of 532 nm (this is the result of a feature called frequency doubling). Compared to inorganic NLO materials such as KTP ($KTiOPO_4$) and $LiNbO_3$ where optical nonlinearities are essentially derived from the polyhedron anion groups,[8] organic molecules with extended π-electron systems have shown exceptionally large molecular nonlinearities and ultra-fast response times because the electron polarization is nearly instantaneous. Therefore, new organic and polymeric NLO materials are expected to speed up the current information superhighway with photonic ("all-optical") or electro-optic technologies.[9] In the early stage of the study, considerable effort was focused on the discovery of organic crystals or films which exhibit larger second order harmonic generation (SHG) efficiencies than conventional inorganic crystals, in order to frequency double infrared lasers to obtain blue and green lasers which are of significant technological importance. However, most polar organic molecules do not crystallize in non-centrosymmetrical lattice, which is essential to macroscopic second order nonlinearity, and even those with very high SHG values could barely be obtained as high quality single crystals suitable for device fabrication.[10] On the other hand, in recent years, there has been continuous improvement in the development of practical blue and green GaN laser diodes.[11] Thus, new organic frequency-doubling materials are no longer the primary goal for NLO material research. Instead, polymers with other NLO properties such as electro-optic, photorefractive (second order) and third order NLO effects, etc., are attracting interest for applications in integrated optics in this information era.[12]

In the past five years, considerable progress has been made toward the rational design of high molecular nonlinearity chromophores; molecules with $\mu\beta$ over 15,000 esu (at 1.9 μm) were obtained.[13] However, turning these molecules into practical NLO devices still presents numerous obstacles. As stated before, a bulk second order NLO material must lack a center of symmetry. There are a number of ways to achieve that, but so far the most successful approach has been the poled-polymer approach.[14] In order to obtain practical polymeric second-order NLO materials, it is necessary to (i) incorporate a high density of chromophores with large $\mu\beta$ values into a polymer, (ii) achieve a high degree of alignment of these chromophores, and (iii) lock in this alignment for long periods (years) even at elevated temperatures (at least 80°C). Usually, the chromophore alignment is locked either by using host polymers with high glass transition temperatures, which are roughly 150 to 200°C above the ultimate operating temperature, or by cross-linking the chromophore-polymer composite. In either cases, the thermal stability of the chromophores is obviously an important factor. In addition, the material must be transparent to the incident and frequency doubled lasers. Therefore, in the process of designing NLO chromophores, the optimization of efficiency (β), thermal stability (T_d) and transparency (λ_{max}) all must be taken into account. Furthermore, their compatibilities with the host polymers, and the respective functionality and cross-linking strategies etc. are all important criteria for molecular design.

The above unsymmetrically substituted BPEB molecules **8-10** exhibit linear (fluorescent) and nonlinear optical properties as well as liquid crystalline phase behavior. In a sense, they can be recognized as multifunctional materials. However, their $\mu\beta$ values are only modest compared to other high $\mu\beta$ chromophores, although very good transparency and considerable thermal stabilities are exhibited. Recently, Jen et al. and others[15] reported that the replacement of benzene rings with heteroaromatic rings could lead to a large increase in $\mu\beta$ as well as in decomposition temperatures. Herein, we wish to propose a general Pd catalyzed route to the thiophene or pyrole containing donor-

acceptor π-conjugated compounds (Scheme **6.1**). The basic synthon *trans*-2,5-I-C_5H_2X-CH=CH-$SiMe_3$ (**15**) can be obtained by the Heck cross-coupling reaction between 2,5-Et_2N_3-C_5H_2-I (**13**) and Me_3Si-CH=CH_2 which will generally gives only the *trans* product.[16] The subsequent transformation to aryl iodide can be accomplished by treatment with Me_3SiI or MeI.[17] The Me_3Si group can be easily removed by electrophilic

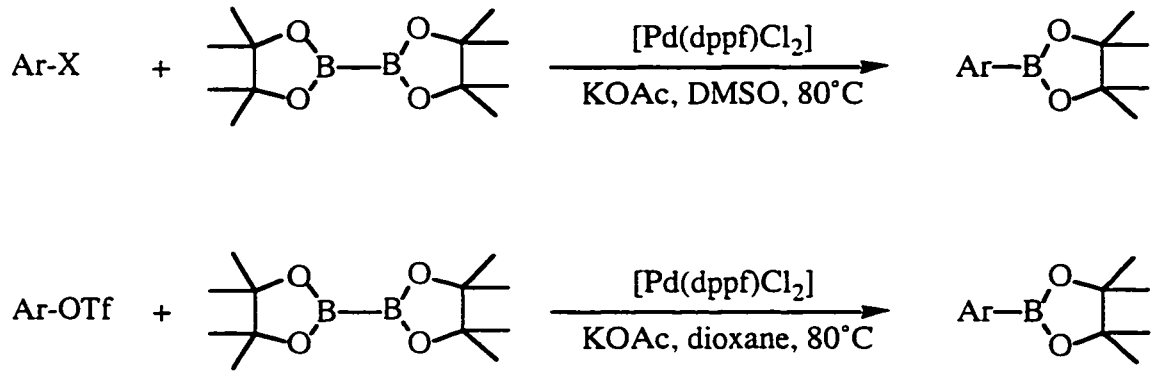


Scheme 6.1 A general route to NLO chromophores with heteroaromatic rings.

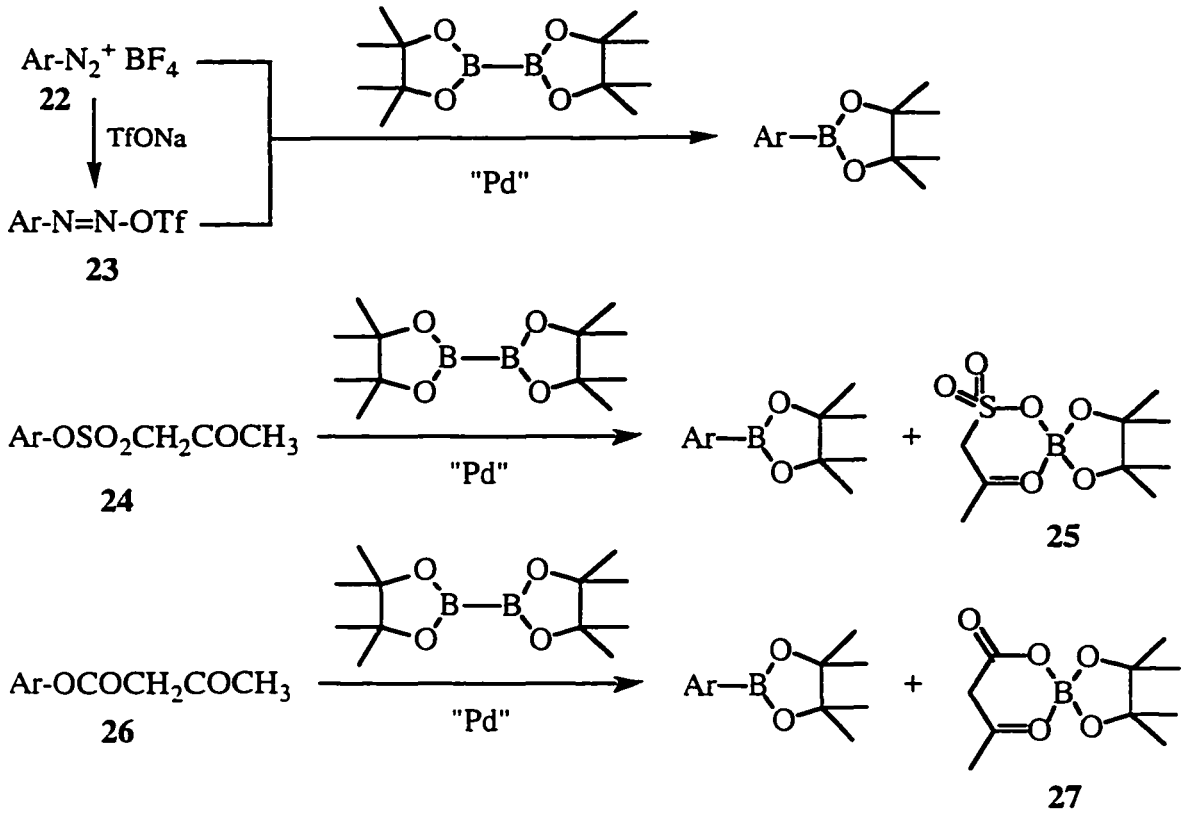
substitution in acid.[18] The triazene group is not stable in acid, so a route resembling the interactive divergent/convergent approach by Tour[19] (see, figure **2.1**) is not suitable for the current situation. However, by applying **15** and the Heck reactions, stepwise growth can be easily achieved, and the D-π-A molecules such as **21** can be fabricated by the respective coupling with the donor and acceptor components. An alternative to the Heck reaction methodology could be the transformation of the Me_3Si group to bromide and then to the $SnBu_3$ group, and subsequently, the Stille coupling method can be applied.[20] The first transformation is reported to be one in which the conformation is retained.[18a] Therefore, not only compounds such as **21** can be made, but also all *trans* polyenes can be prepared through the stepwise coupling of Me_3Si-CH=CH_2.

6.2 Pd Catalyzed Cross-Coupling Reactions to Arylborons.

In the second part of the thesis, we have described our studies on the B-B bond activation of diboron compounds $B_2(RO)_4$ by late transition metal Co(0), Rh(I), and Ir(I) complexes. The reactions between complexes [(acac)RhL_2] and B_2cat_3 to the discovery of the facile synthesis of novel Rh(I) zwitterionic complexes [(η^6-$Bcat_2$)RhL_2], and their catalytic properties for the addition of B_2cat_2 to various alkenes have been investigated. It is always our desire to utilize both knowledge on Pd catalyzed cross-coupling reactions and boron chemistry to develop new methods for organoborane synthesis. However, it was Miyaura[21] who first developed the cross-coupling of diboron compounds with aryl halides and triflates. As a matter of fact, the development of metal catalyzed borylation chemistry (i.e. hydroboration, diboration, silylboration, and stanylboration, etc.) has always been related to the previously developed Si and Sn chemistries. In the cross-coupling of diboron compounds with arylhalides however, 3 equiv. of KOAc have to be added, and half of the diboron reagent is lost to form $AcOB(OR)_2$.



In the various versions of Pd(0) catalyzed cross-coupling reactions between arylmetal (ArM, M = Li, MgX, ZnX, HgX, $B(OH)_2$, AlR_2, SnR_3, etc.) and electrophile (Ar-X) (see, Scheme **2.1** in Chapter 2), the electrophile component has largely been limited to halides and triflates. However, other functional groups are gradually being investigated, such as Ar-COCl, Ar-SO_2Cl, Ar-OSO_2Me, Ar-OTs (Ts = 4-$CH_3C_6H_4SO_2$), Ar-OCOR, Ar-N_2X, Ar-I^+Ar, and so on, among which the aryldiazonium salts or aryltriazenes show some unique properties. The usual basic conditions are not required in their reactions.[22] We anticipate that the reaction between aryldiazonium salts (**22**) or arylazo sulfones (**23**) with diboron compounds may bring some more features to this type of reaction (Scheme **6.2**). Furthermore, we were impressed by the ease of reactions between B_2cat_3 and [(acac)RhL_2] to form the chelating four-coordinated boron compound (acac)Bcat. Therefore, if we start with Ar-$OSO_2CH_2COCH_3$ (**24**) or Ar-$OCOCH_2COCH_3$ (**26**), the side coupling reaction products with B_2pin_2 may have the structure of chelating compounds **25** and **27**, and the catalytic reactions may proceed more smoothly.



Scheme 6.2 Pd(0) catalyzed cross-coupling reactions involving diboron compounds.

6.3 The Implications of Arene-perfluoroarene Interactions in Homogeneous Catalysis.

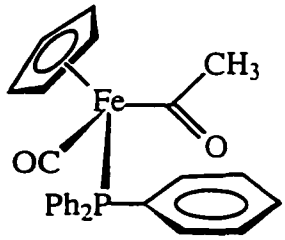
Homogeneous catalysis is the success story of organometallic chemistry. Over the years, numerous novel reactions have been discovered and, as D. Seebach[23] once said, "the discovery of truly new reactions is likely to be limited to the realm of transition-metal organic chemistry, which will almost certainly provide us with additional 'miracle reagents' in the years to come". Homogeneous catalysis also provides reactions with higher efficiency, higher selectivity (chemo-, regio-, diastereo-, and enantioselectivity) and better atom economy.[24] The key feature of transition metal

complexes is that they can be tunable both *electronically* and *sterically* by varying the metal and/or ligands.

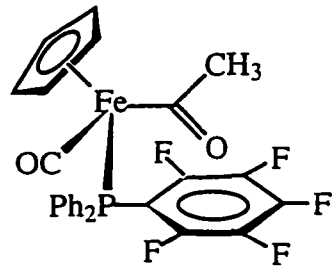
Perfluorocarbon compounds have long been applied to organometallic chemistry, but mainly for *electronic* reasons. In the early days, many transition metal perfluoroalkyl complexes were synthesized and characterized; because of the lack of β hydrogen atoms, they exhibit much higher stabilities than the hydrocarbon analogues. Recently, there has been a major renaissance in the development of catalysts with perfluorocarbon chains because of the application of perfluorinated hydrocarbons as solvent for organic synthesis.[25] In the meantime, perfluorinated aromatics, being realized as electron deficient systems, have gained increasing attention in the last few years. One notable example is the application of tris(pentafluorophenyl)borane, $B(C_6F_5)_3$, as the co-catalyst in metallocene-based polymerization of olefins.[26] The systematic research on the respective phosphines which are the ubiquitous ligands in homogeneous catalysis, on the other hand, has just begun.[27] There were also a few recent reports on the organometallic complexes containing pentafluorocyclopentadienyl[28a,b] and pentakis(trifluoromethyl) cyclopentadienyl[28c] as well as pentafluorophenyl-substituted cyclopentadienyl[28c] ligands. However, in all cases, emphasis has focussed only on their electronic properties.

In the past several years, our understanding of the nature of non-covalent intermolecular arene-arene interactions has been greatly enhanced through intense theoretical and experimental studies (see ref. 19 in Chapter 3). Interactions between aromatic units have been extensively applied to the design of molecular recognition systems or to crystal engineering, and, to some extent, to chiral recognition in organic synthesis (see refs. 25 and 26 in Chapter 3). From the results of our single crystal structural studies on the parent diphenylacetylene (tolan) and 1,4-bis(phenylethynyl)benzene and their partially and fully fluorinated analogs, we can at least conclude that there is always a strong tendency for the offset parallel (or "stacking")

non-covalent arene-perfluoroarene interactions when they are oriented properly. However, despite a few increasing number of recent applications in molecular recognition and crystal engineering (see refs. 39 and 40 in Chapter 3), this unique feature has barely been employed in homogeneous catalytic synthesis. One related example was reported by Ojima and Kwon[29] on the stereoselective reactions of chiral iron acyl complex (**29**) bearing a $PPh_2(C_6F_5)$ ligand. They observed remarkably higher stereoselectivity with the fluorinated PFCHIRC by a factor of between 4 and 5 than the parent CHIRC (**28**), and they attributed this "fluorine" effect to the attractive interaction between the acetyl moiety and the pentafluorophenyl moiety in **29**. We believe that the arene-perfluoroarene interaction must have a much wider application in homogeneous catalysis. Perhaps, complimentary to the conventional catalyst design which is mostly based on repulsive steric interactions in the coordination sphere of the metal, the unique attractive arene-perfluoroarene and related interactions would regulate the direction of the substrate approach and achieve better selectivity.



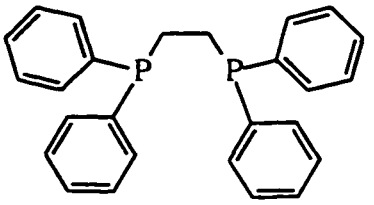
28 CHIRAC



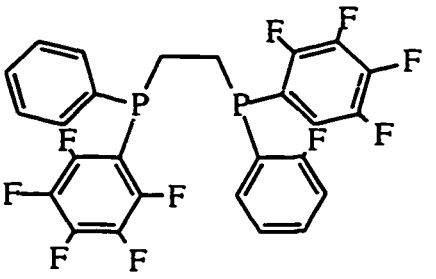
29 PFCHIRAC

Herein, we wish to propose the large application of ligands with perfluoroaryl units in organic synthesis. We speculate that *both* the unique electronic and steric properties of perfluoroaryl groups will make them a valuable system to investigate in homogeneous catalysis. A few examples are depicted in the following.

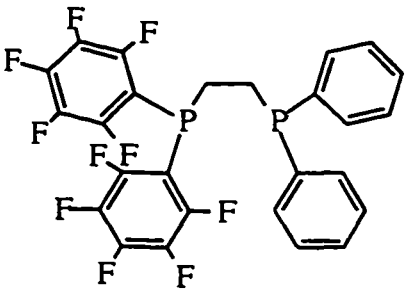
Essentially, one can start with making new fluorinated ligands by partially or fully replacing the aryl groups with perfluoroaryl units wherever applicable. For example, with the versatile bisphosphine ligand dppe (**30**), it would be interesting to examine the reactivities of its three variants **31-33**. However, in reality, it would rely on rational design in each specific situation. Alternatively, combinatorial chemistry methods can be applied to accelerate the process of catalysts screening. In complexes **34**



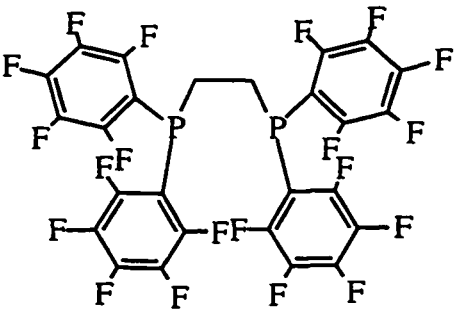
30



31



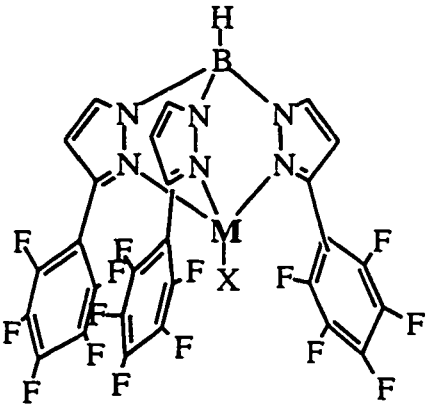
32



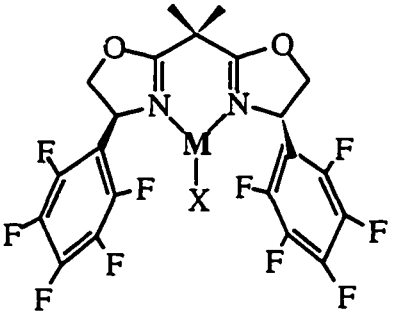
33

and **35**, the pentafluorophenyl groups may help bring aromatic substrates such as styrene and its derivatives into the metal coordination sphere. However, on some occasions, the partially fluorinated complexes may be more advantageous to use. For example, Jacobsen et al.[30] recently reported the crystal structure of a Cu(I) diimine complex with a

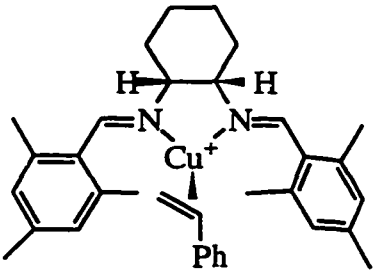
π-bound styrene (**36**). They observed that the C_2-symmetric diimine ligand is arranged such that its two aromatic groups are almost perfectly orthogonal to each other, with the aromatic group of the styrene lying squarely in the resulting cleft. They suggested that there exist simultaneous face-face and face-edge aromatic interactions between the styrene molecule and the two aryl groups of the ligand, and a low temperature NMR study indicated that these interactions were also present in solution. Inspecting the different interaction motifs of phenyl and perfluorophenyl units, we know that phenyl-phenyl systems are prone to adopt the edge-to-face interactions while phenyl-perfluorophenyls prefer face-to-face stackings. So, we may just replace one aryl group in the ligand with C_6F_5 to optimize both types of interactions with the substrates (**36**), and perhaps, even better enantioselectivities would be achieved, and more related catalysts can be developed.



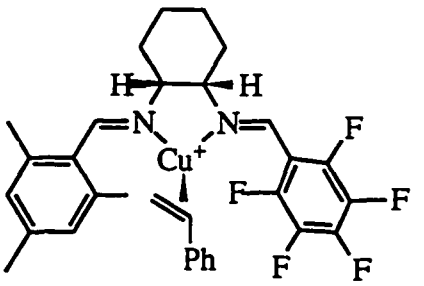
34



35



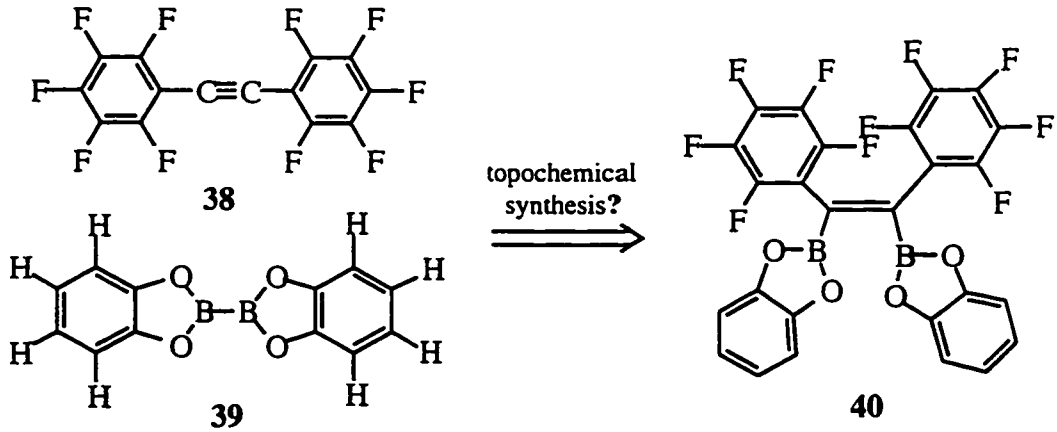
36

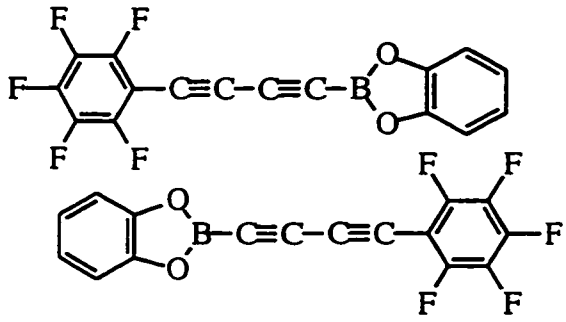


37

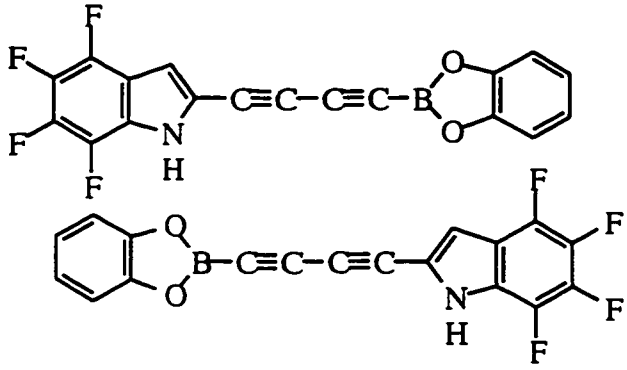
6.4 Topochemical Synthesis of Organoboranes?

The molecules of the diboron compound B_2cat_2 (**38**) in the crystalline phase are essentially planar,[31] so, it may be possible for them to form co-crystals with perfluorinated tolan, C_6F_5-C≡C-C_6F_5 (**39**) driven by the intermolecular arene-perfluoroarene interactions. If this is the case, it would be interesting to investigate the possibility of topochemical synthesis of diborated tolan (**40**) by heating or irradiating the co-crystalline samples. In addition, if the packing configuration of C_6F_5-C≡C-C≡C-Bcat (**41**) in its crystal structure allows appropriate contact between the butyldiynyl unit with those of adjacent parallel molecules, or in the molecule of **42**, the 1,4-butadiyne topochemical polymerization may occur in either *trans* or *cis* fashions. The resulting boron-containing conjugated compounds or polymers would have intersting features in organic syntheis and/or as functional materials.





41



42

6.5 References

1. Cornils, B.; Hermann, W. A. *Applied Homogeneous Catalysis with Organometallic Compounds. A Comprehensive Handbook.* VCH: Weinheim, **1996**. Vol. 1 & 2.

2. (a) Fujita, M.; Yazaki, J.; Ogura, K. *J. Am. Chem. Soc.* **1990**, *112*, 5645. (b) Stang, P. J.; Cao, D. H. *J. Am. Chem. Soc.* **1994**, *116*, 4981. (c) Stang, P. J.; Chen, K. *J. Am. Chem. Soc.* **1995**, *117*, 1667. (d) Stang, P. J.; Cao, D. H.; Saito, S.; Arif, A. M. *J. Am. Chem. Soc.* **1995**, *117*, 6273. (e) Stang, P. J.; Chen, K.; Arif, A. M. *J. Am. Chem. Soc.* **1995**, *117*, 8783. (f) Stang, P. J.; Olenyuk, B. *Angew Chem. Int. Ed. Engl.* **1996**, *35*, 732. (g) Olenyuk, B.; Whiteford, J. A.; Stang, P. J. *J. Am. Chem. Soc.* **1996**, *118*, 8221. (h) Manna, J.; Whiteford, J. A.; Stang, P. J.; Muddiman, D. C.; Smith, R. D. *J. Am. Chem. Soc.* **1996**, *118*, 8731. (i) Stang, P. J.; Persky, N. E.; *Chem. Commun.* **1997**, 77. (j) Stang, P. J.; Persky, N. E.; Manna, J. *J. Am. Chem. Soc.* **1997**, *119*, 4777. (k) Manna, J.; Kuehl, C. J.; Whiteford, J. A.; Stang, P. J.; Muddiman, D. C.; Hofstadler, S. A.; Smith, R. D. *J. Am. Chem. Soc.* **1997**, *119*, 11611. (l) Stang, P. J. *Chem. Eur. J.* **1998**, *4*, 19. (m) Fujita, M.; Oguro, D.; Miyazawa, M.; Oka, H.; Yamaguchi, K.; Ogura, K. *Nature*, **1995** *378*, 469. (n) Fujita, M. *Coord. Chem. Rev.* **1996**, *148*, 249. (o) Slone, R. V.; Hupp, J. T.; Stern, C. L.; Albrecht-Schmitt, T. E. *Inorg. Chem.* **1996**, *35*, 4096. (p) Baxter, P. N. W. *Metal Ion Directed Assembly of Complex Molecular Architectures and Nanostructures* in *Comprehensive Supramolecular Chemistry*; Lehn, J. -M.; Sauvage, J. P.; Hosseini, M. W., Eds.; Pergamon Press: Oxford, **1996**, Vol. 9, Chapter 5, p 165.

3. (a) Fujita, M.; Kwon, Y. J.; Washizu, S.; Ogura, K. *J. Am. Chem. Soc.* **1994**, *116*, 1151. (b) Zaworotko, M. J. *Chem. Soc. Rev.* **1994**, 283. (c) Gardner, G. B.; Venkataraman, D.; Moore, J. S.; Lee, S. *Nature* **1995**, *374*, 792. (d) Yaghi, O. M.;

Li, G.; Li, H. *Nature*, **1995**, *378*, 703. (e) Real, J. A.; Andrés, E.; Muñoz, C.; Julve, M.; Granier, T.; Bousseksou, A.; Varret, F. *Science* **1995**, *268*, 265. (f) Subramanian, S.; Zaworotko, M. J. *Angew Chem. Int. Ed. Engl.* **1995**, *34*, 2127. (g) Losier, P.; Zaworotko, M. J. *Angew Chem. Int. Ed. Engl.* **1996**, *35*, 2779. (h) Venkataraman, D.; Lee, S.; Moore, J. S.; Zhang, P.; Hirsch, K. A.; Gardner, G. B.; Covey, A. C.; Prentice, C. L. *Chem. Mater.* **1996**, *8*, 2030. (i) Kirsch, K. A.; Wilson, S. R.; Moore, J. S. *Inorg. Chem.* **1997**, *36*, 2960. (j) Kirsch, K. A.; Wilson, S. R.; Moore, J. S. *Chem. Eur. J.* **1997**, *3*, 765.

4. Reviews: (a) Aakeröy, C. B.; Seddon, K. R. *Chem. Soc. Rev.* **1993**, 387. (b) Desiraju, G. R. *Angew Chem. Int. Ed. Engl.* **1995**, *34*, 2311. (c) Philp, D.; Stoddart, J. F. *Angew Chem. Int. Ed. Engl.* **1996**, *35*, 1155. (d) Lehn, L. -M. *Supramolecular Chemistry*, VCH Press: New York, 1995.

5. Related systems with hydrogen bonding and arene-arene interactions: (a) Lewis, F. D.; Yang, J. -S.; Stern, C. L. *J. Am. Chem. Soc.* **1996**, *118*, 12029. (b) Endo, K.; Sawaki, T.; Koyanagi, M.; Kobayashi, K.; Masuda, H.; Aoyama, Y. *J. Am. Chem. Soc.* **1995**, *117*, 8341. (c) Aoyama, Y.; Endo, K.; Anzai, T.; Yamaguchi, Y.; Sawaki, T.; Kobayashi, K.; Kanehisa, N.; Hashimoyo, H.; Kai, Y.; Masuda, H. *J. Am. Chem. Soc.* **1996**, *118*, 5562.

6. Nguyen, P.; Lesley, G.; Marder, T. B.; Ledoux, I.; Zyss, J. *Chem. Mater.* **1997**, *9*, 406.

7. More recent reviews: (a) Dalton, L. R. *Chem. & Ind.* **1997**, 510. (b) Marder, S. R.; Kippelen, B.; Jen, A. K. -Y.; Peyghambarian, N. *Nature*, **1997**, *388*, 845.

8. Chen, C. T. in *Laser Science and Technology*, Letoknov, V. S.; Shank, C. V.; Shen, Y. R.; Walther, H. Eds.; Vol. 15, Harwood Academic: Langhorne, PA, 1993.

9. Wilson, E. *C&EN*, August 14, **1995**, p 27.

10. Marder, S. R.; Sohn, J. E.; Stucky, G. D. *Materials for Nonlinear Optics: Chemical Perspectives.* ACS Symposium Series, Vol. 455, American Chemical Society: Washington, 1991.

11. Fasol, G. *Science*, **1996**, *272*, 1751.

12. Lindsay, G. A.; Singer, K. D. *Polymers for Second-order Nonlinear Optics.* ACS Symposium Series, Vol. 601, American Chemical Society: Washington, 1995.

13. (a) Gorman, C. B., Marder, S. R. *Proc. Natl. Acad. Sci. USA*, **1993**, *90*, 11297. (b) Marder, S. R.; Cheng, L. -T.; Tiemann, B. G.; Friedli, A. C.; Blanchard-Desce, M.; Perry, J. W.; Skindhøj, J. *Science* **1994**, *263*, 511. (c) Albert, I. D. L.; Marks, T. J.; Ratner, M. A. *J. Am. Chem. Soc.* **1997**, *119*, 6575. (d) Blanchard-Desce, M.; Alain, V.; Bedworth, P. V.; Marder, S. R.; Fort, A.; Runser, C.; Barzoukas, M.; Lebus, S.; Wortman, R. *Chem. Eur. J.* **1997**, *3*, 1091.

14. Reviews: (a) Yitzchaik, S.; Marks, T. J. *Acc. Chem. Res.* **1996**, *29*, 197. (b) Burland, D. M.; Miller, R. D.; Walsh, C. A. *Chem. Rev.* **1994**, *94*, 31.

15. (a) Rao, V. P.; Jen, A. K. -Y.; Wong, K. Y.; Drost, K. J. *J. Chem. Soc., Chem. Commun.* **1993**, 1118. (b) Jen, A. K. -Y.; Rao, V. P.; Drost, K. J.; Wong, K. Y.; Cava, M. P. *J. Chem. Soc., Chem. Commun.* **1994**, 2057. (c) Rao, V. P.; Jen, A. K. -Y.; Cai, Y. *Chem. Commun.* **1996**, 1237. (d) Shu, C. -F.; Tsai, W. J.; Chen, J. -Y.; Jen, A. K. -Y.; Zhang, Y.; Chen, T. -A. *J. Chem. Soc., Chem. Commun.* **1996**, 2279. (e) Varanasi, P. R.; Jen, A. K. -Y.; Chandraseekhar, J.; Namboothiri, I. N. N.; Rathna, A. *J. Am. Chem. Soc.* **1996**, *118*, 12443.

16. Heck, R. F. *Acc. Chem. Res.* **1979**, *12*, 146.

17. (a) Ku, H.; Barrio, J. R. *J. Org. Chem.* **1981**, *46*, 5239. (b) Moore, J. S.; Weinstein, E. J.; Wu, Z. *Tetrahedron Lett.* **1991**, *32*, 2465.

18. (a) Chan, T. H.; Fleming, I. *Synthesis*, **1979**, 761. (b) Utimoto, K.; Kitai, M.; Nozaki, H. *Tetrahedron Lett.* **1975**, 2825.

19. Schumm, J. S.; Person, D. L.; Tour, J. M. *Angew Chem. Int. Ed. Engl.* **1994**, *33*, 1360.

20. Stille, J. K. *Angew Chem. Int. Ed. Engl.* **1986**, *25*, 508.

21. (a) Ishiyama, T.; Murata, M.; Miyaura, N. *J. Org. Chem.* **1995**, *60*, 7508. (b) Ishiyama, T.; Itoh, Y.; Kitano, T.; Miyaura, N. *Tetrahedron Lett.* **1997**, *38*, 3447.

22. (a) Sengupta, S.; Bhattacharya, S. *J. Chem. Soc., Perkin Trans. 1*, **1993**, 1943. (b) Sengupta, S.; Bhattacharya, S. *J. Org. Chem.* **1993**, *62*, 3405.

23. Seebach, D. *Angew. Chem. Int. Ed. Engl.* **1990**, *29*, 1320.

24. Trost, B. M. *Angew. Chem. Int. Ed. Engl.* **1995**, *34*, 259.

25. (a) Horváth, I. T.; Rabai, J. *Science*, **1994**, *266*, 72. (b) Horváth, I. T. in *Applied Homogeneous Catalysis with Organometallic Compounds*. Cornils, B.; Herrmann, W. Eds. VCH: Weinheim, 1996, p 601.

26. For recent reviews, see: (a) Piers, W. E.; Chivers, T. *Chem. Soc. Rev.* **1997**, *26*, 345. (b) Piers, W. E. *Chem. Eur. J.* **1998**, *4*, 13.

27. (a) Atherton, M. J.; Coleman, K. S.; Fawcett, J.; Holloway, J. H.; Hope, E. G.; Karacar, A.; Peck, L. A.; Saunders, G. C. *J. Chem. Soc., Dalton Trans.* **1995**, 4029. (b) Holloway, J. H.; Hope, E. G.; Russell, D. R.; Saunders, G. C.; Atherton, M. J.;

Polyhedron, **1996**, *15*, 173. (c) Atherton, M. J.; Fawcett, J.; Holloway, J. H.; Hope, E. G.; Russell, D. R.; Saunders, G. C. *J. Chem. Soc., Dalton Trans.* **1997**, 2217.

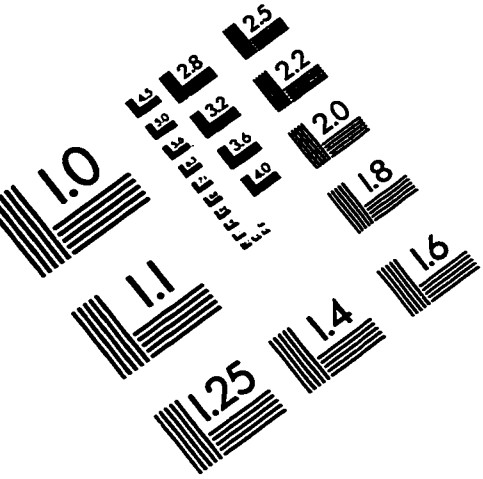
28. (a) Curnow, O. J.; Hughes, R. P. *J. Am. Chem. Soc.* **1992**, *114*, 5895. (b) Hughes, R. P.; Zheng, X.; Ostrander, R. L.; Rheingold, A. L. *Organometallics*, **1994**, *13*, 1567. (c) Chambers, R. D.; Roche, A. J.; Vaughan, J. F. S. *Can. J. Chem.* **1996**, *74*, 1925. (d) Deck, P. A.; Jackson, W. F.; Fronczek, F. R. *Organometallics*, **1996**, *15*, 5287.

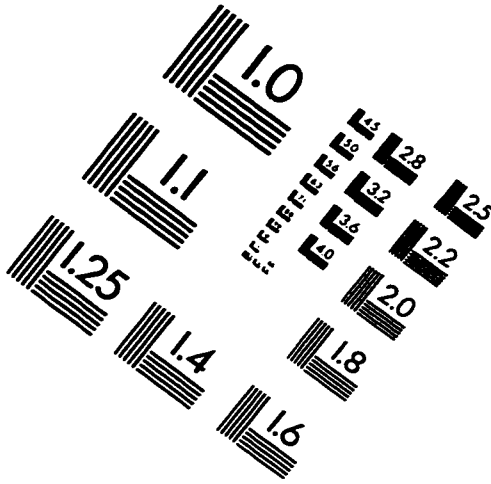
29. Ojima, I.; Kwon, H. B. *J. Am. Chem. Soc.* **1988**, *110*, 5617.

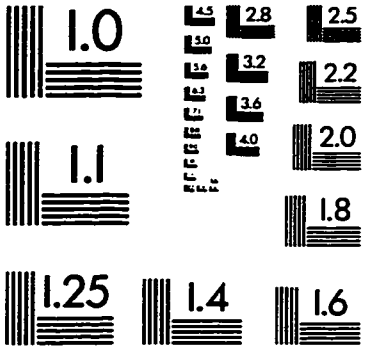
30. Quan, R. W.; Li, Z.; Jacobsen, E. N. *J. Am. Chem. Soc.* **1996**, *118*, 8156.

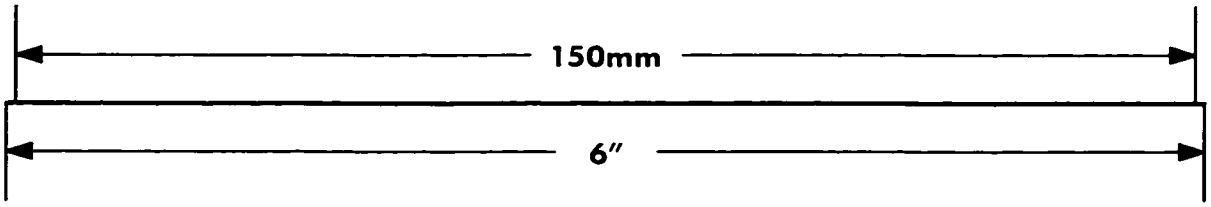
31. Clegg, W.; Elsegood, M. R. J.; Lawlor, F.; Norman, N. C.; Pickett, N. L.; Robins, E. G.; Scott, A. J.; Nguyen, P.; Taylor, N. J.; Marder, T. B. *Inorg. Chem.* (in press)

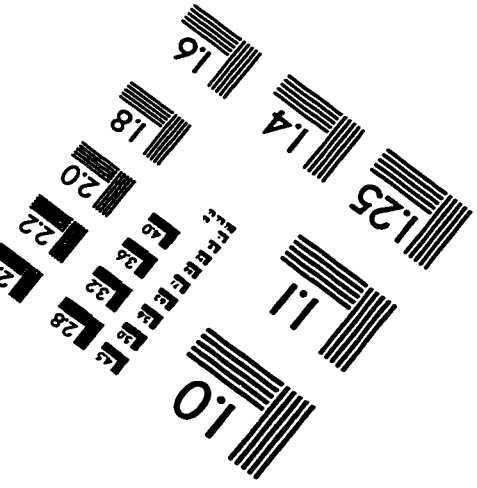
IMAGE EVALUATION
TEST TARGET (QA-3)

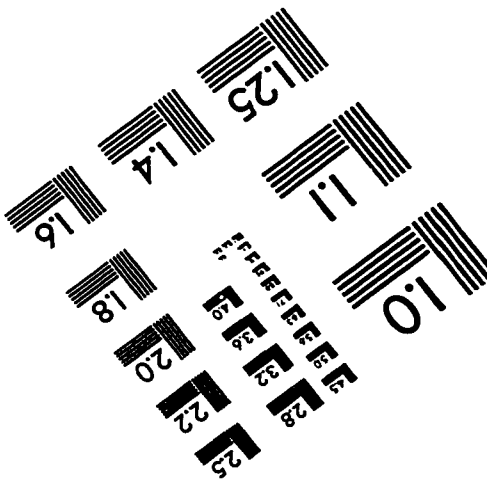












APPLIED IMAGE, Inc
1653 East Main Street
Rochester, NY 14609 USA
Phone: 716/482-0300
Fax: 716/288-5989

© 1993, Applied Image, Inc., All Rights Reserved